Publishing House ASV

begell house, inc. publishers

PAACH

Scientific coordination is carried out by the Russian Academy of Architecture and Construction Sciences (RAACS)

Volume 19 • Issue 2 • 2023

ISSN 2588-0195 (Online)
ISSN 2587-9618 (Print) Continues ISSN 1524-5845

International Journal for

Computational Civil and Structural Engineering

Международный журнал по расчету гражданских и строительных конструкций

http://ijccse.iasv.ru/index.php/IJCCSE
http://raasn.ru/public.php

DOI: 10.22337/2587-9618
GICID: 71.0000.1500.2830

EXECUTIVE EDITOR

Vladimir I. Travush,
Full Member of RAACS, Professor, Dr.Sc.,
Vice-President of the Russian Academy
of Architecture and Construction Sciences;
Urban Planning Institute
of Residential and Public Buildings;
24, Ulitsa Bolshaya Dmitrovka, 107031, Moscow, Russia

EDITOR-IN-CHIEF

Vladimir N. Sidorov,
Corresponding Member of RAACS, Professor, Dr.Sc.,
National Research Moscow State University of Civil
Engineering; Russian University of Transport
(RUT – MIIT); Moscow Institute of Architecture
(State Academy); Perm National Research Polytechnic
University; 26, Yaroslavskoe Shosse, 129337,
Moscow, Russia

EDITORIAL DIRECTOR

Valery I. Telichenko,
Full Member of RAACS, Professor, Dr.Sc.,
The First Vice-President of the Russian Academy
of Architecture and Construction Sciences;
Honorary President of National Research
Moscow State University of Civil Engineering;
24, Ulitsa Bolshaya Dmitrovka, 107031, Moscow, Russia

MANAGING EDITOR

Nadezhda S. Nikitina,
Professor, Ph.D.,
Director of ASV Publishing House;
National Research Moscow State University
of Civil Engineering;
26, Yaroslavskoe Shosse, 129337, Moscow, Russia

ASSOCIATE EDITORS

Pavel A. Akimov,
Full Member of RAACS, Professor, Dr.Sc.,
Acting Rector of National Research
Moscow State University of Civil Engineering;
Vice-President of the Russian Academy
of Architecture and Construction Sciences;
Tomsk State University of Architecture and Building;
Russian University of Friendship of Peoples;
26, Yaroslavskoe Shosse, 129337, Moscow, Russia

Alexander M. Belostotsky,
Full Member of RAACS, Professor, Dr.Sc.,
Research & Development Center "STADYO";
National Research Moscow State University of Civil
Engineering; Russian University of Transport (RUT –
MIIT); Russian University of Friendship of Peoples;
Perm National Research Polytechnic University;
Tomsk State University of Architecture and Building;
Irkutsk National Research Technical University;
8th Floor, 18, ul. Tretya Yamskogo Polya,
125040, Moscow, Russia

Mikhail Belyi, Professor, Dr.Sc.,
Dassault Systèmes Simulia;
1301 Atwood Ave Suite 101W
02919 Johnston, RI, United States

Vitaly Bulgakov, Professor, Dr.Sc.,
Micro Focus;
Newbury, United Kingdom

Nikolai P. Osmolovskii, Professor, Dr.Sc.,
Systems Research Institute, Polish Academy of Sciences;
Kazimierz Pulaski University
of Technology and Humanities in Radom;
29, ul. Malczewskiego, 26-600, Radom, Poland

Gregory P. Panasenko, Professor, Dr.Sc.,
Equipe d'Analise Numerique; NMR CNRS 5585
University Gean Mehnet;
23 rue. P.Michelon 42023, St.Etienne, France

Scientific coordination is carried out by the Russian Academy of Architecture and Construction Sciences (RAACS)

PUBLISHER

ASV Publishing House
(ООО «Издательство АСВ»)
19/1,12, Yaroslavskoe Shosse, 120338, Moscow, Russia
Tel. +7(925)084-74-24; E-mail: iasv@iasv.ru; Интернет-сайт: http://iasv.ru/

ADVISORY EDITORIAL BOARD

Mojtaba Aslami, Ph.D,
Fasa University; Daneshjou blvd,
Fasa, Fars Province, Iran

Klaus-Jurgen Bathe, Professor
Massachusetts Institute
of Technology;
Cambridge, MA 02139, USA

Alexander T. Bekker,
Academician of RAACS,
Professor, Dr.Sc.,
Far Eastern Federal University;
Russian Academy of Architecture
and Construction Sciences;
8, Sukhanova Street, Vladivostok,
690950, Russia

Tomas Bock, Professor, Dr.-Ing.,
Technical University of Munich,
Arcisstrasse 21, D-80333
Munich, Germany

Jan Buynak, Professor, Ph.D.,
University of Žilina;
1, Univerzitná, Žilina, 010 26,
Slovakia

Vladimir T. Erofeev,
Full Member of RAACS,
Professor, Dr.Sc.,
Ogarev Mordovia State University;
68, Bolshevistskaya Str., Saransk
430005, Republic of Mordovia,
Russia

Victor S. Fedorov,
Full Member of RAACS,
Professor, Dr.Sc.,
Russian University of Transport
(RUT – MIIT);
9b9 Obrazcova Street, Moscow,
127994, Russia

Sergey V. Fedosov,
Full Member of RAACS,
Professor, Dr.Sc.,
Russian Academy of Architecture
and Construction Sciences;
24, Ul. Bolshaya Dmitrovka, 107031,
Moscow, Russia

Sergiy Yu. Fialko,
Professor, Dr.Sc.,
Cracow University of Technology;
24, Warszawska Street, Kraków,
31-155, Poland

Vladimir G. Gagarin,
Corresponding Member
of RAACS, Professor, Dr.Sc.,
Research Institute of Building
Physics of Russian Academy
of Architecture and Construction
Sciences;
21, Lokomotivny Proezd,
Moscow, 127238, Russia

Vyatcheslav A. Ilyichev,
Full Member of RAACS,
Professor, Dr.Sc.,
Russian Academy of Architecture
and Construction Sciences;
Podzemproekt Ltd.;
24, Ulitsa Bolshaya Dmitrovka,
Moscow, 107031, Russia

Marek Iwański,
Professor, Dr.Sc.,
Kielce University of Technology;
7, al. Tysiąclecia Państwa Polskiego
Kielce, 25 – 314, Poland

Sergey Yu. Kalashnikov,
Advisor of RAACS,
Professor, Dr.Sc.,
Volgograd State Technical
University; 28, Lenin avenue,
Volgograd, 400005, Russia

Semen S. Kaprielov,
Academician of RAACS,
Professor, Dr.Sc.,
Research Center of Construction;
6, 2nd Institutskaya St., Moscow,
109428, Russia

Nikolay I. Karpenko,
Full Member of RAACS,
Professor, Dr.Sc.,
Research Institute of Building
Physics of Russian Academy
of Architecture and Construction
Sciences; Russian Academy of
Architecture and Construction
Sciences; 21, Lokomotivny Proezd,
Moscow, 127238, Russia

Vladimir V. Karpov,
Professor, Dr.Sc., Saint Petersburg
State University of Architecture and
Civil Engineering;
4, 2-nd Krasnoarmeiskaya Steet,
Saint Petersburg, 190005, Russia

Galina G. Kashevarova,
Corresponding Member
of RAACS, Professor, Dr.Sc.,
Perm National Research
Polytechnic University;
29 Komsomolsky pros., Perm,
Perm Krai, 614990, Russia

John T. Katsikadelis,
Professor, Dr.Eng, PhD, Dr.h.c.,
National Technical University of
Athens; Zografou Campus
9, Iroon Polytechniou str
15780 Zografou, Greece

Vitaly I. Kolchunov,
Full Member of RAACS,
Professor, Dr.Sc., Southwest State
University; Russian Academy of
Architecture and Construction
Sciences; 94, 50 let Oktyabrya,
Kursk, 305040, Russia

Dmitry V. Kozlov, Dr. Sc.
Engineering, Professor, Head of
the Department of Hydraulics and
Hydrotechnical Construction, NRU
MGSU,
26, Yaroslavskoe Shosse., 129337,
Moscow, Russia

Markus König, Professor
Ruhr-Universität Bochum;
150, Universitätsstraße, Bochum,
44801, Germany

Sergey B. Kositsin,
Advisor of RAACS,
Professor, Dr.Sc.,
Russian University of Transport
(RUT – MIIT); 9b9 Obrazcova
Street, Moscow, 127994, Russia

Sergey B. Krylov,
Corresponding Member
of RAACS, Professor, Dr.Sc.,
Research Center of Construction;
6, 2nd Institutskaya St., Moscow,
109428, Russia

Sergey V. Kuznetsov,
Professor, Dr.Sc.,
Ishlinsky Institute for Problems
in Mechanics of the Russian
Academy of Sciences;
101-1, Prosp. Vernadskogo,
Moscow, 119526, Russia

Vladimir V. Lalin,
Professor, Dr.Sc.,
Peter the Great Saint-Petersburg Polytechnic University;
29, Ul. Politechnicheskaya,
Saint-Petersburg, 195251, Russia

Leonid S. Lyakhovich,
Full Member of RAACS,
Professor, Dr.Sc., Tomsk State University of Architecture and Building; 2, Solyanaya Sq., Tomsk, 634003, Russia

Rashid A. Mangushev,
Corresponding Member of RAACS, Professor, Dr.Sc.,
Saint Petersburg State University of Architecture and Civil Engineering;
4, 2-nd Krasnoarmeiskaya Steet,
Saint Petersburg, 190005, Russia

Ilizar T. Mirsayapov,
Advisor of RAACS,
Professor, Dr.Sc., Kazan State University of Architecture and Engineering; 1, Zelenaya Street,
Kazan, 420043, Republic of Tatarstan, Russia

Vladimir L. Mondrus,
Corresponding Member of RAACS, Professor, Dr.Sc.,
National Research Moscow State University of Civil Engineering;
Yaroslavskoe Shosse 26,
Moscow, 129337, Russia

Valery I. Morozov,
Corresponding Member of RAACS, Professor, Dr.Sc.,
Saint Petersburg State University of Architecture and Civil Engineering;
4, 2-nd Krasnoarmeiskaya Steet,
Saint Petersburg, 190005, Russia

Anatoly V. Perelmuter,
Foreign Member of RAACS,
Professor, Dr.Sc., SCAD Soft;
Office 1,2, 3a Osvity street,
Kiev, 03037, Ukraine

Alexey N. Petrov,
Advisor of RAACS, Professor, Dr.Sc., Petrozavodsk State University; 33, Lenina Prospect,
Petrozavodsk, 185910,
Republic of Karelia, Russia

Vladilen V. Petrov,
Full Member of RAACS,
Professor, Dr.Sc.,
Yuri Gagarin State Technical University of Saratov;
77 Politechnicheskaya Street,
Saratov, 410054, Russia

Jerzy Z. Piotrowski,
Professor, Dr.Sc.,
Kielce University of Technology;
al. Tysiąclecia Państwa Polskiego 7,
Kielce, 25 – 314, Poland

Chengzhi Qi, Professor, Dr.Sc.,
Beijing University of Civil Engineering and Architecture;
1, Zhanlanlu, Xicheng District,
Beijing, China

Vladimir P. Selyaev,
Full Member of RAACS,
Professor, Dr.Sc., Ogarev Mordovia State University;
68, Bolshevistskaya Str., Saransk 430005, Republic of Mordovia, Russia

Eun Chul Shin,
Professor, Ph.D.,
Incheon National University;
(Songdo-dong)119 Academy-ro,
Yeonsu-gu, Incheon, Korea

D.V. Singh,
Professor, Ph.D,
University of Roorkee;
Roorkee, India, 247667

Wacław Szcześniak,
Foreign Member of RAACS,
Professor, Dr.Sc.,
Lublin University of Technology;
Ul. Nadbystrzycka 40,
20-618 Lublin, Poland

Tadatsugu Tanaka,
Professor, Dr.Sc.,
Tokyo University; 7-3-1 Hongo,
Bunkyo, Tokyo, 113-8654, Japan

Josef Vican,
Professor, Ph.D,
University of Žilina;
1, Univerzitná, Žilina, 010 26,
Slovakia

Zbigniew Wojcicki,
Professor, Dr.Sc.,
Wroclaw University of Technology;
11 Grunwaldzki Sq., 50-377,
Wrocław, Poland

Artur Zbiciak, Professor, Dr.Sc.,
Warsaw University of Technology;
Pl. Politechniki 1, 00-661 Warsaw, Poland

Segrey I. Zhavoronok, Ph.D.,
Institute of Applied Mechanics of Russian Academy of Sciences;
Moscow Aviation Institute (National Research University);
7, Leningradsky Prt.,
Moscow, 125040, Russia

Askar Zhussupbekov,
Professor, Dr.Sc.,
Eurasian National University;
5, Munaitpassov street, Astana,
010000, Kazakhstan

TECHNICAL EDITOR

Taymuraz B. Kaytukov,
Advisor of RAACS,
Associate Professor, Ph.D.,
Vice-Rector of National Research Moscow State University of Civil Engineering;
Yaroslavskoe Shosse 26,
Moscow, 129337, Russia

EDITORIAL TEAM

Vadim K. Akhmetov, Professor, Dr.Sc., National Research Moscow State University of Civil Engineering; 26, Yaroslavskoe Shosse, 129337 Moscow, Russia

Pavel A. Akimov, Full Member of RAACS, Professor, Dr.Sc., Acting Rector of National Research Moscow State University of Civil Engineering; Vice-President of the Russian Academy of Architecture and Construction Sciences; Tomsk State University of Architecture and Building; Russian University of Friendship of Peoples; 26, Yaroslavskoe Shosse, 129337, Moscow, Russia

Alexander M. Belostotsky, Full Member of RAACS, Professor, Dr.Sc., Research & Development Center "STADYO"; National Research Moscow State University of Civil Engineering; Russian University of Transport (RUT – MIIT); Russian University of Friendship of Peoples; Perm National Research Polytechnic University; Tomsk State University of Architecture and Building; Irkutsk National Research Technical University; 8th Floor, 18, ul. Tretya Yamskogo Polya, 125040, Moscow, Russia

Mikhail Belyi, Professor, Dr.Sc., Dassault Systèmes Simulia; 1301 Atwood Ave Suite 101W 02919 Johnston, RI, United States

Vitaly Bulgakov, Professor, Dr.Sc., Micro Focus; Newbury, United Kingdom

Charles El Nouty, Professor, Dr.Sc., LAGA Paris-13 Sorbonne Paris Cite; 99 avenue J.B. Clément, 93430 Villetaneuse, France

Natalya N. Fedorova, Professor, Dr.Sc., Novosibirsk State University of Architecture and Civil Engineering (SIBSTRIN); 113 Leningradskaya Street, Novosibirsk, 630008, Russia

Darya Filatova, Professor, Dr.Sc., Probability, Assessment, Reasoning and Inference Studies Research Group, EPHE Laboratoire CHART (PARIS) 4-14, rue Ferrus, 75014 Paris

Vladimir Ya. Gecha, Professor, Dr.Sc., Research and Production Enterprise All-Russia Scientific-Research Institute of Electromechanics with Plant Named after A.G. Iosiphyan; 30, Volnaya Street, Moscow, 105187, Russia

Taymuraz B. Kaytukov, Advisor of RAACS, Associate Professor, Ph.D, Vice-Rector of National Research Moscow State University of Civil Engineering; 26, Yaroslavskoe Shosse, 129337, Moscow, Russia

Marina L. Mozgaleva, Professor, Dr.Sc., National Research Moscow State University of Civil Engineering; 26, Yaroslavskoe Shosse, 129337 Moscow, Russia

Nadezhda S. Nikitina, Professor, Ph.D., Director of ASV Publishing House; National Research Moscow State University of Civil Engineering; 26, Yaroslavskoe Shosse, 129337 Moscow, Russia

Nikolai P. Osmolovskii, Professor, Dr.Sc., Systems Research Institute Polish Academy of Sciences; Kazimierz Pulaski University of Technology and Humanities in Radom; 29, ul. Malczewskiego, 26-600, Radom, Poland

Gregory P. Panasenko, Professor, Dr.Sc., Equipe d'Analise Numerique NMR CNRS 5585 University Gean Mehnet; 23 rue. P.Michelon 42023, St.Etienne, France

Andreas Rauh, Prof. Dr.-Ing. habil. Carl von Ossietzky Universität Oldenburg, Germany School II - Department of Computing Science Group Distributed Control in Interconnected Systems D-26111 Oldenburg, Germany

Zhan Shi, Professor LPSM, Université Paris VI 4 place Jussieu, F-75252 Paris Cedex 05, France

Marina V. Shitikova, National Research Moscow State University of Civil Engineering, Advisor of RAACS, Professor, Dr.Sc., Voronezh State Technical University; 14, Moscow Avenue, Voronezh, 394026, Russia

Igor L. Shubin, Corresponding Member of RAACS, Professor, Dr.Sc., Research Institute of Building Physics of Russian Academy of Architecture and Construction Sciences; 21, Lokomotivny Proezd, Moscow, 127238, Russia

Vladimir N. Sidorov, Corresponding Member of RAACS, Professor, Dr.Sc., National Research Moscow State University of Civil Engineering; Russian University of Transport (RUT – MIIT); Moscow Institute of Architecture (State Academy); Perm National Research Polytechnic University; 26, Yaroslavskoe Shosse, 129337, Moscow, Russia

Valery I. Telichenko, Full Member of RAACS, Professor, Dr.Sc., The First Vice-President of the Russian Academy of Architecture and Construction Sciences; National Research Moscow State University of Civil Engineering; 24, Ulitsa Bolshaya Dmitrovka, 107031, Moscow, Russia

Vladimir I. Travush, Full Member of RAACS, Professor, Dr.Sc., Vice-President of the Russian Academy of Architecture and Construction Sciences; Urban Planning Institute of Residential and Public Buildings; 24, Ulitsa Bolshaya Dmitrovka, 107031, Moscow, Russia

INVITED REVIEWERS

Akimbek A. Abdikalikov, Professor, Dr.Sc.,
Kyrgyz State University of Construction, Transport and Architecture n.a. N. Isanov;
34 Maldybayeva Str., Bishkek, 720020, Biskek, Kyrgyzstan

Vladimir N. Alekhin, Advisor of RAACS, Professor, Dr.Sc.,
Ural Federal University named after the first President of Russia B.N. Yeltsin;
19 Mira Street, Ekaterinburg, 620002, Russia

Irina N. Afanasyeva, Ph.D., University of Florida; Gainesville, FL 32611, USA

Ján Čelko, Professor, PhD, Ing., University of Žilina; Univerzitná 1, 010 26, Žilina, Slovakia

Tatyana L. Dmitrieva, Professor, Dr.Sc.,
Irkutsk National Research Technical University; 83, Lermontov street, Irkutsk, 664074, Russia

Petr P. Gaidzhurov, Advisor of RAACS, Professor, Dr.Sc.,
Don State Technical University; 1, Gagarina Square, Rostov-on-Don, 344000, Russia

Jacek Grosel, Associate Professor, Dr inz.
Wroclaw University of Technology; 11 Grunwaldzki Sq., 50-377, Wrocław, Poland

Stanislaw Jemioło, Professor, Dr.Sc.,
Warsaw University of Technology; 1, Pl. Politechniki, 00-661, Warsaw, Poland

Konstantin I. Khenokh, M.Ing., M.Sc.,
General Dynamics C4 Systems; 8201 E McDowell Rd, Scottsdale, AZ 85257, USA

Christian Koch, Dr.-Ing., Ruhr-Universität Bochum;
Lehrstuhl für Informatik im Bauwesen, Gebäude IA, 44780, Bochum, Germany

Gaik A. Manuylov, Professor, Ph.D.,
Moscow State University of Railway Engineering; 9, Obraztsova Street, Moscow, 127994, Russia

Alexander S. Noskov, Professor, Dr.Sc.,
Ural Federal University named after the first President of Russia B.N. Yeltsin;
19 Mira Street, Ekaterinburg, 620002, Russia

Grzegorz Świt, Professor, Dr.hab. Inż.,
Kielce University of Technology; 7, al. Tysiąclecia Państwa Polskiego, Kielce, 25 – 314, Poland

AIMS AND SCOPE

The aim of the Journal is to advance the research and practice in structural engineering through the application of computational methods. The Journal will publish original papers and educational articles of general value to the field that will bridge the gap between high-performance construction materials, large-scale engineering systems and advanced methods of analysis.

The scope of the Journal includes papers on computer methods in the areas of structural engineering, civil engineering materials and problems concerned with multiple physical processes interacting at multiple spatial and temporal scales. The Journal is intended to be of interest and use to researches and practitioners in academic, governmental and industrial communities.

ОБЩАЯ ИНФОРМАЦИЯ О ЖУРНАЛЕ

International Journal for Computational Civil and Structural Engineering

(Международный журнал по расчету гражданских и строительных конструкций)

Международный научный журнал "International Journal for Computational Civil and Structural Engineering (Международный журнал по расчету гражданских и строительных конструкций)" (IJCCSE) является ведущим научным периодическим изданием по направлению «Инженерные и технические науки», издаваемым, начиная с 1999 года (ISSN 2588-0195 (Online); ISSN 2587-9618 (Print) Continues ISSN 1524-5845). В журнале на высоком научно-техническом уровне рассматриваются проблемы численного и компьютерного моделирования в строительстве, актуальные вопросы разработки, исследования, развития, верификации, апробации и приложений численных, численно-аналитических методов, программно-алгоритмического обеспечения и выполнения автоматизированного проектирования, мониторинга и комплексного наукоемкого расчетно-теоретического и экспериментального обоснования напряженно-деформированного (и иного) состояния, прочности, устойчивости, надежности и безопасности ответственных объектов гражданского и промышленного строительства, энергетики, машиностроения, транспорта, биотехнологий и других высокотехнологичных отраслей.

В редакционный совет журнала входят известные российские и зарубежные деятели науки и техники (в том числе академики, члены-корреспонденты, иностранные члены, почетные члены и советники Российской академии архитектуры и строительных наук). Основной критерий отбора статей для публикации в журнале − их высокий научный уровень, соответствие которому определяется в ходе высококвалифицированного рецензирования и объективной экспертизы, поступающих в редакцию материалов.

Журнал входит в Перечень ВАК РФ ведущих рецензируемых научных изданий, в которых должны быть опубликованы основные научные результаты диссертаций на соискание ученой степени кандидата наук, на соискание ученой степени доктора наук по научным специальностям и соответствующим им отраслям науки:

- 1.1.8 – Механика деформируемого твердого тела (технические науки),
- 1.2.2 – Математическое моделирование численные методы и комплексы программ (технические науки),
- 2.1.1 – Строительные конструкции, здания и сооружения (технические науки),
- 2.1.2 – Основания и фундаменты, подземные сооружения (технические науки),
- 2.1.5 – Строительные материалы и изделия (технические науки),
- 05.23.07 – Гидротехническое строительство (технические науки),
- 2.1.9 – Строительная механика (технические науки)

В Российской Федерации журнал индексируется Российским индексом научного цитирования (РИНЦ).

Журнал входит в базу данных Russian Science Citation Index (RSCI), полностью интегрированную с платформой Web of Science. Журнал имеет международный статус и высылается в ведущие библиотеки и научные организации мира.

Издатели журнала – *Издательство Ассоциации строительных высших учебных заведений /АСВ/* (Россия, г. Москва) и до 2017 года *Издательский дом Begell House Inc*. (США, г. Нью-Йорк). Официальными партнерами издания является *Российская академия архитектуры и строительных наук* (РААСН), осуществляющая научное курирование издания, и *Научно-исследовательский центр СтаДиО* (ЗАО НИЦ СтаДиО).

Цели журнала – демонстрировать в публикациях российскому и международному профессиональному сообществу новейшие достижения науки в области вычислительных методов

решения фундаментальных и прикладных технических задач, прежде всего в области строительства.

Задачи журнала:

• предоставление российским и зарубежным ученым и специалистам возможности публиковать результаты своих исследований;

• привлечение внимания к наиболее актуальным, перспективным, прорывным и интересным направлениям развития и приложений численных и численно-аналитических методов решения фундаментальных и прикладных технических задач, совершенствования технологий математического, компьютерного моделирования, разработки и верификации реализующего программно-алгоритмического обеспечения;

• обеспечение обмена мнениями между исследователями из разных регионов и государств.

Тематика журнала. К рассмотрению и публикации в журнале принимаются аналитические материалы, научные статьи, обзоры, рецензии и отзывы на научные публикации по фундаментальным и прикладным вопросам технических наук, прежде всего в области строительства. В журнале также публикуются информационные материалы, освещающие научные мероприятия и передовые достижения Российской академии архитектуры и строительных наук, научно-образовательных и проектно-конструкторских организаций.

Тематика статей, принимаемых к публикации в журнале, соответствует его названию и охватывает направления научных исследований в области разработки, исследования и приложений численных и численно-аналитических методов, программного обеспечения, технологий компьютерного моделирования в решении прикладных задач в области строительства, а также соответствующие профильные специальности, представленные в диссертационных советах профильных образовательных организациях высшего образования.

Редакционная политика. Политика редакционной коллегии журнала базируется на современных юридических требованиях в отношении авторского права, законности, плагиата и клеветы, изложенных в законодательстве Российской Федерации, и этических принципах, поддерживаемых сообществом ведущих издателей научной периодики.

За публикацию статей плата с авторов не взымается. Публикация статей в журнале бесплатная. На платной основе в журнале могут быть опубликованы материалы рекламного характера, имеющие прямое отношение к тематике журнала.

Журнал предоставляет непосредственный открытый доступ к своему контенту, исходя из следующего принципа: свободный открытый доступ к результатам исследований способствует увеличению глобального обмена знаниями.

Индексирование. Публикации в журнале входят в системы расчетов индексов цитирования авторов и журналов. «Индекс цитирования» – числовой показатель, характеризующий значимость данной статьи и вычисляющийся на основе последующих публикаций, ссылающихся на данную работу.

Авторам. Прежде чем направить статью в редакцию журнала, авторам следует ознакомиться со всеми материалами, размещенными в разделах сайта журнала (интернет-сайт Российской академии архитектуры и строительных наук (http://raasn.ru); подраздел «Издания РААСН» или интернет-сайт Издательства АСВ (http://iasv.ru); подраздел «Журнал IJCCSE»): с основной информацией о журнале, его целями и задачами, составом редакционной коллегии и редакционного совета, редакционной политикой, порядком рецензирования направляемых в журнал статей, сведениями о соблюдении редакционной этики, о политике авторского права и лицензирования, о представлении журнала в информационных системах (индексировании), информацией о подписке на журнал, контактными данными и пр. Журнал работает по лицензии Creative Commons типа cc by-nc-sa (Attribution Non-Commercial Share Alike) – Лицензия «С указанием авторства – Некоммерческая – Копилефт».

Рецензирование. Все научные статьи, поступившие в редакцию журнала, проходят обязательное двойное слепое рецензирование (рецензент не знает авторов рукописи, авторы рукописи не знают рецензентов).

Заимствования и плагиат. Редакционная коллегия журнала при рассмотрении статьи проводит проверку материала с помощью системы «Антиплагиат». В случае обнаружения многочисленных заимствований редакция действует в соответствии с правилами COPE.

Подписка. Журнал зарегистрирован в Федеральном агентстве по средствам массовой информации и охраны культурного наследия Российской Федерации. Индекс в общероссийском каталоге РОСПЕЧАТЬ − 18076.

По вопросам подписки на международный научный журнал “International Journal for Computational Civil and Structural Engineering (Международный журнал по расчету гражданских и строительных конструкций)” обращайтесь в Агентство «Роспечать» (Официальный сайт в сети Интернет: http://www.rosp.ru/) или в издательство Ассоциации строительных вузов (АСВ) в соответствии со следующими контактными данными:

ООО «Издательство АСВ»

Юридический адрес: 129337, Россия, г. Москва, Ярославское ш., д. 26, офис 705;

Фактический адрес: 129337, Россия, г. Москва, Ярославское ш., д. 19, корп. 1, 5 этаж, офис 12 (ТЦ Соле Молл);

Телефоны: +7 (925) 084-74-24;

Интернет-сайт: www.iasv.ru. Адрес электронной почты: iasv@iasv.ru.

Контактная информация. По всем вопросам работы редакции, рецензирования, согласования правки текстов и публикации статей следует обращаться к главному редактору журнала члену-корреспонденту РААСН *Сидорову Владимиру Николаевичу* (адреса электронной почты: sidorov.vladimir@gmail.com, sidorov@iasv.ru, iasv@iasv.ru, sidorov@raasn.ru) или к техническому редактору журнала советнику РААСН *Кайтукову Таймуразу Батразовичу* (адреса электронной почты: tkaytukov@gmail.com; kaytukov@raasn.ru). Кроме того, по указанным вопросам, а также по вопросам размещения в журнале рекламных материалов можно обращаться к генеральному директору ООО «Издательство АСВ» *Никитиной Надежде Сергеевне* (адреса электронной почты: iasv@iasv.ru, nsnikitina@mail.ru, ijccse@iasv.ru).

Журнал становится технологичнее. Издательство АСВ с сентября 2016 года является членом Международной ассоциации издателей научной литературы (Publishers International Linking Association (PILA)), осуществляющей свою деятельность на платформе CrossRef. Оригинальным статьям, публикуемым в журнале, будут присваиваться уникальные номера (индексы DOI – Digital Object Identifier), что значительно облегчит поиск метаданных и местонахождение полнотекстового произведения. DOI – это система определения научного контента в сети Интернет.

С октября 2016 года стал возможен прием статей на рассмотрение и рецензирование через онлайн систему приема статей Open Journal Systems на сайте журнала (электронная редакция): http://ijccse.iasv.ru/index.php/IJCCSE.

Автор имеет возможность следить за продвижением статьи в редакции журнала в личном кабинете Open Journal Systems и получать соответствующие уведомления по электронной почте.

В феврале 2018 года журнал был зарегистрирован в Directory of open access journals (DOAJ) (это один из самых известных поисковых сервисов в мире, который предоставляет открытый доступ к материалам и индексирует не только заголовки журналов, но и научные статьи), в сентябре 2018 года включен в продукты EBSCO Publishing.

В ноябре 2020 года журнал начал индексироваться в международной базе Scopus.

International Journal for
Computational Civil and Structural Engineering
(Международный журнал по расчету гражданских и строительных конструкций)
Volume 19, Issue 2 ***2023***

Scientific coordination is carried out by the Russian Academy of Architecture and Construction Sciences (RAACS)

CONTENTS

Modelling of a Three-Dispersed Suspension Filtration **14**
Galina L. Safina

The Effect of Hollow Structure Parameter on the 3d-Printed Wall Bearing Capacity. Experimental Model **31**
Galina S. Slavcheva, Artem V. Levchenko, Maria A. Shvedova, Davut R. Karakchi-Ogli, Dmitriy S. Babenko, Pavel Y. Yurov

Strength of Aluminum Alloy Joints Made by Contact Capacitor Welding **42**
Andrey V. Korgin

Selection of the Rational Parameters of Three-Layer Reinforced Concrete Structures with Monolithic Bonding Layers by the Method of Computer Modeling **51**
Elena A. Korol, Yulia O. Kustikova

On Resonant Vortex Excitation of High-Rise Buildings **60**
Anastasia I.Karakozova, Vladimir L. Mondrus

Problem of Plate Bending in the Moment Asymmetric Theory of Elasticity **71**
Nelly N. Rogacheva, Yulia G. Zheglova

Numerical Study of Ice and Channel Processes on the Bridge Supports Across the Kuibyshev Reservoir (Kazan) **81**
Vitaly V. Belikov, Natalya M. Borisova, Anna V.Glotko, Dmitry V.Kozlov

The Recommendations of Determining the Boundary Conditions of the Model for Assessing the Impact on the Surrounding Development of Tunneling **95**
Armen Z. Ter-Martirosyan, Rustam H. Cherkesov, Ilya O. Isaev, Viktoriya V. Rud, Mariya I. Ambrushkevich

Nonlinear Refinement of the Deformation Model of Orthotropic Materials, the Rigidity of which Depends on the Type of Stress State **109**
Alexander A. Treshchev, Nikita S. Yushchenco, Alexander A. Bobryshev

Strength and Durability of Concretes with a Super Absorbent Polymer Additive
Kamil B. Sharafutdinov, Ksenia A. Saraykina, Galina G. Kashevarova, Yana A. Sanyagina, Vladimir T. Erofeev, Nikolai I. Vatin **120**

Experimental and Theoretical Studies of Dynamic Characteristics of Wooden Frame Buildings **136**
Tatiana L. Dmitrieva, Kristina A. Podshivalova

Calculation Model of a Multi-Storey Reinforced Concrete Frame with Complexly Stressed Beams Under Accidental Impact **150**
Violetta S. Moskovtseva, Sergey S. Fedorov, Margarita A. Amelina

Numerical Analysis of Antiseismic Sliding Belt Performance **161**
Oleg V. Mkrtychev, Salima R. Mingazova

Resudial Stresses In I-Beams and Its Effect on Rods Buckling **172**
Denis V. Konin, Alexander I. Fimkin, Alexander R. Olurombi

Acoustic Emission-Based Damage Detection in Steel Framed Structure - a Review **188**
Anupam Kumar Biswas, Aloke Kumar Datta, Pijush Topdar, Sanjay Sengupta

International Journal for
Computational Civil and Structural Engineering
(Международный журнал по расчету гражданских и строительных конструкций)
Volume 19, Issue 2 ***2023***

Scientific coordination is carried out by the Russian Academy of Architecture and Construction Sciences (RAACS)

СОДЕРЖАНИЕ

Моделирование фильтрации трёхдисперсной суспензии **14**
Г.Л. Сафина

Экспериментальная модель влияния пустотности на несущую способность стен, полученных по аддитивной технологии **31**
Г.С. Славчева, А.В. Левченко, М.А. Шведова, Д.Р. Каракчи-Огли, Д.С. Бабенко, П.Ю. Юров

Прочность соединений из алюминиевых сплавов, выполненных методом контактной конденсаторной сварки **42**
А.В. Коргин

Выбор рациональных параметров трехслойных железобетонных конструкций с монолитными связующими слоями методом компьютерного моделирования **51**
Е.А. Король, Ю.О. Кустикова

О резонансном вихревом возбуждении высотных сооружений **60**
А.И. Каракозова, В.Л. Мондрус

Задача изгиба пластины в моментной асимметричной теории упругости **71**
Н.Н. Рогачева, Ю.Г. Жеглова

Численное моделирование деформаций дна и ледовых явлений на опоры строящегося моста через куйбышевское водохранилище у г. Казани **81**
В.В. Беликов, Н.М. Борисова, А.В. Глотко, Д.В. Козлов

Определение параметров границ расчетной модели при оценке влияния на окружающую застройку от тоннелепроходческих работ **95**
А.З. Тер-Мартиросян, Р.Х. Черкесов, И.О. Исаев, В.В. Рудь, М.И. Амбрушкевич

Нелинейное уточнение модели деформирования ортотропных материалов, жесткость которых зависит от вида напряженного состояния **109**
А.А. Трещев, Н.С. Ющенко, А.А. Бобрышев

Прочность и долговечность бетонов с супервпитывающей полимерной добавкой **120**
К.Б. Шарафутдинов, К.А. Сарайкина, Г.Г. Кашеварова, Я.А. Санягина, В.Т. Ерофеев, Н.И. Ватин

Экспериментально-теоретические исследования динамических характеристик деревянных каркасных зданий **136**
Т.Л. Дмитриева, К.А. Подшивалова

Расчетная модель многоэтажной железобетонной рамы со сложнонапряженными ригелями в запредельном состоянии **150**
В.С. Московцева, С.С. Федоров, М.А. Амелина

Численный анализ эффективности работы антисейсмического скользящего пояса **161**
О.В. Мкртычев, С.Р. Мингазова

Остаточные напряжения в двутаврах и их влияние на устойчивость стержней **172**
Д.В. Конин, А.И. Фимкин, А.Р. Олуромби

Обнаружение повреждений в стальных рамных конструкциях акустическим методом: аналитический обзор **188**
Анупам Кумар Бисвас, Алоке Кумар Датта, Пиюш Тондар, Санджай Сенгупта

О прошедших научных мероприятиях:
О восьмом международном симпозиуме РААСН «Актуальные проблемы компьютерного моделирования конструкций и сооружений» **205**
В.И. Травуш, П.А. Акимов, А.М. Белостоцкий, В.Н. Сидоров, П.В. Монастырев

DOI:10.22337/2587-9618-2023-19-2-14-30

MODELLING OF A THREE-DISPERSED SUSPENSION FILTRATION

Galina L. Safina

Moscow State University of Civil Engineering, Moscow, RUSSIA

Abstract. The injection method of soil stabilization is one of the methods to improve the soil base during the road construction. This method consists in the introduction of special compounds into the ground with the help of special equipment. Such compositions, as a rule, are solutions of polymers or cement, which harden, forming a solid base. The advantages of the injection method of soil stabilization for roads include rapid completion of work, minimal environmental impact, the possibility of application in difficult geological conditions, as well as strengthening the soil base at great depth. Injection solutions penetrate into microcracks and micropores of soils, forming a deposition. The study of liquid filtration in a porous soil system is of great practical importance. The paper considers the filtration of liquid in a porous medium with three types of particles. In the considered problem, each of the three types of suspension particles is characterized by its linear filtration function. It determines the size-exclusion particle capture mechanism, in which particles whose diameter exceeds the size of the pores get stuck in them, the rest pass through them unhindered. Numerical solutions are obtained for the concentrations of suspended particles of three types, as well as the total deposition. Depending on the initial parameters of the problem, the concentrations of suspended particles are either monotonic functions or non-monotonic, reaching the maximum value. In this paper, asymptotic solutions are constructed for the concentrations of suspended and retained particles near the concentration front, which are compared with numerical ones. The solution is obtained at infinity using a traveling wave.

Keywords: suspension filtration, suspended and retained particles, porous medium, filtration function, asymptotic solution, traveling wave

МОДЕЛИРОВАНИЕ ФИЛЬТРАЦИИ ТРЁХДИСПЕРСНОЙ СУСПЕНЗИИ

Г.Л. Сафина

Национальный исследовательский Московский государственный строительный университет, г. Москва, РОССИЯ

Аннотация: Инъекционный способ укрепления грунтов является одним из методов улучшения грунтового основания при строительстве автодорог. Этот метод заключается во введении специальных составов в грунт при помощи специального оборудования. Такие составы, как правило, являются растворами полимеров или цемента, которые затвердевают, образуя прочную основу. К преимуществам инъекционного способа укрепления грунтов для автодорог можно отнести быстрое выполнение работ, минимальное воздействие на окружающую среду, возможность применения в сложных геологических условиях, а также усиление грунтового основания на большой глубине. Инъекционные растворы проникают в микротрещины и микропоры грунтов, образуя осадок. Изучение фильтрации жидкости в пористой системе грунта имеет большое практическое значение. В работе рассматривается фильтрация жидкости в пористой среде с тремя типами частиц. В рассматриваемой задаче каждый из трех видов частиц суспензии характеризуется линейной функцией фильтрации. Это определяет размерный механизм захвата частиц, при котором частицы, диаметр которых превышает размер пор, застревают в них, остальные проходят через них беспрепятственно. Получены численные решения для концентраций взвешенных частиц трех типов, а также полного осадка. В зависимости от исходных параметров задачи концентрации взвешенных частиц являются либо монотонными функциями, либо немонотонными, достигающими максимального значения. В работе построено асимптотические решения для концентраций взвешенных и осажденных частиц вблизи фронта концентраций, которые сравниваются с численными. Получено решение на бесконечности с помощью бегущей волны.

Ключевые слова: фильтрация суспензии, взвешенные и осажденные частицы, пористая среда, функция фильтрации, асимптотическое решение, бегущая волна

INTRODUCTION

Many negative factors affect pavements throughout their service life. The mechanical effects of road transport cause bending stresses in concrete and abrasion of surface layers. Fluctuations in temperature and relative humidity during the day and calendar year, as well as cyclic processes of freezing and thawing, lead to the occurrence of tensile and compressive stresses in concrete. Hydrogeological conditions of the location of the road route, frosting of soil bases as a result of winter freezing and spring thawing lead to non-uniform deformations of concrete. Anti-icing chemical reagents and chemical compounds of the environment aggressively affect the concrete of the road bed. All this leads to the need to solve the problem of durability of road surfaces [1-5].

There are currently many ways to strengthen the ground bases in road construction [6-10], one of them is the soil stabilization by injection [11-15]. This method consists in introducing special compositions (injection solutions) into the soil to strengthen its properties and increase its bearing capacity. The process of injecting soil usually occurs as follows. First, the weak zones, zones with reduced bearing capacity, zones with subsidence, etc. on the ground surface are determined. Then drills are inserted into these zones and an injection fluid is injected through them, which fills the pores and cracks of the soil, strengthening its properties. Usually injection compositions consist of cement, sand and water, as well as additives to improve the properties of the composition.

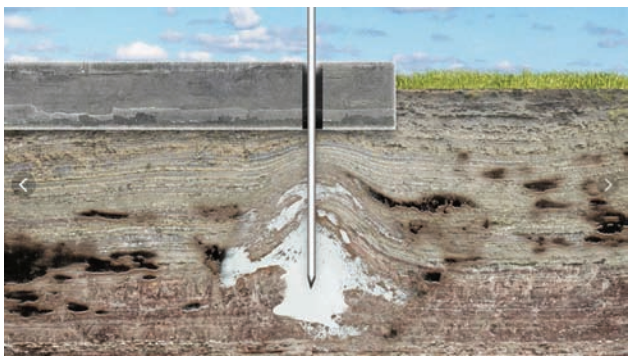


Figure 1. Soil stabilization by injection

Injecting soils during the road construction has a number of advantages. This is a fast and effective method of strengthening the soil foundations, which can significantly reduce the construction time of the road and reduce its cost. Injecting soils can significantly increase the bearing capacity of the soil and reduce the likelihood of subsidence and failures on the road. This method does not require a large amount of equipment and labor, which allows it to be used in the construction of roads in difficult geological conditions. Soil injection is an environmentally safe method of strengthening soil foundations, as it does not require the usage of chemicals or other hazardous substances.

Solving the filtration problem [16, 17] in a porous medium is an integral part of achieving the efficiency of the injection process. Currently, many papers are devoted to the problems of monodisperse [18-20] and polydisperse [21-23] suspension filtration. Suspension filtration in a porous medium with several types of particles is the process of passing a liquid with particles through a porous medium in which particles of various sizes and shapes may be present.

In the case of several types of particles, different filtration processes may occur for each type of particle. For example, larger particles may linger in the pores of the medium, and smaller particles may pass through the pores. It may also be possible for one type of particle to block the pores, which prevents the passage of other types of particles.

To optimize the filtration process in a porous medium with several types of particles, various methods can be used, for example, changing the parameters of the porous medium (pore size, particle packing density), changing the speed of liquid passage through the porous medium, etc. A combination of different methods can also be used to achieve the best result.

The paper is devoted to the numerical solution of the problem of bed deep filtration with three-dispersed suspension. It is assumed that three types of particles, with different sizes move in a

porous medium with a constant velocity. Linear functions for each type of particles differing only by a multiplier are considered as filtration functions. The usage of linear filtration functions trains the size-exlusion capture mechanism [24], in which particles freely pass through pores with a larger diameter than the pore diameter itself and plug pores with a smaller diameter.

THE MATHEMATICAL MODEL

In the domain $\Psi = \begin{cases} 0 \le x \le 1 \\ t \ge 0 \end{cases}$ consider a hyperbolic system of first-order equations defining a mathematical model of filtration of a three-dispersed liquid:

$$\frac{\partial C_i(x,t)}{\partial t} + \frac{\partial C_i(x,t)}{\partial x} + \frac{\partial S_i(x,t)}{\partial t} = 0, \quad (1)$$

$$\frac{\partial S_i(x,t)}{\partial t} = \Lambda_i\left(S_1, S_2, S_3\right) C_i(x,t), \quad (2)$$

$$i = 1, 2, 3,$$

where $C_i(x,t)$ is the concentration of suspended particles of the *i*-th type, $S_i(x,t)$ is the concentration of retained particles of the *i*-th type, $\Lambda_i\left(S_1, S_2, S_3\right)$ is the filtration function of the *i*-th type particles.

The boundary conditions of the problem at $x = 0$ are

$$C_i(0,t) = C_i^0, \ i = 1,2,3, \quad (3)$$

at that $\sum_{i=1}^{3} C_i^0 = 1$.

The initial conditions at $t = 0$ are

$$C_i(x,0) = 0, S_i(x,0) = 0, \ i = 1,2,3. \quad (4)$$

As filtration functions, we will consider functions of the form

$$\Lambda_i = \lambda_i \left(1 - \sum_{i=1}^{3} \beta_i C_i^0 S_i(x,t)\right), \ i = 1, 2, 3, \quad (5)$$

where λ_i and β_i are some positive constants. Assume that $\lambda_1 > \lambda_2 > \lambda_3$, it means that the particles of the first type are the largest, and particles of the third type are the smallest

Let us denote the linear combination in (5) as

$$P = \sum_{i=1}^{3} \beta_i C_i^0 S_i(x,t),$$

it takes into account the different probabilities of deposit for different type particles.

The straight line divides the domain Ψ into two subdomaines Ψ^1 and Ψ^2. In the subdomain $\Psi^1 = \begin{cases} 0 \le x \le 1 \\ 0 \le t < x \end{cases}$, i.e. under the line $t = x$, the solutions $C_i(x,t)$ and $S_i(x,t)$ for every type of particles are zero. Below this line, i.e. in the subdomain $\Psi^2 = \begin{cases} 0 \le x \le 1 \\ t > x \end{cases}$ the solutions $C_i(x,t)$ and $S_i(x,t)$, $i = 1, 2, 3$ are positive. On the line $t = x$ the solutions $C_i(x,t), i = 1, 2, 3$ are positive and the solutions $S_i(x,t), i = 1, 2, 3$ are equal to zero. This line is called the concentration front. So, along the concentration front the solutions $C_i(x,t)$, $i = 1, 2, 3$ are discontinuous and the solutions $S_i(x,t)$, $i = 1, 2, 3$ are continuous.

The solution at x=0

Taking into account the conditions (3) we have the heterogeneous system of equations (2) in the form

$$\begin{cases} \dfrac{\partial S_1}{\partial t} = \lambda_1 \left(1 - P\right) C_1^0, \\ \dfrac{\partial S_2}{\partial t} = \lambda_2 \left(1 - P\right) C_2^0, \\ \dfrac{\partial S_3}{\partial t} = \lambda_3 \left(1 - P\right) C_3^0. \end{cases}$$

Let's solve the corresponding homogeneous system of equations

$$\begin{cases} \dfrac{\partial S_1}{\partial t} = \lambda_1 C_1^0 P, \\ \dfrac{\partial S_2}{\partial t} = \lambda_2 C_2^0 P, \\ \dfrac{\partial S_3}{\partial t} = \lambda_3 C_3^0 P. \end{cases}$$

Write down the characteristic polynomial of the system

$$\begin{vmatrix} \lambda_1\beta_1\left(C_1^0\right)^2 + k & \lambda_1\beta_2 C_1^0 C_2^0 & \lambda_1\beta_3 C_1^0 C_3^0 \\ \lambda_2\beta_1 C_1^0 C_2^0 & \lambda_2\beta_2\left(C_2^0\right)^2 + k & \lambda_2\beta_3 C_2^0 C_3^0 \\ \lambda_3\beta_1 C_1^0 C_3^0 & \lambda_3\beta_2 C_2^0 C_3^0 & \lambda_3\beta_3\left(C_3^0\right)^2 + k \end{vmatrix}$$

and construct the characteristic equation

$$k^3 + \lambda_1\beta_1\left(C_1^0\right)^2 k^2 + \lambda_2\beta_2\left(C_2^0\right)^2 k^2 + \\ + \lambda_3\beta_3\left(C_3^0\right)^2 k^2 = 0,$$

whose solutions are numbers

$$\begin{bmatrix} k_{1,2} = 0, \\ k_3 = -\lambda_1\beta_1\left(C_1^0\right)^2 - \lambda_2\beta_2\left(C_2^0\right)^2 - \lambda_3\beta_3\left(C_3^0\right)^2. \end{bmatrix}$$

Omitting the calculations, we obtain the solution of homogeneous system of equations

$$\begin{cases} S_1 = \alpha_1 \dfrac{\beta_2 C_2^0}{\beta_1 C_1^0} + \alpha_2 \dfrac{\beta_3 C_3^0}{\beta_1 C_1^0} + \alpha_3 \dfrac{\lambda_1 C_1^0}{\lambda_3 C_3^0} e^{-\sum_{j=1}^{3}\lambda_j\beta_j\left(C_j^0\right)^2 t}, \\ S_2 = -\alpha_1 + \alpha_3 \dfrac{\lambda_2 C_2^0}{\lambda_3 C_3^0} e^{-\sum_{j=1}^{3}\lambda_j\beta_j\left(C_j^0\right)^2 t}, \\ S_3 = -\alpha_2 + \alpha_3 e^{-\sum_{j=1}^{3}\lambda_j\beta_j\left(C_j^0\right)^2 t}, \end{cases}$$

where $\alpha_1, \alpha_2, \alpha_3$ are arbitrary constants.

After that we solve the original inhomogeneous system of equations by the method of variation of constants. Taking into account the initial conditions (4) we get the solutions

$$S_i^0 = S_i(0,t) = \frac{\lambda_i C_i^0 \left(1 - e^{-\sum_{j=1}^{3}\lambda_j\beta_j\left(C_j^0\right)^2 t}\right)}{\sum_{j=1}^{3}\lambda_j\beta_j\left(C_j^0\right)^2}, \quad (6)$$

$$i = 1, 2, 3.$$

The solution at the concentration front

Taking into account that $S_i(x,t) = 0$, $i = 1, 2, 3$ at $t = x$ the filtration functions (5) are $\Lambda_i = \lambda_i$, $i = 1, 2, 3$, so equations (2) can be rewritten in the form

$$\frac{\partial S_i(x,t)}{\partial t} = \lambda_i C_i(x,t).$$

Turn in equation (1) to the characteristic variables $\tau = t - x$, $x = x$:

$$\frac{\partial C_i(x,t)}{\partial x} + \lambda_i C_i(x,t) = 0, \; i = 1, 2, 3.$$

Solving the equations with separable variables we obtain the solutions

$$C_i^f = C_i^0 e^{-\lambda_i x}, \; i = 1, 2, 3. \quad (7)$$

ASYMPTOTIC SOLUTION NEAR THE CONCENTRATION FRONT

Let us obtain solutions near the concentration front in the form of expansions

$$\tilde{C}_i(x,t) = \tilde{C}_i^0(x) + \tilde{C}_i^1(x)(t-x), \quad (8)$$

$$\tilde{S}_i(x,t) = \tilde{S}_i^1(x)(t-x) + \frac{1}{2}\tilde{S}_i^2(x)(t-x)^2, \quad (9)$$

$$i = 1, 2, 3.$$

Note, that in expansion (8) there are no terms $\tilde{S}_i^0(x)$, because $S_i(x,t) = 0$ at $t = x$.

Let us calculate partial derivatives of functions (8) and (9)

$$\frac{\partial \tilde{C}_i(x,t)}{\partial x} = \tilde{C}_i^{0\prime}(x) + \tilde{C}_i^{1\prime}(x)(t-x) - \tilde{C}_i^{1}(x),$$

$$\frac{\partial \tilde{C}_i(x,t)}{\partial t} = \tilde{C}_i^{1\prime}(x),$$

$$\frac{\partial \tilde{S}_i(x,t)}{\partial t} = \tilde{S}_i^{1}(x) + \tilde{S}_i^{2}(x)(t-x), \quad i = 1,2,3.$$

Substitute these expressions into (1)-(2) and group the terms at the same degrees of $(t-x)$:

$$\begin{cases} \lambda_i \tilde{C}_i^0 + \tilde{C}_i^{0\prime} + (t-x)\left(\tilde{C}_i^{1\prime} + \lambda_i \tilde{C}_i^1 - \lambda_i \tilde{C}_i^0 \left(\beta_1 C_1^0 \tilde{S}_1^1 + \beta_2 C_2^0 \tilde{S}_2^1 + \beta_3 C_3^0 \tilde{S}_3^1\right)\right) + \ldots = 0, \\ -\lambda_i \tilde{C}_i^0 + \tilde{S}_i^1 + (t-x)\left(\tilde{S}_i^2 - \lambda_i \tilde{C}_i^1 + \lambda_i \tilde{C}_i^0 \left(\beta_1 C_1^0 \tilde{S}_1^1 + \beta_2 C_2^0 \tilde{S}_2^1 + \beta_3 C_3^0 \tilde{S}_3^1\right)\right) + \ldots = 0. \end{cases}$$

Taking into account that $\tilde{C}_i^0 = C_i^0$, $i = 1,2,3$, the solution of the system of equations

$$\begin{cases} \lambda_i \tilde{C}_i^0 + \tilde{C}_i^{0\prime} = 0, \\ -\lambda_i \tilde{C}_i^0 + \tilde{S}_i^1 = 0, \quad i = 1,2,3 \end{cases}$$

$$\begin{cases} \tilde{C}_i^0 = C_i^0 e^{-\lambda_i x}, \\ \tilde{S}_i^1 = \lambda_i C_i^0 e^{-\lambda_i x}, \quad i = 1,2,3. \end{cases}$$

Obviously, solution $\tilde{C}_i^0$ is equal to C_i^f, $i = 1, 2, 3$, obtained in (6).

Solving the system for lower terms is

$$\begin{cases} \tilde{C}_i^{1\prime} + \lambda_i \tilde{C}_i^1 - \lambda_i \tilde{C}_i^0 \left(\beta_1 C_1^0 \tilde{S}_1^1 + \beta_2 C_2^0 \tilde{S}_2^1 + \beta_3 C_3^0 \tilde{S}_3^1\right) = 0, \\ \tilde{S}_i^2 - \lambda_i \tilde{C}_i^1 + \lambda_i \tilde{C}_i^0 \left(\beta_1 C_1^0 \tilde{S}_1^1 + \beta_2 C_2^0 \tilde{S}_2^1 + \beta_3 C_3^0 \tilde{S}_3^1\right) = 0, \end{cases}$$

we obtain

$$\begin{cases} \tilde{C}_i^1 = \lambda_i \tilde{C}_i^0 e^{-\lambda_i x}\left(\beta_1 \left(C_1^0\right)^2 \left(1 - e^{-\lambda_1 x}\right) + \beta_2 \left(C_2^0\right)^2 \left(1 - e^{-\lambda_2 x}\right) + \beta_3 \left(C_3^0\right)^2 \left(1 - e^{-\lambda_3 x}\right)\right), \\ \tilde{S}_i^2 = \lambda_i \tilde{C}_i^0 e^{-\lambda_i x}\left(\beta_1 \left(C_1^0\right)^2 \left(\lambda_i - (\lambda_i + \lambda_1) e^{-\lambda_1 x}\right) + \beta_2 \left(C_2^0\right)^2 \left(\lambda_i - (\lambda_i + \lambda_2) e^{-\lambda_2 x}\right) + \beta_3 \left(C_3^0\right)^2 \left(\lambda_i - (\lambda_i + \lambda_3) e^{-\lambda_3 x}\right)\right), \end{cases}$$
$$i = 1,2,3.$$

So, the asympotic solutions are

$$\tilde{C}_i(x,t) = C_i^0 e^{-\lambda_i x} + \lambda_i \tilde{C}_i^0 e^{-\lambda_i x}\left(\beta_1 \left(C_1^0\right)^2 \left(1 - e^{-\lambda_1 x}\right) + \beta_2 \left(C_2^0\right)^2 \left(1 - e^{-\lambda_2 x}\right) + \beta_3 \left(C_3^0\right)^2 \left(1 - e^{-\lambda_3 x}\right)\right)(t-x), \tag{10}$$

$$\tilde{S}_i(x,t) = \lambda_i C_i^0 e^{-\lambda_i x}(t-x) + \frac{1}{2}\lambda_i \tilde{C}_i^0 e^{-\lambda_i x}\left(\beta_1 \left(C_1^0\right)^2 \left(\lambda_i - (\lambda_i + \lambda_1) e^{-\lambda_1 x}\right) + \beta_2 \left(C_2^0\right)^2 \left(\lambda_i - (\lambda_i + \lambda_2) e^{-\lambda_2 x}\right) + \beta_3 \left(C_3^0\right)^2 \left(\lambda_i - (\lambda_i + \lambda_3) e^{-\lambda_3 x}\right)\right)(t-x)^2, \tag{11}$$

$$i = 1,2,3.$$

THE SOLUTION AT $t\to\infty$

Let us obtain the solution at $t\to\infty$ with usage of travelling wave. Consider $C_i = C_i(\theta)$ and $S_i = S_i(\theta)$, $i=1,2,3$, where $\theta = x - \nu t$ with unknown wave velocity ν. In this case the system (1)-(2) takes the form

$$(\nu-1)\frac{\partial C_i(\theta)}{\partial\theta} + \nu\frac{\partial S_i(\theta)}{\partial\theta} = 0, \qquad (12)$$

$$\nu\frac{\partial S_i(\theta)}{\partial\theta} = -\lambda_i(1-P)C_i(\theta), \qquad (13)$$

$$i = 1, 2, 3$$

with infinity boundary conditions

$$C_i(+\infty) = 0,\ S_i(+\infty) = 0, \qquad (14)$$

$$C_i(-\infty) = C_i^0. \qquad (15)$$

$$i = 1,2,3,$$

where C_i^0, $i=1,2,3$ are determined with conditions (3).
Substituting (13) into (12)

$$(\nu-1)\frac{\partial C_i(\theta)}{\partial\theta} - \lambda_i(1-P)C_i(\theta) = 0, \qquad (16)$$

$$i = 1,2,3,$$

we obtain

$$(1-P) = \frac{\nu-1}{\lambda_i C_i(\theta)}\frac{\partial C_i(\theta)}{\partial\theta},\ i=1,2,3. \qquad (17)$$

Using the expressions (17) we can construct the system of equations

$$\begin{cases} \dfrac{1}{\lambda_1 C_1(\theta)}\dfrac{\partial C_1(\theta)}{\partial\theta} = \dfrac{1}{\lambda_2 C_2(\theta)}\dfrac{\partial C_2(\theta)}{\partial\theta}, \\ \dfrac{1}{\lambda_1 C_1(\theta)}\dfrac{\partial C_1(\theta)}{\partial\theta} = \dfrac{1}{\lambda_3 C_3(\theta)}\dfrac{\partial C_3(\theta)}{\partial\theta}, \end{cases}$$

integrating it with conditions (15) we obtain

$$\begin{cases} C_2(\theta) = C_2^0\left(\dfrac{C_1(\theta)}{C_1^0}\right)^{\frac{\lambda_2}{\lambda_1}}, \\ C_3(\theta) = C_3^0\left(\dfrac{C_1(\theta)}{C_1^0}\right)^{\frac{\lambda_3}{\lambda_1}}. \end{cases} \qquad (18)$$

Let us itegrate the equation (12) over variable θ

$$(\nu-1)C_i(\theta) + \nu S_i(\theta) = 0,\ i=1,2,3$$

and express

$$S_i(\theta) = -\frac{\nu-1}{\nu}C_i(\theta),\ i=1,2,3. \qquad (19)$$

Substite expressions (18) and (19) into (12) for the first type of particles we obtain the equation

$$\frac{\partial C_1(\theta)}{\partial\theta} - \lambda_1\left(\frac{1}{\nu-1} + \frac{1}{\nu}\left(\beta_1 C_1^0 C_1(\theta) + \beta_2\left(C_2^0\right)^2\left(\frac{C_1(\theta)}{C_1^0}\right)^{\frac{\lambda_2}{\lambda_1}} + \beta_3\left(C_3^0\right)^2\left(\frac{C_1(\theta)}{C_1^0}\right)^{\frac{\lambda_3}{\lambda_1}}\right)\right)C_1(\theta) = 0 \qquad (20)$$

with initial condition $C_1(0) = \hat{C}_1$, where $0 < \hat{C}_1 < C_1^0$.
Integrating separable differential equation (20), we obtain

$$\int_{\hat{C}_1}^{C_1}\frac{dC_1}{C_1\left(\frac{1}{\nu-1} + \frac{1}{\nu}\left(\beta_1 C_1^0 C_1(\theta) + \beta_2\left(C_2^0\right)^2\left(\frac{C_1(\theta)}{C_1^0}\right)^{\frac{\lambda_2}{\lambda_1}} + \beta_3\left(C_3^0\right)^2\left(\frac{C_1(\theta)}{C_1^0}\right)^{\frac{\lambda_3}{\lambda_1}}\right)\right)} = \lambda_1\theta. \qquad (21)$$

Taking into account the equality (15) we obtain the formula for velocity ν from (21)

$$\nu = \frac{\beta_1 (C_1^0)^2 + \beta_2 (C_2^0)^2 + \beta_3 (C_3^0)^2}{1 + \beta_1 (C_1^0)^2 + \beta_2 (C_2^0)^2 + \beta_3 (C_3^0)^2}. \tag{22}$$

NUMERICAL SOLUTION

Since the problem (1)-(4) has no analytical solution, we will solve it numerically using explicit difference schemes. To approximate first-order derivatives, we use the values $h_t = h_x = 0.01$ as steps along the coordinate axes, in this case the Courant condition is fulfilled [25]. Let us set the coefficients of the filtration functions Λ_i, $i = 1, 2, 3$: $\lambda_1 = 10$, $\lambda_2 = 5$, $\lambda_3 = 2.5$. We solve the problem for three different sets of parameters C_i^0 and β_i^0, $i = 1, 2, 3$, presented in Table 1.

Table 1

№	C_1^0	C_2^0	C_3^0	β_1	β_2	β_3
1	0.3	0.2	0.5	4	6	12
2	0.3	0.5	0.2	4	6	8
3	0.4	0.5	0.1	8	5	7

The graphs of retained particle concentrations $S_1(x)$ (the black line), $S_2(x)$ (the red line), $S_3(x)$ (the blue line) and the total deposit concentration $S(x)$ (the green line) are shown in Fig. 1 at different times for the first parameter combination from the Table 1. The figure shows that the concentrations $S_1(x)$, $S_2(x)$ and $S(x)$ decrease on the total segment $x \in [0;1]$. The solution $S_3(x)$ decreases monotonically until about time $t \approx 0.2$, then the graph behaves non-monotonically: it first increases, reaching its maximum value, and then begins to decrease. Beginning at a point in time $t \approx 1.3$ the solution $S_3(x)$ is an increasing function for all $x \in [0;1]$. The movement of the maximum point of $S_3(x)$ is shown in Fig. 2.

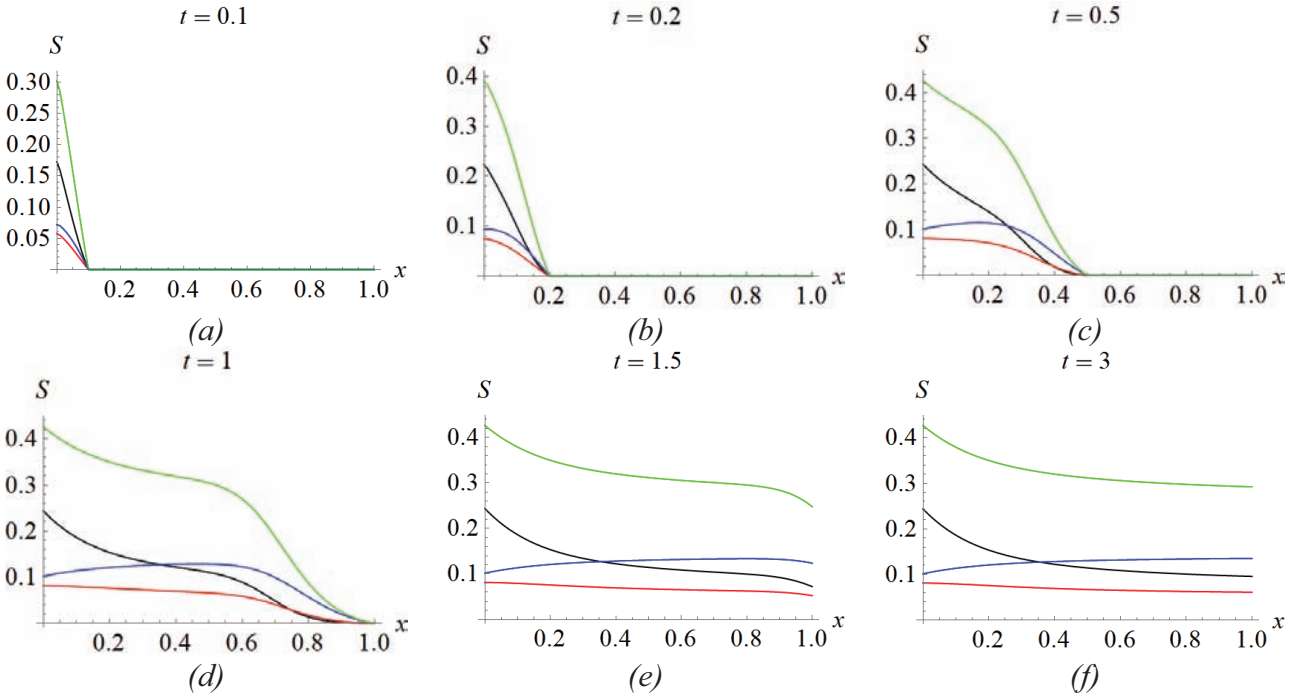


Figure 1. The solutions of retained particles concentrations for three types of particles and total deposit at different times (set 1)

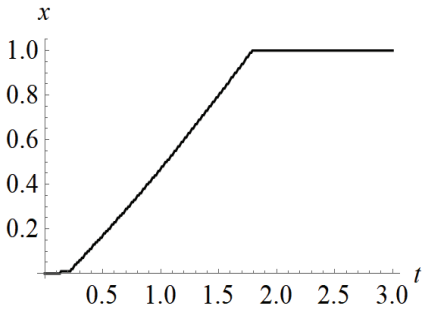


Figure 2. Movement of the maximum point of the concentration $S_3(x)$

The plots of $S_1(x)$ (the black line), $S_2(x)$ (the red line), $S_3(x)$ (the blue line) and $S(x)$ (the green line) for the second parameter combination from the Table 1 are shown in Fig. 3. The solutions $S_1(x)$ and $S(x)$ are monotonously decreasing functions for any time values. $S_2(x)$ is a monotonously decreasing curve until $t \approx 0.23$, after that it is non-monotonic. $S_3(x)$ always decreases until $t \approx 0.15$, after that it has the maximum point. In Fig. 4 the graphs of moving the maximum of the concentrations $S_2(x,t)$ (Fig. 4a) and $S_3(x,t)$ (Fig. 4b) are presented. From Fig. 3 it can be seen that starting from the moment of time $t \approx 0.2$ the solutions $S_2(x,t)$ (Fig. 4(a)) and $S_3(x,t)$ (Fig. 4(b)) have the maximum point which moves along the axis x until it reaches the filter outlet.

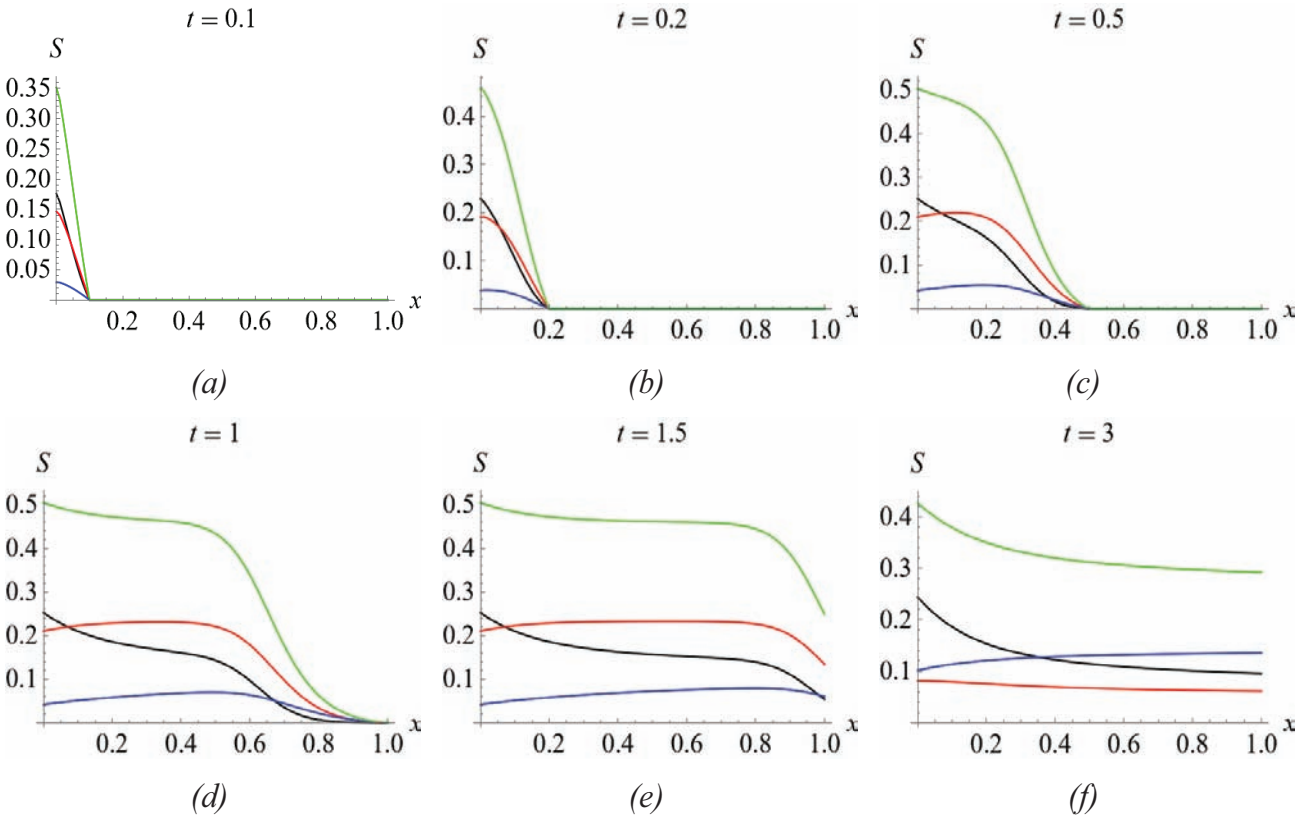


Figure 3. The solutions of retained particles concentrations for three types of particles and total deposit at different times (set 2)

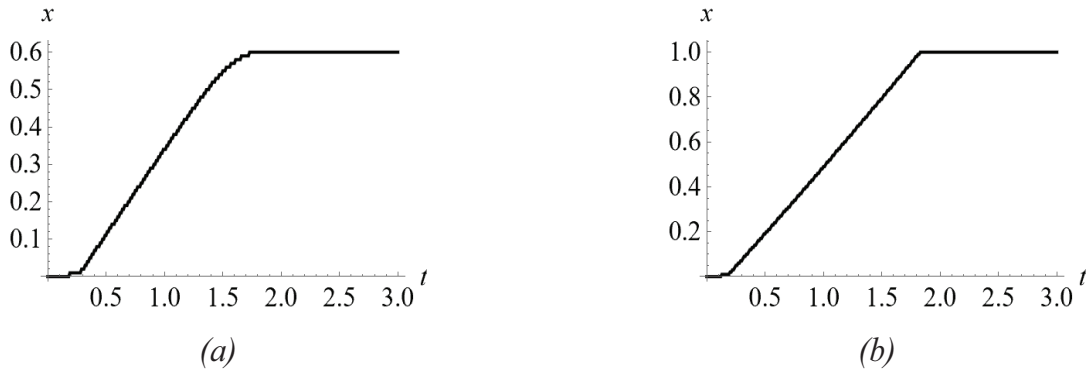


Figure 4. Movement of the maximum point of the concentrations $S_2(x)$ and $S_3(x)$

In Fig. 5 the graphs of functions $S_1(x)$ (the black line), $S_2(x)$ (the red line), $S_3(x)$ (the blue line) and $S(x)$ (the green line) for the third case from Table 1 are shown. The solution $S_1(x)$ always monotonously decreases. There is a decrease in functions $S_2(x)$, $S_3(x)$ and the total deposit $S(x)$: $S_2(x)$ and $S_3(x)$ decrease until $t \approx 0.1$, $S(x)$ decreases until $t \approx 0.15$. After that each function becomes non-monotonic: every maximum point moves from inlet to outlet of filter with increasing time. The graphs of movement of the maximum point of $S_2(x,t)$ (Fig. 6(a)), $S_3(x,t)$ (Fig. 6(b)) and $S_3(x,t)$ (Fig. 6(c)) are presented in Fig. 6.

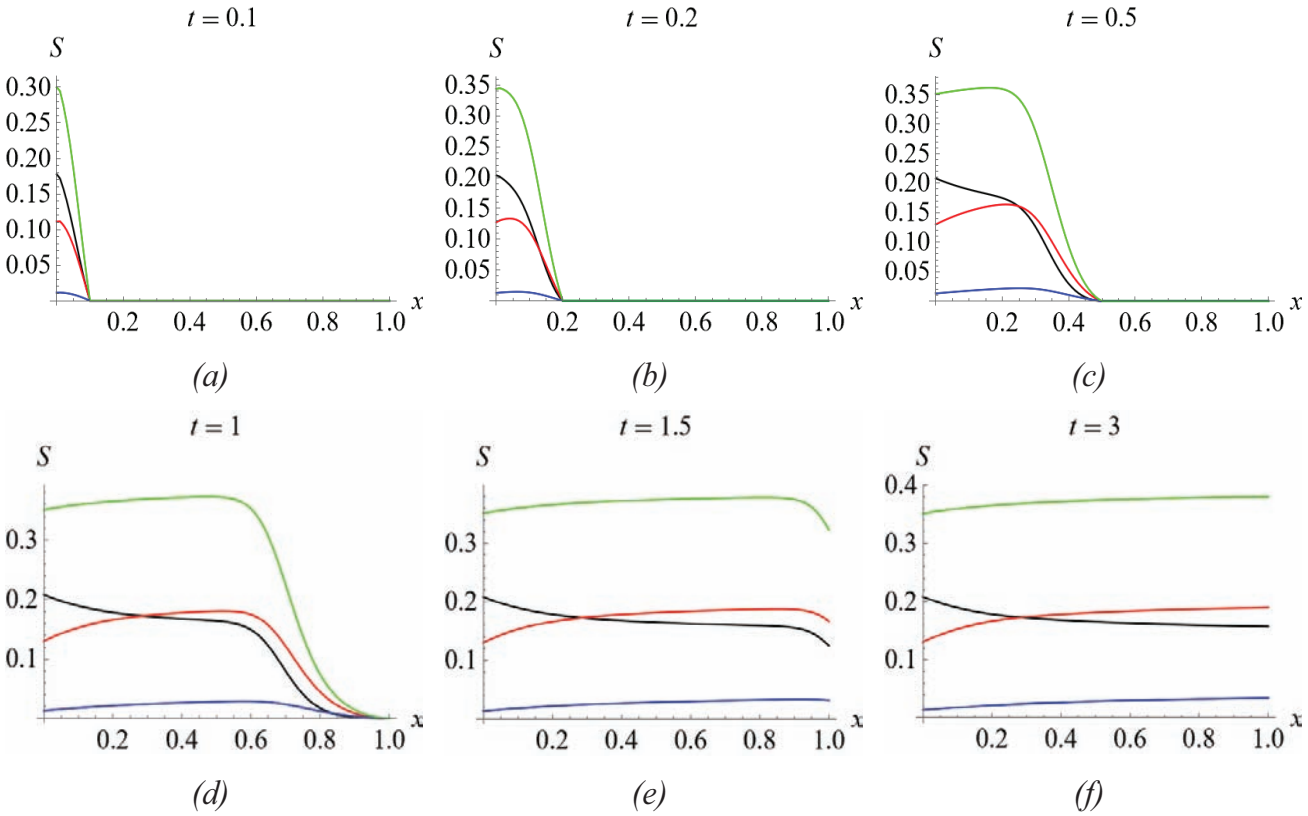


Figure 5. Solutions of retained particles concentrations for three types of particles and total deposit at different times (set 3)

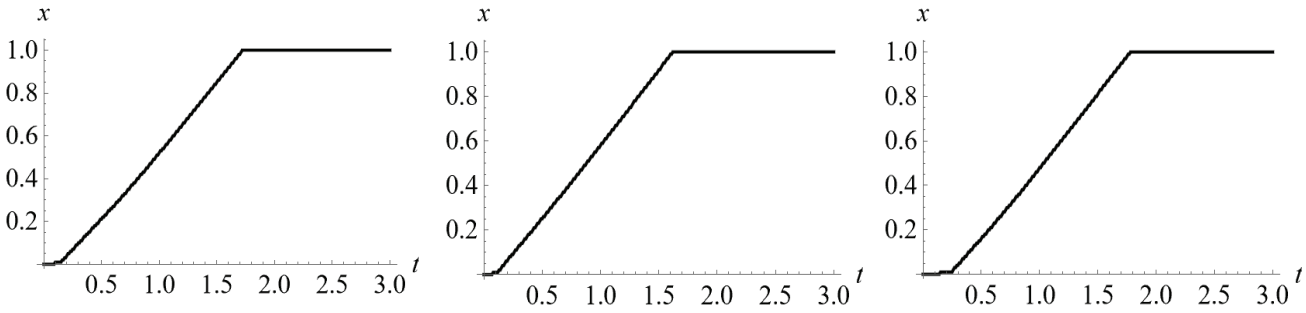


Figure 6. Movement of the maximum point of the concentrations $S_2(x)$, $S_3(x)$ and $S(x)$

The graphs of concentrations $S_1(t)$ (Fig. 7(a)), $S_2(t)$ (Fig. 7(b)) and $S_3(t)$ (Fig. 7(c)) and their asymptotic solutions $\tilde{S}_1(t)$, $\tilde{S}_2(t)$ and $\tilde{S}_3(t)$, obtained by formulas (11), at $x = 0.5$ are shown in Fig. 7. The black curves correspond to the numerical solutions and the red lines correspond to the asymptotic ones. Fig. 8 shows similar graphs at the filter outlet at $x = 1$. The following parameters are choosen: $\lambda_1 = 0.5$, $\lambda_2 = 0.25$, $\lambda_3 = 0.125$, $C_1^0 = 0.2$, $C_2^0 = 0.3$, $C_2^0 = 0.5$, $\beta_1 = 2$, $\beta_2 = 4$, $\beta_3 = 5$. It can be seen from the graphs that the concentration of suspended particles of the first type has the best approximation, while for all three types of suspended particles, the closer to the filter output, the closer the asymptotic solution is to the numerical one. The graphs of relative errors of suspended particles concentration asymptotics $\tilde{S}_1(t)$, $\tilde{S}_2(t)$ and $\tilde{S}_3(t)$ are shown in Fig. 9. The black line corresponds to $x = 0.5$ and the red line corresponds to $x = 1$. With increasing, i.e. with distance from the concentration front, the relative errors of the asymptotics for each type of particles increase. At the same time, it can be seen that the relative errors at $x = 0.5$ are much greater than at $x = 1$. Both at $x = 0.5$ and $x = 1$, the asymptotic $\tilde{S}_1(t)$ has the smallest error and $\tilde{S}_3(t)$ has the largest one. The maximum values of the relative errors are presented in Table 2.

Table 2

	$\tilde{S}_1(t)$	$\tilde{S}_2(t)$	$\tilde{S}_3(t)$
$x = 0.5$	10 %	19 %	23 %
$x = 1$	5 %	4 %	9 %

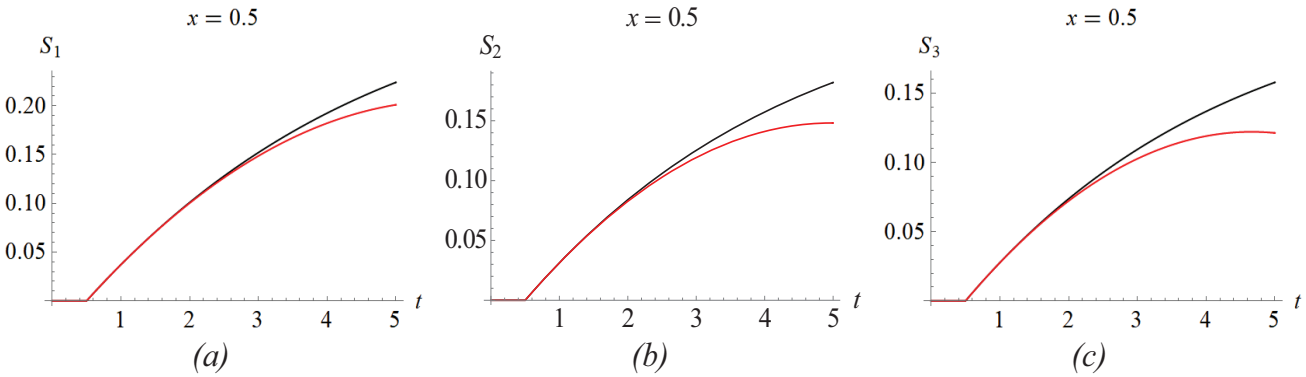
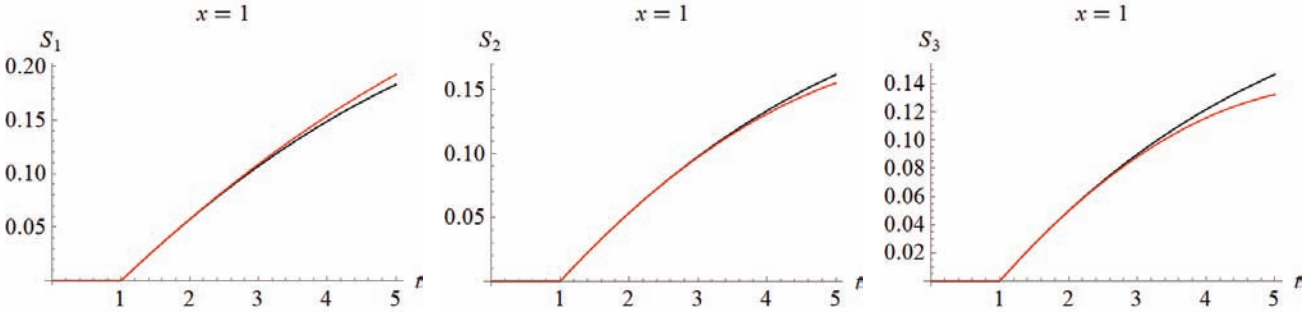
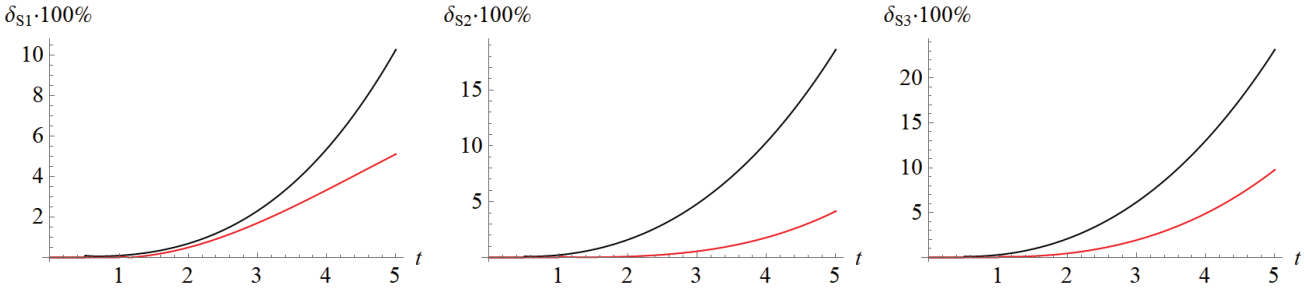


Figure 7. Numerical and asymptotic solutions for three types of retained particles at $x = 0.5$



(a) (b) (c)

Figure 8. Numerical and asymptotic solutions for three types of retained particles at $x = 1$



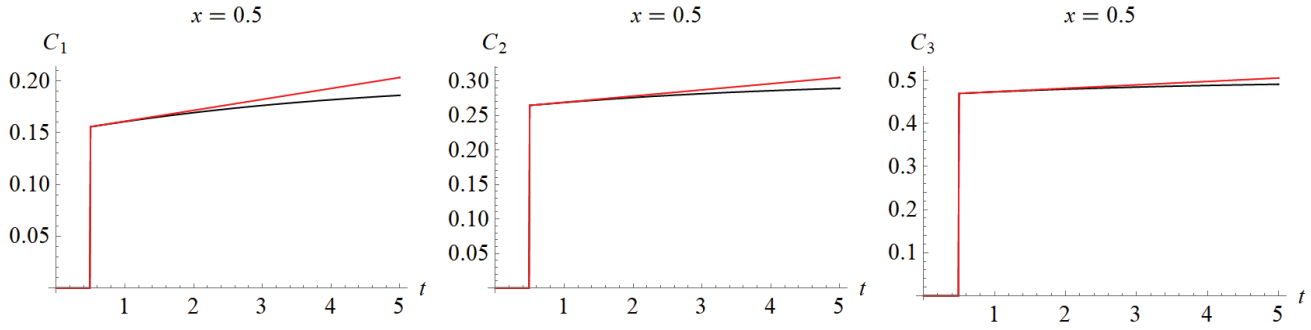
(a) (b) (c)

Figure 9. Relative errors of asymptotics for three types of retained particles for $x = 0.5$ *and* $x = 1$

The graphs of the numerical solutions $C_1(t)$ (Fig. 10(a)), $C_2(t)$ (Fig. 10(b)), $C_3(t)$ (Fig. 10(c)) and their asymptotics $\tilde{C}_1(t)$, $\tilde{C}_2(t)$ and $\tilde{C}_3(t)$, obtained by formulas (10) at $x = 0.5$, are presented in Fig. 10. Numerical solutions are shown with black lines, the asymptotic solutions are shown with red lines. Similar graphs at the filter inlet are shown in Fig. 11. In contrast to the asymptotics of retained particles concentrations, the deviations of asymptotics of suspended particles concentrations do not depend on x, they remain the same at $x = 0.5$ and $x = 1$. The asymptotics of the concentration of the third type of particles approximates the numerical solution in the best way. Fig. 12 shows plots of relative errors of asymptotics for three types of suspended particles at $x = 0.5$ and $x = 1$. The black lines correspond to the case of $x = 0.5$, the red ones correspond to $x = 1$. Analysis of these dependencies shows that the behavior of the relative errors of the asymptotics $\tilde{C}_2(t)$ and $\tilde{C}_3(t)$ are very similar: at first, the relative errors calculated for $x = 0.5$ and $x = 1$, practically coincide, and after reaching a certain point in time ($t \approx 3$ for $\tilde{C}_2(t)$ and $t \approx 2.6$ for $\tilde{C}_3(t)$), the relative error at the filter outlet begins to increase faster than at $x = 0.5$. The relative deviations of the asymptotics $\tilde{C}_1(t)$ at $x = 0.5$ and $x = 1$ by the time $t \approx 2.6$ maximum deviate from each other, then begin to converge again so that by the time $t \approx 9$ they reach the same value. Every function in this case is monotonically increasing. The values of the largest relative errors of asymptotics of suspended particles concentrations are presented in Table 3.

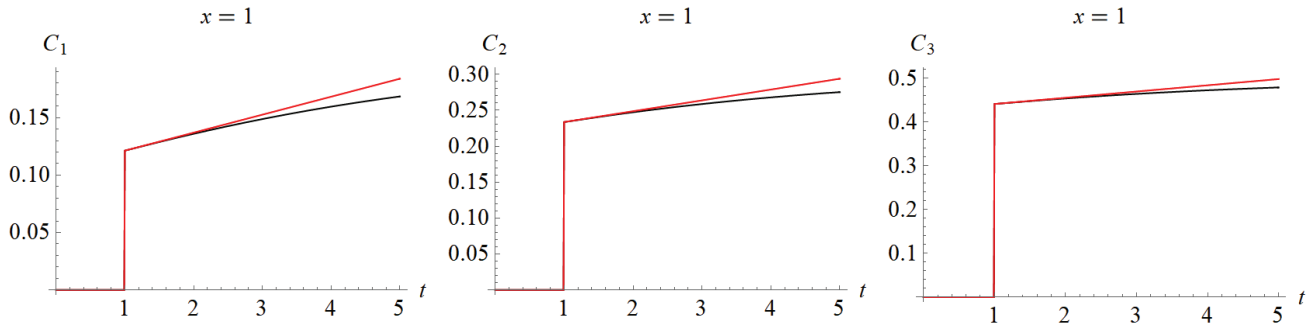
Table 3

	$\tilde{C}_1(t)$	$\tilde{C}_2(t)$	$\tilde{C}_3(t)$
$x = 0.5$	10 %	19 %	23 %
$x = 1$	5 %	4 %	9 %



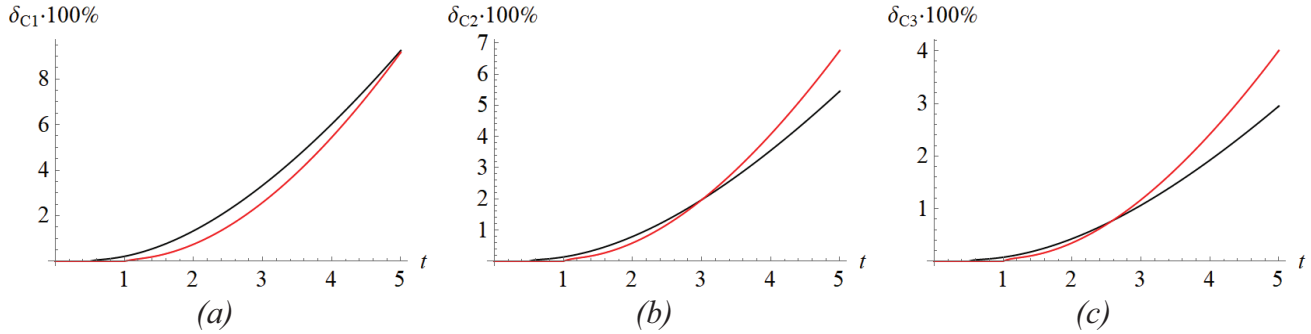
(a) (b) (c)

Figure 10. Numerical and asymptotic solutions for three types of suspended particles at $x = 0.5$



(a) (b) (c)

Figure 11. Numerical and asymptotic solutions for three types of suspended particles at $x = 1$



(a) (b) (c)

Figure 12. Relative errors of asymptotics for three types of suspended particles for $x = 0.5$ *and* $x = 1$

Fig. 13 shows the graphs of travelling waves, that determine the concentrations of suspended particles at $t \to \infty$, obtained using formulas (21) and (18). The values of parameters are: $\lambda_1 = 0.5$, $\lambda_2 = 0.25$, $\lambda_3 = 0.125$, $C_1^0 = 0.4$, $C_2^0 = 0.5$, $C_2^0 = 0.1$, $\beta_1 = 8$, $\beta_2 = 5$, $\beta_3 = 7$. The black curves correspond to the value of $\hat{C}_1 = 0.4$, the red curves correspond to $\hat{C}_1 = 0.3$. Fig. 14 shows similar graphs of retained particles concentrations obtained with equations (19).

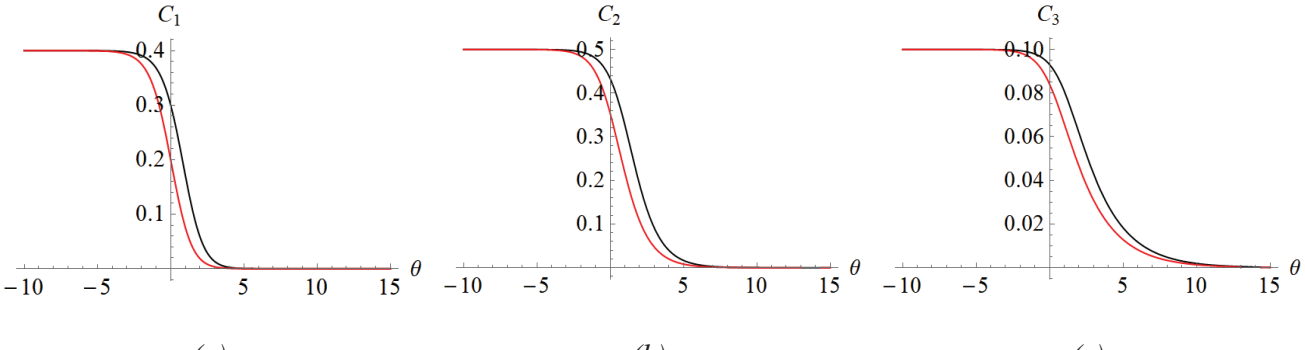


Figure 13. Solutions for three types of suspended particles at $t \to \infty$ with usage of travelling wave

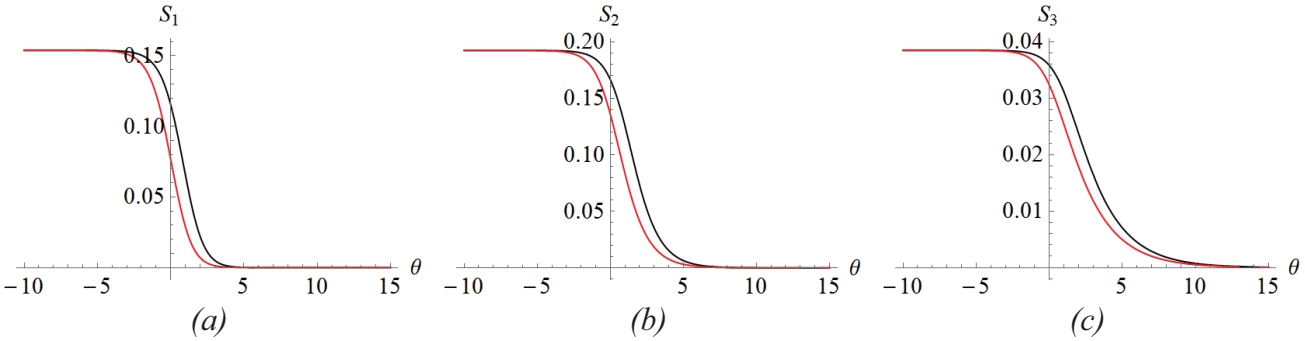


Figure 14. Solutions for three types of retained particles at $t \to \infty$ with usage of travelling wave

CONCLUSION

The problem with 3 types of particles is considered for the first time.

The asymptotics of the solutions near the concentration front are constructed.

The concentrations of partial deposits and total deposit are investigated. Similarly [22], the concentration of large retained particles always decreases monotonically, the concentration of small retained particles is non-monotonic. The concentration of total deposit remains monotonic or non-monotonic depending on the problem parameters. The concentration of medium retained particles can also be monotonic or non-monotonic.

Nonmonotonic particles concentrations have a maximum point. The movements of the maximum points in dependence of time were investigated. It was found that for the chosen parameters the points of maximum of the concentration of total deposit and deposit of small particles grow indefinitely with increasing time, while the point of maximum of the medium retained particles concentration is limited.

The travelling waves, determining the concentrations of retained and suspended particles at $t \to \infty$, are obtained.

REFERENCES

1. **Belev G., Ivanova-Radovanova P., Ivanov V., Chervenkcov H.** Climate change implications on the condition of the road surface in Bulgaria // Lecture Notes in Networks and Systems, 2023, vol. 638, pp. 100-109. DOI: 10.1007/978-3-031-26754-3_9
2. **Levkovich T.I., Mevlidinov Z.A., Rodin P.V., Feshchenko M.A.** Study of crack resistance of asphalt concrete pavements of the streets of the city of Bryansk and roads of the Bryansk region // Russian journal of transport engineering, 2018, vol. 5, No. 3, 01SATS318. DOI: 10.15862/01SATS318

3. **Lysbakken K.R., Norem H.** Processes that control development of quantity of salt on road surfaces after salt application // Transportation Research Record Journal of the Transportation Research Board vol. 2258(-1), pp. 139-146. DOI: 10.3141/2258-17
4. **Novik A., Drozdetskiy I., Petukhov P., Labusov N., Novik V., Popova A.** Justification constructions of the road pavement under conditions of changing road surface temperature // Lecture Notes in Civil Engineering, 2021, vol. 150, pp. 161-172. DOI: 10.1007/978-3-030-72404-7_17
5. **Tolmachov S.** Research of the reasons of Frost destruction of road concrete // Key Engineering Materials, 2020, vol. 864, pp. 175-179. DOI: 10.4028/www.scientific.net/KEM.864.175
6. **Ana Patricia Pérez-Fortes.** Aggregates Properties for Safety Road Surfaces // Advances in Engineering Research, 2020, vol. 40, ch. 4, Nova Science Publishers.
7. **Kosukhin M.M., Kosukhin A.M.** The Modified Composite Binder For Cement-Concrete Road Surfaces // IOP Conference Series: Materials Science and Engineering, 2018, vol. 463, 042036. DOI 10.1088/1757-899X/463/4/042036
8. **Buzikov S., Motovilova M.** Development of a method for improving the quality of the road surface with the addition of asphalt granulate // The Eurasian Scientific Journal, 2022, vol. 14, No. 4, 21SAVN422. DOI: 10.15862/21SAVN422
9. **Levkovich T.I., Mevlidinov Z.A., Tuljankina N.A., Vishtalenko M.V.** The study of strength of sandy soils reinforced with cement with the addition of «DorZem Ds-1», for use in the construction of foundations of roads // Russian Journal of Transport Engineering, 2019, vol 6, No. 2, 09SATS219. DOI: 10.15862/09SATS219
10. **Hongguanga M., Jing W.** Analysis of key points of road and bridge foundation construction technology // IOP Conference Series: Earth and Environmental Science, 2021, vol. 638, 012046. DOI: 10.1088/1755-1315/638/1/012046
11. **Gnaedinger G.P.** Soil Stabilization by Injection Techniques // Industrial and Engineering Chemistry, 1955, vol. 47 (11), pp. 2249-2253. DOI: 10.1021/ie50551a022
12. **Argal E.S.** Modern technologies and problems of ground stabilization by injection // Soil Mechanics and foundation Engineering, 2020, vol. 57 (3), pp. 219-226. DOI: 10.1007/s11204-020-09658-z
13. **Korolev V.M., Smirnov O.E., Argal E.S., V. A. Ashikhmen** Experience with microcement stabilization of soils // Soil Mechanics and Foundation Engineering, 2006, vol. 43, pp. 125-130.
14. **Sabri M., Shashkin K., Zakharin E., Ulybin A.** Soil stabilization and foundation restoration using an expandable polyurethane resin // Magazine of Civil Engineering, 2018, vol. 82, No. 6, pp. 68-80. DOI: 10.18720/MCE.82.7
15. **Zhifeng T., Tang X., Li J., Xiu Z., Xue Z.** Influence of the grouting parameters on microbially induced carbonate precipitation for soil stabilization // Geomicrobiology Journal, 2021, vol. 38, No. 9, pp. 755-767. DOI: 10.1080/01490451.2021.1946623
16. **Herzig J.P., Leclerc D.M., Golf P.L.** Flow of suspensions through porous media – application to deep filtration // Industrial & Engineering Chemistry (American Chemical Society), 1970, vol. 62, is. 5, pp 8-35.
17. **Kanaoka C.** Permeation (flow through porous media) // Powder Technology Handbook, 2004, CRC Press.
18. **Safina G.** Filtration problem with nonlinear filtration and concentration

functions // International Journal for Computational Civil and Structural Engineering, 2022, vol. 18, no. 1, 129-140. DOI:10.22337/2587-9618-2022-18-1-129-140

19. **Kuzmina L.I., Osipov Yu.V., Galaguz Yu.P.** Numerical and asymptotic modeling of a filtration problem with the initial deposit // International Journal for Computational Civil and Structural Engineering, 2017, vol. 13, no. 3, pp. 70-76. DOI: 10.22337/1524-5845-2017-13-3-70-76
20. **Safina G.L.** Calculation of retention profiles in porous medium // Lecture Notes in Civil Engineering, 2021, vol. 170, pp. 21-28.
21. **Kuzmina L.I., Osipov Y.V., Astachov M.D.** Analysis of the filtration problem by bitwise search method // International Journal for Computational Civil and Structural Engineering, 2022, vol. 18, no. 3, 86-94. DOI: 10.22337/2587-9618-2022-18-3-86-94
22. **Kuzmina L.I., Osipov Y.V., Astachov M.D.** Bidisperse fltration problem with non-monotonic retention profles // Annali di Matematica Pura ed Applicata (1923 -), 2022, vol. 201, pp. 2943–2964. DOI: 10.1007/s10231-022-01227-5
23. **Kuzmina L.I., Osipov Y.V., Gorbunova T.N.** Asymptotics for filtration of polydisperse suspension with small impurities // Applied Mathematics and Mechanics, 2021, vol. 42 (1), pp. 109-126. DOI: 10.1007/s10483-021-2690-6
24. **Fallah H., Fallah A., Rahmani A., Afkhami M., Ahmadi A.** Size exclusion mechanism, suspension flow through porous medium // International Journal of Modern Nonlinear Theory and Application, 2012, vol. 1, pp. 113-117.
25. **You Z., Osipov Y., Bedrikovetsky P., Kuzmina L**. Asymptotic model for deep bed filtration // Chemical Engineering Journal, 2014, vol. 258, pp. 374-385.

СПИСОК ЛИТЕРАТУРЫ

1. **Belev G., Ivanova-Radovanova P., Ivanov V., Chervenkcov H.** Climate change implications on the condition of the road surface in Bulgaria // Lecture Notes in Networks and Systems, 2023, vol. 638, pp. 100-109. DOI: 10.1007/978-3-031-26754-3_9
2. **Levkovich T.I., Mevlidinov Z.A., Rodin P.V., Feshchenko M.A.** Study of crack resistance of asphalt concrete pavements of the streets of the city of Bryansk and roads of the Bryansk region // Russian journal of transport engineering, 2018, vol. 5, No. 3, 01SATS318. DOI: 10.15862/01SATS318
3. **Lysbakken K.R., Norem H.** Processes that control development of quantity of salt on road surfaces after salt application // Transportation Research Record Journal of the Transportation Research Board vol. 2258(-1), pp. 139-146. DOI: 10.3141/2258-17
4. **Novik A., Drozdetskiy I., Petukhov P., Labusov N., Novik V., Popova A.** Justification constructions of the road pavement under conditions of changing road surface temperature // Lecture Notes in Civil Engineering, 2021, vol. 150, pp. 161-172. DOI: 10.1007/978-3-030-72404-7_17
5. **Tolmachov S.** Research of the reasons of Frost destruction of road concrete // Key Engineering Materials, 2020, vol. 864, pp. 175-179. DOI: 10.4028/www.scientific.net/KEM.864.175
6. **Ana Patricia Pérez-Fortes.** Aggregates Properties for Safety Road Surfaces // Advances in Engineering Research, 2020, vol. 40, ch. 4, Nova Science Publishers.
7. **Kosukhin M.M., Kosukhin A.M.** The Modified Composite Binder For Cement-Concrete Road Surfaces // IOP Conference Series: Materials Science and

Engineering, 2018, vol. 463, 042036. DOI 10.1088/1757-899X/463/4/042036
8. **Buzikov S., Motovilova M.** Development of a method for improving the quality of the road surface with the addition of asphalt granulate // The Eurasian Scientific Journal, 2022, vol. 14, No. 4, 21SAVN422. DOI: 10.15862/21SAVN422
9. **Levkovich T.I., Mevlidinov Z.A., Tuljankina N.A., Vishtalenko M.V.** The study of strength of sandy soils reinforced with cement with the addition of «DorZem Ds-1», for use in the construction of foundations of roads // Russian Journal of Transport Engineering, 2019, vol 6, No. 2, 09SATS219. DOI: 10.15862/09SATS219
10. **Hongguanga M., Jing W.** Analysis of key points of road and bridge foundation construction technology // IOP Conference Series: Earth and Environmental Science, 2021, vol. 638, 012046. DOI: 10.1088/1755-1315/638/1/012046
11. **Gnaedinger G.P.** Soil Stabilization by Injection Techniques // Industrial and Engineering Chemistry, 1955, vol. 47 (11), pp. 2249-2253. DOI: 10.1021/ie50551a022
12. **Argal E.S.** Modern technologies and problems of ground stabilization by injection // Soil Mechanics and foundation Engineering, 2020, vol. 57 (3), pp. 219-226. DOI: 10.1007/s11204-020-09658-z
13. **Korolev V.M., Smirnov O.E., Argal E.S., V. A. Ashikhmen** Experience with microcement stabilization of soils // Soil Mechanics and Foundation Engineering, 2006, vol. 43, pp. 125-130.
14. **Sabri M., Shashkin K., Zakharin E., Ulybin A.** Soil stabilization and foundation restoration using an expandable polyurethane resin // Magazine of Civil Engineering, 2018, vol. 82, No. 6, pp. 68-80. DOI: 10.18720/MCE.82.7
15. **Zhifeng T., Tang X., Li J., Xiu Z., Xue Z.** Influence of the grouting parameters on microbially induced carbonate precipitation for soil stabilization // Geomicrobiology Journal, 2021, vol. 38, No. 9, pp. 755-767. DOI: 10.1080/01490451.2021.1946623
16. **Herzig J.P., Leclerc D.M., Golf P.L.** Flow of suspensions through porous media – application to deep filtration // Industrial & Engineering Chemistry (American Chemical Society), 1970, vol. 62, is. 5, pp 8-35.
17. **Kanaoka C.** Permeation (flow through porous media) // Powder Technology Handbook, 2004, CRC Press.
18. **Safina G.** Filtration problem with nonlinear filtration and concentration functions // International Journal for Computational Civil and Structural Engineering, 2022, vol. 18, no. 1, 129-140. DOI:10.22337/2587-9618-2022-18-1-129-140
19. **Kuzmina L.I., Osipov Yu.V., Galaguz Yu.P.** Numerical and asymptotic modeling of a filtration problem with the initial deposit // International Journal for Computational Civil and Structural Engineering, 2017, vol. 13, no. 3, pp. 70-76. DOI: 10.22337/1524-5845-2017-13-3-70-76
20. **Safina G.L.** Calculation of retention profiles in porous medium // Lecture Notes in Civil Engineering, 2021, vol. 170, pp. 21-28.
21. **Kuzmina L.I., Osipov Y.V., Astachov M.D.** Analysis of the filtration problem by bitwise search method // International Journal for Computational Civil and Structural Engineering, 2022, vol. 18, no. 3, 86-94. DOI: 10.22337/2587-9618-2022-18-3-86-94
22. **Kuzmina L.I., Osipov Y.V., Astachov M.D.** Bidisperse fltration problem with non-monotonic retention profles // Annali di Matematica Pura ed Applicata (1923 -), 2022, vol. 201, pp.

2943–2964. DOI: 10.1007/s10231-022-01227-5

23. **Kuzmina L.I., Osipov Y.V., Gorbunova T.N.** Asymptotics for filtration of polydisperse suspension with small impurities // Applied Mathematics and Mechanics, 2021, vol. 42 (1), pp. 109-126. DOI: 10.1007/s10483-021-2690-6
24. **Fallah H., Fallah A., Rahmani A., Afkhami M., Ahmadi A.** Size exclusion mechanism, suspension flow through porous medium // International Journal of Modern Nonlinear Theory and Application, 2012, vol. 1, pp. 113-117.
25. **You Z., Osipov Y., Bedrikovetsky P., Kuzmina L**. Asymptotic model for deep bed filtration // Chemical Engineering Journal, 2014, vol. 258, pp. 374-385.

Galina L. Safina, Ph. D, Head of the Department of Fundamental Education, branch of Moscow State University of Civil Engineering in Mytishchi, Associate Professor of the Department of Computer Science and Applied Mathematics, Moscow State University of Civil Engineering; 129337, Russia, Moscow, Yaroslavskoe Shosse, 26, tel. +7(499)1835994, e-mail: minkinag@mail.ru.

Сафина Галина Леонидовна, кандидат технических наук, заведующий кафедрой фундаментального образования филиала НИУ МГСУ в г. Мытищи, доцент кафедры информатики и прикладной математики Национального исследовательского Московского государственного строительного университета; 129337, Россия, г. Москва, Ярославское шоссе, д. 26, тел. +7(499)1835994, e-mail: minkinag@mail.ru.

DOI:10.22337/2587-9618-2023-19-2-31-41

THE EFFECT OF HOLLOW STRUCTURE PARAMETER ON THE 3D-PRINTED WALL BEARING CAPACITY. EXPERIMENTAL MODEL

Galina S. Slavcheva, Artem V. Levchenko, Maria A. Shvedova, Davut R. Karakchi-Ogli, Dmitriy S. Babenko, Pavel Y. Yurov

Voronezh State Technical University (VSTU), Voronezh, RUSSIA

Abstract. We present the results of experimental studies and modelling of the evaluation of the bearing capacity of hollow 3D-printed walls with the printed shell performing bearing functions. The bearing capacity of hollow 3D-printed walls was experimentally assessed depending on the ratio of the void areas and casting layers in the wall structure. It was established that in case of central loading, a 3D-printed wall with bearing casting layers can serve as a bearing wall similar to traditional types of masonry construction without filling voids with structural concrete and reinforcement. We established the value of strength reduction of hollow 3D-printed walls, which amounted to ~0.1 – 0.25 MPa per 1 % of the increased area of voids. The limit value of the hollow structure parameter was determined, which must not exceed $K = 0.75$ in order to ensure the bearing capacity of self-bearing and non-bearing 3D-printed walls. We obtained an experimental model of the relationship between the hollow structure parameter and the bearing capacity, which allowed predicting the bearing capacity of a 3D-printed wall under central loading. It was suggested to take into account the hollow structure parameter K when calculating the elements of unreinforced 3D-printed walls under central compression according to the first group of limit states.

Keywords: 3D-build printing, bearing capacity, strength, wall, experimental model

ЭКСПЕРИМЕНТАЛЬНАЯ МОДЕЛЬ ВЛИЯНИЯ ПУСТОТНОСТИ НА НЕСУЩУЮ СПОСОБНОСТЬ СТЕН, ПОЛУЧЕННЫХ ПО АДДИТИВНОЙ ТЕХНОЛОГИИ

Г.С. Славчева, А.В. Левченко, М.А. Шведова, Д.Р. Каракчи-Огли, Д.С. Бабенко, П.Ю. Юров

Воронежский государственный технический университет (ВГТУ), Воронеж, РОССИЯ

Аннотация. Представлены результаты экспериментальных исследований и моделирования оценки несущей способности пустотелой 3D-напечатанной стены, в которой печатная оболочка выполняет несущие функции. Экспериментально оценена несущая способность 3D-печатных пустотелых стен в зависимости от соотношения площади пустот и печатных слоев в конструкции стены. Установлено, что 3D-напечатанная стена с несущими аддитивными слоями в случае центрального нагружения может выполнять роль несущей стены аналогично традиционным видам каменной кладки без заполнения пустот конструкционным бетоном и армирования. Определена мера снижения прочности 3D-напечатанной стены, которая составляет ~0.1 – 0.25 МПа на 1 % увеличения площади пустот. Установлено предельное значение параметра пустотности, которое не должно превышать $K = 0.75$, для обеспечения несущей способности самонесущих и ненесущих аддитивных стеновых конструкций. Получена экспериментальная модель взаимосвязи пустотности и несущей способности, которая позволяет прогнозировать несущую способность 3D-напечатанной стены при центральном нагружении в зависимости от параметра пустотности K. Предложено учитывать параметр пустотности K при расчете элементов неармированных аддитивных стеновых конструкций при центральном сжатии по первой группе предельных состояний.

Ключевые слова: строительная 3Д-печать, прочность, стена, экспериментальная модель

INTRODUCTION

The most common option of the wall structure in 3D-build printing is in the form of two straight layers connected by a sinusoidal lintel as a diaphragm stiffness [1-3]. Such a wall is actually a space truss with parallel belts, which means that the internal and external parts of the wall are interconnected by a spatial structure in the form of triangles [4]. The rationality of using such walls can be explained by the need to minimise the "idle" movement of the extruder of a construction printer, which ensures the continuity of the printing contour [5]. Precast lintels are installed above window and door frames. Channels are provided in the door profiles for the placement of utility systems and a hollow to be filled with a heat-insulating material [6,7].

In all implemented projects with 3D-build printing objects, the construction of walls includes the following steps:

- 3D printer prints the wall shell;
- Wall cavities are reinforced manually;
- Wall cavities are filled with structural concrete and (for external walls) insulation.

This approach is also typical for the manufacture of precast structural elements of complex curvilinear geometry [8].

The main disadvantage of this practised approach is that the printed shell acts as a fixed formwork and does not have a constructive function. Examples is 3D printed walls made using WinSun technology, CyBe technology, etc.[9-11]., The most operations in these technologies are performed manually, excluding the printing of fixed formwork. It was noted in [12] that the traditional technology of concrete casting was actually used in the formwork instead of the innovative printing technology, Today, this determines the high labour intensity of the process. This approach is an over-simplification of the idea of 3D-build printing as a robotic intelligent construction technology and may lead to its discreditation. From an economic point of view, the use of a printed shell only as a fixed formwork is also inefficient due to its obviously high cost as compared to traditional formworks.

However, in a number of studies it was confirmed that hollow 3D-printed walls that were not filled with structural concrete have sufficient bearing capacity due to the high strength of the material used and the more homogeneous strength properties of the obtained structure as compared to traditional masonry. For example, in [13], a compressive strength of 2.3 MPa was determined as a result of testing a 3D-printed concrete segment. The effective area of the wall with the deduction of the hollow was approximately 60% of the total area. That is confirmed that the hollow3D-printed wall shell carries out bearing function. So, the influence of the hollow parameter on the bearing capacity of 3D-printed walls needs to study in order to use it in design of 3D printed wall. According to the requirements of SP 15.13330.2020 "Masonry and reinforced masonry structures", this corresponds to the strengths that are traditional in the Russian Federation [14] for the following types of walls:

- Masonry of M150 ceramic bricks on an M100 mixture,
- Made from B7.5 cellular concrete blocks on an M100 mixture,
- Made from M150 solid gypsum concrete blocks on an M150 mixture.

Thus, there is a possibility of using a hollow 3D-printed wall as a bearing and self-bearing wall in low-rise construction. This requires sufficient bearing capacity of the hollow wall structure, while their internal space should be used for creating heat-insulating layers instead of being filled with structural heavy concrete. The hollowness of the 3D-printed wall will allow their material consumption and reduce the costs of manual labour in the course of construction. In order to do this, the allowable area of voids per unit area of the wall must be determined as the current regulatory document SP 15.13330 does not in

any way regulate the design of 3D-printed structures.

The goal of the study was to justify the requirements to the effective cross-section area of hollow 3D-printed walls by the criterion of ensuring its bearing capacity based on experimental studies and modelling.

Research objectives:

- Evaluating the bearing capacity of hollow 3D-printed walls depending on the ratio of the void areas and casting layers in the wall structure;
- Obtaining an experimental model of the influence of a hollow structure 3D-printed wall on its bearing capacity;
- Making suggestions for calculations on the strength of 3D-printed walls taking into account their hollow structure.

MATERIALS AND METHODS

The object of the study is a hollow 3D-printed wall with a sinusoidal lintel (Fig. 1). To assess the bearing capacity, we used the model and full-size 3D-printed wall segments the sizes of which are presented in Table 1.

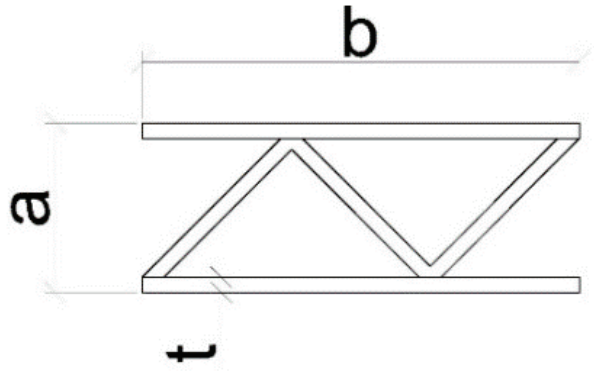


Figure 1. Cross-section of 3D-printed wall

Table 1. Size of experimental samples

Sample	a, mm	b, mm	t, mm	h, mm
3D-printed wall model segment				
IBW -75	75	155	15	150
IBW -90	90	200	15	180
IBW -105	105	245	15	210
EBW -135	135	335	15	270
EBW -150	150	380	15	300
EBW -165	165	425	15	330
3D-printed wall full-size segment				
IBW -75-f	250	520	50	500
IBW -90-f	300	670	50	600
IBW -105-f	350	820	50	700
EBW -135-f	450	1120	50	900
EBW -150-f	500	1270	50	1000
EBW -165-f	550	1420	50	1100

Note: Code EBW-135 means the following: the thickness of the bearing external wall is 135, IBW is the internal bearing wall, index "f" stands for a full-size construction.

The relative effective cross-sectional area A_c/A_{cs}, the ratio of concrete area (A_c) to cross-sectional area ($A_{cs} = a \times b$), was chosen as a variable parameter.

It is reasonable to assume that the following inequality must be satisfied for the relative effective area:

$$X < A_c / A_{cs} \leq 1, \quad (1)$$

where 1 is the value of a layered conventionally monolithic sample,

X is the minimum value of the relative effective cross-sectional area allowable to ensure the bearing capacity.

The range of values of the relative effective cross-sectional area A_c/A_{cs} of the 3D-printed wall segment used in the experiment is presented in Table 2.

Table 2. Parameters of experimental samples

Sample	Concrete area A_c, mm^2	Cross-sectional area ($A_{cs} = a \times b$), mm^2	Relative effective cross-sectional area A_c/A_{cs}	Hollow structure parameter K
3D-printed model wall segment				
IBW -75	7530	11625	0.65	0.35
IBW -90	9825	18000	0.55	0.45
IBW -105	12165	25725	0.47	0.53
EBW -135	16755	45225	0.37	0.63
EBW -150	19050	57000	0.33	0.67
EBW -165	21345	70125	0.30	0.70
3D-printed full-size wall segment				
IBW -75-f	83800	130000	0.64	0.36
IBW -90-f	109450	201000	0.54	0.46
IBW -105-f	134950	287000	0.47	0.53
EBW -135-f	186250	504000	0.37	0.63
EBW -150-f	211750	635000	0.33	0.67
EBW -165-f	237400	781000	0.30	0.70

Materials and 3D-printed wall segment preparation. The cement-sand mixture, patented by the author's team [15], was used for the printing wall model segments. The strength characteristics of the hardened cement-sand mixture are presented in Table 3.

Table 3. Strength test results

Compressive strength (axial), MPa	47.0
Compressive strength (cube), MPa	60.0
Flexible strength (four-point bending), MPa	2.8
Splitting interlayer bond strength, MPa	3.0

Sand-based concrete of B40 strength class was used to obtain a 3D-printed wall full-size segment.

Model and full-scale walls were printed on laboratory and industrial printers, respectively, with similar conditions for manufacturing and curing:

- Constant print speed 2 cm/s,
- Constant distance between nozzle and layer – 2 cm;
- Printing time gap < 1 min;
- Curing for 28 days in the same environment (T = 20 ± 2°C, RH = 60-70 %).

Figure 2 presents an example of 3D-printed model wall segment.



Figure 2. 3D-printed model wall segment after printing

Test conditions of 3D-printed wall segment.

The printed hollow wall segments were tested for axial compression with a central load application according to GOST 32047-2012 "Masonry. Method of compressive test". The choice of the test pattern was due to the following. Testing methods for wall and other structures regarding 3D-build printing are not

currently regulated. We analysed the experience [13] of a compression test of a 3D-printed wall segment 730 × 530 × 504 mm in size with a layer size of 12 × 35 mm. This pattern corresponding to the methodology of GOST 32047-2012 was accepted as adequate. Series of 3 samples were manufactured and tested for each type of a 3D-printed wall segment. 3D-printed wall segments prepared for testing and installed in the testing machine are presented in Figures 3 and 4.

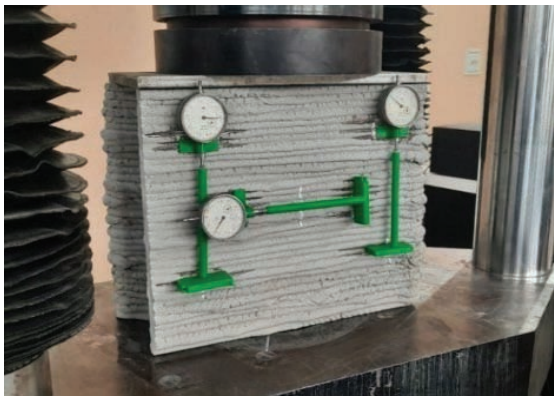


Figure 3. A 3D-printed model wall segment prepared for testing



Figure 4. General view on 3D-printed full-size wall segments before testing

EXPERIMENTAL RESULTS

Test results of 3D-printed wall segments are presented in Table 4.

The nature of destruction of the model and full-size wall segments upon central compression was identical and was characterised by the formation of vertical cracks that crossed the layers without any changes in the crack path. With an increase in the load, the number of cracks increased (Figures 5 and 6).

Table 4. 3D-printed walls axial compression test results

Sample	Cross-sectional area A_{cs}, mm^2	Concrete area A_c, mm^2	Relative effective cross-sectional area A_c/A_{cs}	Force N, kN	Strength of the model wall, related to the sectional area (considering hollows) N/ A_{cs}, MPa	The strength of the model wall, related to the concrete area N/A_c, MPa
3D-printed model wall segment						
IBW -75	13825	11678.3	0.84	126.14	9.10	10.85
IBW -90	20333	15840.4	0.78	191.41	9.37	11.85
IBW -105	29400	18621.3	0.63	223.50	7.60	12.00
EBW -135	49800	28218.5	0.57	279.35	5.59	9.87
EBW -150	62300	33871.1	0.54	384.35	6.25	12.17
EBW -165	73800	36924.0	0.50	407.37	5.54	11.06
3D-printed full-size wall segment						
IBW -75-f	134900	91500.0	0.68	1389.00	10.30	15.18
IBW -90-f	207162	112000	0.54	1380.00	6.66	12.32
IBW -105-f	285363	142630	0.50	1411.00	4.94	9.89
EBW -135-f	490757	172080	0.35	984.00	2.01	5.72
EBW -150-f	633775	199870	0.32	1017.00	1.60	5.09
EBW -165-f	771584	242160	0.31	1121.00	1.45	4.63



Figure 5. Representative example of the 3D-printed model wall segments during the compressive strength test

The effect of the hollow structure on the strength of walls was assessed quantitatively. With an increase in the size of the 3D-printed model wall segments, the ratio of the concrete area to the total cross-sectional area of the A_c/A_{cs} wall decreased within the range from 0.9 to 0.5, while the hollow structure, accordingly, increased from 0.1 to 0.5. The compressive strength of model walls classified as part of the total cross-sectional area N/A_c (which means, taking into account the hollow structure) naturally decreased and changed within the range of 5.5 – 9.4 MPa. The strength values of the bearing layers of concrete remained almost the same for all types of 3D-printed model wall segments and were in the range of 10 – 12 MPa. This showed that the bearing layers used their structural potential equally, regardless of the changes in the usable cross-sectional area of the wall.



Figure 6. A representative example of the 3D-printed-size wall segments during the compressive strength test

With an increase in the size of the model and full-size wall segments, the ratio of the concrete area to the total cross-sectional area of the A_c/A_{cs} wall decreased within the range of 0.7 – 0.3, while the hollow structure increased from 0.3 to 0.7, accordingly. The compressive strength of full-size walls classified as part of the total cross-sectional area N/A_c (which means, taking into account the hollow structure) naturally decreased and changed within the range of 1.45 – 10.3 MPa. The strength values of bearing concrete layers of full-size walls decreased and were within the range of 5 – 15 MPa. This indicated that the structural potential of the bearing layers depended on the change in the useful cross-sectional area of the wall and the scale factor as part of the central loading. The reduction in the strength of full-size wall segments as compared to model segments can be explained by the scale factor. With an increase in the size of the walls, their flexibility of straight layers increased, and as a result, the stability of the 3D-printed full-size wall segment on the whole decreased.

According to the obtained data, it can be stated that the bearing capacity of 3D-printed walls is determined by the following factors:

- The ratio of the concrete area to the total cross-sectional area of the wall or its hollow structure.
- The scale factor and especially its effect on the flexibility and stability of the structure.

The results of the assessment of the bearing capacity of hollow 3D-printed walls were correlated with the requirements to the bearing capacity of masonry from small-piece wall products, regulated by SP 15.13330.2020 “Masonry and reinforced masonry structures”. It can be explained by the fact that the working conditions for masonry and 3D-printed structures in internal and external bearing and self-bearing walls are similar. In the studied range of changes of the concrete area A_c/A_{cs} = 0.3-0.9 in the section of a hollow 3D-printed wall with bearing printed layers, the strength range was 1.45-10.3 MPa. In case of central loading these values corresponded to and, in most cases, exceeded the requirements of SP 15.13330.2020 to the calculated compressive strengths of typical forms of masonry for house construction. In particular, the strength values obtained in experiments corresponded to the strength of masonry from solid concrete, gypsum concrete, and natural stones, which was within the range of 0.38-13.0 MPa in accordance with the requirements of Table 6.5 of SP 15.13330.2020 (with a masonry layer height of 200-300 mm).

EXPERIMENTAL MODEL

The values of 3D-printed model and full-size wall segments were generalised depending on the hollow structure parameter (Figure 7).

$$K = 1 - A_c / A_{cs} \qquad (2)$$

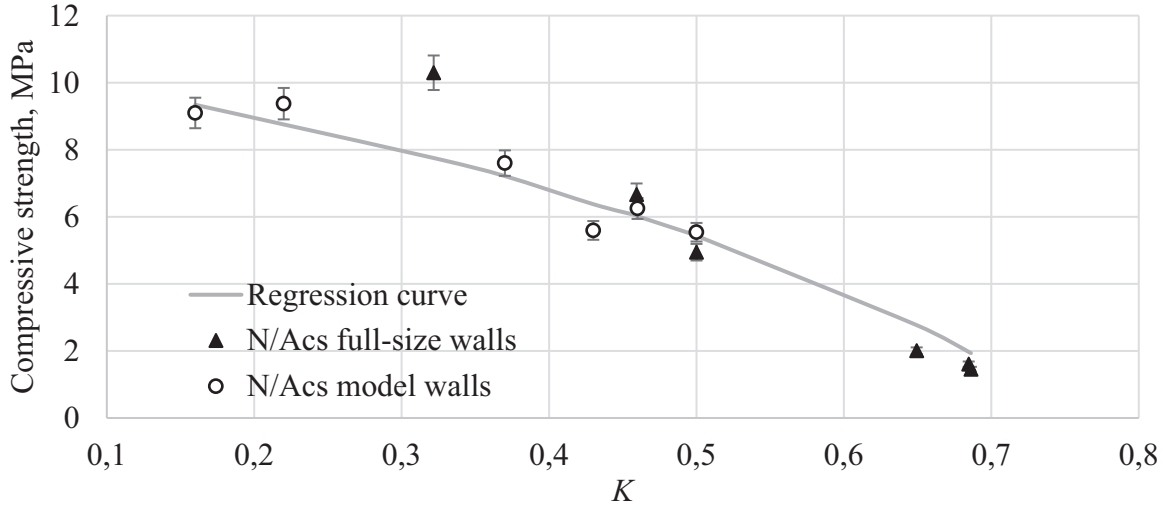


Figure 7. The effect of hollow structure parameter K on the 3d-printed wall bearing capacity.

Based on the regression analysis of experimental data, we obtained an equation that predicted a change in the bearing capacity of 3D-printed walls depending on their hollow structure.

$$N = \ln(1-K)^{7.94 A_{cs}} + 10.89 \cdot A_{cs} \qquad (3)$$

The reliability coefficient of the experimental data approximation was 0.9 for the obtained regression curve (eq. (3))

Therefore, it can be stated that the obtained experimental model described by equation (3) allowed predicting the bearing capacity of 3D-printed walls upon central loading depending on the hollow area in the section. The solution of this equation also allowed determining the minimum allowable boundary of wall void content by the criterion of ensuring enough bearing capacity in case of central compression. Taking into account the root of equation (3), the following inequality is true:

$$0 \le K < 0.75 \qquad (4)$$

High convergence of the experimental data with the calculated data allowed proposing the hollow structure parameter K to be used for the calculation of strength of hollow 3D-printed walls according to the standard method SP 15.13330.2020 "Masonry and reinforced masonry structures". The hollow parameter in this standard is used for masonry blocks. At the same time, in some foreign standards for building blocks the filling ratio is normalized in the range from 40% to 75%, vice versa the hollow of the building blocks is from 25% to 60%. It is corresponded to investigated hollow structure range of 3D-printed wall segments.

When designing 3D-printed walls, the calculations for the first group of limit states were allowed to be performed using existing standard methods, which are regulated in SP 63.13330 "Concrete and reinforced concrete structures. General provisions", SP 15.13330 "Masonry and reinforced masonry structures".

When using the specified standard methods, it is suggested to calculate the bearing capacity upon central compression of an unreinforced hollow 3D-printed wall using the following improved formula:

$$N \le m_r \cdot (1-K) \cdot m_g \cdot \varphi \cdot R \cdot A, \qquad (5)$$

where N is the calculated longitudinal force; R is the calculated compressive strength of 3D-printed layered concrete, determined by new parametric rows; A is the wall cross-sectional area in geometric axes, K is the hollow structure parameter, m_g is the coefficient taking into account the impact of a long-term load, φ is the buckling coefficient.

At the same time, it is proposed to introduce the coefficient m_r into relation (5) which takes into account a decrease in the strength potential of 3D-printed layered concrete in the structure. Systematic studies must be performed in order to determine it. Extended experimental studies are also required to determine the impact of such parameters as concrete class, reinforcement, and wall configuration in combination with hollow structure on the bearing capacity of 3D-printed walls.

CONCLUSION

1. It was established that in case of central loading the strength of an unreinforced hollow 3D-printed wall corresponded to and/or exceeded SP 15.13330.2020 "Masonry and reinforced masonry structures" and amounted to 1.45–10.3 MPa within the range of a hollow structure 0.15–0.75. Therefore, in case of central loading a hollow 3D-printed wall can serve as a bearing wall similar to traditional types of masonry with no need to fill the voids with structural concrete and reinforcement.
2. According to the test results of model and full-size 3D-printed walls, it was established that the main factor determining their bearing capacity was the hollow structure. We determined the value of strength reduction of 3D-printed walls, which was ~0.1 – 0.25 MPa per 1% of the increased area of the hollow structure.
3. An experimental model was obtained that allowed predicting the bearing capacity of 3D-printed walls upon central loading depending on the hollow structure parameter K. According to the obtained model, the calculated value of the hollow structure parameter should not exceed 0.75 in order to ensure the bearing capacity of self-bearing and non-bearing 3D-printed walls. Thus, it is suggested to perform the calculation for the first group of limit states of the bearing capacity of unreinforced hollow 3D-printed walls upon central compression using the hollow structure parameter K.

ACKNOWLEDGEMENT

This research was supported by the Russian Science Foundation, No. 22-19-00280, https://rscf.ru/en/project/22-19-00280/.
The experimental studies have been carried out

using the facilities of the Collective Research Center named after Professor Yu. M. Borisov, Voronezh State Technical University, which is partly supported by the Ministry of Science and Education of the Russian Federation, Project No. 075-15-2021-662.

REFERENCES

1. **Monastyrev P.V., Ezerskij V.A., Ivanov I.A., Bal'tozar A. D.** (2019) Analiz tekhnologij 3d -pechati sten maloetazhnyh zdanij i ih klassifikaciya **[**Analysis of 3d printing technologies for walls of low-rise buildings and their classification]. Sovremennye problemy v stroitel'stve: postanovka zadach i puti ih resheniya. Kursk, 2019, pp. 70-80. (in Russian)
2. **Karpova E., Skripkiunas G., Sedova A., Tsimbalyuk Y.** (2021) Additive manufacturing of concrete wall structures. E3S Web of Conferences, no 281, pp. 03007.https://doi.org/10.1051/e3sconf/202128103007.
3. **Suleymanova L.A., Ognev N.V.** (2017) Ocenka vozvedeniya sten zdaniya s pomoshch'yu 3d-printera v sravnenii s tradicionnym stroitel'stvom iz betonnyh blokov **[**Building evaluation with a 3D printer in search of concrete block construction applications]. Universitetskaya nauka, no. 2 (4). pp. 13-15. (in Russian)
4. **Luneva D.A., Kozhevnikova E.O., Kaloshina S.V.** (2017) Tekhnologiya 3D-pechati s ispol'zovaniem metoda poslojnogo ekstrudirovaniya v stroitel'stve [3D printing technology using layer-by-layer extrusion in construction]. Material IX Vserossijskoj molodezhnoj konferencii aspirantov, molodyh uchenyh i studentov «Sovremennye tekhnologii v stroitel'stve. Teoriya i praktika», no 9, pp. 251-261. (in Russian)
5. **Watson N.D., et al.** (2019) Large-scale additive manufacturing of concrete using a 6-axis robotic arm for autonomous habitat construction. Solid Freeform Fabrication: Proceedings of the 30th Annual International, Austin, Texas, 2019, pp. 1583-1595.
6. **Aleksanin A.V., Makarevich A.I.** (2017) Ispol'zovanie additivnyh tekhnologij pri vozvedenii zdanij **[**The use of additive technologies in the construction of buildings]. Vestnik Belgorodskogo gosudarstvennogo tekhnologicheskogo universiteta im. V.G. Shuhova, no 6, pp. 66-69. (in Russian)
7. **Krushelnitskaya E.A., Ognev N.V., Zhang Jiandong Xie Di.** (2018) Materialy dlya stroitel'nyh 3d-printerov i varianty konstruktivnogo resheniya zdanij **[**Materials for construction 3D printers and options for constructive solutions for buildings]. Mezhdunarodnyj studencheskij stroitel'nyj forum, Belgorod, 2018, pp. 255-259. (in Russian)
8. **Khoshnevis B., et al.** (2006) Mega-scale fabrication by contour crafting. Int. J. Ind. Syst. Eng., no 1, pp. 301-320. http://dx.doi.org/10.1504/IJISE.2006.009791.
9. **Mechtcherine V., et al.** (2018) 3D-printed steel reinforcement for digital concrete construction - Manufacture, mechanical properties and bond behavior. Construction and Building Materials, no 179, pp. 125-137. https://doi.org/10.1016/j.conbuildmat.2018.05.202.
10. **Pessoa S., Guimarães A.S., Lucas S.S., Simões N.** (2021) 3D printing in the construction industry - A systematic review of the thermal performance in buildings. Renewable and Sustainable Energy Reviews, vol. 141, pp. 110794. https://doi.org/10.1016/j.rser.2021.110794
11. **Furet B., Poullain P., Garnier S.** (2019) 3D printing for construction based on a complex wall of polymer-foam and concrete. Additive Manufacturing, vol. 28, pp. 58-64. https://doi.org/10.1016/j.addma.2019.04.002.
12. **Molodin V.V., Gasenko I.I., Timi P.L.** (2020) Tekhnologiya 3d-pechati

odnostadijnym polistirolbetonom [3D printing technology with single-stage polystyrene concrete]. Nauka i Innovacionnye tekhnologii, no 1 (14), pp. 278-287, DOI: 10.33942/sit.nes033 (in Russian)
13. **Ferretti E., et al.** (2022) Mechanical Properties of a 3D Printed Wall Segment made with an Earthen Mixture. Materials (Basel), no 15(2), pp. 438, DOI: 10.3390/ma15020438.
14. **Lukina E.V.** (2021) Obzor populyarnyh stroitel'nyh materialov, primenyaemyh v maloetazhnom stroitel'stve (kirpich, gazobeton). Sravnenie ih osnovnyh harakteristik [Overview of popular building materials used in low-rise construction (brick, aerated concrete). Comparison of their main characteristics]. Innovacionnaya nauka, no 8-1, pp. 66-68. (in Russian)
15. RU 2729085 C1, 04.08.2020. Dvuhfaznaya smes' na osnove cementa dlya kompozitov v tekhnologii stroitel'noj 3D-pechati [Two-phase mixture based on cement for composites in the construction 3D printing technology], 8p. (in Russian)
16. Brick Industry Association: Reston, Virginia (2007) Technical Notes on Brick Construction. Specifications and classification of Brick, Virginia, BIA, 13p
17. ASTM C652-21. (2021) Standard Specification for Hollow Brick (Hollow Masonry Units Made From Clay or Shale). ASTM International, 7p.

СПИСОК ЛИТЕРАТУРЫ

1. **Монастырев П.В., Езерский В.А., Иванов И.А., Бальтозар А.Д.** Анализ технологий 3d -печати стен малоэтажных зданий и их классификация // Современные проблемы в строительстве: постановка задач и пути их решения. Курск. 2019. С. 70-80.
2. **Karpova E., Skripkiunas G., Sedova A., Tsimbalyuk Y.** Additive manufacturing of concrete wall structures // E3S Web of Conferences. 2021. №281. pp. 03007. https://doi.org/10.1051/e3sconf/202128103007.
3. **Сулейманова Л.А., Огнев Н.В.** Оценка возведения стен здания с помощью 3d-принтера в сравнении с традиционным строительством из бетонных блоков // Университетская наука. 2017. № 2 (4). С. 13-15.
4. **Лунева Д.А., Кожевникова Е.О., Калошина С.В.** Технология 3D-печати с использованием метода послойного экструдирования в строительстве // Материал IX Всероссийской молодежной конференции аспирантов, молодых ученых и студентов «Современные технологии в строительстве. Теория и практика». 2017.№ 9. С. 251-261.
5. **Watson N.D., et al.** Large-scale additive manufacturing of concrete using a 6-axis robotic arm for autonomous habitat construction // Solid Freeform Fabrication: Proceedings of the 30th Annual International. 2019. pp. 1583-1595
6. **Алексанин А.В., Макаревич А.И.** Использование аддитивных технологий при возведении зданий // Вестник Белгородского государственного технологического университета им. В.Г. Шухова. 2017. № 6. С. 66-69.
7. **Крушельницкая Е.А., Огнев Н.В., Чжан Цзяньдун Се Ди.** Материалы для строительных 3d-принтеров и варианты конструктивного решения зданий // Международный студенческий строительный форум. Белгород. 2018. С. 255-259.
8. **Khoshnevis B., et al.** Mega-scale fabrication by contour crafting // Int. J. Ind. Syst. Eng. 2006. № 1. pp. 301-320. http://dx.doi.org/10.1504/IJISE. 2006.009791.
9. **Mechtcherine V., et al.** 3D-printed steel reinforcement for digital concrete construction - Manufacture, mechanical properties and bond behaviour // Construction and Building Materials. 2018. № 179. pp. 125-137.

https://doi.org/10.1016/j.conbuildmat.2018.05.202.

10. **Pessoa S., Guimarães A.S., Lucas S.S., Simões N.** 3D printing in the construction industry - A systematic review of the thermal performance in buildings // Renewable and Sustainable Energy Reviews. Vol. 141. 2021. pp. 110794. https://doi.org/10.1016/j.rser.2021.110794
11. **Furet B., Poullain P., Garnier S.** 3D printing for construction based on a complex wall of polymer-foam and concrete // Additive Manufacturing. Vol. 28. 2019. pp. 58-64. https://doi.org/10.1016/j.addma.2019.04.002.
12. **Молодин В.В., Гасенко И.И., Тими П.Л.** Технология 3d-печати одностадийным полистиролбетоном // Наука и Инновационные технологии. 2020. № 1 (14). С. 278-287. DOI: 10.33942/sit.nes033
13. **Ferretti E., et al.** Mechanical Properties of a 3D Printed Wall Segment made with an Earthen Mixture // Materials (Basel). 2022. № 15(2). pp. 438. DOI: 10.3390/ma15020438.
14. **Лукина Е.В.** Обзор популярных строительных материалов, применяемых в малоэтажном строительстве (кирпич, газобетон). Сравнение их основных характеристик // Инновационная наука. 2021. № 8-1. С. 66-68.
15. RU 2729085 C1, 04.08.2020. Двухфазная смесь на основе цемента для композитов в технологии строительной 3D-печати. 8с.
16. Technical Notes on Brick Construction. Specifications and classification of Brick. Brick Industry Association: Reston, Virginia, 2007. 13p
17. ASTM C652-21. Standard Specification for Hollow Brick (Hollow Masonry Units Made From Clay or Shale). ASTM International, 2021. 7p.

Galina S. Slavcheva, Associate Professor, Doctor of Technical Sciences, Professor, Voronezh State Technical University, 84, 20 letiya Oktyabrya st. Voronezh, 394006. Russia, e-mail: gslavcheva@yandex.ru

Artem V. Levchenko, Candidate of Technical Sciences, Senior lecturer, Voronezh State Technical University, 84, 20 letiya Oktyabrya st. Voronezh, 394006. Russia, e-mail: alevchenko@vgasu.vrn.ru

Maria A. Shvedova, Candidate of Technical Sciences, Junior Researcher, Voronezh State Technical University, 84, 20 letiya Oktyabrya st. Voronezh, 394006. Russia, e-mail: marishwedowa@mail.ru

Davut R. Karakchi-Ogli, Junior Researcher, Voronezh State Technical University, 84, 20 letiya Oktyabrya st. Voronezh, 394006. Russia, e-mail: karakchiogli.david@mail.ru

Dmitriy S. Babenko, Engineer, Voronezh State Technical University, 84, 20 letiya Oktyabrya st. Voronezh, 394006. Russia, e-mail: teleperedoz@mail.ru

Pavel Y. Yurov, PhD student Voronezh State Technical University, 84, 20 letiya Oktyabrya st. Voronezh, 394006. Russia, e-mail: yurov.py@yandex.ru

Славчева Галина Станиславовна, доцент. д.т.н., проф., Воронежский государственный технический университет, 394006. Россия, г. Воронеж, ул. 20-летия Октября. 84, e-mail: gslavcheva@yandex.ru

Левченко Артем Владимирович, к.т.н., старший преподаватель Воронежского государственного технического университета, 394006. Россия, г. Воронеж, ул. 20-летия Октября. 84, e-mail: alevchenko@vgasu.vrn.ru

Шведова Мария Александровна, к.т.н., младший научный сотрудник Воронежского государственного технического университета, 394006. Россия, г. Воронеж, ул. 20-летия Октября. 84, e-mail: marishwedowa@mail.ru

Каракчи-Огли Давут Ресулович, младший научный сотрудник Воронежского государственного технического университета, 394006. Россия, г. Воронеж, ул. 20-летия Октября. 84, e-mail: karakchiogli.david@mail.ru

Бабенко Дмитрий Сергеевич, инженер Воронежского государственного технического университета, 394006. Россия, г. Воронеж, ул. 20-летия Октября. 84, e-mail: teleperedoz@mail.ru

Юров Павел Юрьевич аспирант Воронежского государственного технического университета, 394006. Россия, г. Воронеж, ул. 20-летия Октября. 84, e-mail: yurov.py@yandex.ru

International Journal for Computational Civil and Structural Engineering, 19(2) 42–50 (2023)

DOI:10.22337/2587-9618-2023-19-2-42-50

JOINT STRENGTH OF ALUMINUM ALLOYS STRUCTURES CONNECTED WITH CONTACT CAPACITOR WELDING

Andrey V. Korgin

National Research Moscow State University of Civil Engineering, Moscow, RUSSIA

Abstract. Currently, aluminum alloys are widely used in various industrial productions and constructions due to the unique properties, which allows creation of lightweight, durable, reliable, corrosion-resistant and aesthetic structures and products for different purposes. Nevertheless, aluminum alloys have a number of disadvantages, the main of which is a more complex and expensive process of manufacturing of welded structures. It requires the use of more advanced technologies such as argon arc welding and friction welding with mixing and qualified personnel in contrary with classical electric welding of steel structures. Such technologies also include the modern method of contact capacitor spot welding, the equipment for which is compact and mobile enough. And its usage does not require highly qualified personnel compared to other aluminum welding technologies. The existing regulatory documentation of the Russian Federation on contact capacitor spot welding does not provide sufficient recommendations for the design and calculation of the strength of joints of this type, which requires additional experimental studies of such joints. The purpose of this work is to determine experimentally the strength of two types of joints made using condenser welding technology and working on tension and shear units of ceiling suspension of sheets and profiles of aluminum alloy AMG2M to rod threaded rods made of aluminum alloy AMG3. For this purpose, 18 joints of these types were tested. Control calculations by standard methods for tension and for shear were performed in order to assess their applicability for analyses of these types of joints.

Keywords: aluminum alloy, spot capacitor welding, tension, shear, stress, strength, fracture

ПРОЧНОСТЬ СОЕДИНЕНИЙ ИЗ АЛЮМИНИЕВЫХ СПЛАВОВ, ВЫПОЛНЕННЫХ МЕТОДОМ КОНТАКТНОЙ КОНДЕНСАТОРНОЙ СВАРКИ

А.В. Коргин

Национальный исследовательский Московский государственный строительный университет, г. Москва, РОССИЯ

Аннотация. В настоящее время алюминиевые сплавы находят широчайшее применение в самых разнообразных сферах промышленного производства и строительства за счет уникальных свойств физико-механических, позволяющих создавать легкие, прочные, надежные, коррозионностойкие и эстетичные конструкции и изделия самого разнообразного назначения. Тем не менее, алюминиевые сплавы обладают рядом недостатков, основным из которых является более сложный и дорогостоящий процесс изготовления сварных конструкций, требующий применения более совершенных технологий – аргонодуговой сварки и сварки трением с перемешиванием, а также квалифицированного персонала по сравнению с классической электросваркой конструкций из стали. К подобным технологиям также относятся современные методы лазерной сварки и контактной конденсаторной точечной сварки, оборудование для которой достаточно компактно и мобильно, а его использование не требует персонала высокой квалификации по сравнению с другими технологиями сварки алюминия. Существующая нормативная документация РФ по контактной конденсаторной точечной сварке не дает достаточных рекомендаций по проектированию и расчету прочности соединений данного типа, что требует дополнительных экспериментальных исследований таких соединений. Целью настоящей работы явилось экспериментальное определение прочности соединений двух типов, выполненных с помощью технологии конденсаторной сварки и работающих на растяжение и срез – узлов потолочной подвески листов и профилей алюминиевого сплава АМГ2М к стержневым резьбовым тягам, выполненным из алюминиевого сплава АМГ3. Для этого были испытаны 18 соединений указанных типов и выполнены контрольные расчеты нормативными методами на растяжение и срез с целью оценки их применимости для расчетов соединений данных типов.

Ключевые слова: алюминиевый сплав, точечная конденсаторная сварка, растяжение, срез, напряжение, прочность, разрушение

INTRODUCTION

At present, the use of various aluminum alloys is rapidly developing, finding the widest application in the most diverse areas of industrial production and construction due to their unique properties, allowing to create light, strong, reliable, corrosion-resistant and aesthetic structures and products of various purposes. Nevertheless, aluminum alloys have a number of disadvantages compared to steels, the main of which is a more complicated and costly process of producing welded structures, that requires the use of more advanced technologies such as argon arc welding, friction stir welding [1,2,3,4,5,6,7,8] and qualified personnel in contrast to the classical electric welding of steel structures. Such technologies also include various modern methods of laser welding and contact capacitor spot welding [9,10,11,12,13,14], the equipment for which is quite compact and mobile, and its use does not require highly qualified personnel compared to other aluminum welding technologies.

The existing regulatory documents of the Russian Federation on contact welding technologies, including condensation welding presented in GOST 15878-79 "Contact welding", do not give sufficient recommendations on the design and calculation of the strength of joints of this type, which requires additional experimental research of such joints.

The purpose of this work was to carry out tests and calculations of two types of joints consisting of sheet and T-type profiles of aluminum alloy AMG2M with threaded rods for mounting suspended rods of aluminum alloy AMG3 welded to them by the method of spot welding in order to determine the values of ultimate loads for these welded joints. Examples of similar studies in Russia and abroad are given in [15,16].

The main stages of the study are as follows:

- manufacture and installation of loading devices of the tested joints;
- testing of specimen joints of two types;
- performing verification analysis of the strength of these joints in order to assess the possibility of using the standard calculation methods for the design of such joints to determine the values of the ultimate loads by calculation;
- conclusions and recommendations for manufacturing and operation of structures with the joints of this type.

METHODS

Two types of specimens were tested: a connection of plates with dimensions 100×100 mm made of sheet metal of 3 mm thickness and parts of a rolling Taurus with dimensions 100×70×70 mm made of aluminum alloy AMG2M, with studs having internal thread M4 made of aluminum alloy AMG3, connected by spot-condensation welding [18].

Welding was performed using a C99 welding machine [19].

Number of specimens of each type is 9 pieces, a total of 18 pieces (Fig. 1)

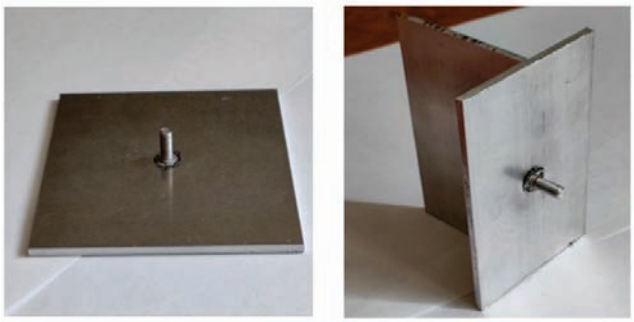


Figure 1. General view of tensile and shear test specimens

Joints were tested in tension under the action of a concentrated force perpendicular to the plane of the plates (type 1) and a concentrated force parallel to the plane of the taurus flange (type 2).

Tests were performed on an Instron 3382 universal testing machine in static loading mode [20].

For the tests, joint elements were fastened in specially designed equipment consisting of steel plates, high-strength bolts and rods, installed in the grips of the testing machine (Fig. 2).

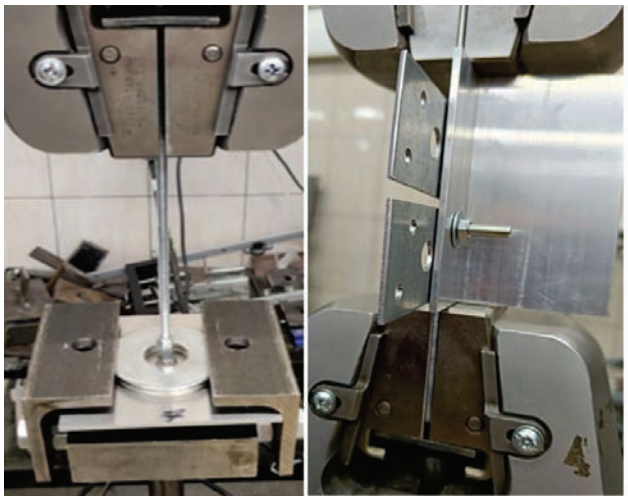


Figure 2. General view of the tensile and shear test of specimens installed in the testing machine

RESULTS AND DISCUSSION

Tensile tests

The tensile tests used a tensile force with control of the rate and magnitude of loading. In these tests, specimen fracture occurs solely by welding (Fig.3-4).

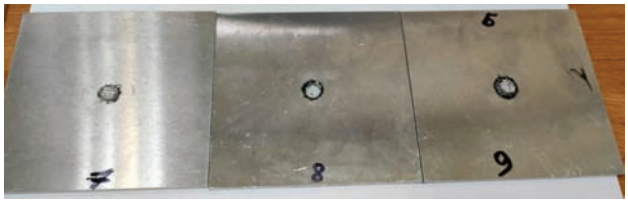


Figure 3. General view of specimens Type 1 after tensile test

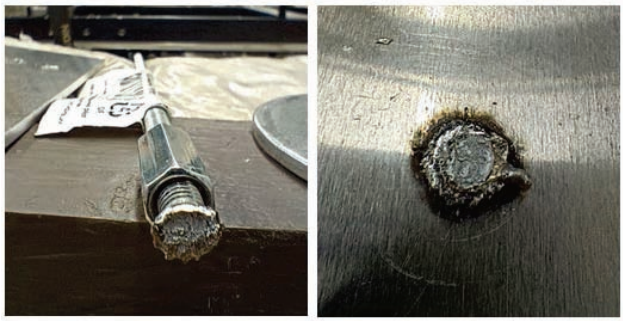


Figure 4. Type of destruction in the welded zone during tensile tests

In the course of loading, the axial load - longitudinal displacement relation was fixed by the recording unit of the Instron 3382 testing machine in the form of corresponding graphical diagrams (Fig. 5).

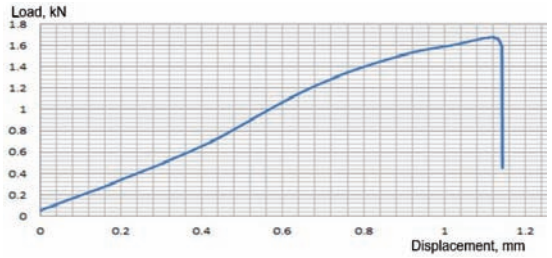


Figure 5. Diagram of displacements during the tensile test of the Type 1 sample

The results of the tensile tests are presented in Table 1. The estimation of the average obtained values of the ultimate load was made both without rejection and with rejection of the value for specimen No. 9 based on the condition of deviation from the average value by more than 50%.

Table 1. Destructive forces during tensile tests

Sample№	Maximal force, kN	Deviation from average value %	
		Before rejection	After rejection
1	1,68	-19	-17
2	2,32	13	14
3	1,75	-15	-14
4	1,63	-21	-20
*5	2,90	41	42
6	2,41	17	18
7	1,74	-16	-15
8	1,86	-10	-9
***9**	**0,74**	**-64**	**-**
Average value before rejection			**2,06**
Standard deviation			0.608
Coefficient of variation			32%
Average value after rejection			**2.04**
Standard deviation			0.457
Coefficient of variation			22%

* – samples subjected to rejection.

Shear tests

During shear testing of a batch of specimens, the failure of this type of connection occurred solely by welding (Fig. 6). In the course of specimen preparation for the test, the welded joint of specimen No. 8 failed before the test while manually tightening the tie rod fastening nut.



Figure 6. General view of Type 2 specimens after the shear tests

During loading, the relationship between the shear force and linear displacement in the shear plane was recorded in the form of appropriate graphical diagrams (Fig. 7).

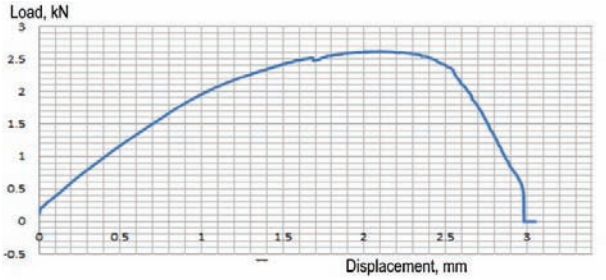


Figure 7. Displacement diagram when testing a type 2 sample on a shear

The results of the shear test are shown in Table 2.

Table 2. Destructive forces during shear tests

Sam-ple№	Maximal force, kN	Deviation from average value %	
		Before rejection	After rejection
1	14	26	14
2	-6	4	-6
3	-21	-12	-21
4	0,5	11	0,5
*5	5	15	5
6	-	-72	-
7	0,9	18	0,9
***8**	-	-	-
9	7	18	7
Average value before rejection			**2,08**
Standard deviation			0,608
Coefficient of variation			32%
Average value after rejection			**2,29**
Standard deviation			0,25
Coefficient of variation			11%

* – samples subjected to rejection.

Verification calculations

Tensile and shear calculations of two types of joints were performed in accordance with the provisions of normative document SP 128.13330.2016 "Aluminum structures".

Dimensions of the threaded rod M4 RT according to DIN EN ISO 13918 (Fig.8):

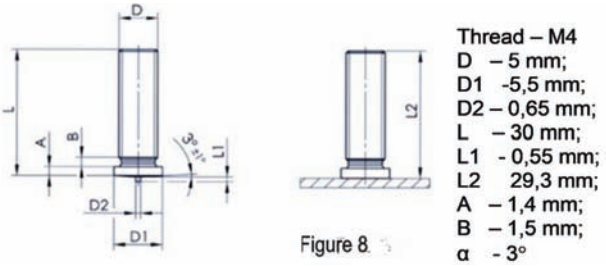


Figure 8

Diameter of welding zone (D_1+0,5 mm) D_w=6 mm.

Welding area:

$$A = \frac{\pi \cdot D_w^2}{4} = \frac{3{,}14 \cdot 6^2}{4} = 28{,}3\ mm^2.$$

The strength parameters of the aluminum alloys used in the tested assemblies are given in accordance with the current regulatory documents GOST 21631-2019 "Sheets of aluminium and aluminium alloys. Specifications", SP 128 and materials [17] with rounding to 5 MPa (Table 3).

Table 3. Strength parameters of aluminum alloys

Node element	Растяжение [МПа]		Сдвиг (срез) [МПа]	
	Yield strength $\sigma_{0,2}$	Maximum resistance $\sigma_в$	Yield strength $\tau_{0,2}$	Maximum resistance $\tau_в$
Plate АМГ2М	70	125	55	90
Threaded stud АМГ3	100	165	70	115

Tensile Calculation

Experimental values of normal tensile stresses (Table 4).

Table 4. Normal tensile stresses during tensile

Sample №	P (kN)	δP (%)	σ (Pa)	δσ (%)	$\delta\sigma_B$ (%)
1	1,68	-17	5,94E+07	-17	-26
2	2,32	14	8,20E+07	14	2
3	1,75	-14	6,18E+07	-14	-23
4	1,63	-20	5,76E+07	-20	-28
5	2,90	42	1,02E+08	42	28
6	2,41	18	8,52E+07	18	6
7	1,74	-15	6,15E+07	-15	-23
8	1,86	-9	6,57E+07	-9	-18
Average	**2,04**	**0**	**7,20E+07**	**0**	**-10**

Tension in the welding zone for the average value of the fracturing force *P*=2.04 kN:

$$\sigma = \frac{P}{A} = \frac{2{,}04 \cdot 10^3}{28{,}3 \cdot 10^{-6}} = 72 \cdot 10^6 = 72\ MPa \leq \sigma_B = 80\ MPa\ (\delta = -10\%).$$

Stress range at failure of 8 specimens:

σ=68,5÷122 MPa (deviation from σ_B –±28%)

Shear calculation

The experimental values of shear tangential stresses are presented in Table 5.

Table 5. Shear stresses during cutting

Sample №	P (kN)	δP (%)	τ (Pa)	δτ (%)	$\delta\tau_B$ (%)
1	2,61	14	9,22E+07	28	54
2	2,16	-6	7,63E+07	6	27
3	1,82	-21	6,43E+07	-11	7
4	2,3	0	8,13E+07	13	35
5	2,39	4	8,45E+07	17	41
6	2,31	1	8,16E+07	13	36
7	2,44	7	8,62E+07	20	44
Average	**2,29**	**0**	**8,09E+07**	**12**	**35**

Tangential stress in the welding area for the average value of the destructive force *P*=2.29 kN:

$$\tau = \frac{P}{A} = \frac{2{,}29 \cdot 10^3}{28{,}3 \cdot 10^{-6}} = 80{,}9 \cdot 10^6 = 80{,}9\ MPa > \tau_B = 55\ \text{МПа}\ MPa(35\%).$$

Stress range at failure of 7 specimens:

τ=64.3÷92.2 MPa (deviation from τ_B 7÷54%).

Conclusions on the results of tests and verification calculations

1. According to the test results, the failure of all specimens of types 1 and 2 occurred in the welded area.
2. Tensile fracture force of type 1 junction is within 1.68÷2.9 kN, the average value is 2.04 kN (Table 1).
3. The divergence of calculation results in tension with the experiment is satisfactory, lies in the range of -28÷+28%, from 59.4 MPa to 102 MPa, the average value is 72 MPa. The average deviation from the value of tensile strength of 80 MPa is -10% (Table 4).
4. Fracture force at shear for the joint of type 2 is in the range of 1,68÷2,9 kN, average value 2,29 kN. (table 2). During the preparation of type 2 specimens for shear tests, the effect of the tightening force on the strength of the welded joint was recorded. At the applied insignificant force the considerable decrease of fracturing load down to 0,57 kN (specimen No.6) and complete fracture of the weld (specimen No.8) took place.
5. The divergence of calculation results on a shear with experiment is more essential, than at a tension, and lies in the limits of 7÷54%, from 64,3 MPa to 92,2 MPa, average value of 80,9 MPa. The average deviation from the value of shear time resistance of 55 MPa is 35% (Table 5).
6. Significantly greater difference of the results of calculations for shear with the data of

experiments than for tensile is a consequence of more complex actual stress state when loading the joint with shear force, created by the construction of the joint, than in pure shear (shear). As a consequence, the values of fracturing tangential stresses for all the tested specimens noticeably exceed the calculated value for pure shear (shear), which goes into the joint strength reserve in the calculations of connections of this type by the normative method.

7. Reducing the dispersion of values of destructive loads and ensuring operational reliability of joints can be achieved in the process of their production when performing the following preparatory actions:

- stripping followed by de-greasing of the welded surfaces of the stud head and the plate area [22];
- control of the amount of preliminary pressing of the stud to the plate surface before the weld pulse [23,24].
- control loading of the manufactured assemblies with the force that exceeds the value of the planned operational load by 50%.

8. To ensure the strength of the nodes during installation and operation, it is necessary to provide a hinged connection of the stud with the loading rod to avoid the appearance of additional bending stresses that may occur at a rigid connection.

9. In order to guarantee compliance with the regulatory requirements of SP 128 to ensure the strength of aluminum alloy structures, the value of maximum load for both types of assemblies investigated should not exceed 1 kN (100 kg) per assembly. In this case, the requirements for preparation and quality control of manufacturing and installation of the assemblies shall be observed (clauses 6-7).

СПИСОК ЛИТЕРАТУРЫ

1. **Шавнев А.А., Курбаткина Е.И., Косолапов Д.В.** Методы соединения алюминиевых композиционных материалов (обзор) // Материалы и технологии, 2017, № 3 (48), стр. 35-42.
2. **Крылов Д.С., Назаров С.В.** Некоторые особенности аргонодуговой сварки алюминиево-магниевых сплавов // В сборнике: Актуальные проблемы авиации и космонавтики, Сборник материалов VI Международной научно-практической конференции, посвященной Дню космонавтики, в 3-х томах под общей редакцией Ю.Ю. Логинова, 2020, стр. 466-467.
3. **Drits A.M., Ovchinnikov V.V.** Weldability and properties of welds of high-strength aluminum alloys of the Al - Cu - Li system // Metal Science and Heat Treatment, 2012, V. 53, № 9-10, pp. 445-449.
4. **Овчинников В.В., Дриц А.М.** Сварка трением с перемешиванием алюминиевых сплавов с дополнительным охлаждением соединения // Электрометаллургия, 2021. № 10, стр. 2-14.
5. **Овчинников В.В., Березина В.А., Скакова Т.Ю.** Механические свойства соединений алюминиевых сплавов, выполненных сваркой трением с, при статическом и динамическом нагружении // Наукоемкие технологии в машиностроении, 2021, № 11 (125), стр. 20-29.
6. **Лаптев Е.А., Михайлицын С.В., Беляев А.И.** Сварка трением с перемешиванием алюминиевых сплавов // Актуальные проблемы современной науки, техники и образования, 2013, Т. 1, № 71.стр. 377-379.
7. **Drits A.M., Ovchinnikov V.V.** Properties of the joints of sheets of 1565ch alloy in combination with other aluminum alloys that were performed by friction welding with mixing // Russian Metallurgy (Metally), 2016, V. 2016, № 6, pp. 537-546.
8. **Amirov A.I., Beloborodov V.A., Ivanov A.N., Zhukov L.L.** Lap welded joint of aluminum and titanium alloy by friction stir welding // Collection of AIP Conference

Proceedings, Proceedings of the Advanced Materials with Hierarchical Structure for New Technologies and Reliable Structures, 2018, 020013.
9. **Милютин В.С., Близник М.Г. Катаев Р.Ф.** Теория и технология контактной сварки // Екатеринбург, изд-во Уральского университета, 2015, 255 стр.
10. **Маликов А.Г., Оришич А.М., Витошкин И.Е., Карпов Е.В., Анчаров А.И.** Лазерная сварка разнородных материалов на основе термически упрочняемых алюминиевых сплавов // Прикладная механика и техническая физика, 2021, Т. 62, № 5 (369), стр. 161-171.
11. **Wang Z., Shao X., Bu X., Oliveira J.P., Zeng Z., Peng B.** Laser beam oscillating welding of 5a06 aluminum alloys: microstructure, porosity and mechanical properties // Optics & Laser Technology, 2019, V. 11, pp. 58-65.
12. **Кучук А.В.,-Яценко С.И., Чвертко П.Н., Семёнов Л.А., Гущин К.В. Самотрясов С.М.,** Контактная стыковая сварка изделий из высокопрочных сплавов на основе алюминия // Автоматическая сварка, 2013, № 7 (723), стр. 3-7.
13. **Чвертко П.Н., Семенов Л.А., Гущин К.В.** Контактная стыковая сварка оплавлением тонкостенных профилей из термически упрочняемых алюминиевых сплавов // Автоматическая сварка, 2014, № 12 (738), стр. 37-40.
14. **Dimitrescu A., Alecusan A.M., Babiş C., Chivu O., Ungureanu L.** Alternative non-demountable assembly technologies for aluminium alloy // In collection of 18th International Multidisciplinary Scientific GeoConference SGEM 2018., Conference proceedings, 2018, pp. 17-24.
15. **Гуреева М.А., Грушко О.Е., Клочков Г.Г.** Исследование свойств сварных соединений алюминиевого сплава В1341, выполненных контактной точечной сваркой // Заготовительные производства в машиностроении. 2016, № 7, стр. 8-12.
16. **Hasan I.Kh., Pan'kin N.A., Kyashkin V.M.** Xrd study of the surface of aluminum alloy AK5M7 after electric-spark alloying // Letters about materials, 2021, V. 11. № 1 (41), pp. 84-89.
17. **НИЛ ИИМСК НИУ МГСУ** Технический отчет для АО «Русал ТД» «Разработка свода правил «Мосты с конструкциями из алюминиевых сплавов. Правила проектирования // НИУ МГСУ, Москва, 2020, 230 стр.
18. **Калеко Д.М.** Приварка стальных шпилек к алюминиевым листам // Автоматическая сварка, 2013, № 8 (724), стр. 38-42.
19. Аппарат для приварки шпилек методом конденсаторной сварки С99, http://mossklad.ru.
20. Универсальная электромеханическая машина Instron 3382, Руководство пользователя, Instron, USA, 2015, 235 стр.
21. **Анисимов А.Г., Ахмед С.М.** Экспериментальное исследование и численное моделирование метания алюминиевого образца для магнитно-импульсной сварки // Наука и инновации, 2022, № 3 (123), стр. 58-62.
22. **Максимов Н.Н., Сергеев В.Ю.** Совершенствование технологического процесса контактной сварки деталей из алюминиевых сплавов // Аллея науки, 2017, Т. 4, № 10, стр. 150-157.
23. **Андреева Л.П., Овчинников В.В., Сидоров А.А.** Оптимизация размеров точечных соединений при электроконтактной сварке алюминиевых сплавов // Современные материалы, техника и технологии, 2015, № 3 (3), стр. 23-32.
24. **Han L., Thornton M., Boomer D., Shergold M.** Effect of aluminium sheet surface conditions on feasibility and quality of resistance spot welding // Journal of Materials Processing Technology, 2010, V. 210, № 8, pp. 1076-1082.

REFERENCES

1. **Shavnev A.A., Kurbatkina E.I., Kosolapov D.V.** Methods of joining aluminum composite materials (review) // Materials and technologies, 2017, No. 3 (48), pp. 35-42.
2. **Krylov D.S., Nazarov S.V.** Some features of argon arc welding of aluminum-magnesium alloys // In the collection: Actual problems of aviation and cosmonautics, Collection of materials of the VI International Scientific and Practical Conference dedicated to the Day of Cosmonautics, in 3 volumes under the general editorship of Yu.Yu. Loginov, 2020, pp. 466-467.
3. **Drits A.M., Ovchinnikov V.V.** Weldability and properties of welds of high-strength aluminum alloys of the Al - Cu - Li system // Metal Science and Heat Treatment, 2012, V. 53, No. 9-10, p.p. 445-449.
4. **Ovchinnikov V.V., Drits A.M.** Welding friction with mixing of aluminum alloys with additional cooling of the joint // Electrometallurgy, 2021. No. 10, pp. 2-14.
5. **Ovchinnikov V.V., Berezina V.A., Skakova T.Y.** Mechanical properties of aluminum alloy joints made by friction welding with static and dynamic loading // High-tech technologies in mechanical engineering, 2021, No. 11 (125), pp. 20-29.
6. **Laptev E.A., Mikhailitsyn S.V., Belyaev A.I.** Friction welding with mixing of aluminum alloys // Actual problems of modern science, technology and education, 2013, Vol. 1, No. 71. pp. 377-379.
7. **Drits A.M., Ovchinnikov V.V.** Properties of the joints of sheets of 1565ch alloy in combination with other aluminum alloys that were performed by friction welding with mixing // Russian Metallurgy (Metally), 2016, V. 2016, № 6, p.p. 537-546.
8. **Amirov A.I., Beloborodov V.A., Ivanov A.N., Zhukov L.L.** Lap welded joint of aluminum and titanium alloy by friction stir welding // Collection of AIP Conference Proceedings, Proceedings of the Advanced Materials with Hierarchical Structure for New Technologies and Reliable Structures, 2018, 020013.
9. **Milyutin V.S., Bliznik M.G. Kataev R.F.** Theory and technology of contact welding // Yekaterinburg, Ural University Publishing House, 2015, 255 p.
10. **Malikov A.G., Orishich A.M., Vitoshkin I.E., Karpov E.V., Ancharov A.I.** Laser welding of heterogeneous materials based on thermally hardened aluminum alloys // Applied Mechanics and Technical Physics, 2021, Vol. 62, No. 5 (369), pp. 161-171.
11. **Wang Z., Shao X., Bu X., Oliveira J.P., Zeng Z., Peng B.** Laser beam oscillating welding of 5a06 aluminum alloys: microstructure, porosity and mechanical properties // Optics & Laser Technology, 2019, V. 11, p.p. 58-65.
12. **Kuchuk A.V., Yatsenko S.I., Chvertko P.N., Semenov L.A., Gushchin K.V., Sabotryasov S.M.** Contact butt welding of products made of high-strength alloys based on aluminum // Automatic welding, 2013, No. 7 (723), pp. 3-7.
13. **Chvertko P.N., Semenov L.A., Gushchin K.V.** Contact butt welding by melting thin-walled profiles from thermally hardened aluminum alloys // Automatic welding, 2014, No. 12 (738), pp. 37-40.
14. **Dimitrescu A., Alecusan A.M., Babiş C., Chivu O., Ungureanu L.** Alternative non-demountable assembly technologies for aluminum alloy // In collection of 18th International Multidisciplinary Scientific GeoConference SGEM 2018., Conference proceedings, 2018, pp. 17-24.
15. **Gureeva M.A., Grushko O.E., Klochkov G.G.** Investigation of the properties of welded joints of aluminum alloy B1341 made by contact spot welding // Procurement production in mechanical engineering. 2016, No. 7, pp. 8-12.
16. **Hasan I.Kh ., Pan'kin N.A., Kyashkin V.M.** Xrd study of the surface of aluminum alloy AK5M7 after electric-spark alloying //

Letters about materials, 2021, V. 11. No. 1 (41), pp. 84-89.
17. **NIL IIMSK NIU MGSU** Technical report for JSC Rusal TD "Development of a set of rules "Bridges with structures made of aluminum alloys. Design rules // NRU MGSU, Moscow, 2020, 230 p.
18. **Kaleko D.M.** Welding of steel studs to aluminum sheets // Automatic welding, 2013, No. 8 (724), pp. 38-42.
19. Apparatus for welding studs by condenser welding C99, http://mossklad.ru .
20. Universal electromechanical machine Instron 3382, User Manual, Instron, USA, 2015, 235 p.
21. **Anisimov A.G., Ahmed S.M.** Experimental investigation and numerical modeling of aluminum sample throwing for magnetic pulse welding // Nauka i innovatsii, 2022, No. 3 (123), pp. 58-62.
22. **Maksimov N.N., Sergeev V.Y**. Improving the technological process of contact welding of aluminum alloy parts // Alley of Science, 2017, Vol. 4, No. 10, pp. 150-157.
23. **Andreeva L.P., Ovchinnikov V.V., Sidorov A.A.** Optimization of point joint sizes during electric contact welding of aluminum alloys // Modern Materials, Technique and Technology, 2015, No. 3 (3), pp. 23-32.
24. **Han L., Thornton M., Boomer D., Shergold M.** Effect of aluminum sheet surface conditions on feasibility and quality of resistance spot welding // Journal of Materials Processing Technology, 2010, V. 210, No. 8, p.p. 1076-1082.

Korgin Andrey Valentinovich, Doctor of Technical Sciences, Professor, Professor of the Department of Testing Structures of the National Research Moscow State University of Civil Engineering (NRU MGSU), Moscow, 129337, Yaroslavskoye sh., 26, e-mail: korguine@mgsu.ru, anvakorg@gmail.com. tel. +7 495 183-54-29 (office) +7 985 765-46-38 (mobile) home. address: Moscow, 129110, 2nd Krestovsky lane, 4, sq. 96

Коргин Андрей Валентинович, Доктор технических наук, профессор, профессор кафедры испытаний сооружений Национального Исследовательского Московского Государственного Строительного Университета (НИУ МГСУ), Москва, 129337, Ярославское ш., д.26, e-mail: korguine@mgsu.ru, anvakorg@gmail.com. тел. +7 495 183-54-29 (раб.) +7 985 765-46-38 (моб.), дом. адрес: Москва, 129110, 2-й Крестовский пер., д.4, кв.96.

International Journal for Computational Civil and Structural Engineering, 19(2) 51–59 (2023)

DOI:10.22337/2587-9618-2023-19-2-51-59

SELECTION OF THE RATIONAL PARAMETERS OF THREE-LAYER REINFORCED CONCRETE STRUCTURES WITH MONOLITHIC BONDING LAYERS BY THE METHOD OF COMPUTER MODELING

Elena A. Korol, Yulia O. Kustikova

National Research Moscow State University of Civil Engineering, Moscow, RUSSIA

Abstract. For the selection of the rational physical, mechanical and geometric parameters of three-layer reinforced concrete structures with monolithic bonding layers, it is necessary to have numerous data on the stress field and patterns of their deformation upon loading, changes in the energy parameters of the strength of concrete and the thickness of the layers. The important condition for the analysis of the stress-strain state by computer simulation is verification with experimental studies. This research is a confirmation of the reliability of the partitioning of the model into finite elements, the choice of their size and configuration. Modeling of three-layered enclosing structures with overall dimensions of attic overlappings allows obtaining strains and deformations in the outer and middle layers at different levels of loads and performing their comparison with limiting values. Due to the high rigidity of the three-layered enclosing structures with a monolithic bond of the layers and the use of structural concrete in the outer layers, the strength of which is more than 10 times higher than that of the middle layer, there are no cracks in the operating loads. In order to recommend considering the stress-strain state, there are more dimensional three-layer coating plates with monolithically bonded layers with different geometric and strength parameters, with different degrees of reinforcement and levels.

Keywords: three-layer reinforced concrete structures, monolithic binding layers, computer modeling, deformations, stress-strain state, enclosing structures, concrete strength

ВЫБОР РАЦИОНАЛЬНЫХ ПАРАМЕТРОВ ТРЕХСЛОЙНЫХ ЖЕЛЕЗОБЕТОННЫХ КОНСТРУКЦИЙ С МОНОЛИТНЫМИ СВЯЗУЮЩИМИ СЛОЯМИ МЕТОДОМ КОМПЬЮТЕРНОГО МОДЕЛИРОВАНИЯ

Е.А. Король, Ю.О. Кустикова

Национальный исследовательский Московский государственный строительный университет (НИУ МГСУ); г. Москва, РОССИЯ

Аннотация. Для выбора рациональных физико-механических и геометрических параметров трехслойных железобетонных конструкций с монолитными связующими слоями необходимо располагать многочисленными данными о поле напряжений и закономерностях их деформации при нагружении, изменениях энергетических параметров прочности бетона и толщины слоев. Важным условием для анализа напряженно-деформированного состояния с помощью компьютерного моделирования является верификация экспериментальными исследованиями. Это исследование является подтверждением надежности разделения модели на конечные элементы, выбора их размера и конфигурации. Моделирование трехслойных ограждающих конструкций с учетом габаритных размеров чердачных перекрытий позволяет получать напряжения и деформационные сдвиги во внешнем и среднем слоях при разных уровнях нагрузок и проводить их сравнение с предельными значениями. Благодаря высокой жесткости трехслойных ограждающих конструкций с монолитным соединением слоев и использованию конструкционного бетона во внешних слоях, прочность которого более чем в 10 раз выше, чем у среднего слоя, при эксплуатационных нагрузках трещины отсутствуют. Для того чтобы рекомендовать учитывать напряженно-деформированное состояние, существуют пластины с трехслойным покрытием большего размера с мо-

нолитно соединенными слоями с различными геометрическими и прочностными параметрами, с разной степенью усиления и уровнями.

Ключевые слова: трехслойные железобетонные конструкции, монолитные связующие слои, компьютерное моделирование, деформации, напряженно-деформированное состояние, ограждающие конструкции, прочность бетона

1. INTRODUCTION

This research is aimed at studying the development of methods for calculating multi-layer reinforced concrete structures, that based on the use of the results of both experimental and theoretical studies, including computer modeling.
Multilayer structures consisting of materials with different physical and mechanical characteristics have a contact layer on the contact boundary, the influence of which on the construction of computational models has been investigated by numerical methods [1-7].
The experimental results reflect within the limits of the accuracy of the experiment the actual parameters of the stress-strain state of the structures and are associated with the correct development of physical models.
As shown by the theoretical and experimental studies, which were carried out earlier by the author [8-10], the stresses in the stretched zone of the investigated three-layer reinforced concrete structures under the operational load do not reach the ultimate tensile strength, therefore formation of cracks does not occur. This is the basis for accepting the work of concretes of the middle and outer layers of the structure under such elastic loads. However, when analyzing the results of model calculation, it is necessary to consider the ratio of the obtained values of tensile stresses for each layer of concrete and the corresponding design tensile strength. When these values approach or exceed the first one above the second one, it is necessary to correct the model taking into account the cracking.

2. MATERIALS AND METHODS

The cross-section of the investigated three-layer bending reinforced concrete structures consists of two types of concrete. Their outer layers are made of structural concrete of class B12.5 - B30, and the middle layer is made of structural and heat-insulating class B1.5 and less.
After preliminary analysis for further work, the ZSOIL software package developed by Zace Service Ltd. (Switzerland). The possibilities of this program are allowed to enter various material parameters without their mutual dependence. The program allows you to set the data and generate the grid CE in manual mode. This software allows the use of flat, isoparametric and subparametric finite elements of the second order.
To approximate a three-layer structure from different types of concrete with a monolithic bond of layers, as preliminary studies have shown, rectangular or triangular flat finite elements are most suitable. The dimensions of the final elements were correlated with the thickness of the layers of the structure, the smallest of which was 40 mm. In order to be able to compare the results of the simulation with the actual picture of the deformation of the tested three-layer reinforced concrete beam-type samples, the parameters of the layers of beam samples were taken for the first model [8] based on the results of previous experimental studies. In the first approximation, taking into account the rare arrangement of the reinforcement and the low percentage of reinforcement (up to 0.05%), the beam reinforcement was not taken into account in the calculation.
In the first version of the model, the three-layer construction was represented by rectangular finite elements - the lower and upper layers in one row, the middle one in the form of 4 rows of finite elements (Fig. 1, a).

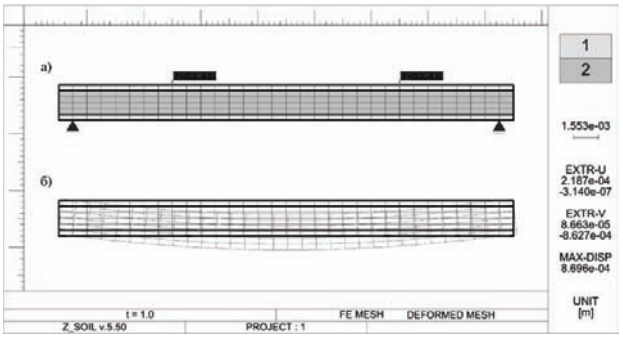


Figure 1. FE model of beam with rectangular grid: a) scheme for grid layout of FE model; b) beam deformations

The parameters of the finite elements (FE) and the characteristics of the concrete layers of the structure are given in Table 1.

Table 1

Construction layer	External	Internal
The size of rectangular elements, m	0,04×0, 10	0,0425×0, 10
Prismatic strength of concrete R_b, MPa	10,1	1,15
Strength of concrete for tensile strength R_{bt}, MPa	1,02	0,35
Initial modulus of elasticity E0, MPa	10400	950
Poisson's ratio ν = 0.00189 | R_b | + 0.12	0,139	0,122
The shear modulus G = E_0 / 2 (1 + ν), MPa	4570	423
Average density of concrete, kg / m3	1700	440

The results of the calculation for a load corresponding to the elastic stage of operation of a beam sample are shown in Fig. 1 and Fig. 2.
As the calculation results showed, the deflections of beam models correspond to the results of full-scale tests with an accuracy of up to 95%. The magnitudes of the principal stresses in the layers of the elements are also close to those experienced at the corresponding load levels. However, the direction of the main tensile and principal compressive stresses, shown in adjacent finite elements on opposite diagonals, somewhat distorts the true picture of the stress field. Therefore, the representation of the structural layers by rectangular finite elements with a length more than two times the height of the element is not convenient in deriving the calculation results in the form of principal stresses.

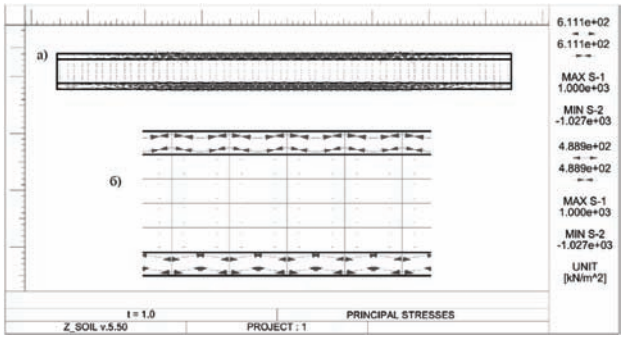


Figure 2. Pattern of the distribution of principal stresses in model 1
a) general diagram of the location of the principal stresses along the length of the beam;
b) enlarged fragment in the middle of the span

In the second model, the length of the rectangular finite elements is reduced to 0.05 m. Fig. 3 shows the main stresses in the middle of the beam model. With a decrease in the size of the final element by half, the overall picture of the stresses did not change, but the angle of inclination of the principal stresses decreased somewhat. Differences in stress level do not exceed 0.1% upwards.

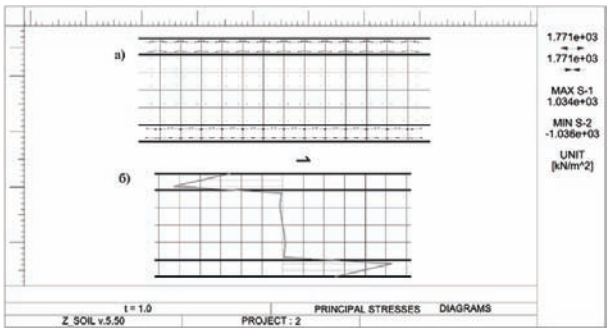


Figure 3. Stresses in the beam by model 2
a) enlarged fragment of the main stresses in the middle of the span;
b) diagram of normal stresses in the middle of the span

In the third model, the same construction is represented in the form of triangular finite elements (Figure 4), that is, each rectangular FE with a width of 0.1 m is replaced by four triangular elements, dividing it by diagonals. In this case, we obtain triangular FEs of two types-with the side of the parallel lines separating the layers (1a) and with the side perpendicular to these lines (1b).
The properties of the materials are taken from Table. 1. As the analysis shows (Fig. 4, Fig. 5), the transition to smaller triangular FEs clarifies the results downwards by about 1.3%. In this case, the diagram of normal stresses in the middle of the span of the beam completely corresponds to the experimental data.

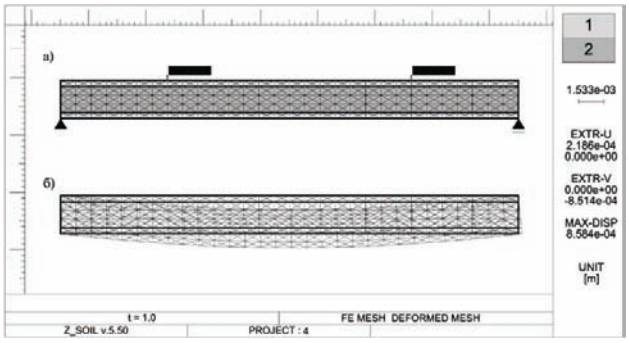


Figure 4. FE model of beam with triangular grid a) scheme for grid layout of FE model; b) beam deformations

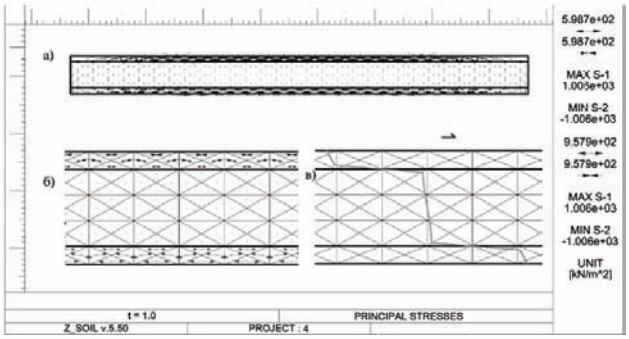


Figure 5. Stress distribution pattern in model 3 a) distribution of principal stresses along the length of the beam; b) enlarged fragment of principal stresses along the length of the beam; c) diagram of normal stresses in the middle section of the beam

The reliability of the model, when the beam is divided into triangular FEs, has a significant importance. Comparison of the calculation results with the experimental data on deflections, strain measurements along the direction of the main stresses in the middle of the span and on the landing areas gives a convergence in the range 95-97%.
In general, the analysis of the operation of the three-layer beam element model without longitudinal reinforcement shows that the bulk of the effort is assumed by the outer layers of the construction made of structural concrete, and in the middle layer of low strength concrete, the level of maximum stresses is lower by an average of 15 times. The destruction of the structure will occur starting with the outer layers, and on the average, a layer of internal destruction and excessive deformation is not observed.
In this research there is also well-considered issue, how the introduction into the stretched zone of the beam of longitudinal reinforcement will affect the operation of the layered structure. For this, in the middle of the height of the lower layer of the beam we arrange the reinforcement layer. In this case, for the possibility of comparing the results of the characteristics of reinforcement and concrete layers, we take as previous tests of beam samples [8] (Table 2).

Table 2

Construction layer	External	Internal
The size of rectangular elements, m	0,04×0,10 0,02×0,10	0,0425×0, 10
Prismatic strength of concrete R_b, MPa	21,0	1,01
Strength of concrete for tensile strength R_{bt}, MPa	1,75	0,28
Initial modulus of elasticity E0, MPa	12000	890
Poisson's ratio $\nu = 0.00189 \mid R_b \mid + 0.12$	0,16	0,122
The shear modulus $G = E_0 / 2 (1 + \nu)$, MPa	5172	397
Average density of concrete, kg / m3	1800	440
Modulus of elasticity of reinforcement, MPa	200000	

The reinforcement was adopted with a diameter of 8 mm in increments of 15 cm, the reinforcement percentage was 0.29%. The FE model grid and the results of the the loading of beam calculations are shown in Fig. 6 - 8.

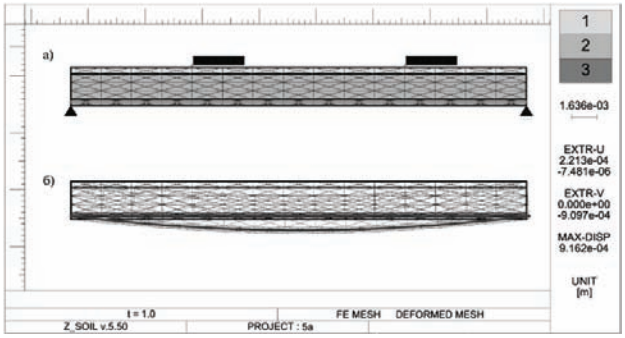


Figure 6. Model of a beam with longitudinal reinforcement
a) scheme of grid layout of the FE model 4;
b) deformation of the beam

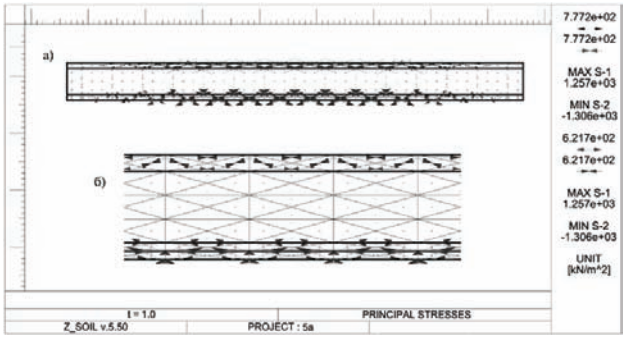


Figure 7. Pattern of the distribution of principal stresses in a model with longitudinal reinforcement: a) distribution of principal stresses in the model; b) enlarged fragment of principal stresses

As shown by the calculation results, the deflections of the models of beam samples (Fig. 6) correspond to the results of the tests with an accuracy of up to 96%, the deformations in the middle layer of the beam near the supports (Fig. 8b) are also close to those experienced at this stage of loading. The effect of reinforcement on the operation of such rigid beams at such a low percentage of reinforcement (0.29%) is very slight. The difference in the absolute values of the boundary compressive and tensile stresses in the considered models without reinforcement is from 0 to 0.3%, and in the reinforced sample this difference amounts to 3.75%.

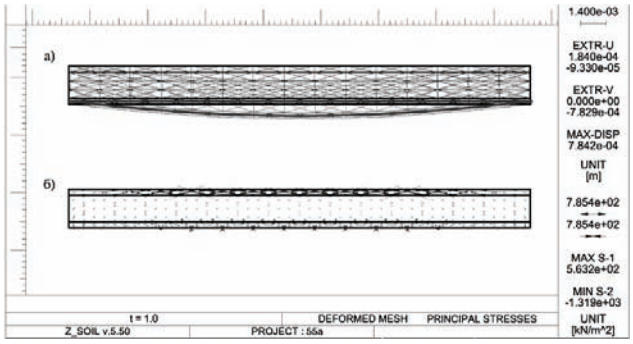


Figure 8. The field of distribution of the relative deformations of concrete in the beam of model 4
a) along the length of the beam; b) enlarged fragment near the support

In this study the following model of the effect of increasing the degree of reinforcement on the work of a three-layer structure was considered. With an increase in the percentage of reinforcement to 3% and a decrease in the strength of the concrete of the outer layers to the value indicated in Table. 1, the stress field in concrete changes and the reinforcement will have a significant effect on the design work (Figure 9). The main tensile stresses in the lower zone of the beams in the middle of the span are below the boundary compressive stresses by 57.3%.

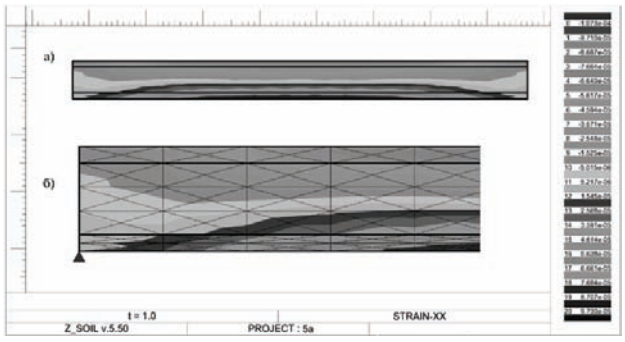


Figure 9. Beam model with an increased percentage of reinforcement
a) deformation of the beam; b) distribution of principal stresses

Comparison of the results of experimental studies of three-layer beam elements with their models developed with the help of the ZSOIL

software complex showed that it is possible to reproduce with sufficient accuracy the modeling of the operation of a multilayer element using plane triangular cells with dimensions close to the thickness of the layers.

3. RESULTS

In the practice important means has studying the work of the slabs and attic overlaps of a three-layer structure with a monolithic bond of layers: a slab of a 6.0 m length and a thickness of 50 cm with external layers of structural concrete 8 and 4 cm thick and a medium layer of low strength concrete - 38 cm; minimum allowable reinforcement level of 0.05% (a reinforcement with a diameter of 8 mm step of 15 cm). The total calculated value of the uniformly distributed load from the roof mass and the temporary snow load is 2.2 kN / m^2.

The model with the bottom layer of concrete 8 cm thick is divided in height into two rows of FE - 2 cm and 6 cm, reinforcement is provided between layers 2 cm and 6 cm thick, was composed in this researching. Further, the middle layer of 38 cm thick is represented by three rows of FE with a height of 5.6 cm. The upper layer 4 cm thick is single-row. The length of the element is divided into 15 sections, i.e., the maximum length of the FE is 20 cm. The FEs are triangular (Fig. 9 and Fig.10).

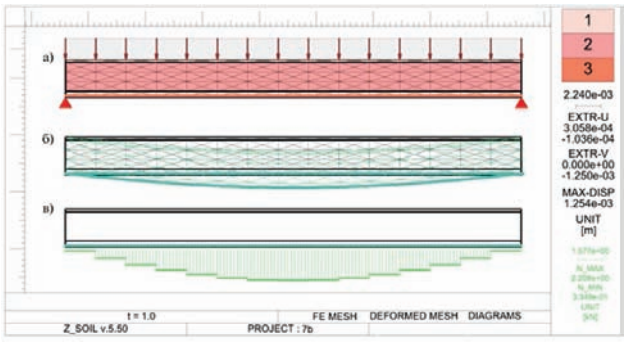


Figure 10. Model of a plate of a covering: a) scheme of splitting on final elements; b) deformation of the plate; c) diagram of the distribution of longitudinal forces in the reinforcement

Deflections, the pattern of distribution of principal stresses, the diagram of normal stresses and also the distribution fields of normal stresses and relative deformations of concrete are shown in Fig. 10 – 12. The maximum vertical deflection of the structure was 0.125 cm. As can be seen in Fig. 11, at such value of ratio of the layers thickness, the tensile force in the middle layer practically does not arise.

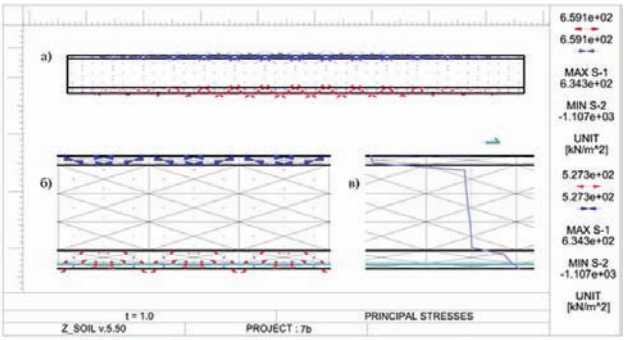


Figure 11. The pattern of stress distribution in the plate model: a) the main stresses along the length of the plate; b) enlarged fragment of principal stresses; c) diagram of normal stresses in the middle section of the plate

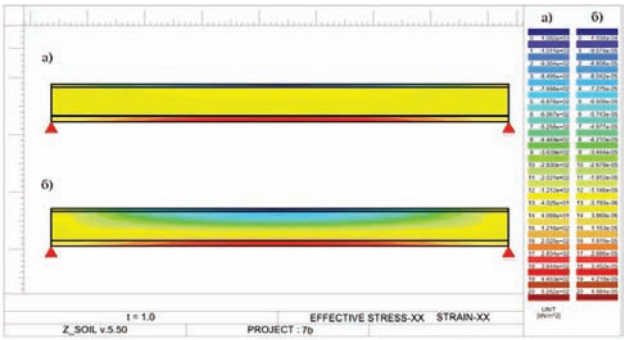


Figure 12. distribution of stresses and strains in the model plate: a) field distribution of normal stresses in the plate; b) field of distribution of the relative deformations

In addition, the cross section in the middle of the span of the plate was considered. In the 5 upper triangular cells of the cross-section 1, normal compressive stresses of the level of 0.086-0.012 MPa (at Rb = 1.15 MPa) act in the middle of the slab of the structural concrete layer; and only in the lower FE there is an insignif-

icant stretching of 0.022 MPa (at Rbt = 0.35 MPa). Such a distribution of efforts will positively affect the reliability of the work of such a design. Efforts in the outer layers of the plate are as follows: in the stretched zone 0.259-0.526 MPa (at Rbt = 1.02 MPa); in the compressed zone 0,96 - 1,1 MPa (at Rb = 10,1 MPa).

The stress diagram for the reinforcement, shown in Fig. 10, shows that the effect of reinforcement due to the rigidity of the structure is insignificant, since at the design load the ratio of the maximum force in the armature (2.2 kN) to the design (18.34 kN) is 12%.

As the calculation of the design model with the dimensions of the offered full-scale plates has shown, the concrete of the middle layer of such boards will experience compressive stresses of 85% of the thickness that do not exceed 8% of the prismatic strength of concrete, while the remaining part exhibits insignificant tensile stresses that do not exceed 6% of the tensile strength of the concrete.

4. CONCLUSIONS

The well convergence of the experimental and calculated results makes it possible to recommend considering the stress-strain state of large-sized layered slabs with different thicknesses of monolithically bonded layers at different reinforcement levels and loading levels on the recommended finite element models.

The use of modern calculating software on the basis of the finite element method (FE) makes it possible to simulate the stress-strain state of a reinforced layered structure with monolithically bonded layers. It is recommended to use flat triangular cells with dimensions close to the thickness of the layers.

The analysis of the operation of three-layer beam structures shows that the middle layer of low-strength concrete undergoes insignificant stresses, which are close to the operational ones, 5-10% of the design tensile strength of concrete, which confirms the rational layout of the section from the point of view of the stress-strain state,

These researches with application of a computer modeling method allow to vary in a wide range by changing the design parameters (thickness of layers, strength properties of concrete, types of reinforcement and the degree of reinforcement) and, ultimately, to choose a rational design solution.

REFERENCES

1. **Andreev V.I., Barmenkova E.V., Matveeva A.V.** The Stress State in Inhomogeneous Elastic Beam at Combined Strength // Applied Mechanics and Materials. 2014. Vols. 501-504. pp. 645-648.
2. **Andreev V.I., Barmenkova E.V**. The modeling of the real building objects by using the model of a two-layer beam of variable rigidity on an elastic basis // Applied Mechanics and Materials. 2012. Vols. 204-208. pp. 3596-3599.
3. **Vladimir I. Andreev, Robert A.** Turusov, Nikita Yu. Tsybin Application of the Contact Layer in the Solution of the Problem of Bending the Multilayer Beam // Procedia Engineering, Volume 153, 2016, Pages 59-65.
4. **Vladimir I. Andreev, Elena V. Barmenkova, Ivan A. Potekhin.** Way of Optimization of Stress State of Elements of Concrete Structures. Procedia Engineering, Volume 153, 2016, Pages 37-44.
5. **Vladimir Andreev, Robert Turusov and Nikita Tsybin.** The edge effects in layered beams //FORM 2018 IOP Conf. Series: Materials Science and Engineering 365 (2018) 042049
6. **Andreev V.I., Turusov R.A.** The contact layer method in the problem of bending of a multilayer beam. Fourier series solution: 2nd International Conference on Mechanics, Materials and Structural Engineering (ICMMSE 2017).
7. **Elena Korol, Vu Dinh Tho and Yuliya Kustikova**. Model of stressed-strained state of multi-layered reinforced concrete struc-

ture with the use of composite reinforcement IOP Conference Series: Materials Science and Engineering, Volume 365, Reliability Of Buildings And Constructions.
8. **Korol E.A.** Three-layer enclosing reinforced concrete structures made of lightweight concrete and features of their calculation. M., ASV, (2001)
9. **Bujnak I., Korol E. A., Latushkin V. E.** Design model from three-layer composite reinforcement of reinforced concrete structures. Communication, T. 14, № 1, P. 101-105 (2012)
10. **Korol E. A. and Kharkin Yu. A.** To the question of choosing a software package for modeling the stress-strain state of three-layer reinforced concrete elements and structures with a monolithic bond of layers. Scientific and technical journal on construction and architecture (The Bulletin of MGSU). № 3. p156-163 (2010)
11. **Korol E. A., Pugach E. M. and Kharkinua A.** The influence of technological factors on the formation of communication layers of multi-layered enclosing structures. Scientific and technical journal on construction and architecture (The Bulletin of MGSU). № 3. p67-75 (2014)
12. **Korol E.A.** Deformation model for calculating three-layer reinforced concrete elements. News of higher educational institutions. Bulletin of MGSU. № 5. p11 (2004).
13. **Korol E.A.** and Kharkin Yu. A. Investigation of stress-strain state of three-layer reinforced concrete elements and monolithic section constructions by computer simulation Bulletin of MGSU. 117-120 (2010)
14. **Korol E.A.** Analysis the operating conditions of the polystyrene in the middle of three layer structures // Loaf. No 2.- P. 5-7 (2000)

СПИСОК ЛИТЕРАТУРЫ

1. **Andreev V.I., Barmenkova E.V., Matveeva A.V.** The Stress State in Inhomogeneous Elastic Beam at Combined Strength // Applied Mechanics and Materials. 2014. Vols. 501-504. pp. 645-648.
2. **Andreev V.I., Barmenkova E.V**. The modeling of the real building objects by using the model of a two-layer beam of variable rigidity on an elastic basis // Applied Mechanics and Materials. 2012. Vols. 204-208. pp. 3596-3599.
3. **Vladimir I. Andreev, Robert A.** Turusov, Nikita Yu. Tsybin Application of the Contact Layer in the Solution of the Problem of Bending the Multilayer Beam // Procedia Engineering, Volume 153, 2016, Pages 59-65.
4. **Vladimir I. Andreev, Elena V. Barmenkova, Ivan A. Potekhin.** Way of Optimization of Stress State of Elements of Concrete Structures. Procedia Engineering, Volume 153, 2016, Pages 37-44.
5. **Vladimir Andreev, Robert Turusov and Nikita Tsybin.** The edge effects in layered beams //FORM 2018 IOP Conf. Series: Materials Science and Engineering 365 (2018) 042049
6. **Andreev V.I., Turusov R.A.** The contact layer method in the problem of bending of a multilayer beam. Fourier series solution: 2nd International Conference on Mechanics, Materials and Structural Engineering (ICMMSE 2017).
7. **Elena Korol, Vu Dinh Tho and Yuliya Kustikova**. Model of stressed-strained state of multi-layered reinforced concrete structure with the use of composite reinforcement IOP Conference Series: Materials Science and Engineering, Volume 365, Reliability Of Buildings And Constructions.
8. **Korol E.A.** Three-layer enclosing reinforced concrete structures made of lightweight concrete and features of their calculation. M., ASV, (2001)
9. **Bujnak I., Korol E. A., Latushkin V. E.** Design model from three-layer composite reinforcement of reinforced concrete structures. Communication, T. 14, № 1, P. 101-105 (2012)

10. **Korol E. A. and Kharkin Yu. A.** To the question of choosing a software package for modeling the stress-strain state of three-layer reinforced concrete elements and structures with a monolithic bond of layers. Scientific and technical journal on construction and architecture (The Bulletin of MGSU). № 3. p156-163 (2010)
11. **Korol E. A., Pugach E. M. and Kharkinua A.** The influence of technological factors on the formation of communication layers of multi-layered enclosing structures. Scientific and technical journal on construction and architecture (The Bulletin of MGSU). № 3. p67-75 (2014)
12. **Korol E.A.** Deformation model for calculating three-layer reinforced concrete elements. News of higher educational institutions. Bulletin of MGSU. № 5. p11 (2004).
13. **Korol E.A.** and Kharkin Yu. A. Investigation of stress-strain state of three-layer reinforced concrete elements and monolithic section constructions by computer simulation Bulletin of MGSU. 117-120 (2010)
14. **Korol E.A.** Analysis the operating conditions of the polystyrene in the middle of three layer structures // Loaf. No 2.- P. 5-7 (2000)

Elena A. Korol – Doctor of Technical Sciences, Professor, Head of the Department of Housing and Communal Utility; Moscow State University of Civil Engineering (National Research University) (MGSU); 26 Yaroslavskoe shosse, Moscow, 129337, Russian Federation; professorkorol@mail.ru.

Kustikova Yulia Olegovna – Candidate of Technical Sciences, Associate Professor, Associate Professor of the Department of Housing and Communal Complex, National Research Moscow State University of Civil Engineering (National Research University MGSU); 26 Yaroslavskoe shosse, Moscow, e-mail: KustukovaYO@mgsu.ru, 8(926)179-20-74.

Елена Анатольевна Король – доктор технических наук, профессор, заведующая кафедрой жилищно-коммунального комплекса; Национальный исследовательский Московский государственный строительный университет (НИУ МГСУ); 129337, г. Москва, Ярославское шоссе, д. 26; professorkorol@mail.ru.

Кустикова Юлия Олеговна – кандидат технических наук, доцент, доцент кафедры Жилищно-коммунальный комплекс, Национальный исследовательский Московский государственный строительный университет (НИУ МГСУ) ; 129337, г. Москва, Ярославское шоссе, д. 26; e-mail: KustukovaYO@mgsu.ru, 8(926)179-20-74.

DOI:10.22337/2587-9618-2023-19-2-60-70

RESONANT VORTEX EXCITATION OF HIGH-RISE STRUCTURES

Anastasia I. Karakozova, Vladimir L. Mondrus

National Research Moscow State University of Civil Engineering, Moscow, RUSSIA

Abstract. Subject of the research: Today, the design of flexible, extended in length and height structures of transport, industry, communication is one of the important directions of construction development. Such structures include continuous extended metal constructions such as chimneys, poles, billboards, monuments, bridges, pipelines. Besides ensuring the limit states for strength and deformability, there is another important condition for the durable operation of metal structures which is the absence of aerodynamic instability phenomena (mainly wind resonance) during the whole service life. Objectives: Review of the background, analysis of accidents that have occurred, proposals to avoid such situations at the design stage and in the occurrence of emergency conditions at existing facilities. Materials and methods: Review and analysis of existing data and proposals for further improvement of calculation and design methods. Results: The paper analyzes the mechanisms of the main types of aerodynamic instability (wind resonance, flutter, galloping, oscillations in the airfoil) on different types of structures, presents particular cases of the history of famous unique constructions and the authors' calculation practice, describes the ways to avoid this type of phenomena in the design of new buildings or in emergency situations on existing structures. Conclusions: The phenomena described in the article are applicable to an extremely narrow area of construction and are often ignored in calculation and design. This article is intended to draw special attention to these phenomena not only for designers, but also for research engineers in order to create new mechanisms for their analysis.

Keywords: high-rise metal structures, wind resonance, galloping, flutter, wind loads, vortex excitation, aerodynamic wake, towers, masts, ice load, chimneys, unique structures

О РЕЗОНАНСНОМ ВИХРЕВОМ ВОЗБУЖДЕНИИ ВЫСОТНЫХ СООРУЖЕНИЙ

А.И. Каракозова, В.Л. Мондрус

Национальный исследовательский Московский государственный строительный университет, г. Москва, РОССИЯ

Аннотация: Предмет исследования: Проектирование гибких, протяженных в длину и высоту сооружений, для нужд транспорта, промышленности, связи является одним из важных направлений развития строительства на сегодняшний день. К таким сооружениям относятся сплошностенчатые протяженные металлические конструкции – дымовые трубы, столбы, рекламные щиты, монументы, мосты, трубопроводы. Помимо обеспечения предельных состояний по прочности и деформативности, для долговечной эксплуатации металлических конструкций существует еще одно важное условие - невозникновение явлений аэродинамической неустойчивости (главным образом, ветрового резонанса) на протяжении всего срока службы. Цели: Обзор истории вопроса, анализ имевших место аварийных ситуаций, предложения по избежанию подобных ситуаций на этапе проектирования и при возникновении аварийных состояний на существующих объектах. Материалы и методы: Обзор и анализ существующих данных и предложения по дальнейшему совершенствованию методик расчета и проектирования. Результаты: В статье проанализированы механизмы возникновения основных видов аэродинамической неустойчивости (ветровой резонанс, флаттер, галопирование, колебания в аэродинамическом следе) на разных видах конструкций, приведены частные случаи из истории строительства известных уникальных сооружений и расчетной практики авторов, описаны способы избежания данного типа явлений при проектировании новых сооружений или при возникновении аварийных ситуаций на существующих конструкциях. Выводы: Явления, описанные в статье, применимы к крайне узкой области строительного производства и часто игнорируются при расчете и проектировании. Данная статья призвана обратить на эти явления особое внимание не только проектировщиков, но и инженеров-исследователей для создания новых механизмов их анализа.

Ключевые слова: высотные металлические сооружения, ветровой резонанс, галопирование, флаттер, ветровые нагрузки, вихревое возбуждение, аэродинамический след, башни, мачты, гололедная нагрузка, дымовые трубы, уникальные сооружения

INTRODUCTION

High-rise structures due to their design features (length in height and small size in the plan) are most susceptible to wind loads, which increase in proportion to the distance from the ground. Bridge structures and pipelines extended in length, which are also flexible structures with low structural damping, should not be neglected. Seismic loads can also have a significant impact if the structure is located in an earthquake-prone area [1], however, in this work we focus mainly on the wind effects. In addition to ensuring the limit states for strength and deformability, there is another important condition for the durable operation of metal structures that is the non-occurrence of aerodynamic instability phenomena (mainly wind resonance) throughout the service life. In the article the mechanisms of the appearance of the main kinds of aerodynamic instability (wind resonance, flutter, galloping, and oscillations in the aerodynamic trace) are analyzed. The special cases of the well-known unique constructions construction history and the authors' calculation practice are adduced and the ways to avoid this type of phenomena at the designing of new structures or occurrence of emergency situations at the existing constructions are described.

LITERATURE REVIEW

High solid-wall steel structures became widespread in the middle of the last century. To analyze their performance and refine the calculation methods, experimental data of blowing down structural models in wind tunnels were used [2, 3]. The main place for testing in those years was the TsAGI wind tunnel. Only in the beginning of this century wind tunnels began to appear in scientific and educational institutes (in particular, in Scientific and Research Institute of Moscow State University of Civil Engineering). Parallel to the development of experimental studies, mathematical modeling has been actively developed: modern program complexes (Ansys, Nastran) allow modeling any building objects in their interaction with the wind flow [4, 5, 6]. Simulation (experimental, numerical) is an integral part of design of unique, technically complex objects. An important role is still given to numerical simulation methods, experiments on existing structures as it allows corrections and clarifications to regulatory documents, according to which typical objects are designed [7-11].

MATERIALS AND METHODS

It is known that the wind load has a static (average) and dynamic (pulsation) component. And, if the average component is fully enough described in the regulatory documents (SP[1]), the dynamic component, although considered in the standards (SP[1]), is still a subject of research and debate. In terms of mechanics, the wind load is represented as a system of forces that cause dynamic oscillations. Classical mechanics gives a strict and clear, widely known solution of this problem [12], as well as the definition of "resonance" as the coincidence of natural frequency of vibrations of the structure and the frequency of oscillations of the driving load (in our case wind load). The materials, of which the structures are made, have different degrees of susceptibility to the phenomenon of resonance, which is described by the logarithmic damping decrement δ [13] (as the logarithm of the ratio of two neighboring amplitudes of vibrations y_i):

$$\delta = \ln \frac{y_n}{y_{n+1}} = nT_1, \qquad (1)$$

where n is the damping coefficient, T_1 is the damped period.

The value of the logarithmic decrement is used in paragraph 11.1.10 (SP[1]) to calculate the dynamic amplification factor for the pulsation component of wind load and is adopted as in the Table 1.

[1] SP 20.13330.2018 Loads and Actions

Table 1. Logarithmic decrement for different materials

Material	decrement of damping
Reinforced concrete and masonry structures, including those with a steel frame	0.3
Glass, steel and reinforced concrete structures	0.22
Steel structures, lined chimneys	0.15

As can be seen from Table 1, the steel structures have the smallest logarithmic decrement. This means that, being taken out of equilibrium state, they can perform long-term oscillations, the decay of which can occur extremely slowly and lead to an emergency situation [14, 15].

Let's consider further the peculiarities of aerodynamic instability in high-rise (extended) flexible structures and ways to combat the phenomena of aerodynamic instability.

Such forms of aerodynamic instability as flutter, galloping, vortex excitation, oscillations in the aerodynamic trace are inherent to flexible structures.

Vortex excitation (wind resonance) is an intensive increase in the amplitudes of aero elastic vibrations of the structure across the wind flow [16].

Self-excited oscillations (self-oscillations) are undamped oscillations, which are maintained by energy sources that do not have oscillatory properties, such as a uniform wind flow. They can be observed when one of the natural frequencies of the structure coincides with the frequency of Karman vortices, which alternately bounce off the surface of the elements [16].

$$\lambda_e = \frac{l}{d} \tag{2}$$

where l is the height of a facility, d is the minimum cross-sectional dimension;

If the ratio of the dimensions of the solid-wall structure having the form (2) is λ_e>20, then one should perform the check for the possibility of resonant vortex excitation according to Section 11.3 (SP[2]). The critical wind velocities $V_{cr.i}$, m/s, at which resonant vortex excitation by the i^{th} eigenform of vibration occurs, are determined by the formula

$$V_{cr.i} = \frac{k_V f_i d}{St} \tag{3}$$

where f_i, Hz, is the eigenfrequency of the i^{th} bending eigenform; d, m, is the cross-sectional dimension of the structure; St is the Struhal number of cross-section, determined experimentally or by reference data; for circular cross-sections St = 0.2; for sections with sharp edges (including rectangular sections) it is St = 0.11. The coefficient k_v takes account of the effect of capturing the natural frequency of oscillations. It is assumed to be 0.9...1.1 from the condition of realization of the worst variant of loading.

Then, comparison of speeds is performed: critical wind speed for the considered structure (3) and maximum wind speed for the given area $V_{max}(z_{eq})$ at the equivalent height z_{eq}.

$$V_{\max} = 1{,}5\sqrt{w_0 k\left(z_{эк}\right)} \tag{4}$$

where w_0 is the characteristic wind pressure, and $k(z_{эк})$ is the coefficient of wind pressure variation by height (11.1.4 and 11.1.6 SP).

Resonant vortex excitation does not occur if

$$V_{cr.i} > V_{\max} \tag{5}$$

If condition (5) is not satisfied, then various measures are taken, which will be discussed below.

The most typical is vortex excitation for structures with circular cross section. In a certain flow velocity range, the vortex trace behind such profiles takes the form of the so-called Karman track which is a double row of

[2] SP 20.13330.2018 Loads and Actions

point vortices with a staggered arrangement [16], [17] (Fig. 1).

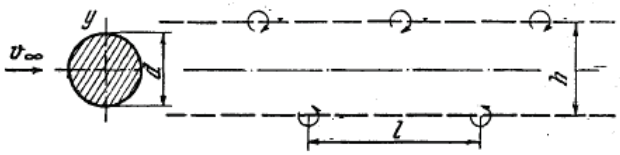


Figure 1. Karman vortex track.
d is the size of the cross section, l, h are the step and width of the track.

The frequency of Karman vortex formation is proportional to the velocity of the incoming flow V and inversely proportional to the cross-sectional size d:

$$\omega_k = \frac{V}{d} St \tag{6}$$

with the coefficient of proportionality (Struhal number St), depending on the shape of the profile.

High-rise solid-wall metal structures most susceptible to wind resonance are chimneys and stacks (Fig. 2).



(a) A chimney in a cage



(b) chimneys connected by platforms



(c) chimney with interceptors

Figure 2. Metal chimneys

When designing this type of structures, checking for wind resonance is an obligatory stage of calculation [19, 20]. Contrary to popular belief, the presence of cage (Fig. 2, a) has no effect on wind resonance and comes from technical necessity. Interceptors (Fig. 2, c) help to reduce the value of vortex formation, but cannot prevent resonance. A special difficulty is represented by chimneys arranged in a row (Fig. 2, b) (this case of aerodynamic instability will be considered below). Pillars with height of 20-50 m (Fig. 3) are used for placement of antenna equipment along with towers and masts [14], [15] when there is no necessity of antenna arrangement at high height (for comparison, standard height of lattice towers is 20-100 m). Despite of small height there is also a danger of occurrence of wind resonance for them.

Consider also other types of aerodynamic instability.

Galloping is the self-excited oscillations of flexible structures in the direction across the wind flow. The basis of the galloping process is the following phenomenon: the transverse motion of the body leads to the fact that the resultant relative velocity of the flow on the

body is oriented at an angle to the original position of the flow vector, i.e. the effect of changing the angle of attack and there is a negative aerodynamic damping. As soon as it becomes larger than the normal damping (and this circumstance is indicated by Scruton number Sc). The process becomes unstable and galloping oscillations occur [4].

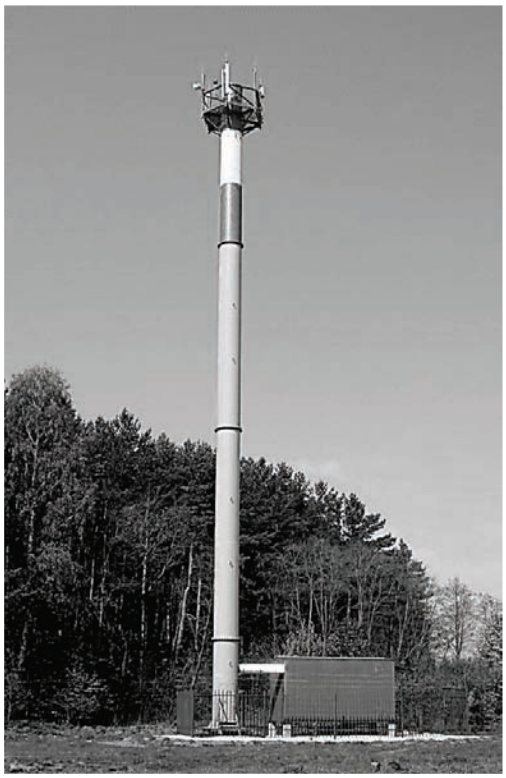


Figure 3. The pole with a height of 35 m

Galloping does not occur in the elements of circular cross section, since the angle of attack does not affect the aerodynamic coefficient, and is inherent in the sections of L-, I-, U-, T-shaped profile. However, this term is very often applied to wires with circular cross-section: galloping or "dancing" of wires. It is explained as follows: during the cold season, icing of wires (Fig.4), ice changes the shape of the cross-section (Fig.5), and at a certain initial wind speed the oscillations of galloping occur. The amplitudes increase rapidly with increasing wind speed and reach tens of cross-sectional body sizes. A similar effect of ice can have on mast structures of great height (Fig.6).



Figure 4. Ice on wires



Figure 5. Possible forms of ice deposits on wires

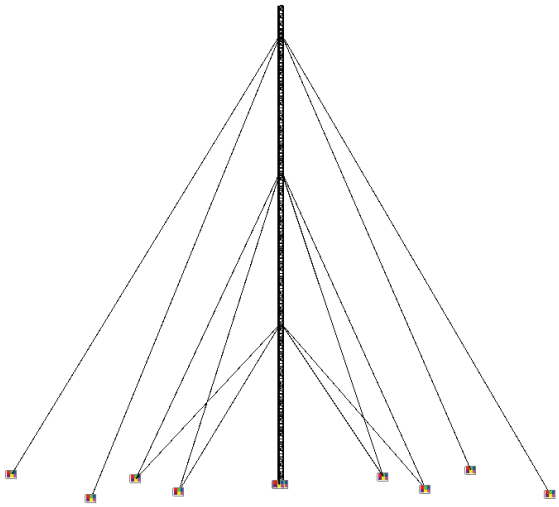


Figure 6. Calculation scheme of a mast structure in SCAD Software

Flutter is an instability that can occur for flexible plate or box structures. A change in the angle of attack in this case causes the profile to twist (disruptive flutter) or to twist together with a displacement across the flow (classical flexural-torsional flutter). A widely known case of flexural-torsional flutter resulted in the collapse of the Tacoma Bridge on November 7, 1940 (Figure 7) [16].

An example of high-rise structures capable of experiencing flutter are billboards and road signs (Fig.6).

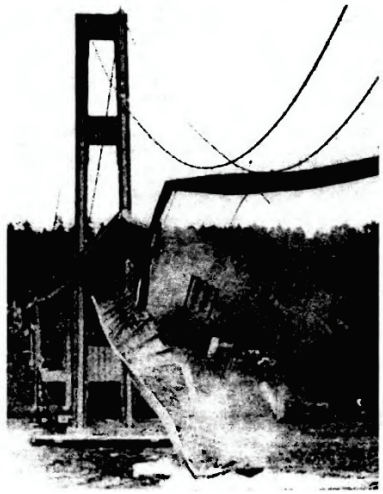


Figure 7. Collapse of the Tacoma Bridge

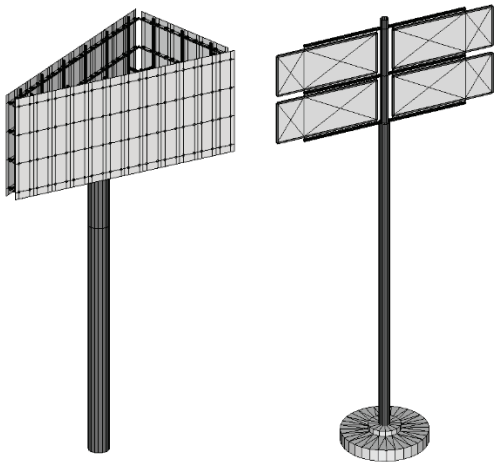
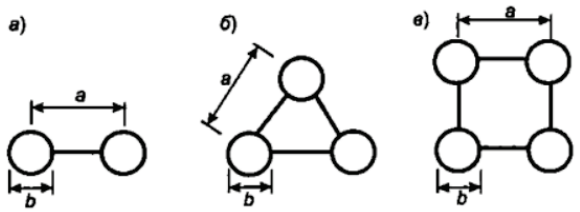


Figure 8. Billboards. Calculation scheme in SCAD Software.

Flexible structures or structural elements, such as trunks or cables, may be arranged in a row or group, may or may not stand in pairs. This leads to the excitation of self-oscillations in the aerodynamic trace. Depending on the a/b ratio (Figure 9), vortex resonance or interferential galloping can occur. Interferential galloping can be excited if two or more cylinders are close to each other without coupling [16].



a) b) c)

Figure 9. Arrangement of cylinders in a row or as a group

Flexible structures or structural elements, such as trunks or cables, may be arranged in rows or groups, may or may not stand in pairs

In addition to structures for industrial purposes, special attention in terms of the occurrence of vibrations such as wind resonance should be paid to monuments. Thus, during the construction and operation of several famous domestic monuments accidents occurred because of wind resonance.

The highest and most technically complex in Russia, the Victory Monument is located in the Victory Park in Moscow (Fig. 10). It has a height of 141.8 m and was designed and erected in the shortest possible time for the 50th anniversary of the Victory in the Great Patriotic War [18-21].

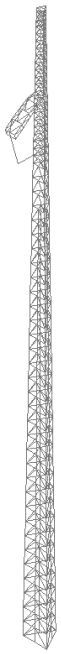
Under the direction of the chief engineer of the project, B.V. Ostroumov, the Melnikov Central Research Institute of Construction Materials developed a project of lattice frame in the form of a triangular prismatic tower, on which the half-tower and then decorative bronze panels was mounted. A similar lattice frame is located inside the statue of the goddess Nika.

The frame of the Monument is high and lined with solid panels, which automatically creates an aerodynamically unstable form, unlike the tall lattice-type radio and television towers. Already at the initial stage of the design it

became clear that such a tall, flexible structure clad with decorative bronze panels would not pass the "wind resonance" type of vortex excitation test, and additional measures would be required to protect it from this atmospheric phenomenon.



a) General view of the Monument on Poklonnaya Hill



b) The metal frame of the Monument in SCAD

Figure 10. Victory Monument on Poklonnaya Hill in Moscow

During the design and installation of the structure, several ways had to be used to combat wind resonance. During the installation of the frame, when the bronze panels covered 2/3 of the monument's height, a strong wind rose. The monument was in wind resonance, the vibrations were visible to the naked eye and did not fade. Then the simplest and most urgent way to protect against vortex excitement was used - the installation of stragglers. At the corners of unfinished monument were installed steel cables in the number of three (because the structure in plan is close to the triangle). One end of the cable was fixed to the corners of the frame at a height of 2/3 and the other was fixed to the quickly erected foundations of reinforced concrete blocks within a radius of 10-15 meters from the center of the monument. The scheme of the construction turned from free-console to mast and until the completion of the monument allowed to dampen any dangerous fluctuations in the wind impact.

At the final stage, the dynamic dampers were installed before the removal of cables, which violated the architectural design of the author. Dynamic vibration dampers (DVD) - a device designed to damp the vibrations of the structure. It consists of the inertial mass suspended on the spring and the dampers connected to it. To preserve the architectural appearance of the Monument DVD were placed inside the framework. The main part of the dampers is located inside the sculptural group "Nica", and another is placed along the central axis of the monument at levels above the mark of 90 meters. Dynamic vibration dampers for the Monument were developed simultaneously with the basic design, their characteristics were obtained experimentally by examining the behavior of the structure model in the wind tunnel TsAGI.

Vibration dampers are activated not only at the moments of wind resonance, they also contribute to the reduction of horizontal displacement of the structure under the action of wind load. The efficiency of DVD is provided by their specific location on the structure, in most cases not less than 2/3 of the total height. At a mass of almost 800 tons the total mass of all DVD is equal to 27.5 tons, which is 3.5% of the mass of the structure.

RESULTS

At the end of the article, let's structuring all the mentioned ways to reduce wind resonance of high-rise flexible structures. If condition (5) turned out not to be met at the design stage, use the following ways to increase the damping of the structure:

1. Structural changes in the shape and size of the structure at the design stage allow to change

the components of formulas (2) and (3) and the period of natural vibrations of the structure. Such measures are permissible if allowed by the Technical Design Assignment.

2. Changing the design scheme in principle: use of guy wire as a transition from the cantilever scheme to the scheme with intermediate supports; increasing the throughness of the structure by adding holes. These measures are often used on already constructed structures in case of unforeseen circumstances.

3. Installation of vibration dampers, dynamic or shock dampers. This measure can act as an emergency, but usually dampers are designed at the same time as the construction, when no structural changes can not help to avoid the phenomena of wind resonance. The design must take into account the mass of the dampers, as well as the design of sites for their placement. Vibration dampers require regular inspections and additional adjustments.

CONCLUSIONS

The article analyzes modern studies on the impact of wind flow on extended flexible metal structures such as chimneys, poles, billboards, icy wires, monuments and monuments. Construction of modern unique structures is accompanied by modeling in FE software such as Ansys, Nastran etc., which allows an engineer to get a complete picture of the flow of wind around the structure and to analyze the possible unfavorable factors. However, for typical structures or already built structures, the authors recommend using the methods described in the article.

ACKNOWLEDGMENTS

The authors express their special gratitude to the team of the Department of High-Rise Structures of TsNIIPSK im. Melnikov represented by the head of the department, doctor of technical sciences, honored builder of the Russian Federation, Ostroumov B.V., and leading engineer Karakozova V.I.

REFERENCES

1. **Karakozova A.I. Mondrus V.L**. Analysis of loads on high-rise tower structures in earthquake-prone areas // Izvestiya VUZov. Building No. 2 2021 p.112-119
2. **Besprozvannaya I.M., Sokolov A.G., Fomin G.M.** Wind impact on high solid-wall structures. M.: Stroyizdat, 1976.
3. **Ostroumov B.V.** Development, research and implementation of new constructive forms of high-rise buildings on the basis of their experimental and theoretical studies with a wind flow. Diss. ... Cand. tech. sciences. M.: TsNIIPSK them. Melnikov, 1985.
4. **Poddaeva O.I., Ageev N.D., Fedosova A.N.** Investigation of the influence of various factors on the results of a calculation-experimental assessment of frequencies and amplitudes during vortex excitation of bending vibrations of building structures// Journal of Physics: Conference Series. International Scientific Conference on Modelling and Methods of Structural Analysis 2019, MMSA 2019. 2020. C. 012135.
5. **Marchevsky I.K., Ivanova O.A.** Numerical modeling of wind resonance of a circular profile by the vortex element method // Problems of mechanical engineering and machine reliability. 2009. No. 5. S. 8-12.
6. **Dubinsky S.I.** Numerical modeling of wind effects on high-rise buildings and complexes. Diss. ... Cand. tech. sciences. M.: MGSU, 2010.
7. **Y. Suna, Z. Lib, X. Suna, N. Suc, S. Pengc.** Inteference effects between two tall chimneys on wind loads and dynamic responses// Journal of Wind Engineering and Industrial Aerodynamics. Volume

206, November 2020, 104227 https://doi.org/10.1016/j.jweia.2020.104227
8. **Sule. S, Nwofor T.C.** Wind Induced Vibration of a Tall Steel Chimney// Canadian Journal on Environmental, Construction and Civil Engineering Vol. 3, No. 2, February 2012
9. **J.Kaweckia, J.A.Żurańskib.** Cross-wind vibrations of steel chimneys// Journal of Wind Engineering and Industrial Aerodynamics Volume 95, Issues 9–11, October 2007, Pages 1166-1175
10. **F. Lupia, H.-J. Niemannb, R. Höffera.** A novel spectral method for cross-wind vibrations: Application to 27 full-scale chimneys// Journal of Wind Engineering and Industrial Aerodynamics. Volume 171, December 2017, Pages 353-365. https://doi.org/10.1016/j.jweia.2017.10.014
11. **A.V. Belvera, A.L. Ibán, C.E.L. Martína** Coupling between structural and fluid dynamic problems applied to vortex shedding in a 90 m steel chimney// Journal of Wind Engineering and Industrial Aerodynamics. Volume 100, Issue 1, January 2012, Pages 30-37 https://doi.org/10.1016/j.jweia.2011.10.007
12. **Anokhin N.N**. Structural mechanics in examples and problems. Part III. Dynamics of structures. Ed. ASV: - M., 2018.
13. **Ostroumov B.V., Karakozova A.I.** A method for calculating the actual logarithmic decrements of oscillations of high-rise structures Industrial and civil construction №06 / 2011
14. **Mondrus V.L. Karakozova A.I.** On the features of the calculation of tower structures // Structural mechanics and calculation of structures. 2020. No. 6. S. 56-60.
15. **Karakozova A.I.** Calculation of high-rise structures with low structural damping and taking into account the effect of wind speed pulsations. Diss. ... Cand. technical sciences. Moscow 2013.
16. **Gordeev V.N., Lantukh-Lyashchenko A.I., Pavshinsky V.A., Perelmuter A.V., Pichugin S.F.** Loads and impacts on buildings and structures / ed. Perelmutera A.V. - 3rd ed., Rev. Moscow: ASV Publishing House, 2009.480 p.
17. **Fomin G.M.** On the circulation of vortices and the speed of displacement of the Karman track // Uchenye zapiski TsAGI Volume II 1974 №4
18. **Ostroumov B.V., Karakozova A.I., Karakozova V.I.** Embodiment of B.G. Korenev's ideas in the field of equipping high-rise structures with dynamic vibration dampers // Industrial and Civil Engineering №11 / 2010
19. **Ostroumov B.V**. Research, development and implementation of high-rise buildings with vibration dampers. Diss. ... Dr. Tech. sciences. M.: TsNIIPSK them. Melnikov, 2003.
20. **Nikitin P.N., Onosov G.V.** Experience in designing chimneys // Industrial and civil construction. 2009. No. 5. S. 24-27.
21. Ministry of Culture of the Russian Federation. Order dated July 16, 2020 N 798. On the approval of the subject protection of the object of cultural heritage of federal significance "sculpture" Motherland is calling! "(the main monument)", which is part of the cultural heritage site of federal significance "memorial complex" to the heroes of the battle of Stalingrad "on Mamaev Kurgan (1960, 1967)
22. **Ostroumov B.V., Patrikeev A.V., Gusev M.A.** Monitoring the state of the supporting structures of the main monument of the Victory Monument on Poklonnaya Gora // Promyshlennoe i grazhdanskoe stroitel'stvo. 2004. No. 5. S. 19-21.

СПИСОК ЛИТЕРАТУРЫ

1. **Каракозова А.И. Мондрус В.Л.** Анализ нагрузок на высотные башенные сооружения в сейсмоопасных районах//

Известия ВУЗов. Строительство №2 2021 с.112-119
2. **Беспрозванная И.М., Соколов А.Г., Фомин Г.М.** Воздействие ветра на высокие сплошностенчатые сооружения. М. : Стройиздат, 1976.
3. **Остроумов Б.В.** Разработка, исследование и внедрение новых конструктивных форм высотных сооружений на основе экспериментально-теоретических исследований их взаимодействия с ветровым потоком. Дисс. … канд. техн. наук. М. : ЦНИИПСК им. Мельникова, 1985.
4. **Poddaeva O.I., Ageev N.D., Fedosova A.N.** Investigation of the influence of various factors on the results of a calculation-experimental assessment of frequencies and amplitudes during vortex excitation of bending vibrations of building structures// Journal of Physics: Conference Series. International Scientific Conference on Modelling and Methods of Structural Analysis 2019, MMSA 2019. 2020. С. 012135.
5. **Марчевский И.К., Иванова О.А.** Численное моделирование ветрового резонанса кругового профиля методом вихревых элементов // Проблемы машиностроения и надежности машин. 2009. № 5. С. 8-12.
6. **Дубинский С.И.** Численное моделирование ветровых воздействий на высотные здания и комплексы. Дисс. … канд. техн. наук. М. : МГСУ, 2010.
7. **Y. Suna, Z. Lib, X. Suna, N. Suc, S. Pengc.** Inteference effects between two tall chimneys on wind loads and dynamic responses// Journal of Wind Engineering and Industrial Aerodynamics. Volume 206, November 2020, 104227 https://doi.org/10.1016/j.jweia.2020.104227
8. **Sule. S, Nwofor T.C.** Wind Induced Vibration of a Tall Steel Chimney// Canadian Journal on Environmental, Construction and Civil Engineering Vol. 3, No. 2, February 2012
9. **J.Kaweckia, J.A. Żurańskib.** Cross-wind vibrations of steel chimneys// Journal of Wind Engineering and Industrial Aerodynamics Volume 95, Issues 9–11, October 2007, Pages 1166-1175
10. **F. Lupia, H.-J. Niemannb, R. Höffera.** A novel spectral method for cross-wind vibrations: Application to 27 full-scale chimneys// Journal of Wind Engineering and Industrial Aerodynamics. Volume 171, December 2017, Pages 353-365. https://doi.org/10.1016/j.jweia.2017.10.014
11. **A.V. Belvera, A.L. Ibán, C.E.L. Martína** Coupling between structural and fluid dynamic problems applied to vortex shedding in a 90 m steel chimney// Journal of Wind Engineering and Industrial Aerodynamics. Volume 100, Issue 1, January 2012, Pages 30-37 https://doi.org/10.1016/j.jweia.2011.10.007
12. **Анохин Н.Н.** Строительная механика в примерах и задачах. Часть III. Динамика сооружений. Изд. АСВ: - М., 2018.
13. **Остроумов Б.В., Каракозова А.И.** Способ вычисления фактических логарифмических декрементов колебаний высотных сооружений Промышленное и гражданское строительство №06/ 2011
14. **Мондрус В.Л. Каракозова А.И.** Об особенностях расчета башенных сооружений // Строительная механика и расчет сооружений. 2020. №6. С. 56-60.
15. **Каракозова А.И.** Расчет высотных сооружений с низким конструкционным демпфированием и учетом воздействия пульсаций скорости ветра. Дисс. … канд. техн.наук. Москва, 2013.
16. **Гордеев В.Н., Лантух-Лященко А.И., Павшинский В.А., Перельмутер А.В., Пичугин С.Ф.** Нагрузки и воздействия на здания и сооружения/ под общей ред. Перельмутера А.В. – 3-е изд., перераб. М.: Издательство АСВ, 2009. 480 с.
17. **Фомин Г.М**. О циркуляции вихрей и скорости перемещений дорожки Кармана// Ученые записки ЦАГИ Том II 1974 №4

18. **Остроумов Б.В., Каракозова А. И., Каракозова В.И.** Воплощение идей Б.Г. Коренева в области оснащения высотных сооружений динамическими гасителями колебаний// Промышленное и гражданское строительство №11/ 2010
19. **Остроумов Б.В.** Исследование, разработка и внедрение высотных сооружений с гасителями колебаний. Дисс. … д-ра техн. наук. М. : ЦНИИПСК им. Мельникова, 2003.
20. **Никитин П.Н., Оносов Г.В.** Опыт проектирования дымовых труб// Промышленное и гражданское строительство. 2009. № 5. С. 24-27.
21. **Остроумов Б.В., Патрикеев А.В., Гусев М.А.** Контроль за состоянием несущих конструкций главного монумента Памятника победы на Поклонной горе// Промышленное и гражданское строительство. 2004. № 5. С. 19-21.

Karakozova Anastasia Ivanovna - CSc, Associate Professor of the Department of STM NRU MGSU, 405 ulk, 26, Yaroslavskoe sh., Moscow, 129337, Russia, karioca@mail.ru, 89151694001.

Mondrus Vladimir Lvovich - DSc, Professor, Corresponding Member of the RAASN, Head of the Department of STM NRU MGSU, 405 ulk, 26, Yaroslavskoe sh., Moscow, 129337, Russia, mondrus@mail.ru, 89057209122.

Каракозова Анастасия Ивановна – к.т.н., доцент кафедры СиТМ НИУ МГСУ, 405 улк, д.26, Ярославское ш., Москва, 129337, Россия, karioca@mail.ru, 89151694001.

Мондрус Владимир Львович – д.т.н., профессор, член-корреспондент РААСН, заведующий кафедрой СиТМ НИУ МГСУ, 405 улк, д.26, Ярославское ш., Москва, 129337, Россия, mondrus@mail.ru, 89057209122.

International Journal for Computational Civil and Structural Engineering, 19(2) 71–80 (2023)

DOI:10.22337/2587-9618-2023-19-2-71-80

PROBLEM OF PLATE BENDING IN THE MOMENT ASYMMETRIC THEORY OF ELASTICITY

Nelly N. Rogacheva, Yulia G. Zheglova

National Research Moscow State University of Civil Engineering, Moscow, RUSSIA

Abstract. For a number of materials used in modern practice, calculations according to the classical theory of elasticity give incorrect results. To ensure the reliable operation of structures, there is a need for new theories. At present, of particular interest for practical applications is the asymmetric moment theory of elasticity. In the work, by the method of hypotheses, the three-dimensional equations of the moment asymmetric theory of elasticity are reduced to the equations of the theory of plates. The hypotheses of the theory of plates in the moment theory of elasticity are formulated on the basis of previously obtained our results of the reduction of three-dimensional equations to two-dimensional theories by a mathematical method. Just as in the classical theory of elasticity, the complete problem of the moment theory of plates is divided into two problems - a plane problem and a problem of plate bending. The equations of the plane problem have been obtained in many papers. The situation is different with the construction of the theory of plate bending in the moment theory of elasticity. In this work, for the first time, substantiated hypotheses are formulated and a consistent theory of plate bending is presented. A numerical calculation of the bending of a rectangular hinged plate is carried out according to the obtained applied theory. The calculation results are presented in the form of graphs.

Keywords: plate bending, moment asymmetric theory of elasticity

ЗАДАЧА ИЗГИБА ПЛАСТИНЫ В МОМЕНТНОЙ АСИММЕТРИЧНОЙ ТЕОРИИ УПРУГОСТИ

Н.Н. Рогачева, Ю.Г. Жеглова

Национальный исследовательский Московский государственный строительный университет, г. Москва, РОССИЯ

Аннотация. Для ряда материалов, используемых в современной практике, расчеты по классической теории упругости дают неверные результаты. Для обеспечения надежной работы конструкций необходимы новые теории. В настоящее время особый интерес для практических приложений представляет асимметричная моментная теория упругости. В работе методом гипотез трехмерные уравнения моментной несимметричной теории упругости сведены к уравнениям теории пластин. Гипотезы теории пластин моментной теории упругости сформулированы на основе ранее полученных нами результатов сведения математическим методом трехмерных уравнений к двумерным теориям. Как и в классической теории упругости, полная задача теории моментов пластин делится на две задачи — плоскую задачу и задачу об изгибе пластин. Уравнения плоской задачи получены во многих работах . Иначе обстоит дело с построением теории изгиба пластин в моментной теории упругости. В данной работе впервые сформулированы обоснованные гипотезы и представлена непротиворечивая теория изгиба пластин. По полученной прикладной теории проведен численный расчет на изгиб прямоугольной откидной пластины. Результаты расчета представлены в виде графиков.

Ключевые слова: изгиб пластин, моментная ассиметричная теория упругости

1. INTRODUCTION

In connection with the appearance and application of new materials interest in non-classical theories of asymmetric elasticity has recently grown [1-13]. Experiments confirm that for a number of materials, for example, polymers, porous materials, the moment asymmetric theory of elasticity should be used [6, 8] . Many papers focus on plates and shells

is often constructed by means of hypotheses [1, 2, 3. 10, 12, 13]. As a rule, the well known Kirchhoff's hypotheses are used for the sought-for quantities of symmetric elasticity and new hypotheses are adopted for quantities which do not exist in the symmetric theory of elasticity, such as the components of moment stress tensor and an independent rotation vector. The use of a false hypotheses leads to considerable errors.

The methods to reduce 3D equations to 2D type will be further called reduction methods.

Another reduction method is the asymptotic method. This method allows to qualitatively investigate the behavior stress-strain state, passing from 3D to 2D problem without applying any hypotheses, next to estimate the errors of the resulting theories. The asymptotic reduction method was tested for many problems [14, 15].

We reduced the 3D problem of asymmetric elasticity to the plate theory by the asymptotic method in [9]. Two iterative processes are used in order to pass from a 3D problem to a 2D problem. The first iterative process allows to construct the internal stress-strain state which can be approximately described by the plate theory in asymmetric elasticity. The second iterative process is used to create a quickly decreasing stress-strain state; i.e. the boundary layer localized near the edge. The boundary layer and the internal stress-strain state interact at the edge provided 3D boundary conditions are satisfied. The investigation of this interaction gives the boundary conditions for the plate theory and boundary layer. Note that the linear problem of asymmetric elasticity has the only solution and the unique asymptotics. It is very important to choose a correct asymptotics. Incorrect asymptotics leads to a wrong theory.

2. BASIC EQUATIONS

We write a complete system of equations for asymmetric theory of elasticity in a tensor form [1].

The equilibrium equations:

$$\sigma_{nm,n} = 0, \quad \mu_{nm,n} + э_{mnk}\, \sigma_{nk} = 0; \qquad (1)$$

The constitutive relations:

$$\begin{aligned} \sigma_{nm} &= (\mu+\alpha)e_{nm} + (\mu-\alpha)e_{mn} + \lambda e_{kk}\delta_{nm}, \\ \mu_{nm} &= (\gamma+\varepsilon)\chi_{nm} + (\gamma-\varepsilon)\chi_{mn} + \beta\chi_{kk}\delta_{nm}. \end{aligned} \qquad (2)$$

The geometrical relations:

$$e_{nm} = u_{m,n} - э_{knm}\, \omega_k, \quad \chi_{nm} = \omega_{m,n}. \qquad (3)$$

Here σ_{nm}, μ_{nm} are the components of the force and moment stress tensors, e_{nm} are the components of the asymmetric strain tensor, χ_{nm} are the components of the asymmetric bending-torsion tensor, $\lambda, \mu, \alpha, \beta, \gamma, \varepsilon$ are the constants of the material of asymmetric elasticity, u_n are the components of the displacement vector, ω_n are the components of the rotation vector at the point of the body, $э_{nmk}$ is the Levi-Civita symbol. The subscripts *n, m* after a comma denote differentiation with respect to the coordinates x_n and x_m respectively. Here and henceforth, the subscripts *n, m, k* take the values 1, 2, 3 and the subscripts *i, j* ($(i \neq j)$ take the values 1, 2.

A thin plate is located in Cartesian coordinates. The plane $x_1\, x_2$ coincides with the middle plane of the plate and the x_3 axis is orthogonal to the middle plane.

The boundary conditions on the plate faces $x_3 = \pm h$ are written as

$$\sigma_{i3} = q_i^{\pm}, \ \sigma_{33} = q_3^{\pm}, \ \mu_{3i} = m_i^{\pm}, \ \mu_{33} = m_3^{\pm}, \qquad (4)$$

where $q_n^{\pm}$, $m_n^{\pm}$ are the components of the given external forces and moments.

On the edge of the plate $x_i = const$ six boundary conditions are given. For example, they can be written at the free edge as follows:

$$\begin{aligned} &\sigma_{ii} = 0, \ \sigma_{ji} = 0, \ \sigma_{i3} = 0, \\ &\mu_{ii} = 0, \ \mu_{ji} = 0, \ \mu_{i3} = 0, \end{aligned} \qquad (5)$$

and at the rigidly fixed edge they can be written at the free edge as follows:

$$u_i = 0,\ u_j = 0,\ u_3 = 0,$$
$$\omega_i = 0,\ \omega_j = 0,\ \omega_3 = 0. \quad (6)$$

3. CONSTRUCTING THE EQUATIONS OF THE PLATE THEORY

Here we will use the hypotheses method since the asymptotical method is complex and requires special knowledge. The hypotheses way is very simple and clear.

The plate theory in asymmetric elasticity was constructed by asymptotical method in [9].

Using the results of the mathematical reduction 3D asymmetric elasticity theory to 2D plate theory we can formulate the correct hypotheses.

In the considered asymmetric elasticity, the equations of state include six physical constants $\gamma, \beta, \varepsilon,\ \mu, \lambda, \alpha$. We assume that the quantities $\mu R^2,\ \lambda R^2,\ \alpha R^2, \gamma, \beta, \varepsilon$ are of the same order, where value R is the characteristic size of the plate.

Just as in the classical theory of elasticity, in the moment asymmetric theory of elasticity, the complete system of plate equations is divided into two independent systems for a plane problem and plate bending.

We divide all the required values of the theory of plates into two groups (7) and (8)

$$u_i,\ \omega_3,\ e_{ij},\ e_{ii},\ \chi_{i3},\ \chi_{3i},\ \sigma_{ij},\ \sigma_{ii},\ \sigma_{33},\ \mu_{i3},\ \mu_{3i} \quad (7)$$
$$u_3, \omega_i, e_{i3}, e_{3i}, \chi_{ij}, \chi_{ii}, \sigma_{i3}, \sigma_{3i}, \mu_{ii}, \mu_{ij}, \mu_{33}. \quad (8)$$

In the plane problem, the required quantities (7) are even functions of the x_3 coordinate, and the quantities (8) are odd functions of the coordinate x_3. In the bending problem, the opposite is true: quantities (7) are odd functions of the x_3 coordinate, and quantities (8) are even functions of the coordinate x_3.

Let us formulate hypotheses for constructing the equations of the plane problem for the asymmetric theory of elasticity

The first hypothesis.

The tangential displacement u_i does not depend on the x_3-coordinate (it is constant along the thickness)

$$u_i\big|_{x_3=0} = v_i$$

The second hypothesis.

The angle of rotation ω_3 does not depend on x_3

$$\omega_3\big|_{x_3=0} = \psi_3$$

The third hypothesis.

The components of moment stresses μ_{i3} do not depend on x_3.

From the equilibrium equation (1) it can be seen that if generalized displacements u_i, ω_3, do not depend on x_3, then from formulas (3) it is obvious that deformations e_{ii}, e_{ij}, χ_{i3}, also do not depend on x_3.

Let us apply these hypotheses to the 3D equation of asymmetric elasticity, just as it is done when constructing the theory of Kirchhoff plate. Then we will move on to the forces and moments accepted in the theory of plate according to the following formulas:

$$T_{ii} = \int_{-h}^{+h} \sigma_{ii} dx_3, \quad T_{ij} = \int_{-h}^{+h} \sigma_{ij} dx_3,$$
$$M_{i3} = \int_{-h}^{+h} \mu_{i3} dx_3, \quad i \neq j = 1,2. \quad (9)$$

As a result of simple transformations, we obtain the following equations of a plane problem in the asymmetric theory of elasticity

The equilibrium equations

$$\frac{\partial T_{ii}}{\partial x_i}+\frac{\partial T_{ji}}{\partial x_j}+X_i=0,$$
$$\frac{\partial M_{13}}{\partial x_1}+\frac{\partial M_{23}}{\partial x_2}+T_{12}-T_{21}+\mathrm{M}=0, \qquad (10)$$
$$X_i=q_i^+ + q_i^-, \quad \mathrm{M}=m_3^+ + m_3^-.$$

The constitutive relations

$$T_{ii}=\frac{4h\mu(\mu+\lambda)}{2\mu+\lambda}\varepsilon_i+\frac{2h\mu\lambda}{2\mu+\lambda}\varepsilon_j+\frac{h\lambda}{2\mu+\lambda}(q_3^+-q_3^-),$$
$$T_{ij}=2h[(\mu+\alpha)\varepsilon_{ij}+(\mu-\alpha)\varepsilon_{ji}], \qquad (11)$$
$$M_{i3}=\frac{8h\gamma\varepsilon}{\gamma+\varepsilon}\varphi_{i3}+\frac{h(\gamma-\varepsilon)}{(\gamma+\varepsilon)}(m_i^+-m_i^-).$$

The geometrical relations

$$\varepsilon_i=\frac{\partial v_i}{\partial x_i},\ \varepsilon_{ij}=\frac{\partial v_j}{\partial x_i}+(-1)^i\psi_3,\ \phi_{i3}=\frac{\partial \psi_3}{\partial x_i} \qquad (12)$$

where

$$\phi_{i3}=\chi_{i3}\big|_{x_3=0},\ \psi_3=\omega_3\big|_{x_3=0}.$$

Equations (10)-(12) have been obtained in many papers [1, 2, 3. 10, 12, 13]. This is explained by the fact that in this case the hypotheses very similar to those of Kirchhoff are used for the construction classical plane plate theory. There is a difference only in relations for the forces T_{ii} and the moments M_{i3}. In these relations we have small additional terms taking into account the external load components $(q_3^+-q_3^-)$ and $(m_i^+-m_i^-)$.

Let us formulate hypotheses for constructing equations for the problem of plate bending.

The first hypotheses.

The components of generalized displacements u_3, ω_i do not depend on the coordinate x_3, i.e. they are constant across the plate thickness

$$u_3\big|_{x_3=0}=w,\ \omega_i\big|_{x_3=0}=\psi_i \qquad (13)$$

The second hypothesis.

The components of the stress tensor σ_{i3} are much larger than the stress σ_{3i}.

By virtue of hypothesis 2, in the second relation (14), the quantity σ_{3i} can be neglected

$$\sigma_{i3}=(\mu+\alpha)e_{i3}+(\mu-\alpha)e_{3i},$$
$$\sigma_{3i}=(\mu+\alpha)e_{3i}+(\mu-\alpha)e_{i3}. \qquad (14)$$

Resolving after discarding σ_{3i} equation (14) with respect to the deformation components e_{i3}, e_{3i} we obtain the following formulas:

$$e_{3i}=-\frac{(\mu-\alpha)}{(\mu+\alpha)}e_{i3}, \qquad \sigma_{i3}=\frac{4\mu\alpha}{(\mu+\alpha)}e_{i3} \qquad (15)$$

By virtue of the first hypothesis, the quantities u_3 and ω_i do not depend on the variable x_3, so it follows from relations (15), that e_{3i}, e_{i3} and σ_{i3} do not depend on the variable x_3.

Let us introduce the notation adopted in the theory of plates

$$N_{i3}=\int_{-h}^{+h}\sigma_{i3}dx_3, \qquad N_{3i}=\int_{-h}^{+h}\sigma_{3i}dx_3,$$
$$G_{ii}=\int_{-h}^{+h}\sigma_{ii}x_3dx_3, \quad G_{ij}=\int_{-h}^{+h}\sigma_{ij}x_3dx_3,$$
$$M_{ii}=\int_{-h}^{+h}\mu_{ii}dx_3, \quad M_{ij}=\int_{-h}^{+h}\mu_{ij}dx_3, \qquad (16)$$
$$i\neq j=1,2,\ w=v_3\big|_{x_3=0},\ \psi_i=\omega_i\big|_{x_3=0}.$$

Continuing such simplifications in the equations of the 3D asymmetric theory of elasticity, we obtain the following 2D equations of the bending problem in the notation of the theory of plates:

The equilibrium equations

$$\frac{\partial N_{13}}{\partial x_1}+\frac{\partial N_{23}}{\partial x_2}+Z=0,$$
$$\frac{\partial M_{ii}}{\partial x_i}+\frac{\partial M_{ji}}{\partial x_j}+\mathrm{M}_i+(-1)^j N_{j3}=0, \quad (17)$$
$$\frac{\partial G_{ii}}{\partial x_i}+\frac{\partial G_{ji}}{\partial x_j}-N_{3i}+Y_i=0,$$

where Z, M_i, Y_i are the surface load

$$Z=h(q_3^+ + q_3^-),\ \ \mathrm{M}_i=(m_i^+ + m_i^-),$$
$$Y_i=h(q_i^+ - q_i^-).$$

The constitutive relations

$$N_{i3}=\frac{8h\mu\alpha}{(\mu+\alpha)}\varepsilon_{i3},$$
$$M_{ii}=2h\left(\frac{4\gamma(\gamma+\beta)}{2\gamma+\beta}\phi_i+\frac{2\gamma\beta}{2\gamma+\beta}\phi_j\right),$$
$$M_{ij}=2h[(\gamma+\varepsilon)\phi_{ij}+(\gamma-\varepsilon)\phi_{ji}],$$
$$G_{ii}=\frac{2h^3}{3}\left(\frac{4\mu(\mu+\lambda)}{2\mu+\lambda}\kappa_{ii}+\frac{2\mu\lambda}{2\mu+\lambda}\kappa_{jj}\right)+ \quad (18)$$
$$+\frac{\lambda}{2\mu+\lambda}\frac{h^2}{3}(q_3^+ + q_3^-),$$
$$G_{ij}=\frac{2h^3}{3}\left((\mu+\alpha)\kappa_{ij}+(\mu-\alpha)\kappa_{ji}\right).$$

The geometrical relations

$$\varepsilon_{i3}=\frac{\partial w}{\partial x_i}+(-1)^j\psi_j,\ \ \varphi_i=\frac{\partial\chi_i}{\partial x_i},\ \ \varphi_{ij}=\frac{\partial\psi_j}{\partial x_i}$$
$$\kappa_{ii}=-\frac{(\mu-\alpha)}{(\mu+\alpha)}\frac{\partial^2 w}{\partial x_i^{\,2}}+(-1)^j\frac{2\alpha}{(\mu+\alpha)}\varphi_{ij},$$
$$\kappa_{ij}=-\frac{(\mu-\alpha)}{(\mu+\alpha)}\frac{\partial^2 w}{\partial x_i\partial x_j}+(-1)^i\frac{2\alpha}{(\mu+\alpha)}\frac{\partial\psi_i}{\partial x_i}- \quad (19)$$
$$-(-1)^i\frac{\beta}{2\gamma+\beta}\left(\frac{\partial\psi_1}{\partial x_1}+\frac{\partial\psi_2}{\partial x_2}\right).$$

For this system of differential equations of the sixth order, it is necessary to specify three boundary conditions at each edge. For example, the conditions at the free edge and the rigidly fixed edge $x_i=const$ have the form respectively components

$$N_{i3}=0,\quad M_{ji}=0,\quad M_{ii}=0,$$
$$w=0,\quad \frac{\partial w}{\partial x_i}+(-1)^j\psi_j=0,\quad \psi_i=0.$$

3. NUMERICAL EXAMPLE

Let us perform the calculation of the stress-strain state of the bend of a rectangular hinge-operated plate along all edges of the plate. Длины сторон пластины равны l_i $(-l_i\le x_i\le l_i)$.

We introduce dimensionless coordinates

$$x_i=l_i\xi_i \quad (20)$$

Let us write down all the required quantities in the dimensionless form

$$w_*=\frac{w}{l_1},\quad \psi_{i*}=\psi_i,$$
$$N_{i3*}=N_{i3}\frac{\mu+\alpha}{8h\mu\alpha},\ \ N_{3i*}=N_{3i}\frac{\mu+\alpha}{8h\mu\alpha},$$
$$M_{ii*}=\frac{M_{ii}}{l_1}\frac{\mu+\alpha}{8h\mu\alpha},\ \ M_{ij*}=\frac{M_{ij}}{l_1}\frac{\mu+\alpha}{8h\mu\alpha}, \quad (21)$$
$$G_{ii*}=\frac{G_{ii}}{l_1}\frac{\mu+\alpha}{8h\mu\alpha},\ \ G_{ij*}=\frac{G_{ij}}{l_1}\frac{\mu+\alpha}{8h\mu\alpha},$$
$$\varepsilon_{i3*}=\varepsilon_{i3},\ \ \kappa_{ii*}=l_1\kappa_{ii},\ \kappa_{ij*}=l_1\kappa_{ij},$$
$$\varphi_{i*}=l_1\varphi_i,\quad \varphi_{ij*}=l_1\varphi_{ij}.$$

We write out a complete system of equations with respect to dimensionless desired quantities. The equilibrium equations

$$\frac{\partial N_{13*}}{\partial \xi_1}+\frac{l_1}{l_2}\frac{\partial N_{23*}}{\partial \xi_2}+Z_*=0,$$
$$\frac{\partial M_{11*}}{\partial \xi_1}+\frac{l_1}{l_2}\frac{\partial M_{21*}}{\partial \xi_2}+\mathrm{M}_{1*}+N_{23*}=0,$$
$$\frac{l_1}{l_2}\frac{\partial M_{22*}}{\partial \xi_2}+\frac{\partial M_{12*}}{\partial \xi_1}+\mathrm{M}_{2*}-N_{13*}=0, \quad (22)$$
$$\frac{\partial G_{11*}}{\partial \xi_1}+\frac{l_1}{l_2}\frac{\partial G_{21*}}{\partial \xi_2}-N_{31*}+Y_{1*}=0,$$
$$\frac{l_1}{l_2}\frac{\partial G_{22*}}{\partial \xi_2}+\frac{\partial G_{12*}}{\partial \xi_1}-N_{32*}+Y_{2*}=0,$$
$$Z_*=\frac{l_1}{h}\frac{\mu+\alpha}{8\mu\alpha}Z,\ \mathrm{M}_{i*}=\frac{\mu+\alpha}{8h\mu\alpha}\mathrm{M}_i,\ Y_{i*}=\frac{\mu+\alpha}{8h\mu\alpha}Y_i.$$

The constitutive relations

$$N_{i3*}=\varepsilon_{i3*},\quad M_{ii*}=A_1\phi_{i*}+A_2\phi_{j*}$$
$$M_{ij*}=A_{12}\phi_{ij*}+A_{21}\phi_{ji*} \quad (23)$$
$$G_{ii*}=c_1\kappa_{ii*}+c_2\kappa_{jj*}+cZ_*,\quad G_{ij*}=c_{12}\kappa_{ij*}+c_{21}\kappa_{ji*}.$$

The geometrical relations

$$\varepsilon_{i3*}=\frac{\partial w_*}{\partial \xi_i}+\psi_{j*},\ \varphi_{i*}=\frac{\partial \psi_{i*}}{\partial \xi_i},\ \varphi_{ij*}=\frac{\partial \psi_{j*}}{\partial \xi_i},$$
$$\kappa_{ii*}=-\frac{(\mu-\alpha)}{(\mu+\alpha)}\frac{\partial^2 w_*}{\partial \xi_i^{\,2}}-(-1)^i\frac{2\alpha}{(\mu+\alpha)}\phi_{ij*}, \quad (24)$$
$$\kappa_{ij*}=-\frac{l_1}{l_2}\frac{(\mu-\alpha)}{(\mu+\alpha)}\frac{\partial^2 w_*}{\partial \xi_i\partial \xi_j}+(-1)^i\frac{2\alpha}{(\mu+\alpha)}\varphi_{i*}-$$
$$-(-1)^i\frac{\beta}{2\gamma+\beta}\left(\varphi_{i*}+\varphi_{j*}\right).$$

In formulas (23), the following designations are introduced:

$$A_1=\frac{1}{l_1^{\,2}}\frac{(\mu+\alpha)}{\mu\alpha}\frac{\gamma(\gamma+\beta)}{2\gamma+\beta},$$
$$A_2=\frac{1}{l_1 l_2}\frac{(\mu+\alpha)}{2\mu\alpha}\frac{\gamma\beta}{2\gamma+\beta},$$
$$A_{12}=\frac{1}{l_1^{\,2}}\frac{(\mu+\alpha)}{4\mu\alpha}(\gamma+\varepsilon),$$
$$A_{21}=\frac{1}{l_1 l_2}\frac{(\mu+\alpha)}{4\mu\alpha}(\gamma-\varepsilon),$$
$$c_1=\frac{h^2}{3l_1^2}\frac{(\mu+\alpha)(\mu+\lambda)}{\alpha(2\mu+\lambda)},\quad c_2=\frac{h^2}{6l_1^2}\frac{(\mu+\alpha)\lambda}{\alpha(2\mu+\lambda)},$$
$$c_{12}=\frac{h^2}{12l_1^2}\frac{(\mu+\alpha)^2}{\mu\alpha}\quad c_{21}=\frac{h^2}{12l_1^2}\frac{(\mu^2-\alpha^2)}{\mu\alpha},$$
$$c=\frac{h^2}{3l_1^2}\frac{(\mu+\alpha)\lambda}{\mu\alpha(2\mu+\lambda)}.$$

The solution of the problem that satisfies the boundary conditions will be sought in the following form

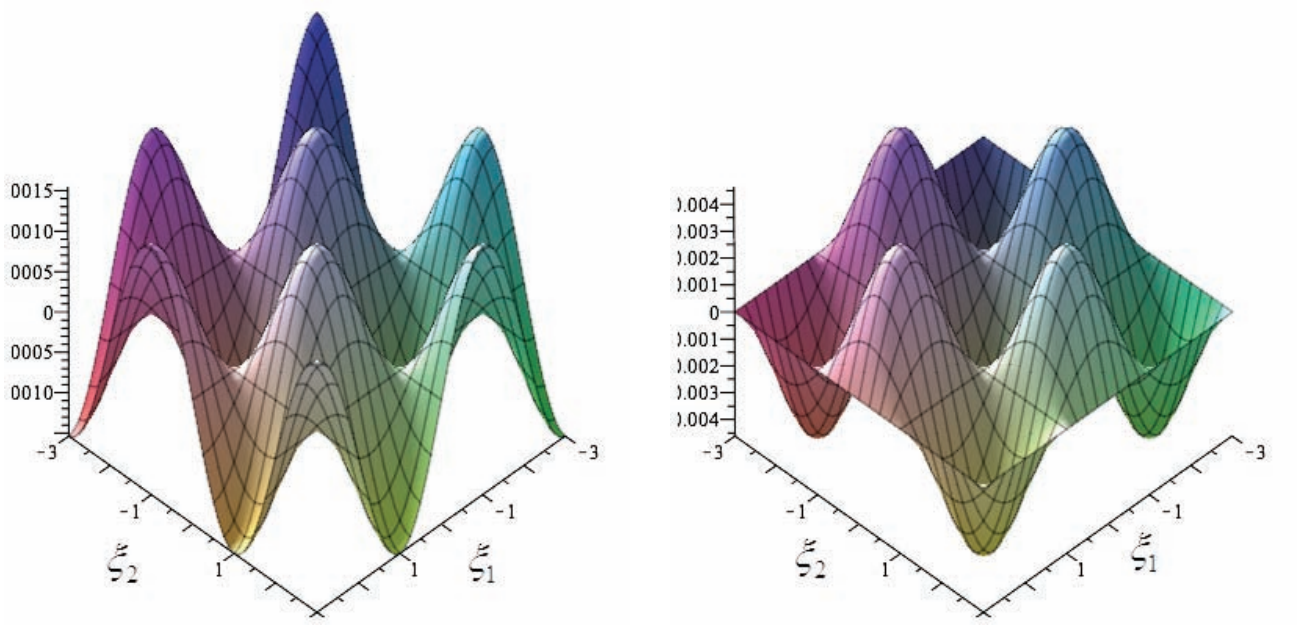
$$f_{1*}=f_{1nm}\cos k_n\xi_1\cos k_m\xi_2,$$
$$f_{2*}=f_{2nm}\cos k_n\xi_1\sin k_m\xi_2,$$
$$f_{3*}=f_{3nm}\sin k_n\xi_1\cos k_m\xi_2, \quad (25)$$
$$f_{4*}=f_{4nm}\sin k_n\xi_1\sin k_m\xi_2,$$

where $k_n=\frac{\pi}{2l_1}(2n-1)$, $k_m=\frac{\pi}{2l_2}(2m-1)$.

In formulas (25), f_{1*} means the quantities w_*, ϕ_{ij*}, κ_{ii*}, G_{ii*}, M_{ij*}, Z_*; f_{2*} means the quantities ψ_{1*}, ε_{23*}, N_{23*}, N_{32*}, Y_{2*}, M_{1*}; f_{3*} means the quantities ψ_{2*}, ε_{13*}, N_{13*}, N_{31*}, Y_{1*}, M_{2*}; f_{4*} means the quantities ϕ_{i*}, M_{ii*}, G_{ij*}.

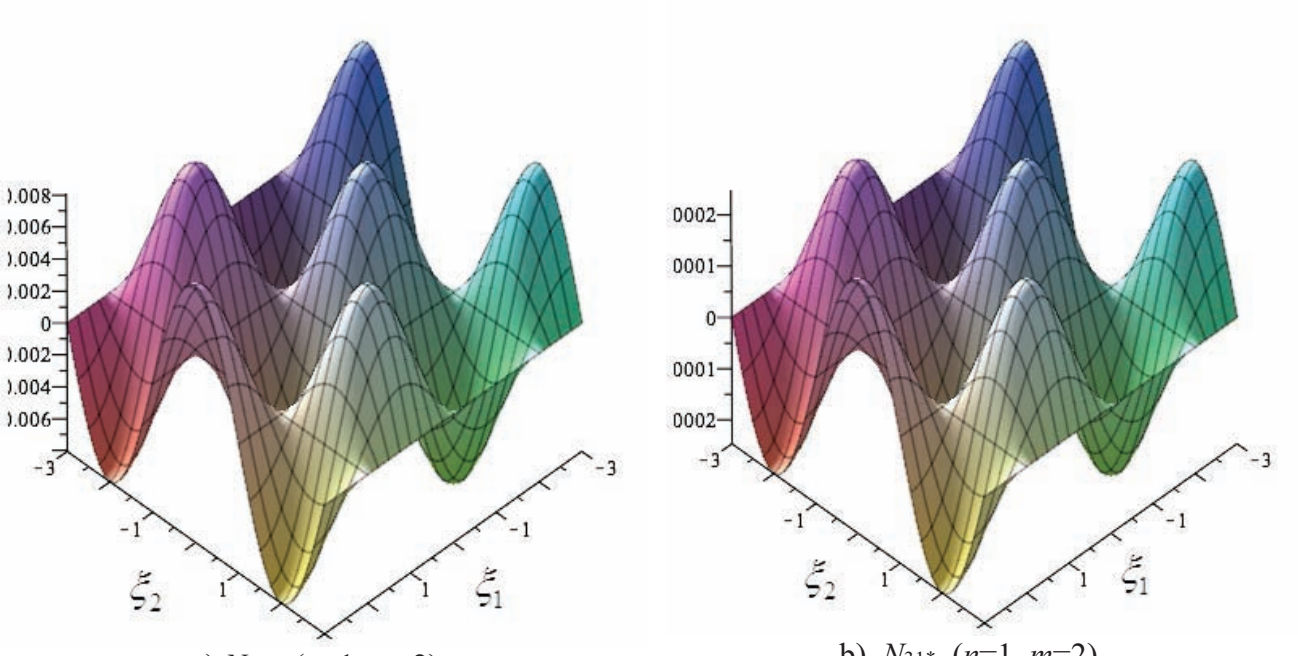
The solution of the problem for the required quantities was reduced to solving the system of linear algebraic equations. Below are the results of the calculation in the form of graphs of the desired values as functions of the dimensionless coordinates ξ_1, ξ_2 the middle plane of the plate.

During the numerical example, we took $\alpha=1{,}6\cdot10^6$ N/m^2, $\mu=2\cdot10^6$ N/m^2, $\lambda=3\cdot10^6$ N/m^2, $\beta=1{,}2$ kN, $\gamma=\varepsilon=3$ kN.



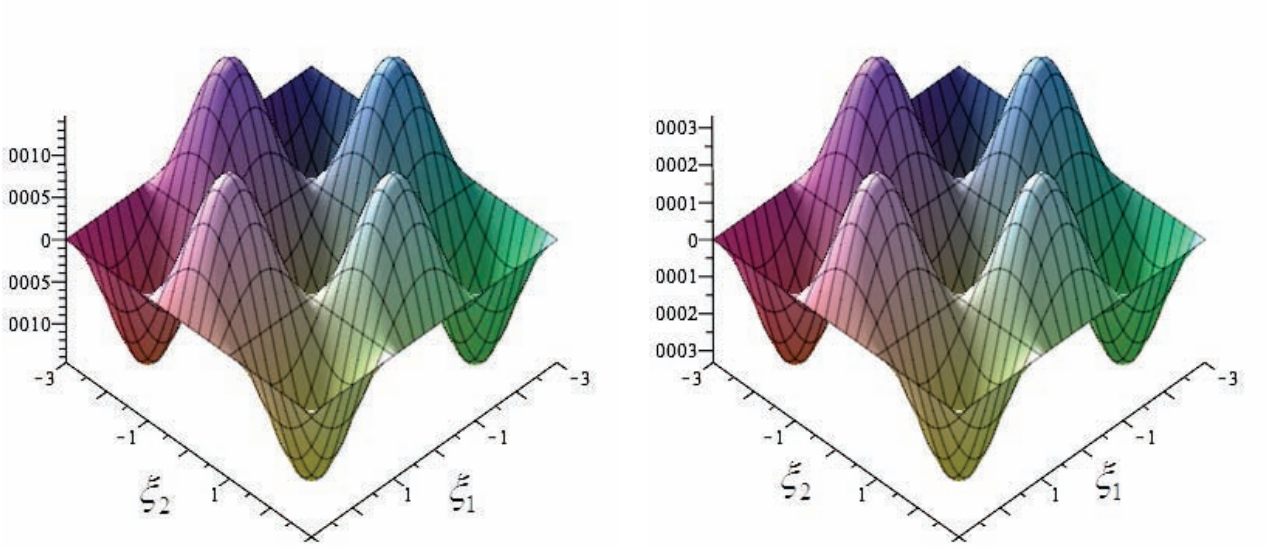
a) M_{11*}, (n=1, m=2) b) M_{12*}, (n=1, m=2)

Figure 1. The moments M_{11*} fig. 1(a) and M_{12*} fig. 1(b) is a function of the coordinates x_1, x_2.



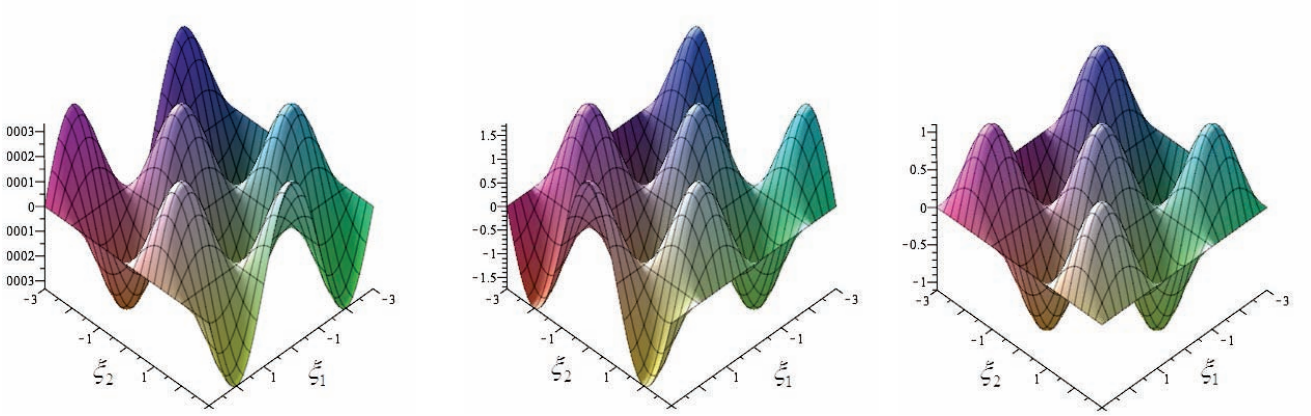
a) N_{13*}, (n=1, m=2) b) N_{31*}, (n=1, m=2)

Figure 2. Graphs of N_{13*} fig. 2(a) and N_{31*} fig. 2(b) is a function of the coordinates x_1, x_2.



a) G_{11*}, (n=1, m=2) b) G_{12*}, (n=1, m=2)

Figure 3. Graphs of G_{11*} fig. 3(a) and G_{12*} fig. 3(b) is a function of the coordinates x_1, x_2.



a) ψ_{1*}, (n=1, m=2) b) ψ_{2*}, (n=1, m=2) c) w_*, (n=1, m=2)

Figure 4. The dependence generalized displacement ψ_{1*}, ψ_{2*}, w_* on the variables x_1, x_2.

The obtained dependences of the dimensionless desired quantities on the coordinates of the middle plane of the plate make it possible to understand the behavior of the stress-strain state. We especially note that for forces and moments, the symmetry conditions known in the classical theory of elasticity are not satisfied, the transverse forces N_{i3*} are significantly greater than the forces N_{3i*}.

4. CONCLUSIONS

It is known that the classical theory of elasticity is unsuitable for describing the behavior of structures made of a number of materials widely used in practice. As the results of experiments show (for example, [6, 8]), in these cases one should use the moment asymmetric theory of elasticity. Thin-walled structures according to the three-dimensional asymmetric theory of

elasticity are almost impossible to calculate in view of the complexity of the problem.

For the construction of applied theories of plates, as in the classical theory of elasticity, a three-dimensional problem is reduced to a two-dimensional problem. As a rule, the reduction is performed by the method of hypotheses, using some simplifying assumptions. Hypotheses are accepted by analogy with Kirchhoff's hypotheses. The choice of hypotheses for a complex problem based on known hypotheses for a simple problem often leads to incorrect hypotheses for the desired quantities that are present in a complex problem and are absent in a simple problem. For example, when constructing the theory of thin-walled electroelastic elements by the hypothesis method for entire classes of problems, incorrect hypotheses were adopted for the desired electrical quantities. The reason is that there are no electrical quantities in the theory of elasticity and there are no analogues for the corresponding hypotheses. Mathematically grounded theories of electroelastic thin-walled elements were first constructed without using hypotheses by the asymptotic method of reducing 3D problems of the theory of electroelasticity to 2D problems [15]. The same situation has developed in the moment asymmetric theory of elasticity: the correct equations of the plane problem of the moment theory of elasticity were obtained by the method of hypotheses by many authors in view of the simplicity of the problem. In the problem of plate bending, the correct theory was obtained only by mathematical method [9]. Here, this theory of plate bending in the asymmetric theory of elasticity is presented by the method of hypotheses for simplicity.

REFERENCES

1. **Nowacki, W.** Theory of Asymmetric Elasticity. Pergamon, Oxford (1986).
2. **Erigen A.C.** Theory of mikropolar plates. Z. angew. Math. Phys. 18 (1), 12-30 (1967).
3. **Green A.E., Naghdi P.M.** The linear elastic cosserat surface and shell theory. Intern. J. Solids Structures 4 (6), 585-592 (1968).
4. **Cowin C.S.** An incorrect inequality in micropolar elasticity theory. ZAMP 21, 494-497 (1970).
5. **Cowin C.S.** Stress functions for cosserat elasticity. Int.J. Solids Struct. 6 (4), 389-398 (1970).
6. **Lakes, R.** Experimental methods for study of Cosserat elastic solids and other generalized elastic continua. In H. Muhlaus. and J. Wiley. (eds.), Continuum models for materials with micro-structure. Wiley and sons, New York (1995).
7. **Forest S., Barbe F., Cailletauci G.** Cosserat modeling of size effects in the mechanical behavior of polycrystals and multi-phase materials. Intern. J. Solids Structures 37 (46/47), 7105-7126 (2000).
8. **Lakes R.S.** Physical meaning of elastic constants in Cosserat, void, and microstretch elasticity. Mech. Mater. Struct. (2016).
9. **Rogacheva N.N.** Theory of thin plate in asymmetric elasticity Shell Structures: Theory and Applications. CRC Press. 4, 149-153 (2018).
10. **Vanin G.A.**. Moment mechanics of thin shells. Izv. RAN Solid Body Mechanics 4, 116-138 (2004).
11. **Brovko G.L., Ivanova O.A.** Modeling of the properties and motions of an inhomogeneous one-dimensional continuum of a complex microstructure of the Cosserat type. Izv. RAN Solid Body Mechanics 1, 22-36 (2008).
12. **Sargsyan, S.O.** Boundary-value problems of the asymmetric theory of elasticity for thin plates. Journal of Applied Mathematics and Mechanics 72(1), 77-86 (2008).
13. **Altenbach H., Eremeyev V.A.** On the linear theory of micropolar plates. Z. agnew. Math. Mech 89 (4), 242-256 (2009).
14. **Gol'denveizer, A.L.** The Theory of Thin Elastic Shells. 2nd ed. Nauka, Moscow (1976).
15. **Rogacheva N.N.** The Theory of Piezoelectric Plates and Shells. CRC Press, Boca Raton (1994).

СПИСОК ЛИТЕРАТУРЫ

1. **Nowacki, W.** Theory of Asymmetric Elasticity // Oxford: Pergamon, 1986.
2. **Erigen A.C.** Theory of mikropolar plates // Z. angew. Math. Phys., Volume 18, Issue 1, 1967, p. 12-30.
3. **Green A.E., Naghdi P.M.** The linear elastic cosserat surface and shell theory // Intern. J. Solids Structures, Volume 4, Issue 6, 1968, p. 585-592.
4. **Cowin C.S.** An incorrect inequality in micropolar elasticity theory // ZAMP, Volume 21, 1970, p. 494-497.
5. **Cowin C.S.** Stress functions for cosserat elasticity // Int.J. Solids Struct., Volume 6, Issue 4, 1970, p. 389-398.
6. **Lakes, R.** Experimental methods for study of Cosserat elastic solids and other generalized elastic continua. // In H. Muhlaus. and J. Wiley. (eds.), Continuum models for materials with micro-structure. New York: Wiley and sons, 1995.
7. **Forest S., Barbe F., Cailletauci G.** Cosserat modeling of size effects in the mechanical behavior of polycrystals and multi-phase materials // Intern. J. Solids Structures, Volume 37, Issues 46/47, 2000, p. 7105-7126.
8. **Lakes R.S.** Physical meaning of elastic constants in Cosserat, void, and microstretch elasticity // Mech. Mater. Struct., 2016.
9. **Rogacheva N.N.** Theory of thin plate in asymmetric elasticity Shell Structures: Theory and Applications // CRC Press, Volume 4, 2018, p.149-153.
10. **Ванин Г.А.** Моментная механика тонких оболочек // Изв. РАН Механика твердого тела, 2004, №4, с. 116-138.
11. **Бровко Г.Л., Иванова О.А.** Моделирование свойств и движений неоднородного одномерного континуума сложной микроструктуры типа Коссера // Изв. РАН Механика твердого тела, 2008, №1, с. 22-36.
12. **Sargsyan, S.O.** Boundary-value problems of the asymmetric theory of elasticity for thin plates // Journal of Applied Mathematics and Mechanics, Volume 72, Issue 1, 2008, p. 77-86.
13. **Altenbach H., Eremeyev V.A.** On the linear theory of micropolar plates // Z. agnew. Math. Mech., Volume 89, Issue 4, 2009, p. 242-256.
14. **Gol'denveizer, A.L.** The Theory of Thin Elastic Shells. 2nd ed. // Moscow: Nauka, 1976.
15. **Rogacheva N.N.** The Theory of Piezoelectric Plates and Shells // Boca Raton: CRC Press, 1994.

Nelly N. Rogacheva, Doctor of Physical and Mathematical Sciences, laureate of the State Prize of the Russian Federation in the field of science and technology, Associate Professor, Department of Informatics and Applied Mathematics, Moscow State University of Civil Engineering, 129337, Russia, Moscow, Yaroslavskoe Shosse, 26, tel. +7(499)1835994, e-mail: rogachevann@mgsu.ru;

Yulia G. Zheglova, Candidate of Tehnical Sciences, Associate Professor, Department of Information Systems, Technologies and Automation in Construction, Moscow State University of Civil Engineering, 129337, Russia, Moscow, Yaroslavskoe Shosse, 26, tel. +7(495)2874919, e-mail: uliagermanovna@yandex.ru.

Рогачева Нэлля Николаевна, доцент, доктор физико-математических наук, лауреат Государственной премии Российской Федерации в области науки и техники, кафедра информатики и прикладной математики Национального исследовательского Московского государственного строительного университета; 129337, Россия, г. Москва, Ярославское шоссе, д. 26; тел. +7(499)1835994; e-mail: rogachevann@mgsu.ru;

Жеглова Юлия Германовна, доцент, кандидат технических наук, кафедра информационных систем, технологий и автоматизации в строительстве Национального исследовательского Московского государственного строительного университета; 129337, Россия, г. Москва, Ярославское шоссе, д. 26; тел. +7(495)2874919 доб. 30-44; e-mail: uliagermanovna@yandex.ru.

International Journal for Computational Civil and Structural Engineering, 19(2) 81–94 (2023)

DOI:10.22337/2587-9618-2023-19-2-81-94

NUMERICAL STUDY OF ICE AND CHANNEL PROCESSES ON THE BRIDGE SUPPORTS ACROSS THE KUIBYSHEV RESERVOIR (KAZAN)

Vitaly V. Belikov [1], Natalya M. Borisova [1], Anna V. Glotko [1,2], Dmitry V.Kozlov [1,2]

[1] Water Problems Institute of the Russian Academy of Sciences (WPI RAS), Moscow, RUSSIA
[2] National Research Moscow State University of Civil Engineering, Moscow, RUSSIA

Abstract: Numerical hydrodynamic modeling of water movement at discharges of 1% and 10% supply is considered in order to study the effect of ice effects and bottom deformations on the bridge supports across the reservoir of the Kuibyshev hydroelectric complex, and to predict the general erosion of the channel. The calculations use two-dimensional shallow water and sediment transport equations implemented in the STREAM 2D CUDA software package.

Keywords: numerical modeling, shallow water equations, bridge crossing, general erosion, ice effects

ЧИСЛЕННОЕ МОДЕЛИРОВАНИЕ ДЕФОРМАЦИЙ ДНА И ЛЕДОВЫХ ЯВЛЕНИЙ НА ОПОРЫ СТРОЯЩЕГОСЯ МОСТА ЧЕРЕЗ КУЙБЫШЕВСКОЕ ВОДОХРАНИЛИЩЕ У Г. КАЗАНИ

В.В. Беликов [1], Н.М. Борисова [1], А.В. Глотко [1,2], Д.В. Козлов [2]

[1] Институт водных проблем РАН (ИВП РАН), г. Москва, РОССИЯ
[2] Национальный исследовательский Московский государственный строительный университет, г. Москва, РОССИЯ

Аннотация: Рассматривается численное гидродинамическое моделирование движения воды при расходах 1%-ной и 10%-ной обеспеченности с целью исследования влияния ледовых воздействий и деформаций дна на опоры моста через Куйбышевское водохранилище, прогнозирование общих размывов русла. В расчетах применяются двумерные уравнения мелкой воды и транспорта наносов, реализованные в программном комплексе STREAM 2DCUDA.

Ключевые слова: численное моделирование, уравнения мелкой воды, мостовой переход, общий размыв, ледовые воздействия

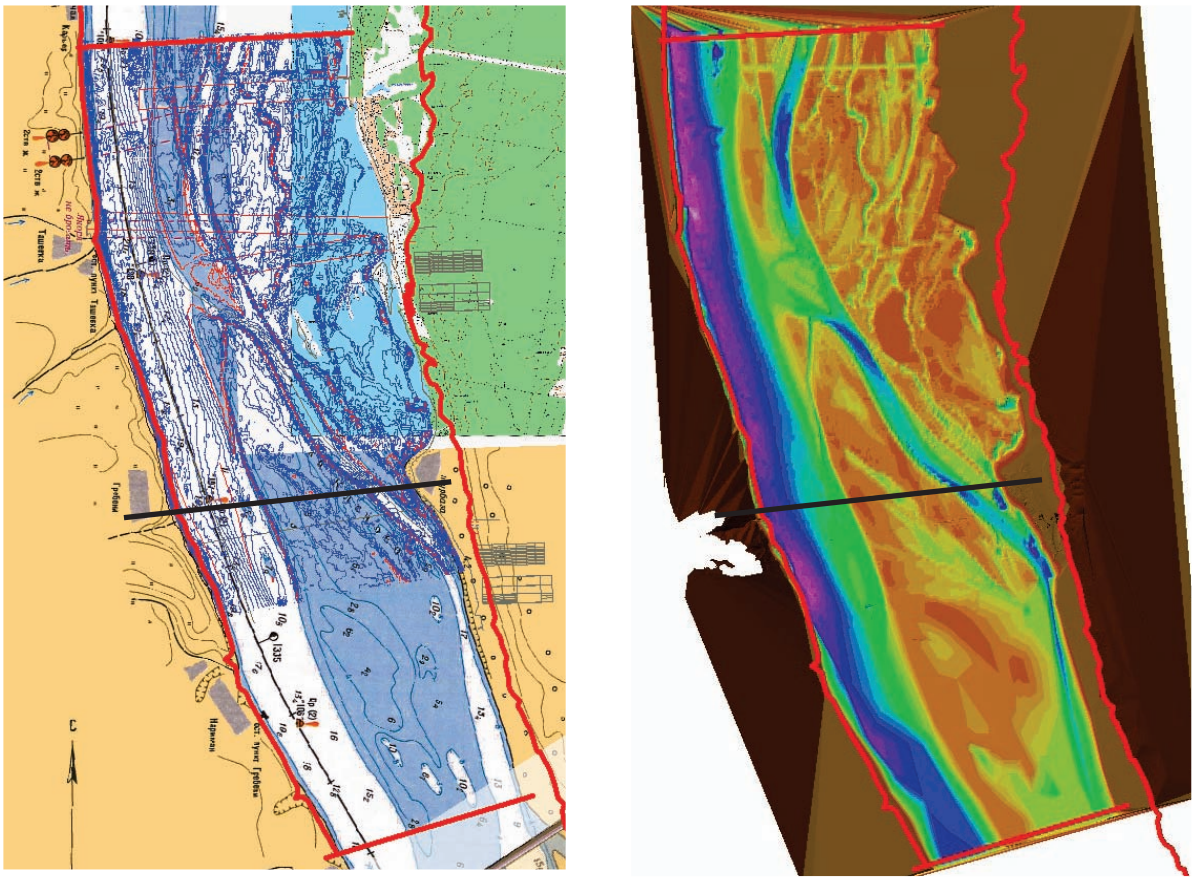
INTRODUCTION

The projected bridge across the Kuibyshev reservoir is a part of the Moscow-Nizhny Novgorod-Kazan highway and is located in the Republic of Tatarstan, 17 km to the south from Kazan. Complex natural and anthropogenic processes take place at this site, which require a comprehensive study, including engineering surveys and scientific research.

The main objective of the numerical simulation is to calculate the possible complex impact on the bridge during construction and operation under various hydrological conditions. Among natural factors, special attention was paid to hydraulic flow characteristics in spring period considering ice phenomena, reservoir bottom deformations at maximum water discharges, which can be observed during the bridge construction and operation period. The technogenic impact on the studied area from the temporary bridge, as well as from the permanently operating quarry was also assessed.

Large-scale cartographic materials [1, 2] and engineering-hydrographic plan were used to build a digital relief model (Figure 1, a). The

data were reduced to a unified system of coordinates and heights. At the next stage a continuous surface was built by the Delaunay triangulation method, edited by semi-automatic method. The resulting digital relief model (hereinafter DRM) (Figure 1, b) was used as the initial relief data for the numerical hydrodynamic model. The data on the hydrological regime in the construction area were obtained from observations at the nearest hydrological stations in Uslon settlement. Verkhniy Uslon (upstream of the projected bridge) and the village of Kirelskoye (downstream of the projected bridge, below the confluence of the Volga and Kama rivers). In accordance with them, water discharges (1% and 10% probability) and levels typical for the flood period were selected for modeling. During the winter period of 2021 observations of ice conditions in the construction area were performed and based on their results ice parameters were specified in the model.



a *b*

Figure 1. The stages of building a digital relief model: a - data source; b - final result (black line - bridge span).

To calculate the deformations of the reservoir bottom, the results of engineering-geological surveys were used [1, 2]. Forty-four wells were analyzed in the channel part of the bridge crossing. In the span of the bridge there are predominantly sandy sediments, which in the upper part are covered with loam and silt. The cohesive soils had a small thickness in the section and are mostly withdrawn in the process of construction, losing their resistance to scouring. Therefore, they were not considered in the calculations. Among sandy sediments, medium and fine sands occupy the largest volume. Since the fine and medium sands are unevenly distributed along the depth and alternate with each other, the mathematical modeling assumed that the deformable soil consists of two

fractions of different sizes at a 50%:50% ratio. Cumulative curves were drawn for these sediments based on their grain size distribution, from which d50 and d90 values were derived to calculate deformation.
Fraction 1 (fine) d_{50}=0.13 mm, d_{90}= 0.28 mm.
Fraction 2(medium) d_{50}=0.25 mm, d_{90}=0.55 mm.
On the top border of limestone deposits the non-degradable surface has been appointed.
In the process of modeling, it was also necessary to consider man-made factors arising during the construction and operation of the structure. During the construction period the working (temporary) bridge will be operated. It consists of spans of 110 x 21.4 m on one-row and two-row pile piers of 1.02 m diameter pipes with the ice-breakers device. The permanent bridge crosses the active quarry with a length of almost 6km and a width of 80 to 540 m. Extraction of soil is expected on a constant basis for a long time under low-water conditions. The minimum level of the quarry bottom was assumed to be 26 m.

CALCULATION OF POSSIBLE COMPLEX IMPACT DURING SPRING ICE DRIFT ON TEMPORARY STRUCTURES (WORKING BRIDGE)

The objective of this part of the study is to assess the ice impact on temporary structures (temporary bridge) during the construction period (without the supports of the main bridge). The work was conducted in two stages. On the first stage there was an ice flood modeling to determine the dependence of discharge, levels, speed and gradients in the investigated area. At the second stage ice load on the temporary bridge piers was calculated using the results of previous calculations as initial data.

Simulation of river flow to assess water flow velocities and water surface gradients, including ice jam conditions

For numerical modeling in the computational domain, a hybrid mesh of triangular quadrangular structure (variant 1), with the number of cells about 63 thousand, was constructed. As boundary conditions on the inlet boundary (in the upper part of the computational domain) the water discharge in the river with 10% probability was set equal to 30 000 m3/s. On the outlet boundary (in the lower part) the water level was set. Because of ambiguity of the level modes (among other reasons because of distribution of the head from the downstream hydraulic facility) the calculation was made for two variants of the water level marks on the outlet boundary, which were 53.0 m and 54.0 m.
The roughness coefficient of the river bottom in Manning's formula was accepted to be 0.025, the additional roughness coefficient of the bottom surface of fixed solid ice in the ice jam was also taken to be 0.025, i.e., the total reduced roughness coefficient in the ice jam section was taken to be 0.05.
It was assumed that a temporary bridge as a disturbance in the channel would provoke ice jam upstream. Therefore, ice cover was modeled in the upstream part of the bridge structure, and the water surface downstream was set as ice-free. The ice thickness was assumed to be 10% probability and equal to 0.73 m according to the design data. The close average value was obtained from the data of full-scale measurements in the beginning of March, 2021.
Numerical studies were performed using the widely tested [3-9] Russian software package for hydrodynamic modeling STREAM 2D CUDA developed at the NPP "Aquarius Analytic" Ltd. [10]. High-precision original algorithms [11-15] used in the calculations allow accounting for the complex orography of the underlying surface [16-18], sediment transport and bottom deformations, taking into account soil heterogeneity and self-bedding phenomena [19-20], as well as the presence of ice phenomena.
Comparative calculations showed that water gradients above the bridge increase more than doubled from 3 cm/km to 6.7 cm/km in the presence of ice jam (Figure 2). Other parameters showed insignificant changes.

The calculation variant with the boundary condition at the outlet of 54 m showed the closest value with the in-situ measurements at the given roughness coefficients, which was accepted for the further modeling.

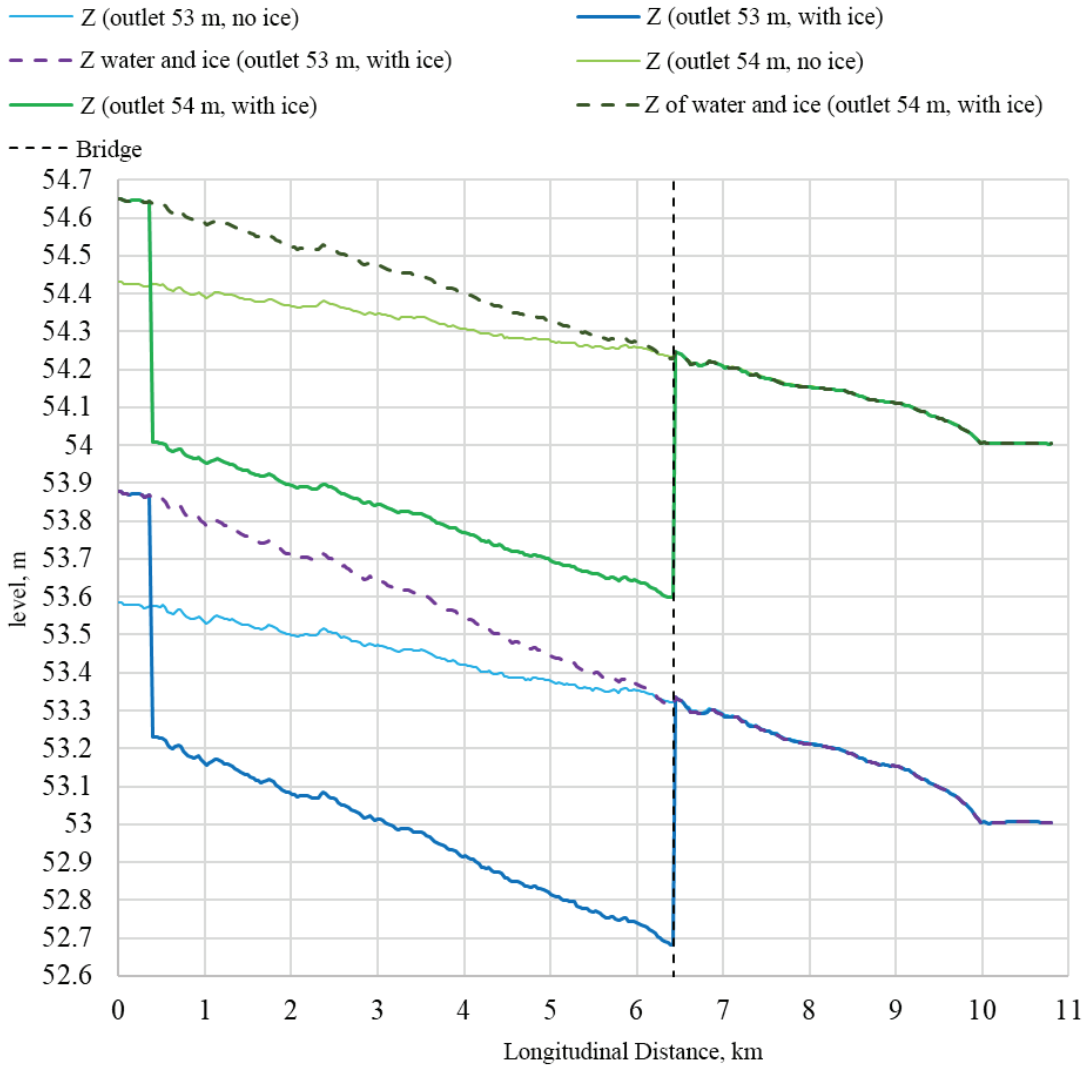


Figure 2.Longitudinal profiles of calculated water levels at Q=30000 m³/s.

Determination of ice forces on temporary technological structures (working bridge)

Based on the simulation results, the following values of the determining parameters and design features were adopted for the design conditions of the construction period during the ice drift to estimate the ice load on temporary structures:

- ice thickness is 0.73 m (10% probability, close to actual measured values for the 2021 flood);
- the depth average speed of stream flow in the deep-water part (in the area of the main fairway) for the conditions of 10% of the flood with the discharge of 30 000 m³/s is 2 m/s (almost the same under ice, and without ice, as the results of modeling show);
- the depth-averaged flow velocity in the main shallow left bank water area is 1 m/s (practically the same under ice and without ice, as the simulation results show);
- for simplicity of calculations, the flow depth in the deep-water part under the right bank is assumed to be 20 m (will not actually be used in

the calculations), and in the shallow-water part it is 5 m;
- slope of water surface in the jam above the bridge is equal to 6.7 cm/km (I=0.000067);
- The temporary bridge is supposed to be built on the supports of relatively small diameter (1 m) with distance between supports 20 m, therefore it does not create essential additional resistance to water flow, however it is an obstacle for moving ice.

Two scenarios were considered to solve the set problems. According to the first scenario we considered the case of unfavorable natural conditions that could lead to a significant jam, i.e., provoke ultimate loads from ice pressure on the working bridge supports. The second scenario is based on the forecast of the spring flood of 2021, in which an insignificant ice jam is formed above the working bridge, and the main danger arises during the ice drift from the impact of floating ice floes.

According to **scenario 1**, based on calculations with ice (performed on the model with mesh variant 1), it can be assumed that an opening of 700 meters in width will let ice floes and ice fields through freely (current velocities reach 2 m/s in the deep-water part of the fairway bottom), but a jam of several kilometers in length and up to 2 km in width can arise on the left bank part above the temporary bridge.

The bridge supports (ice-cutters) will be impacted by the ice field approximately uniformly along the whole length of the temporary bridge, because the current velocity on the whole shallow-water part is equal to 1 m/s on average when the structure flow is passing through. The pressure force application point on the icebreaker will be at the middle of the ice field thickness, i.e., approximately 0.3 m below water level, or approximately at the mark of 54.0 m.

The total pressure of the ice field on one pier of the bridge (i.e., 20 linear meters) is composed of two components: the rolling force (projection of gravity force acting on the ice), equal to (in Newton)

$$F_1 = \rho_i g H_i IBL = 8.64xL \text{ н}$$

and the friction force of the lower part of the ice against the water surface, that, assuming the above assumptions about the equality of the roughness coefficients of the channel bottom and the lower surface of the ice, is equal to half of the total friction resistance of the flow

$$F_2 = 0.5\rho_w g H_w IBL = 32.7xL \text{ н.}$$

Thus, the resulting ice pressure on the support (ice cutter) of the temporary bridge is equal:

$$F = 41.3\ L.$$

Assuming that the length of the jam is 10 km (according to expert opinion, may be less, or maybe more), we get F=413,000 N, or about 40 Tf.

In the calculations of the "ice cutter-piles" system performed by the designers, the ice load is assumed to be equal to F ice = 29.6 Tf. Ice cutters will cut through the ice with a greater load, which will happen when the jam length is close to 7.5 km. When ice is weakened by temperature effects and its thickness decreases, ice breakup on the ice cutters can also start at shorter ice jam lengths.

However, if ice-cutting speed increases rapidly (such situations are possible), ice breaking speed may be insufficient, and then the actual loads on the temporary bridge supports may exceed the calculated ones. This question requires special research and observations. It should be reminded that all the above mentioned refers to the fully constructed temporary bridge.

On this basis, consider that ice jam is formed only at that width of the channel (in its shallow part), which is overlapped by the temporary bridge. Then the load on the outermost supports from static ice pressure will be about 2 times less than on the middle supports, but will not be able to exceed them in any way.

According to scenario 2, the length of ice jams was expertly estimated as 1 km in the situation existing at the beginning of April 2021 (with short sections of the built bridge). Thus, the load

on the support will not exceed 4 Tf, there will be no danger of the support collapse.
However, there is a risk of impact load in this case (especially on the end supports of the bridge sections, and especially for the section in the central part). Due to increased flow velocities there (up to 2 m/s), a large impact load can arise with large sizes of ice floes.
The impact kinetic energy of a 100x100 m ice block of 0.73 m thickness at 2 m/sec velocity is $E=mV^2/2$ =1340 kilotons m, which is comparable to the collapse of a ship of 5000 T displacement on the footing at 2 m/s (tangentially to the footing).
The energy of a 10x10 m ice floe would be 100 times less, and would be 13.4 kilotonnes.

Modeling of bottom deformations for domestic conditions (before construction), during bridge crossing operation, and in the presence of an open pit

To estimate the effect on the reservoir bottom deformations in the area of the bridge piers, two design meshes were prepared by modifying the design mesh of variant 1: with all bridge piers highlighted (variant 2), and an identical mesh for domestic conditions (variant 3), so that the results of calculations with the bridge and in domestic conditions can be compared on these meshes by subtracting values in the cells. The mesh with cut-out bridge supports consists of 76556 cells, while the one without bridge supports consists of 76758 cells (Figure 3).
Modeling of currents and bottom deformations was performed for two constant water flows Q=30000 m3/s (10% flow rate) and Q=39400 m^3/s (1% flow rate) during 1 month (approximate time of high flood passage).
Based on the conducted calculations it can be concluded that in the considered section of the Volga River channel near the projected bridge crossing in domestic conditions during high floods the bottom is on average in steady state of dynamic equilibrium, the balance between volumes of scour and bottom sediments is observed, there is no systematically expressed lowering or raising of erosion base.

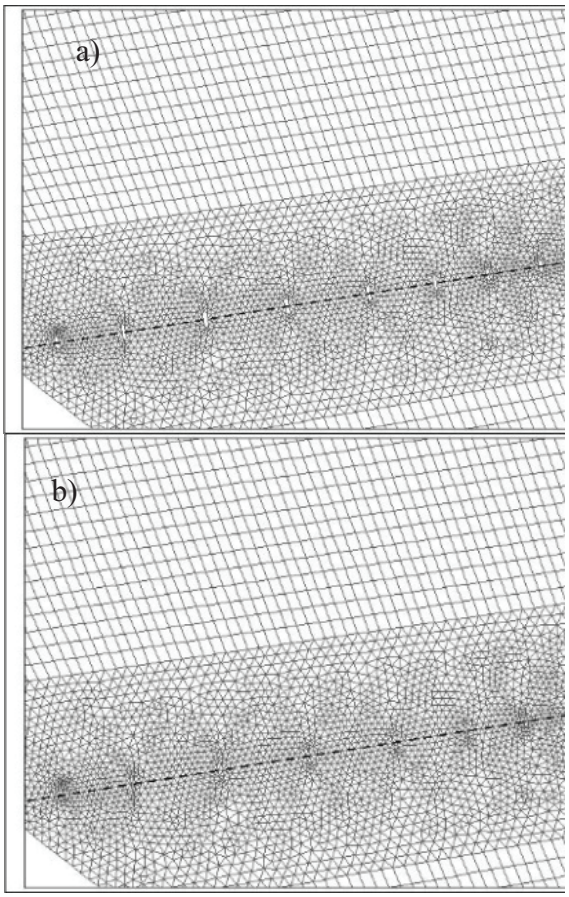


Figure 3. Calculation meshes with and without bridge supports cut out (fragment in the alignment of the bridge near the right bank). Dashed line - the bridge span

Next, the effect of bridge supports on water flow and bottom deformations was analyzed. Namely, channel deformations, flow rates and water levels obtained by calculation in the presence and absence of the bridge crossing were compared. For this purpose, the corresponding results obtained from the model with a bridge crossing (Variant 3) were subtracted from the mesh values of the results obtained from the model for domestic conditions (Variant 2). The results for the two design water flow rates are almost indistinguishable. Figure 4 shows the results for the 10% flow rate.
It should be noted that in the immediate vicinity of the bridge piers (about 10 m radius from the piers) the bottom deformations may not fully correspond to the real values because of the

failure to consider in the applied mathematical model the three-dimensional helical flow near the piers, which leads to additional (local) scouring (should be considered separately, for example, by empirical dependencies).

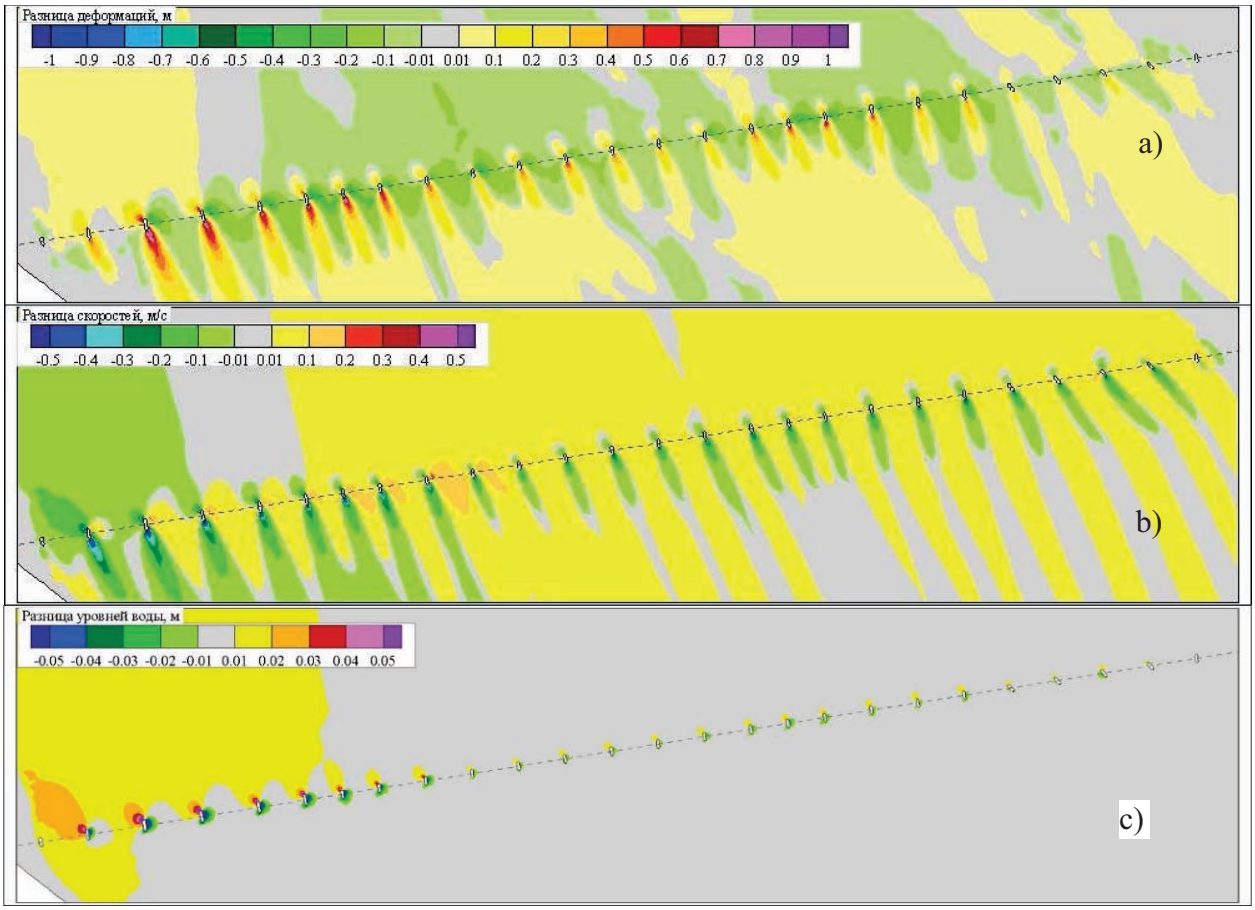


Figure 4. Difference in channel deformations, flow velocities and water levels in the calculation with Q=30000 m³/s (10% flow, fragment near the bridge).

The three-dimensional character of the flow has practically no effect on water surface levels and average flow velocities in depth, so these flow characteristics obtained by calculation, as well as general bottom deformations (scour) between the bridge piers can be considered quite reliable. It should also be noted that most of the piers, especially in deep water, have a small current slant. In the presence of a bridge, channel deformations are characterized by a stronger bottom washout in front of the supports themselves (by ≈10 cm) and between them (by ≈10-30 cm), which is associated with an increase in flow velocity in these places (by ≈0.1-0.2 m/s), and a more intensive scour (sedimentation) behind the bridge supports (by ≈ 10-80 cm), which is associated with a decrease in flow velocity behind them (by ≈0.1-0.5 m/s). Above the section closer to the right bank in front of the bridge there is an increase of the bottom washout (by ≈10 cm), which is associated with a decrease in flow velocity in this area (by ≈0.1 m/s). Water levels in the presence of the bridge crossing change mainly just in this area. Namely, they increase by about 1-3 cm (i.e., the pre-bridge backwater is practically absent), and also change locally at each pier. Before the pier they increase, behind the pier they decrease.

Modeling of the flows and deformations of the bottom in the presence of the bridge crossing

and open pit was performed for the same boundary conditions. Calculation mesh with bridge supports (variant 3) was used, for which an additional DRM with the quarry was prepared.

Outside the quarry, the deformations, as in the previously presented calculation results for domestic conditions and with bridge supports, are not very intensive and mainly lie in the range from +1 m to -1 m. In front of the quarry, the bottom of the river is eroded, and the quarry itself is brought in from the upstream side (slightly at an angle, which is caused by the direction of the stream). The landslide of the slope of the quarry is observed. The similar picture of deformations and for the second flow Q=39400 m3/sec. Flow velocities almost do not change after erosion, levels also change in the process of calculation insignificantly, about 2 cm. It is interesting, that in the pit itself the average depth velocities of flow are less than in the fairway, and decrease in the transverse direction from the right side of the pit to the left.

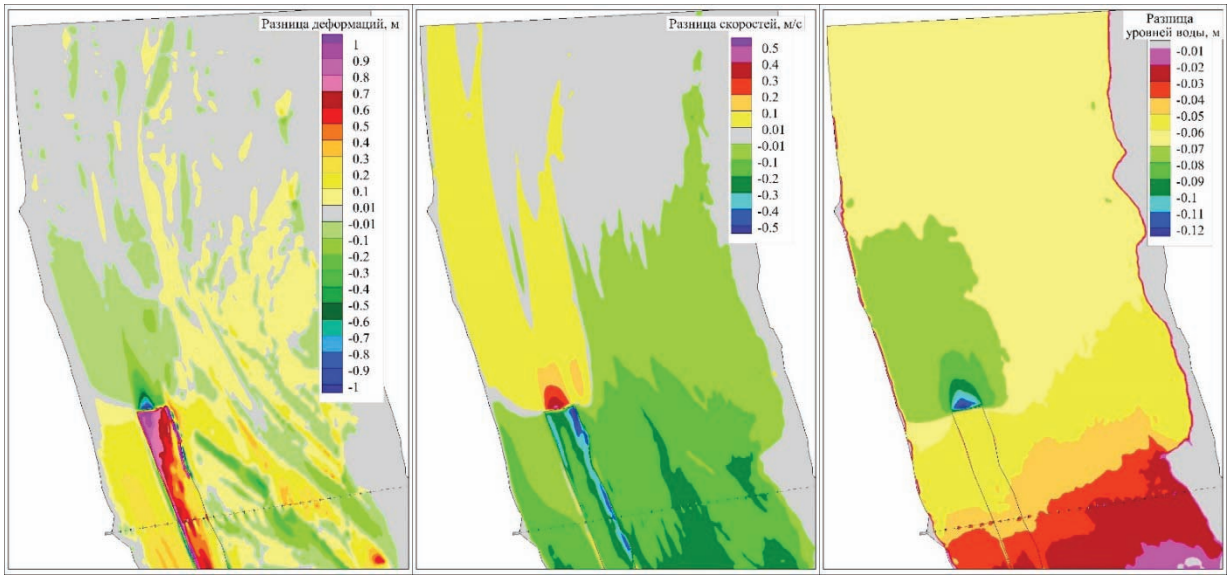


Figure 5. Difference in channel deformations, flow velocities and water levels at calculation with Q=30000 m^3 /s (10% probability)

To analyze the influence of the quarry in detail, the corresponding results obtained from the model with bridge crossing and quarry were subtracted from the grid values of the results obtained from the model with bridge crossing only. Calculation results for the 10% flow rate are shown in Figure 5.

For both discharges the character of changes is the same. The difference of channel deformations showed that in the presence of the quarry we observe more intensive bottom erosion before the quarry (up to 90 cm) and on the approach to it (up to 10 cm), which is because of the flow speed increase before the quarry (up to 0.4 m/s) and on the approach to it (by ≈0.1 m/s), and further mostly more intensive washout in the quarry (up to 1m) and along the channel (up to 30 cm), which is connected with flow speed lowering. Water levels in the presence of the quarry decrease throughout the calculated area, in the vicinity of the bridge section water levels in the presence of the quarry are lower by 3 - 5 cm for the flow of 30000 m^3 /s in comparison with the model without the quarry, and for the flow 39400 m^3 /s - by 1 - 4 cm. Thus, the presence of the quarry leads to the landing of water levels in the alignment of the bridge up to 5 cm, and in the head of the quarry up to 10-12 cm.

Water levels in the crossing section after the construction of the quarry decrease by several

centimeters, and to the greatest extent in the deep-water part and in the territory of the quarry itself. Current velocities decrease in the section of the bridge mainly by 0.1-0.3 m/s, but in some sections even more. Bottom deformations, on the contrary, are mainly positive, i.e., there is a kind of "general rewashing" of ground in the bridge alignment, except for local areas.

However, it should be noted that all these bottom changes will take place within the first tens of centimeters per one flood of rare recurrence, and in the vast majority of cases will be minimal, and cannot affect the choice of design solutions in any way. In this regard, an additional simulation of the situation for the period of 100 years (12 high floods) has been performed.

Deformations of the reservoir bottom, due to the uncertainty of the hydrological situation forecast and unpredictability of anthropogenic factors, it is impossible to forecast with high accuracy quantitatively, especially for a century period. However, the main tendencies of bottom deformation in the bridge area, predicted by numerical modeling, are quite clear and explainable from the point of view of reservoir bottom deformations development in time.

According to the results of calculations with the bridge without the quarry for the century period, it was obtained that flow velocities will change insignificantly, water levels will decrease insignificantly, up to 4-6 cm in the alignment of the bridge.

During modeling, considering the quarry, it was found that it influences bottom reshaping, including changing conditions of connection of the main (flooded channel of Volga River) and additional (flooded floodplain channel) fairways, as well as leading to sedimentation under the right bank in alignment of the bridge on the value up to 2-3 m. The quarry itself from the upstream side is subject to silting (sedimentation), but this process is quite long-term and can take hundreds of years. The matter is that the quarry is stretched along the channel (near the fairway), and its width is only about 10% of the river width. Therefore, it intercepts only a small portion of the river's solid flow. The velocity field is generally flattened while maintaining the same velocity values. Water levels drop by 8 cm on average (from 10 to 11 cm in the upper part to 6 to 7 cm in the lower part), which is largely due to the impact of the quarry, which has increased the area of the river cross-section.

The scour in the quarry itself can reach 5-7 m, and the total scour under the bridge in some sections will not exceed 1.5-2.0 m. It is interesting that the presence of the quarry reduces the intensity of deformation and scour depth in the side channel (the second fairway) compared with the variant without the quarry, which leads to some reduction in the size of scour at piers 19-22 (Figures 6,7). The quarry as if draws a part of the water flow to itself, reducing the share of the flow that enters the side channel. Current velocities with regard to the quarry will change within the range of plus 0.2 m/s - minus 0.1 m/s. Water levels in the bridge alignment will "sit" by 6-8 cm.

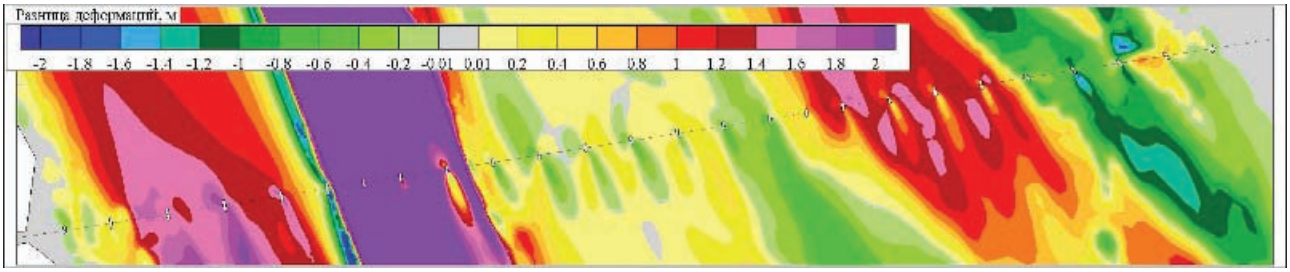


Figure 6. Difference in channel deformations over 100 years in the models with the bridge in the presence and absence of the quarry (fragment at the bridge)

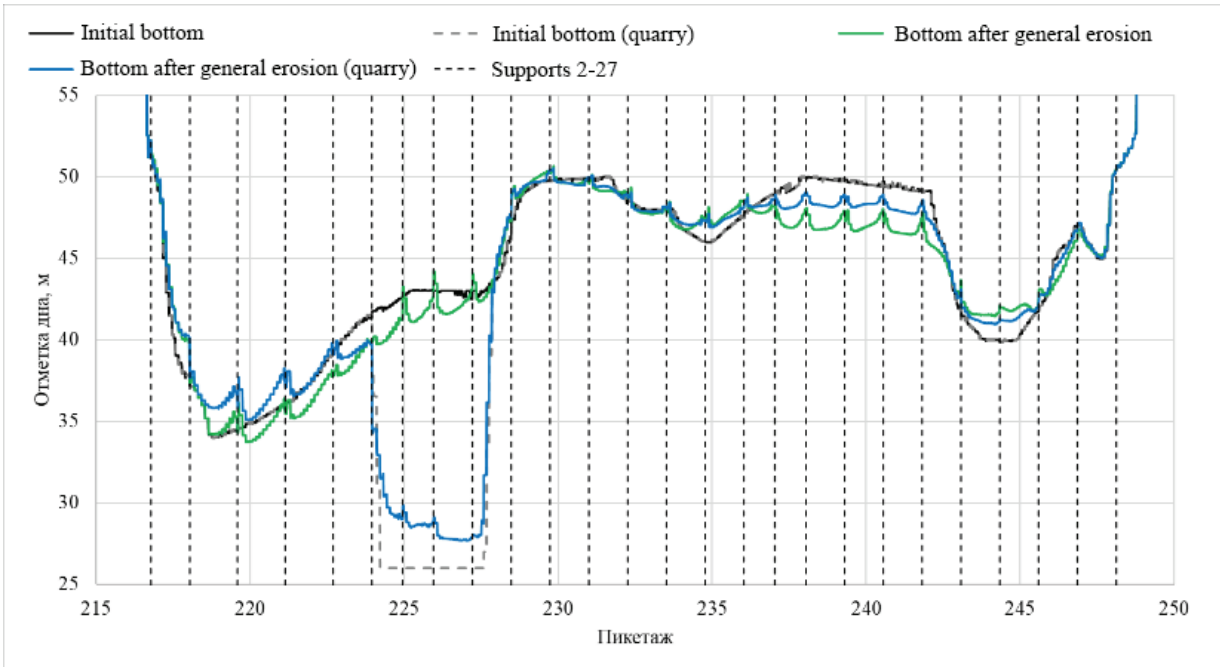


Figure 7. Profiles of the initial bottom and after 100 years in the bridge alignment with and without consideration of the quarry

CONCLUSIONS

In accordance with the stated objectives of the research work for the calculation of the possible complex impact during the spring ice drift on the temporary structures built for the construction of the bridge over the Volga River (ice loads, support, overflow). As well as modeling the deformation of the reservoir bottom near the bridge piers considering possible underwater sand pit development on the M-12 "Moscow-Nizhny Novgorod-Kazan highway under construction", the initial data for modeling were prepared and the scenarios for the modeling were developed.

The main conclusions are as follows:

1. ice phenomena, which may appear on the investigated section, do not pose a threat for the working bridge (which was confirmed in 2021) and for the designed bridge crossing.
2. the bridge piers have an insignificant influence on the hydrodynamic parameters and deformations of the reservoir bottom in the case of the high-water level (1% probability), in the spring period (10% probability) if ice phenomena occur, and in the long term (for 100 years).
3. At quarry excavations more intensive deformations of a reservoir bottom are observed, especially in the long time period. However, these phenomena are not dangerous for the bridge piers due to the actual location and configuration of the active quarry.

ACKNOWLEDGEMENT

This work was performed within the framework of the State Task of IWP RAS (subject FMWZ-2022-0003 "Development of numerical models of hydrological, hydrodynamic and hydro chemical processes in water bodies and their watersheds, creation of decision support technologies based on the developed models in the field of water safety for information modernization of water industry in Russia" – целесообразно привести в соответствии с официальным переводом или продублировать на русском).

Работа выполнена в рамках Государственного задания ИВП РАН (тема FMWZ-2022-0003 “Разработка численных моделей гидрологических, гидродинамических и гидрохи-

мических процессов в водных объектах и их водосборных бассейнах, создание на основе разработанных моделей технологий поддержки решений в сфере водной безопасности для информационной модернизации водохозяйственной отрасли России")

REFERENCES

1. Proektnaya dokumentaciya DSiR-2020-1163 Razdel 1. Poyasnitel`naya zapiska Podrazdel 2. Otchetnaya dokumentaciya po rezul`tatam inzhenerno-geologicheskix izy`skanij Chast` 1. Kniga 1. Poyasnitel`naya zapiska DSiR 2020-1163-P1-IGI-2.1.1 Tom 2.1.1 Moskva. 2020 (in Russian, unpublished).
2. Proektnaya dokumentaciya DSiR-2020-1163 Razdel 1. Poyasnitel`naya zapiska Podrazdel 2. Otchetnaya dokumentaciya po rezul`tatam inzhenerno-geologicheskix izy`skanij Chast` 1. Kniga 1. Poyasnitel`naya zapiska DSiR 2020-1163-P1-IGI-2.1.1 Tom 2.3.11 Moskva 2020(in Russian, unpublished).
3. **Belikov V.V., Aleksyuk A.I.** Modelimelkojvody` v zadachaxrechnojgidrodinamiki. Monografiya [Shallow water models in problems of river hydrodynamics. Monograph] M.: RAN, 2020. – 346 s. (in Russian)
4. **Vasil'eva E. S., Aleksyuk A. I., Belyakova P.A., Belikov V. V., Fedorova T.A.** (2019) Numerical Modeling of the Behavior of a Destructive Rain Flood on a Mountain River . Journal ofWater Resources,vol. 46, no. S1, pp. 43-55. doi:10.1134/S0097807819070169.
5. **Belikov V. V., Aleksyuk A. I., Borisova N.M., Fedorova T. A**. (2019) Use of Accumulation Basins to Reduce Silting of Reservoirs of Hydroelectric Power Plants Located on Mountain Rivers. Journal of Power Technology and Engineering, vol. 53, no. 4, pp. 429-439. doi:10.1007/s10749-019-01095-9.
6. **Fedorova T. A., Vasil'eva E. S., Belikov V.V.** (2020) Numerical Simulation of Triangular Dam Overflow. Journalof Power Technology and Engineering, vol. 54, no. 3,pp. 354-357. doi: 10.1007/s10749-020-01215-w.
7. **Belikov V.V., Aleksyuk A.I., Borisova N.M., Rumyantsev A.B., Glotko A.V.** (2022) Estimation of the Level of Floodplain Inundation in the Lower Don under the Effect of Economic Activity. Retrospective Hydrodynamic Modeling. Journalof Water Resources,vol. 49, no. 6,pp. 941-949. doi: 10.1134/S0097807822060021.
8. **Vasil`eva E.S., Belikov V.V., Glotko A.V.** (2022) Chislennoe modelirovanie kolichestvenny`x parametrov proxozhdeniya rasxodov vody` cherez Uspenskuyu plotinunu r. Klyaz`me. [Numerical modeling of the quantitative parameters of the passage of water flow through the Uspenskaya dam on the river. Klyazma]. Gidrotexnicheskoe stroitel`stvo, № 5,s. 30-35 (in Russian).
9. **Vasil`eva E.S., Belikov V.V., Glotko A.V.** (2022) Chislennoe modelirovanie volny` prory`va gidrouzla № 10 Belomorsko-Baltijskogokanala. [Numerical modeling of the breakthrough wave of the hydroelectric complex No. 10 of the White Sea-Baltic Canal].Gidrotexnicheskoestroitel`stvo, № 7,s. 25-29 (in Russian).
10. **Aleksyuk A.I., Belikov V.V.** Programmny`jkompleks STREAM 2D CUDA dlyaraschetatechenij, deformacijdnaiperenosazagryaznenij v otkry`ty`xpoto-kax s ispol`zovaniemtexnologij Compute Unified Device Architecture (nagraficheskixprocessorax NVIDIA). Svidetel`stvo o gosudarstvennojregi-straciiprogrammdlya E`VM № 2017660266 ot 20.09.2017 (in Russian).
11. **Aleksyuk A.I., Belikov V.V. (**2017) Modeli-rovanie techenijmelkoj vody` s obla-styamiobmeleniyairazry`vamidna. Vy`chislitel`naya matematika i matematicheskaya fizika, T. 57. № 2. S. 316-338 (in Russian).

12. **Aleksyuk A.I., Belikov V.V.**(2017) Simulation of shallow water flows with shoaling areas and bottom discontinuities. Journalof Comput. Math. Math. Phys., vol. 57, no.2, pp. 318–339. doi:10.1134/S0965542517020026
13. **Aleksyuk A.I., Belikov V.V.** (2019) The uniqueness of the exact solution of the Riemann problem for the shallow water equations with discontinuous bottom. Journal of Computational Physics, vol. 390, pp. 232-248.doi:10.1016/j.jcp.2019.04.001
14. **Aleksyuk A.I., Malakhov M.A., Belikov V.V.**(2022) The exact Riemann solver for the shallow water equations with a discontinuous bottom. Journal of Computational Physics, 450, 110801. doi: 10.1016/j.jcp.2021.110801.
15. **Aleksyuk A.I., Malaxov M.A., Belikov V.V.** Reshatel` zadachi Rimana dlya uravnenij melkojvody` s razry`vny`mdnom. Svidetel`stvo o gosudarstvennoj regi-stracii programmy` dlya E`VM №2020660617, 2020 (in Russian).
16. **Belikov V.V., Borisova N.M., Aleksyuk A.I., Rumyantsev A.B., Shurukhin L.A., Glotko A.V.** (2018) Hydraulic substantiation of the Bagaevskaya hydro complex project based on numerical hydrodynamic modeling.Journal of Power Technology and Engineering, vol. 52, no. 4, pp. 372-388. doi:10.1007/s10749-018-0962-9.
17. **Rumyantsev A. B., Borisova N. M., Belikov V. V.**(2022) Assessing the Hazard Due to the Effect of Heat Discharges from the Novocherkasskaya SDPP on the Hydroecological Regime of the Lower Don Taking into Account the Future Bagaevskoe Reservoir. Journal of Power Technology and Engineering,vol. 49, no. 3,pp. 448-457.doi.org/10.1134/S0097807822030125.
18. **Belikov V.V., Borisova N.M., Glotko A.V.**(2021) Numerical Hydrodynamic 2D-Simulation of the Inundation of Tulun Town on the Iya R. during Flood 2019.Journal of Water Resources, vol. 48, no. 5,pp. 713-725. doi 10.1134/S0097807821040023.
19. **Aleksyuk A. I., Belikov V. V., Borisova N. M., Fedorova T. A.** (2018) Numerical Modeling of Non-Uniform Sediment Transport in River Channels Journal of Water Resources,vol. 45, no. S1, pp. 11-17. doi:10.1134/S0097807818050275.
20. **Belikov, V.V. Vasil'eva E.S.**(2020) Numerical Modeling of a Hydrodynamic Accident at an Earth-and-Rockfill Dam on the Dyurso River. Journal of Power Technology and Engineering, vol. 54, no. 3,pp. 326-331. doi:10.1007/s10749-020-01210-1

СПИСОК ЛИТЕРАТУРЫ

1. Проектная документация ДСиР-2020-1163 Раздел 1. Пояснительная записка Подраздел 2. Отчетная документация по результатам инженерно-геологических изысканий Часть 1. Книга 1. Пояснительная записка ДСиР2020-1163-П1-ИГИ-2.1.1 Том 2.1.1 Москва 2020 г.
2. Проектная документация ДСиР-2020-1163 Раздел 1. Пояснительная записка Подраздел 2. Отчетная документация по результатам инженерно-геологических изысканий Часть 1. Книга 1. Пояснительная записка ДСиР2020-1163-П1-ИГИ-2.1.1 Том 2.3.11 Москва 2020 г.
3. **Беликов В.В., Алексюк А.И.**Модели мелкой воды в задачах речной гидродинамики. Монография М.: РАН, 2020. – 346 с.
4. **Vasil'eva E. S., Aleksyuk A. I., Belyakova P.A., Belikov V. V., Fedorova T.A.** Numerical Modeling of the Behavior of a Destructive Rain Flood on a Mountain River //Water Resources. – 2019. – Vol. 46, No. S1. – P. 43-55. – doi:10.1134/S0097807819070169.
5. **Belikov V. V., Aleksyuk A. I., Borisova N.M., Fedorova T. A**. Use of Accumulation Basins to Reduce Silting of Reservoirs of Hydroelectric Power Plants Located on

Mountain Rivers // PowerTechnology and Engineering. – 2019. – Vol. 53, No. 4. – P. 429-439. – doi:10.1007/s10749-019-01095-9.

6. **Fedorova T. A., Vasil'eva E. S., Belikov V.V.** Numerical Simulation of Triangular Dam Overflow // Power Technology and Engineering. – 2020. – Vol. 54, No. 3. – P. 354-357. – doi 10.1007/s10749-020-01215-w
7. **Belikov V.V., Aleksyuk A.I., Borisova N.M., Rumyantsev A.B., Glotko A.V.**Estimation of the Level of Floodplain Inundation in the Lower Don under the Effect of Economic Activity. Retrospective Hydrodynamic Modeling. // Water Resources. – 2022. – Vol. 49, No. 6. – P. 941-949. – doi 10.1134/S0097807822060021
8. **Васильева Е.С., Беликов В.В., Глотко А.В.**Численное моделирование количественных параметров прохождения расходов воды через Успенскую плотину на р. Клязьме. // Гидротехническое строительство. – 2022. – № 5. – С. 30-35
9. **Васильева Е.С., Беликов В.В., Глотко А.В.**Численное моделирование волны прорыва гидроузла № 10 Беломорско-Балтийского канала. // Гидротехническое строительство. – 2022. – № 7. – С. 25-29
10. **Алексюк А.И., Беликов В.В**. Программный комплекс STREAM 2DCUDA для расчета течений, деформаций дна и переноса загрязнений в открытых потоках с использованием технологий ComputeUnifiedDeviceArchitecture (на графических процессорах NVIDIA). // Свидетельство о государственной регистрации программ для ЭВМ № 2017660266 от 20.09.2017.
11. **Алексюк А.И., Беликов В.В.** Моделирование течений мелкой воды с областями обмеления и разрывами дна // Вычисл. матем. и матем. физ., 2017 г. Т. 57. № 2. С. 316-338.
12. **Aleksyuk A.I., Belikov V.V.** Simulation of shallow water flows with shoaling areas and bottom discontinuities. // Comput. Math. Math. Phys., 2017, Vol. 57, No.2, P. 318–339. doi:10.1134/S0965542517020026
13. **AleksyukA.I., Belikov V.V.**The uniqueness of the exact solution of the Riemann problem for the shallow water equations with discontinuous bottom // Journal of Computational Physics, vol. 390, pp. 232-248, Aug.2019. https://doi:10.1016/j.jcp.2019.04.001
14. **Aleksyuk A.I., Malakhov M.A., Belikov V.V.** The exact Riemann solver for the shallow water equations with a discontinuous bottom // Journal of Computational Physics. 2022, vol. 450, p. 110801, 2022, doi:10.1016/j.jcp.2021.110801
15. **Алексюк А.И., Малахов М.А., Беликов В.В.**Решатель задачи Римана для уравнений мелкой воды с разрывным дном // Свидетельство о государственной регистрации программы для ЭВМ №2020660617, 2020.
16. **Belikov V.V., Borisova N.M., Aleksyuk A.I., Rumyantsev A.B., Shurukhin L.A., Glotko A.V.** Hydraulic substantiation of the Bagaevskaya hydro complex project based on numerical hydrodynamic modeling.// Power Technology and Engineering. - 2018. Vol. 52, No. 4. – P. 372-388. – doi:10.1007/s10749-018-0962-9.
17. **Rumyantsev A. B., Borisova N. M., Belikov V. V.** Assessing the Hazard Due to the Effect of Heat Discharges from the Novocherkasskaya SDPP on the Hydroecological Regime of the Lower Don Taking into Account the Future Bagaevskoe Reservoir. // Power Technology and Engineering – 2022. – Vol. 49, No. 3. – P. 448-457.doi.org/10.1134/S0097807822030125
18. **Belikov V.V., Borisova N.M., Glotko A.V.** Numerical Hydrodynamic 2D-Simulation of the Inundation of Tulun Town on the Iya R. during Flood 2019 //Water Resources. - 2021. – Vol. 48, No. 5. – P. 713-725. – DOI 10.1134/S0097807821040023
19. **Aleksyuk A. I., Belikov V. V., Borisova N. M., Fedorova T. A.** Numerical Modeling of Non-Uniform Sediment Transport in

River Channels // Water Resources. – 2018. – Vol. 45, No. S1. – P. 11-17. – doi:10.1134/S0097807818050275.

20. **Belikov, V.V. Vasil'eva E.S.** Numerical Modeling of a Hydrodynamic Accident at an Earth-and-Rockfill Dam on the Dyurso River // Power Technology and Engineering. – 2020. – Vol. 54, No. 3. – P. 326-331. – doi:10.1007/s10749-020-01210-1

Vitaly V. Belikov, Doctor of Technical Sciences, Head of Laboratory of Numerical Hydrodynamic Modelling; Water Problems Institute of the Russian Academy of Sciences; 3, Gubkinst., Moscow, 119333, Russia; e-mail: belvv@bk.ru.

Natalya M. Borisova, Candidate of Science in Physics and Mathematics, senior researcher; Water Problems Institute of the Russian Academy of Sciences; 3, Gubkinst., Moscow, 119333, Russia; e-mail: borisovanm@mail.ru.

Anna V. Glotko, Candidate of Technical Sciences senior researcher; Water Problems Institute of the Russian Academy of Sciences; 3, Gubkinst., Moscow, 119333, Russia; Associate Professor, Department of "Hydraulics and Hydrotechnical Engineering" NRU MGSU 26, YaroslavskoyeShosse, Moscow, 129337,Russia. e-mail: annaglotko@mail.ru

Dmitry V. Kozlov, Doctor of Technical Sciences, Professor, Head of Department of "Hydraulics and Hydrotechnical Engineering" NRU MGSU 26, YaroslavskoyeShosse, Moscow, 129337,Russia. e-mail: kozlovdv@mgsu.ru

Беликов Виталий Васильевич, доктор технических наук, главный научный сотрудник, заведующий лабораторией численного гидродинамического моделирования; Институт водных проблем Российской академии наук; 119333, Москва, ул. Губкина, 3; e-mail: belvv@bk.ru.

Борисова Наталья Михайловна, кандидат физико-математических наук, старший научный сотрудник; Институт водных проблем Российской академии наук; 119333, Москва, ул. Губкина, 3; e-mail: borisovanm@mail.ru.

Глотко Анна Владимировна, кандидат технических наук, старший научный сотрудник; Институт водных проблем Российской академии наук; 119333, Москва, ул. Губкина, 3, доцент кафедры гидравлики и гидротехнического строительства НИУ МГСУ; 129337, Москва, Ярославское шоссе, д. 26 annaglotko@mail.ru

Козлов Дмитрий Вячеславович, доктор технических наук, профессор, заведующий кафедрой гидравлики и гидротехнического строительства НИУ МГСУ; 129337, Москва, Ярославское шоссе, д. 26; kozlovdv@mgsu.ru

DOI:10.22337/2587-9618-2023-19-2-95-108

DETERMINATION OF BOUNDARIES PARAMETERS OF THE COMPUTATIONAL MODEL FOR ASSESSING THE IMPACT ON THE SURROUNDING FACILITIES FROM TUNNELING

Armen Z. Ter-Martirosyan [1], Rustam H. Cherkesov [2], Ilya O. Isaev [2], Viktoriya V. Rud [1], Mariya I. Ambrushkevich [1]

[1] National Research Moscow State University of Civil Engineering, Moscow, RUSSIA
[2] Institute Mosinzhproekt Limited Liability Company, Moscow, RUSSIA

Abstract. As a result of active development of Moscow underground space, as well as due to the increased density of urban development, it is necessary to forecast additional displacements of surrounding buildings from new construction in order to prevent emergency situations. For this reason, one of the important directions is mathematical modeling of the additional displacements of the surrounding building after erection. Establishing the parameters of design boundaries of a geotechnical model is one of the factors that greatly influence the results of the simulation. This study deals with the assignment of the lower boundary of the scheme when estimating the impact from tunneling works in a two-dimensional formulation. A review of international experience in simulating the design scheme depth for various geotechnical problems and its comparison with Russian experience in modeling schemes has been made. The deformation marks located on the ground surface in the zone of influence of the Rublevo-Arkhangelskaya and Troitskaya (Kommunarskaya) lines of the Moscow Metro under construction were selected for the analysis. The authors carried out the selection of the lower boundary of the scheme by changing it in proportion to the outer diameter of the tunnels in dispersed and rocky soils. The obtained data were compared with geodetic monitoring one. Calculations were made for three different soil models such as Mohr-Coulomb, Mohr-Coulomb with increasing deformation modulus of the prism under the excavation and Hardening soil. In addition, calculations were made for two cases of assignment of the overburden coefficient - according to normative documentation and available research on the subject. As a result of this work, more than 600 calculated cases were obtained. Based on these cases, recommendations were developed for adjusting the scheme depth for the considered soil models.

Keywords: Impact zone, the finite element method, vertical deformations, Mohr-Coulomb, Hardening Soil, forecast settlements, tunneling, Plaxis 2D

ОПРЕДЕЛЕНИЕ ПАРАМЕТРОВ ГРАНИЦ РАСЧЕТНОЙ МОДЕЛИ ПРИ ОЦЕНКЕ ВЛИЯНИЯ НА ОКРУЖАЮЩУЮ ЗАСТРОЙКУ ОТ ТОННЕЛЕПРОХОДЧЕСКИХ РАБОТ

А.З. Тер-Мартиросян [1], Р.Х. Черкесов [2], И.О. Исаев [2], В.В. Рудь [1], М.И. Амбрушкевич [1]

[1] Национальный исследовательский Московский государственный строительный университет, г. Москва, РОССИЯ
[2] Институт Мосинжпроект, г. Москва, РОССИЯ

Аннотация. В результате активного освоения подземного пространства города Москвы, а также вследствие повышенной плотности застройки города необходимо осуществлять прогноз дополнительных перемещений окружающей застройки от нового строительства с целью предотвращения аварийных ситуаций. По этой причине одним из важных направлений является математическое моделирование прогноза дополнительных перемещений окружающей застройки после строительства. Установление параметров расчетных границ геотехнической модели - один из факторов, в значительной степени влияющих на результаты расчета. В данном исследовании рассматривается назначение нижней границы схемы при оценке влияния от тоннелепроходческих

работ в двумерной постановке. Произведен обзор международного опыта моделирования глубины расчетной схемы для различных геотехнических задач и его сравнение с российским опытом моделирования схем. Для анализа были подобраны деформационные марки, располагающиеся на грунтовой поверхности в зоне влияния строящихся перегонных тоннелей Рублево-Архангельской и Троицкой (Коммунарской) линий Московского метрополитена. Авторы осуществили подбор нижней границы схемы, путем ее изменения пропорционально внешнему диаметру тоннелей в дисперсных и скальных грунтах. Полученные расчетные данные сравнивались с данными геодезического мониторинга. Расчеты производились для трех различных моделей грунта Mohr-Coulomb, Mohr-Coulomb с увеличением модуля деформации грунта призмы под выработкой и Hardening soil. Дополнительно расчеты производились для двух случаев назначения коэффициента перебора грунта - согласно нормативной документации и имеющимся исследованиям по данной теме. В результате проделанной работы было получено более 600 расчетных случаев, на основании которых были разработаны рекомендации по корректированию глубины схемы для рассмотренных моделей грунта.

Ключевые слова: зона влияния, метод конечных элементов, вертикальные деформации, Mohr-Coulomb, Hardening Soil; прогнозируемые осадки, тоннелирование, Plaxis 2D

INTRODUCTION

The subway plays a significant role in the transport unloading of megacities. Over the past decades, the shield tunneling method has gained enormous popularity all over the world, since this method is the most efficient and has a minimal impact on the environment [1].

Currently, in Moscow an active construction of the subway is being carried out. As a result of development of underground space in one way or another there is a need for mathematical simulation of surrounding buildings in order to determine the impact of construction of new tunnels on existing facilities. Based on the results of the impact assessment, a monitoring program is developed. It is necessary to trace the ground massif movements and, in case of necessity, to work out anti-damage actions [2]. Thus, it seems important to correctly simulate the calculation scheme, which is one of the main tasks of engineers.

In one of the previous papers [3], several most important factors of mathematical modeling, which affect the accuracy of calculation results in the software Plaxis 2D, were considered. Namely: soil model; computational modeling scheme; discretization of finite element mesh; modeling of work stages; construction dewatering by needle filters and open dewatering system; consideration of strength and rigidity of contact elements. According to the research, the factors that have the greatest influence on the accuracy of calculations are the choice of a soil model, type of a calculation model (2D or 3D) and compliance with the technology when specifying the construction phases.

In this paper, one of the factors affecting the results of construction impact assessment calculations is the area occupied by a computational model. On this basis, the authors perform the selection of the lower bound of the computational model for the tasks of impact assessment from tunneling works.

Researchers around the world have raised the issue of the applicability boundaries of the mathematical modeling scheme. One of the first who studied this issue were the authors of the article [4], which was published back in 1996. The mentioned paper argued that it is necessary to reduce the physical domain, thus introducing one or more artificial boundaries in the numerical simulation of displacement processes. This action leads to the fact that the calculation may not be justified and its results will not be correct.

Indeed, setting boundaries in mathematical models is one of the most important conditions. For example, the influence of scheme boundaries on the correctness of calculations is investigated in geophysics as well. Researchers in the article [5] consider simulation of circuit boundaries in electric tomography. It is argued

that the most correct calculation can be done when the computational domain is expanded, but at the same time, this leads to an intractable problem and a large amount of time spent on the simulation. These problems are solved by setting simulation bounds, which in turn lead to calculation errors. Therefore, the authors in their study propose solutions to correct the errors associated with truncation of the computational domain in order to optimize prediction.

Lidija Zdravkovic and Stavroula Kontoe [6] considered the reduction of soil domain boundaries in geotechnical earthquake analysis. Simulation of correct boundaries for such a problem is problematic, since the earthquake source may be located at a considerable distance from the structure, and its inclusion in the geotechnical prediction would lead to simulation of a very large-sized model. The authors studied the behavior of three types of boundary conditions during an earthquake. As a result, the researchers identified the most acceptable scheme boundary setting in terms of calculation correctness as well as in terms of time consumption.

Table 1 shows the international experience of modeling the boundaries of calculation schemes depending on the tunnel diameter for various geotechnical problems.

Table 1. Analysis of international experience in mathematical modeling

No	Problem formulation	Ссылка на исследование	Модель грунта	Расстояние от низа тоннеля до низа схемы в зависимости от диаметра тоннеля, м	Диаметр тоннеля D, м
1	Assessment of the impact of tunneling on the surrounding area	[7]	HS	3.3D	8.5
		[8]	MC	2.5D	6.15 9.15 10.65 12.15
		[9]	MC	3.5D	4.35
		[10]	MC	3.5D	10
		[11]	HSS	1,8D	6.7
2	Simulation of soil-foundation interaction	[12]	MC	1D	6
		[13]	MC	2D 6.3D	11 4.9
3	Determination of surface settlement as a function of loading pressure	[14]	MC	1.5D	6
4	Creation of universal 3D models during TBM tunneling	[15]	MC	3D	6.9
		[16]	MC, Modified Cam-Clay, Linear-Elastic	3.5D	9.3

However, one should note that the definition of the boundaries of the modelling schemes currently being modeled in Russia differs significantly from the international experience. Recommendations on the choice of the size of the calculation area and geomechanical soil model for our country are set out in Table E.2 of SP 249.1325800.2016 "Underground utilities. Design and construction by closed and cut-and-cover methods". The recommended value of the model design domain depth (b) is determined by the formula (1), when modeling closed excavations according to the normative document.

$$b=0,5D_s \quad (1)$$

where D_s id the diameter or cross-sectional dimension of the closed excavation [17].

In this regard, it is important to note that according to international experience, the lower limits of schemes in geotechnical modeling take values from 1D to 6.3D. In comparison with the Russian documentation, this distance is 2-12 times greater.

One of the studies on this issue [18] examined the influence of the boundaries of the soil model on the calculation results. According to the results of that experiment, limiting the size of the computational domain has the greatest effect on the ideal elastic-plastic Mohr-Coulomb (MC) soil model [19], while for the Hardening soil (HS) [20], an elastic-plastic model with soil strengthening, and the Hardening soil model with small-strain stiffness (HSS) [21], a model of strengthening soil at small strains, limiting the computational domain has much less effect.

The purpose of this work is to analyze the international experience in the selection of the lower boundaries and to choose appropriate model sizes for calculating the impact assessment of construction on the surrounding structure in PC Plaxis 2D from tunnel drilling, increasing the lower bound of the scheme and comparing the obtained results of the calculations with the results of geotechnical monitoring.

METHODS

In this paper, deformation marks located on the ground surface in the zone of influence of the construction of the Rublevo-Arkhangelskaya and Troitskaya (Kommunarskaya) line of the Moscow Metro were selected to correct the scheme boundary. All projected tunnels are reinforced concrete with external diameter D=6.0 m and thickness 0.3 m. Geotechnical monitoring of engineering communications are performed from the surface of the ground, therefore for this task the marks were selected according to the following advantages:

- perpendicular to the sinking in order to have several geodetic marks in the section at once with the possibility of fixing the movements of these marks by the width of the trough;
- in different engineering-geological and hydrogeological conditions with different layering of soils.

Marks on communications that showed heaving instead of settlement based on the results of geotechnical monitoring were not included in the calculation.

Figure 1 shows a typical plan of the location of the deformation marks of the communications. The following input data are available for each of the selected communications:

-engineering and geological conditions of the site where the communication is located, well columns and engineering and geological cross sections;

-soil characteristics, including the verified geotechnical indicators required for calculation in the HS model;

-project for the organization of construction of the main line tunnels;

-data of communications monitoring with indication of absolute settlement of marks.

The width of a separate calculation scheme is constant and accepted in accordance with the current normative documentation [17].

In addition, during the calculations in the PC Plaxis 2D the contact elements - interfaces necessary for simulation of the interaction between the structure and the soil were used. The discretization of the finite element mesh was adopted with the standard element distribution "Very fine".

The excess excavation value was set using the tool "Line contractions" with the set value C_{ref} value in accordance with previous studies of the authors [22-25], in order to test the value of the calculated parameter. Then, the excess excavation value was set in a similar way, but its value was set according to Table Z1 of SP 249.1325800.2016 [17]. The results obtained using the excess excavation value according to the regulatory documentation and the same coefficient obtained from the research were analyzed.

Rocky soils, represented by fractured limestone, were simulated using the Linear Elastic soil model.

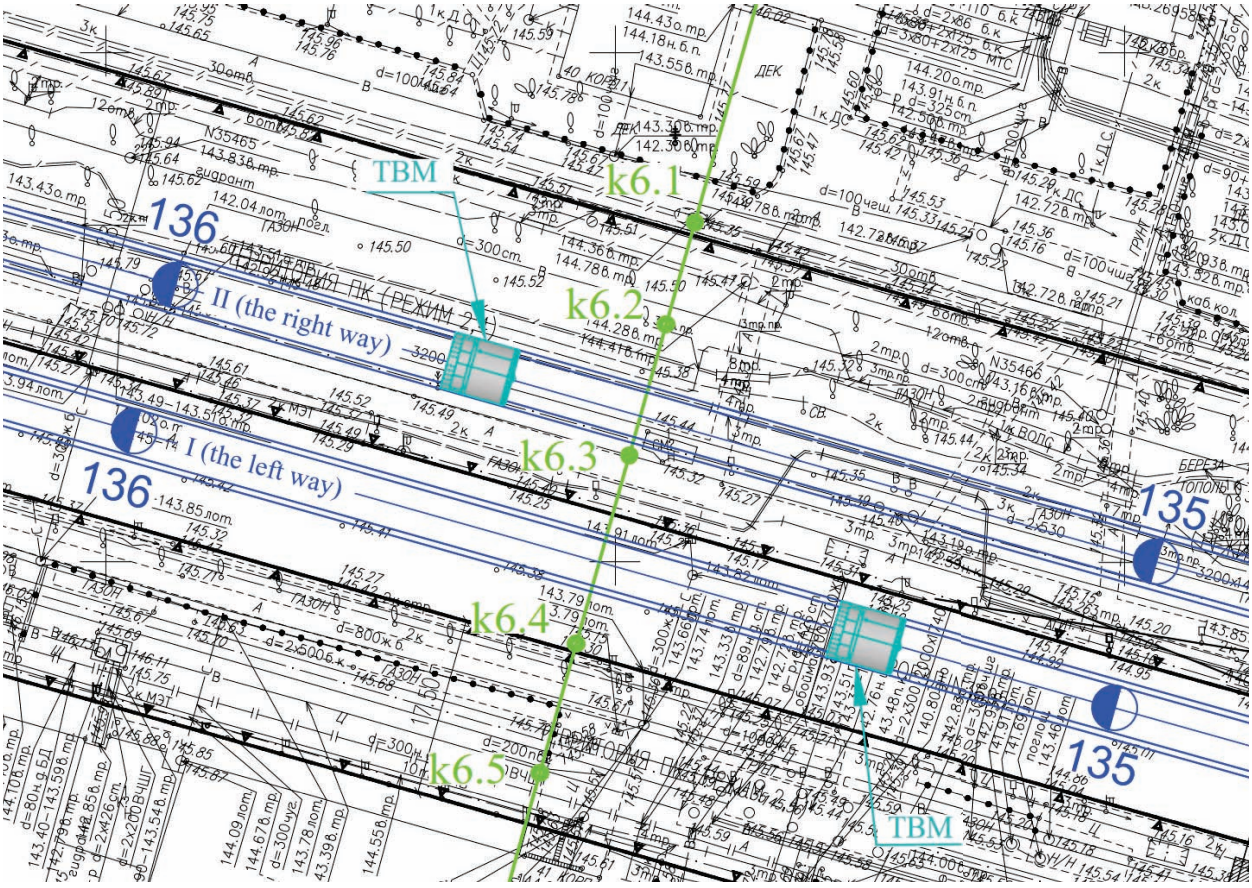


Figure1. Typical plan of the selected communication with the indication of geodetic marks on the example of communication k6

The computational model in Plaxis 2D considers all the stages of the tunneling work. Accordingly, the calculation is performed in the following steps:

- simulation of the initial natural stresses preceding the construction. The engineering-geological and hydrogeological structure of the site corresponds to the layering of soils on the longitudinal profile;
- activation of the objects of the surrounding buildings, nullification of displacements;
- driving of the left main tunnel;
- driving of the right main tunnel.

A representative calculation of the scheme was performed using the MC model at a distance of

0.5D from the bottom of the tunnel to the end of the scheme, and the calculated displacements of the marks were recorded in tabular form. Then, the distance to the bottom of the scheme was increased again by 0.5D and a new calculation of the scheme was made with fixing the obtained displacements at this distance to the bottom of the scheme. The action was repeated until the additional surface deformations had completed the change depending on the geometry of the scheme or had become equal to the settlements obtained by geotechnical monitoring.

In addition, after completing the calculation using the MC model, the prism with increased deformation moduli was modeled using the MC model with increased deformation modulus of the prism soil under the excavation (Fig. 2) according to the recommendations [26]. And all schemes were recalculated similarly to the previous ones.

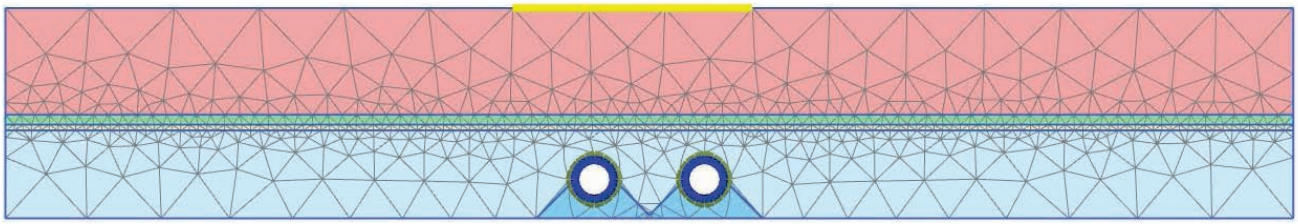


Figure 2. Calculation scheme for evaluating the effect of tunneling with increased soil deformation modulus (areas with darker color) under the tunnels

Separately, the scheme with soils specified by the HS model was also calculated using a sectional calculation pattern using the MC soil model with a tabular fixation of displacements at each increase in the distance to the bottom of the scheme.

Thus, more than 600 design cases were simulated and 6 comparison plots were obtained. Subsequently, the calculation results were analyzed by comparing the obtained displacements with geotechnical monitoring data.

RESULTS AND DISCUSSION

The results of geometry optimization of schemes with different depths of the tunnels are presented below. The average depth in 5 sections was from 20.0 to 26.6 m. However, in section 1-1 the depth of tunneling was 16.5 m.

The number of iterations in the schemes was limited to "soil heaving" the ground surface in the scheme to the opposite side.

Table 2 summarizes the results of the calculations.

Plots of additional vertical displacements vs. distance from tunnel's bottom to the bottom of the computational scheme as a function of tunnel diameter D according to the results of schemes calibration are shown in Fig. 3-4. The graphs are demonstrated for the schemes with the C_{ref} excess excavation value set according to the studies [22-25]. The red dot on the graph indicates the iteration in which the calculated vertical displacement reached the closest value to the results of geodetic monitoring.

The results of scheme calibration with MC model showed that a reliable settlement is obtained when the distance from the tunnel flume to the bottom of the scheme is 0.5-1.5D during the first-third iteration. As the distance increases, the settlement decreases rather quickly (as compared to calculations in other ground models) already at 7-9 iterations the surface bulges out.

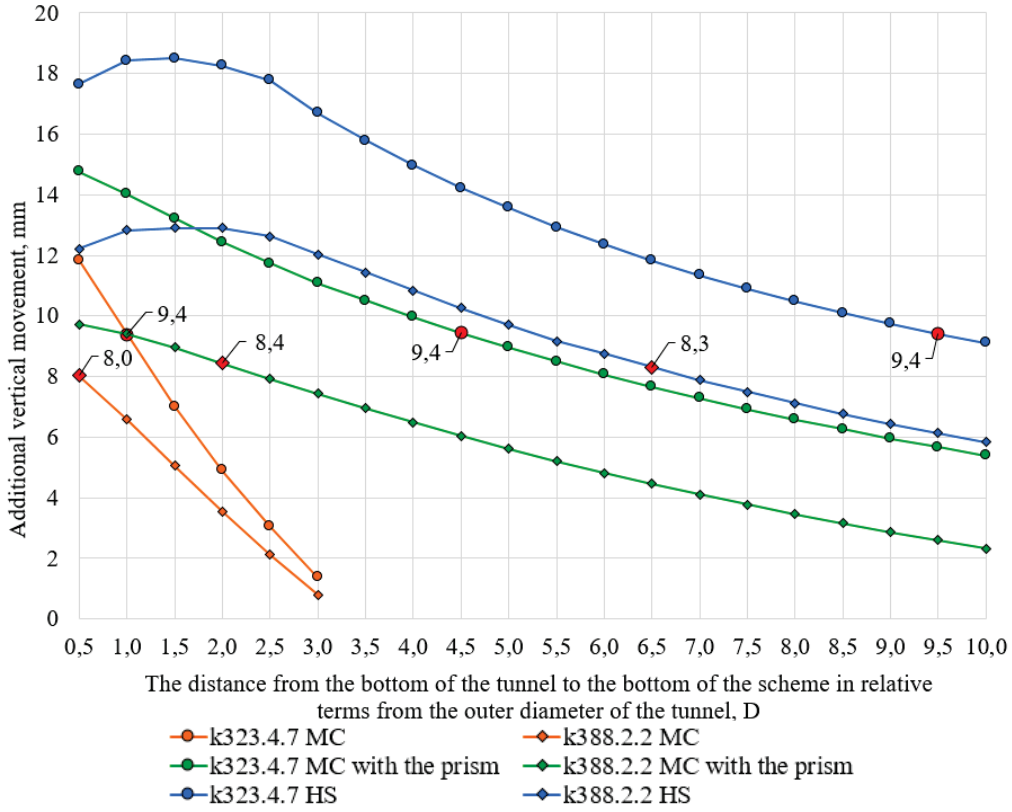


Figure 3. Displacements at H=16.5m in dispersed soils (section 1-1)

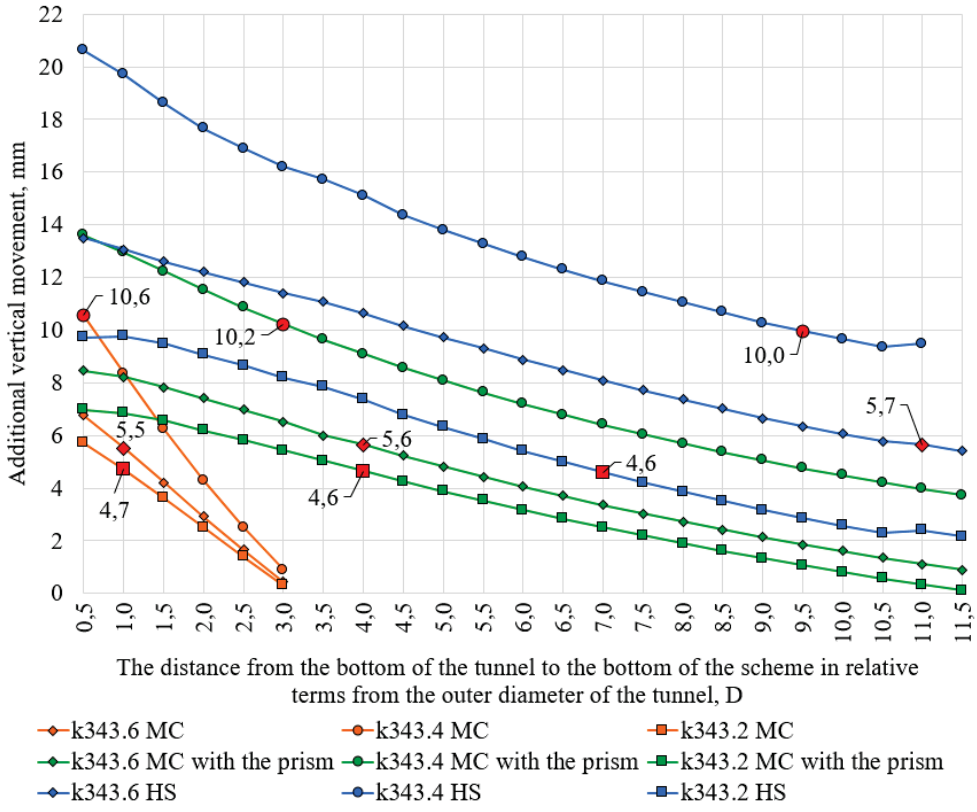


Figure 4. Displacements at H=25m in dispersed soils (section 2-2)

At the same time, the results obtained using the MC model with increased strain modulus in prism and HS are different from MC. The settlement decreases smoothly with increasing distance to the bottom of the scheme, especially in the schemes with the HS ground model. Meanwhile, in the MC model with prism, the displacement reaches the approximate value of actual settlement according to geotechnical monitoring at 2-7D, but in the HS model only at 6-16D.

Besides, there is an increase in settlement with increasing distance to the bottom in the first iterations, and only then the settlement starts to decrease in the HS ground model schemes with shallow tunneling depths.

The results of calibration of the scheme with the MC soil model and using a prism show similarity with HS at shallow depths, at greater depths this method of modeling gives a difference in the results up to 2 times.

In addition, the authors investigated the influence of the lower boundary in the schemes with rocky soils represented by fractured limestone. It was found that changing the boundary from the distance from the tunnel flume to the bottom of the scheme equal to 2.5D does not affect the calculation results.

The calculation of the model using the excess excavation value according to Table Z1 of SP 249.1325800.2016 showed insufficient similarity with the results of field monitoring in that the settlement reached extremely high values during the calculation with these coefficients. This was especially noticeable when calculating using MC model with increasing deformation modulus of the prism soil under the excavation and HS model. It was not possible to reach a suitable lower boundary of the scheme when calculating using these ground models due to a huge distance to the end of the scheme at which the displacement obtained by monitoring would be achieved. As a consequence, the results of calculations with excess excavation value given by the regulatory documentation are presented in Table 1 only for calculations using the classical elastic-plastic MC model. The results of scheme calibration using the MC model and the excess excavation value set according to the regulatory documentation showed that the settlement reaches the value obtained from the monitoring results at the distance from the tunnel flume to the bottom of the scheme equal to 7-12D.

For convenience of the analysis, the graphs constructed by the results of calibration of schemes with characteristic excess excavation value were excluded from the figures, because in their nature they repeat the graphs presented above, differing by a huge number of iterations.

As a result of the study, the authors have developed recommendations for the choice of the lower boundary of the scheme according to the following principle: it is proposed to use the minimum value of the obtained distance, depending on the soil model used. As a result, the authors recommend using the algorithm for selecting the lower bound of the computational scheme shown in Fig. 9 (depending on the given C_{ref} excess excavation value) when solving the problems of influence estimation.

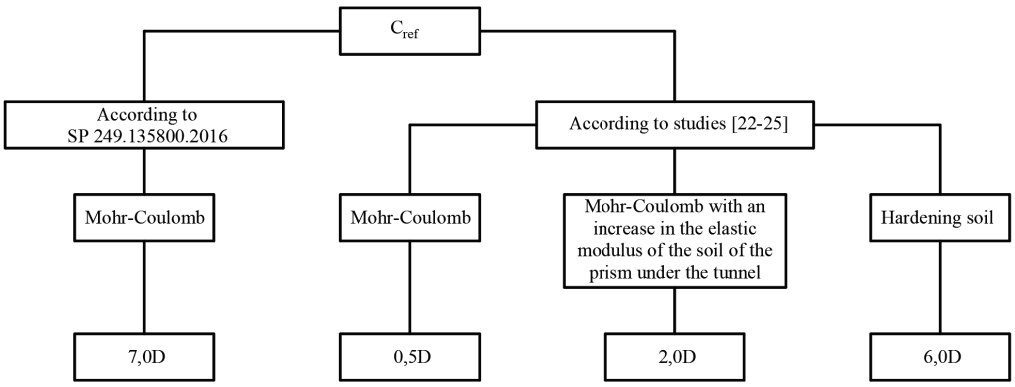


Figure 5. Block diagram for determining the lower boundary of the calculation scheme in a two-dimensional setting in dispersed soils

CONCLUSION

Analysis of international experience shows that the lower boundary of the design scheme regardless of the soil model is set from 1.0D to 6.3D in the cases considered by the authors. Moreover, there is no possibility to determine the regularity of the decision regarding the lower boundary, since the depth of the scheme is set arbitrarily, unlike the Russian designers, who refer to the regulatory document and set the lower boundary at 0.5D for the construction of closed excavations.

The studies presented in this article show the importance of determining a suitable scheme geometry for impact assessment calculations. It is recommended to choose the depth of the scheme depending on the way of assigning the excess excavation value (according to the regulatory documentation or existing studies) and the adopted soil model:

1. In the schemes for estimating the effect from tunneling works in dispersed soils using different soil models, the assignment of the lower limit of the scheme when taking into account the excess excavation value on the basis of SP 249.1325800.2016 and studies [22-25] is recommended to take according to the flowchart in Fig. 5, based on the results of the analysis of Table 2
2. Due to the large scatter of data, in order to ensure the safety of structures, it is proposed to use the minimum values of the obtained distances from the tunnel flume to the bottom of the calculation scheme when creating the calculation schemes:
   - MC (according with SP 249. 1325800.2016) – 7.0D;
   - MC – 0.5D;
   - MC with prism – 2.0D;
   - HS – 6.0D.
3. Using Linear Elastic as the soil model for the rock, at a certain depth (2.5D) the displacements stop changing, which is clearly shown in Figure 4. A similar development of additional deformations occurs when specifying Cref according to the regulatory documents. Thus, there is no need to set the boundary more than 2.5D in the problems of impact assessment in the presence of rocky soils.
4. The C_{ref} value significantly affects the final surface settlement. Depending on the purpose of the excess excavation value, a different lower boundary should be set in the calculated section. In turn, increasing the boundary also affects the reduction of additional surface displacements.
5. The use of the MC soil model with an increased strain modulus under the excavation is permitted to be used in the calculation schemes when considering the lower boundary according to the flowchart in Fig. 5. However, it should be considered that the results of prediction in this way of modeling the soil mass differ from the results of prediction with the HS soil model.
6. It is recommended to recalculate the model at each stage of construction on the basis of monitoring data to optimize its input parameters in order to improve the accuracy of geotechnical prediction.

Since the results of the scheme calibration were not sufficiently pronounced, especially for the MC soil models with increased strain modulus under the excavation and HS, this issue requires further investigations.

Table 2. Optimization results for the calculation scheme

Section number			Section 1-1 H=16.5 m, dispersed soils		Section 2-2, H=24.8 m, dispersed soils			Section 3-3, H=26.6 m, dispersed soils				Section 4-4, H=25.5 m, dispersed soils				Section 5-5, H=20.0 m, dispersed soils			Section 6-6, H=20.1 m, rock soil		
Название точки			k388.2.2	k323.4.7	k343.6	k343.4	k343.2	k10	k307.2	k307.1	k304.3	k376.1	k376.2	k376.3	k323.2.1	k316.7.1	k392.1.1	k392.2.6	K6.3	K6.2	K6.1
Settlement according to the results of monitoring S, mm			8.20	9.20	5.50	9.7	4.5	4.30	9.40	9.00	4.30	5.60	6.60	5.90	3.90	8.00	9.80	6.60	5.9	19.2	11.9
At which boundary the displacement is reached	C_{ref} according to [22-25]	MC	0.5 D	1D	1D	0.5 D	1D	1.5 D	0.5 D	0.5 D	0.5 D	1D	1.5 D	1.5 D	1.5 D	0.5 D	1D	1D	-	-	-
		MC with prism	2D	4.5D	4D	3D	4D	6D	3D	3D	3D	3.5D	6.5D	7D	6.5D	2.5D	5D	4.5D	-	-	-
		HS	6.5D	9.5D	11D	9.5D	7D	13.5D	8D	7.5D	6D	10D	16D	15D	11.5D	7D	15D	9D	-	-	8D
	according to SP 249	MC	7.5D	10.5D	8.5D	9.5D	7.5D	9.5D	9D	9D	7D	8D	11.5D	11.5D	10D	8D	12D	9.5D	4.5D	15.5D	2.5D
Distance to the center of the left tunnel, m			8.8	18.1	9.9	10.2	30.1	8.3	12.0	16.0	34.5	11.3	4.9	15.3	26.0	9.1	7.8	24.5	21.5	0	32.5
Distance to the center of the right tunnel, m			25.8	1.1	26.9	6.8	13.1	26.3	6.0	2.0	16.5	28.3	12.1	1.7	9.0	26.1	9.2	7.5	36.5	15	17.5

REFERENCES

1. **Znamenskaya E., Zertsalov M**. (2022) Issledovanie vliyaniya shchitovoj prohodki tonnelya metropolitena na okruzhayushchuyu gorodskuyu zastrojku [Study of the influence of the shield driving of the metro tunnel on the surrounding urban development]. *Innovacii i investicii,* no 6, pp. 167-170
2. **Hao Liu, Jinjiang Shi, Jiasen Li, Chao Liu** (2021) Investigation on the Influence Caused by Shield Tunneling: WSN Monitoring and Numerical Simulation. *Advances in Civil Engineering*, vol. 2021, Article ID 6620706, 11 pages

3. **Ter-Martirosyan A., Kivlyuk V., Isaev I., Shishkina V.** (2022) Analiz raschetnyh predposylok geotekhnicheskogo prognoza novogo stroitel'stva na okruzhayushchuyu zastrojku [Analysis of the Calculated Prerequisites for the Geotechnical Forecast of New Construction on the Surrounding Buildings]. *Zhilishchnoe stroitel'stvo*, vol. 9, pp. 57-66
4. **Idelsohn S. R., Oñate E., Vionnet C. A., Heinrich J. C.** (1996) Boundary conditions for finite element simulations of convective flows with artificial boundaries. *International journal for numerical methods in engineering,* vol. 39, pp. 1053-1071
5. **Lehikoinen A, Finsterle S., Voutilainen A., Kaipio J. P. et al.** (2007) Approximation errors and truncation of computational domains with application to geophysical tomography. *Inverse Problems and Imaging*, vol. 1, no. 2, pp. 371-389
6. **Zdravkovic L., Kontoe S.** (2008) *Some Issues in Modeling Boundary Conditions in Dynamic Geotechnical Analysis.* The 12th International Conference of International Association for Computer Methods and Advances in Geomechanics (IACMAG), Goa, India, 1-6 October, 2008.
7. **Miro S., König M., Hartmann D., Schanz T.** (2015) A probabilistic analysis of subsoil parameters uncertainty impacts on tunnel-induced ground movements with a back-analysis study. *Computers and Geotechnics*, vol. 68, pp. 38-53
8. **Hamid Chakeri, Yılmaz Ozcelik, Bahtiyar Unver** (2013) Effects of important factors on surface settlement prediction for metro tunnel excavated by EPB. *Tunnelling and Underground Space Technology*, vol. 36, pp. 14-23
9. **Golpasand M.R.B., Nikudel, M.R., Uromeihy A.** (2016) Specifying the real value of volume loss (V_L) and its effect on ground settlement due to excavation of Abuzar tunnel, Tehran. *Bull Eng Geol Environ*, vol. 75, pp. 485-501
10. **Norouzi H**. (2020) The effect of loading type on the amount of effect of loading on the surface settlement during forepoling tunnel excavation in different geotechnical conditions. *Journal of applied engineering sciences*. vol. 10(23), issue 1/2020, art.no. 284, pp. 55-60
11. **V. Fargnoli, D. Boldini, A. Amorosi** (2015) Twin tunnel excavation in coarse grained soils: Observations and numerical back-predictions under free field conditions and in presence of a surface structure. *Tunnelling and Underground Space Technology*, vol. 49, pp. 454-469
12. **D. Dias, R. Kastner** (2013) Movements caused by the excavation of tunnels using face pressurized shields — Analysis of monitoring and numerical modeling results. *Engineering Geology*, vol. 152, pp. 17–25
13. **H.J. Burd , W.N. Yiu, S. Acikgoz, C.M. Martin** (2022) Soil-foundation interaction model for the assessment of tunnelling-induced damage to masonry buildings. *Tunnelling and Underground Space Technology incorporating Trenchless Technology Research,* vol. 119, no 104208
14. **Chuan tan Hou, Qiujing Pan, Tao Xu, Fu Huang, Xiaoli Yang** (2022) Three-dimensional tunnel face stability considering slurry pressure transfer mechanisms. *Tunnelling and Underground Space Technology incorporating Trenchless Technology Research,* vol. 125, no 104524
15. **A. Mirhabibi, A. Soroush** (2013) Effects of building three-dimensional modeling type on twin tunneling-induced ground settlement. *Tunnelling and Underground Space Technology*, vol. 38, pp. 224-234
16. **A. Lambrughi, L. Medina Rodríguez, R. Castellanza** (2012) Development and validation of a 3D numerical model for TBM–EPB mechanised excavations. *Computers and Geotechnics*, vol. 40, pp. 97-113
17. SP 249.1325800.2016 Underground utilities. Design and construction by closed and cut-and-cover methods. Design code.

Basic statements. Moscow: Ministry of Construction, 2016. 66 p. (in Russian)
18. **Ermonin E.** (2023) Raschet tonnelej, sooruzhaemyh shchitovym sposobom, i ocenka vliyaniya stroitel'stva. Rezul'taty vtoroj serii raschetov [Calculation of tunnels constructed by the shield method and assessment of the impact of construction. Results of the second series of calculations] *Geoinfo* (electronic journal) Available at: https://geoinfo.ru/product/ermonin-evgenij-alekseevich/raschet-tonnelej-sooruzhaemyh-shchitovym-sposobom-i-ocenka-vliyaniya-stroitelstva-rezultaty-vtoroj-serii-raschetov-48327.shtml (accessed 10 February 2023).
19. PLAXIS 2D Manual (2012) Edited by R.B.J. Brinkgreve, E. Engin, W.M. Swolfs 132 p.
20. **T. Schanz, P.A. Vermeer, P.G. Bonnier** (1999) The hardening soil model: Formulation and verification. In the book*: Beyond 2000 in Computational Geotechnics*. London: Routledge, pp. 281-296
21. **Mirnyy A., Ter-Martirosyan A.** (2017) Oblasti primeneniya sovremennyh mekhanicheskih modelej gruntov [Areas of application of modern mechanical models of soils] *Geotechnics*, vol. 1 pp. 20-26
22. **Ter-Martirosyan A., Isaev I., Almakaeva A.** (2020) Opredelenie fakticheskogo koefficienta perebora (uchastok «Stahanovskaya ulica» - «Nizhegorodskaya ulica») [Identification of the actual excess excavation ratio (Stakhanovskaya street - Nizhegorodskaya street site)] *Vestnik MGSU*, vol. 15, no 12, pp. 1644-1653
23. **Ter-Martirosyan A., Babushkin N., Isaev I., Shishkina V.** (2020) Opredelenie raschetnogo koefficienta perebora putem analiza dannyh monitoring [Determining the actual ground loss of soil by analyzing monitoring data] *Geotechnics*, vol. 12, no 1, pp. 6-14
24. **Ter-Martirosyan A., Kivlyuk V., Isaev I., Shishkina V.** (2021) Opredelenie fakticheskogo koefficienta perebora (uchastok «Kosino» – «Yugo-Vostochnaya») [Determination of the actual excess excavation ratio (section “Kosino” - “Yugo-Vostochnaya”)] *Construction and Geotechnics*, vol. 12, no 2, pp. 5–14
25. **Ter-Martirosyan A., Kivlyuk V., Isaev I., Shishkina V.** (2021) Opredelenie fakticheskogo koefficienta perebora v skal'nyh gruntah [Determination of the actual coefficient of busting in] *Zhilishchnoe stroitel'stvo*, vol. 9, pp. 3-9
26. **A. Golubev, A. Seleckij** (2010) Vybor modeli grunta i eyo parametrov v raschyotah geotekhnicheskih ob’ektov [Selection of the soil model and its parameters in the calculations of geotechnical objects]. *NIP-Informatika* (electronic journal) Available at: (accessed 10 March 2023).

СПИСОК ЛИТЕРАТУРЫ

1. **Знаменская Е., Зерцалов М.** Исследование влияния щитовой проходки тоннеля метрополитена на окружающую городскую застройку // Инновации и инвестиции, 2022, №6. С. 167-170.
2. **Hao Liu, Jinjiang Shi, Jiasen Li, Chao Liu** Investigation on the Influence Caused by Shield Tunneling: WSN Monitoring and Numerical Simulation // Advances in Civil Engineering, 2021, vol. 2021, Article ID 6620706, 11 pages
3. **Тер-Мартиросян А.З., Кивлюк В.П., Исаев И.О., Шишкина В.В.** Анализ расчетных предпосылок геотехнического прогноза нового строительства на окружающую застройку // Жилищное строительство, 2022, №9. С. 57-66.
4. **Idelsohn S. R., Oñate E., Vionnet C. A., Heinrich J. C.** Boundary conditions for finite element simulations of convective flows with artificial boundaries // International journal for numerical methods in engineering, 1996, Vol. 39, pp. 1053-1071.
5. **Lehikoinen A, Finsterle S., Voutilainen A., Kaipio J.P. et al.** Approximation errors

and truncation of computational domains with application to geophysical tomography // Inverse Problems and Imaging, 2007, Vol. 1, No. 2, pp. 371-389.
6. **Zdravkovic L., Kontoe S.** Some Issues in Modeling Boundary Conditions in Dynamic Geotechnical Analysis // The 12th International Conference of International Association for Computer Methods and Advances in Geomechanics (IACMAG). Goa, India, 2008, 1-6 October.
7. **Miro S., König M., Hartmann D., Schanz T.** A probabilistic analysis of subsoil parameters uncertainty impacts on tunnel-induced ground movements with a back-analysis study // Computers and Geotechnics, 2015, Vol. 68, pp. 38-53.
8. **Hamid Chakeri, Yılmaz Ozcelik, Bahtiyar Unver** Effects of important factors on surface settlement prediction for metro tunnel excavated by EPB // Tunnelling and Underground Space Technology, 2013, Vol. 36, pp. 14-23.
9. **Golpasand M.R.B., Nikudel, M.R., Uromeihy A.** Specifying the real value of volume loss (V_L) and its effect on ground settlement due to excavation of Abuzar tunnel, Tehran // Bull Eng Geol Environ, 2016, Vol. 75, pp. 485-501.
10. **Norouzi H.** The effect of loading type on the amount of effect of loading on the surface settlement during forepoling tunnel excavation in different geotechnical conditions // Journal of applied engineering sciences, 2020, Vol. 10(23), Issue 1/2020, Art.no. 284, pp. 55-60.
11. **Fargnoli V., Boldini D., Amorosi A.** Twin tunnel excavation in coarse grained soils: Observations and numerical back-predictions under free field conditions and in presence of a surface structure // Tunnelling and Underground Space Technology, 2015, Vol. 49, pp. 454-469.
12. **Dias D., Kastner R.** Movements caused by the excavation of tunnels using face pressurized shields — Analysis of monitoring and numerical modeling results // Engineering Geology, 2013, Vol. 152, pp. 17–25.
13. **Burd H.J., Yiu W.N., Acikgoz S., Martin C.M.** Soil-foundation interaction model for the assessment of tunnelling-induced damage to masonry buildings // Tunnelling and Underground Space Technology incorporating Trenchless Technology Research, 2022, Vol. 119, No. 104208.
14. **Chuan tan Hou, Qiujing Pan, Tao Xu, Fu Huang, Xiaoli Yang** Three-dimensional tunnel face stability considering slurry pressure transfer mechanisms // Tunnelling and Underground Space Technology incorporating Trenchless Technology Research, 2022, Vol. 125, No. 104524.
15. **Mirhabibi A., Soroush A.** Effects of building three-dimensional modeling type on twin tunneling-induced ground settlement // Tunnelling and Underground Space Technology, 2013, Vol. 38, pp. 224-234.
16. **Lambrughi A., Medina Rodríguez L., Castellanza R.** Development and validation of a 3D numerical model for TBM–EPB mechanised excavations // Computers and Geotechnics, 2012, Vol. 40, pp. 97-113.
17. СП 249.1325800.2016 Коммуникации подземные. Проектирование и строительство закрытым и открытым способами. Минстрой России 2016.
18. **Ермонин Е. А.** Расчет тоннелей, сооружаемых щитовым способом, и оценка влияния строительства. Результаты второй серии расчетов [Электронный ресурс]. URL: https://geoinfo.ru/product/ermonin-evgenij-alekseevich/raschet-tonnelej-sooruzhaemyh-shchitovym-sposobom-i-ocenka-vliyaniya-stroitelstva-rezultaty-vtoroj-serii-raschetov-48327.shtml (дата обращения 10.02.2023).
19. PLAXIS 2D Manual Edited by Brinkgreve R.B.J., Engin E., Swolfs W.M., 2012, 132 p.
20. **Schanz T., Vermeer P.A., Bonnier P.G.** The hardening soil model: Formulation and verification // Beyond 2000 in

Computational Geotechnics. London: Routledge, 1999, pp. 281-296.
21. **Мирный А.Ю., Тер-Мартиросян А.З.** Области применения современных механических моделей грунтов // Геотехника, 2017, №1. С. 20-26.
22. **Тер-Мартиросян А.З., Исаев И.О., Алмакаева А.С.** Определение фактического коэффициента перебора (участок «Стахановская улица» - «Нижегородская улица») // Вестник МГСУ, 2020, Том 15, №12. С. 1644-1653.
23. **Тер-Мартиросян А.З., Бабушкин Н.Ф., Исаев И.О., Шишкина В.В.** Определение расчетного коэффициента перебора путем анализа данных мониторинга // Геотехника, 2020, Том 12. №1. С. 6-14.
24. **Тер-Мартиросян А.З., Кивлюк В.П., Исаев И.О., Шишкина В.В.** Определение фактического коэффициента перебора (участок «Косино» – «Юго-Восточная») // Construction and Geotechnics, 2021, Том 12, №2. С. 5–14.
25. **Тер-Мартиросян А.З., Кивлюк В.П., Исаев И.О., Шишкина В.В.** Определение фактического коэффициента перебора в скальных грунтах // Жилищное строительство, 2021, №9. С. 3-9.
26. **Голубев И., Селецкий А.В.** Выбор модели грунта и её параметров в расчётах геотехнических объектов «НИП-Информатика» [Электронный ресурс]. URL: http://www.nipinfor.ru/publications/10063/ (дата обращения 10.03.2023).

Armen Z. Ter-Martirosyan – Vice-Rector, Doctor of Science, Professor; National National Research Moscow State University of Civil Engineering, 26, Yaroslavskoye Shosse, 129337 Moscow, Russia; Tel.: +7 (495) 025-28-65, доб. 2263; E-mail: gic-mgsu@mail.ru

Rustam H. Cherkesov – General Director, Institute Mosinzhproekt Limited Liability Company, 4/1, Sverchkov Ln, 101000 Moscow, Russia; Tel.: +7(495)225-19-40, доб. 1001; E-mail: Cherkesov.R@mosinzhproekt.ru.

Ilya O. Isaev – Director of Scientific and Technical Activities; Institute Mosinzhproekt Limited Liability Company, 4/1, Sverchkov Ln, 101000 Moscow, Russia; Tel.: +7(495) 225-19-40, доб. 6107; E-mail: IsaevIO@mosinzhproekt.ru.

Viktoriya V. Rud - graduate student; National Research Moscow State University of Civil Engineering, 26, Yaroslavskoye Shosse, 129337 Moscow, Russia; Tel.: +7-977-806-55-02; E-mail: victo-riadll@yandex.ru.

Mariya I. Ambrushkevich - master's student; National Research Moscow State Civil Engineering University, 26, Yaroslavskoye Shosse, 129337 Moscow, Russia; Tel.: +7-982-763-80-33; E-mail: m_ambrushkevich@mail.ru.

Тер-Мартиросян Армен Завенович – проректор, доктор технических наук, профессор кафедры механики грунтов, оснований и фундаментов; Национальный исследовательский Московский государственный строительный университет (НИУ МГСУ), 129337, Россия, г. Москва, Ярославское шоссе, д. 26; Тел.: +7 (495) 025-28-65, доб. 2263; E-mail: gic-mgsu@mail.ru.

Черкесов Рустам Хасанович – генеральный директор; ООО Институт Мосинжпроект, 101000, Россия, г. Москва, Сверчков переулок, д. 4/1, стр.1; Тел.: +7(495)225-19-40, доб. 1001; E-mail: Cherkesov.R@mosinzhproekt.ru.

Исаев Илья Олегович - директор по научно-технической деятельности; ООО Институт Мосинжпроект, 101000, Россия, г. Москва, Сверчков переулок, д. 4/1, стр.1; Тел.: +7(495) 225-19-40, доб. 6107; E-mail: IsaevIO@mosinzhproekt.ru.

Рудь Виктория Владимировна – аспирант; Национальный исследовательский Московский государственный строительный университет (НИУ МГСУ); 129337, Россия, г. Москва, Ярославское шоссе, д. 26; Тел.: +7-977-806-55-02; E-mail: victoriadll@yandex.ru.

Амбрушкевич Мария Игоревна – магистрант; Национальный исследовательский Московский государственный строительный университет (НИУ МГСУ), 129337, Россия, г. Москва, Ярославское шоссе, д. 26; Тел: +7-982-763-80-33; E-mail: m_ambrushkevich@mail.ru.

International Journal for Computational Civil and Structural Engineering, 19(2) 109–119 (2023)

DOI:10.22337/2587-9618-2023-19-2-109-119

NONLINEAR REFINEMENT OF THE DEFORMATION MODEL OF ORTHOTROPIC MATERIALS, THE RIGIDITY OF WHICH DEPENDS ON THE TYPE OF STRESS STATE

Alexander A. Treshchev [1], Nikita S. Yushchenco [1], Alexander A. Bobryshev [2]

[1] Tula State University, Tula, RUSSIA
[2] Kazan Federal University, Naberezhnye Chelny, RUSSIA

Annotation. As a result of numerous experimental and theoretical studies, it has been established that when deforming both traditional and new structural materials, which are polymers, composites and synthetic structures used in construction, mechanical engineering, and power engineering devices, complicated mechanical properties manifest themselves.Most of these materials have an orthotropic structure complicated by the dependence of deformation and strength characteristics on the type of stress state, which can be interpreted as deformation anisotropy. These properties contradict the generally accepted theories of deformation. Therefore, a number of models have been specially developed for such materials over the past 56 years, taking into account the complicated properties of materials. However, all of them have disadvantages and certain contradictions with the fundamental rules for constructing equations of state. The previous works of the authors of the presented studies establish general approaches to the construction of energetically nonlinear deformation models of composite materials with recommendations for calculating their constants based on a wide range of experiments.It turned out that the set of necessary experiments should include experiments on complex stress states, most of which are technically unrealizable. In another work of the authors in 2021, using the tensor space of normalized stresses, the deformation potential was formulated in a quasi-linear form, constructed in the main axes of orthotropy of materials, for determining constants, which is sufficient for the data of the simplest experiments. Along with the obvious advantages of the introduced potential, it has one drawback, which is to replace real nonlinear diagrams with direct rays with minimal error. Despite the unconditional adequacy of the quasi-linear potential, the use of this level of approximations leads to quantitative errors.Therefore, simplified nonlinear equations of state for composite materials are proposed here, the simplest experiments are sufficient to determine the material functions of which. These equations are based on the general laws of mechanics, on the basis of which the constants of material polynomials for a carbon-graphite composite are calculated, taking into account the Drucker constraints.

Keywords: material functions, nonlinear deformation anisotropy, dimensional orthotropy, defining equations, strain and stress tensors, least squares method, main axes of orthotropy

НЕЛИНЕЙНОЕ УТОЧНЕНИЕ МОДЕЛИ ДЕФОРМИРОВАНИЯ ОРТОТРОПНЫХ МАТЕРИАЛОВ, ЖЕСТКОСТЬ КОТОРЫХ ЗАВИСИТ ОТ ВИДА НАПРЯЖЕННОГО СОСТОЯНИЯ

А.А. Трещев [1], Н.С. Ющенко [1], А.А. Бобрышев [2]

[1] Тульский государственный университет, г. Тула, РОССИЯ
[2] Казанский федеральный университет, г. Набережные Челны, РОССИЯ

Аннотация. В результате многочисленных экспериментальных и теоретических исследований установлено, что при деформировании как традиционных, так и новых конструкционных материалов, которыми являются полимеры, композиты и синтетические структуры, используемые в строительстве, машиностроении и энергетических устройствах, проявляются сложные механические свойства. Большинство из этих материалов имеют ортотропную структуру, осложненную зависимостью деформационных и прочностных характеристик от типа напряженного состояния, что можно интерпретировать как деформационную анизотропию. Эти свойства противоречат общепринятым

теориям деформирования. Поэтому за последние 56 лет для таких материалов был специально разработан ряд моделей, учитывающих усложненные свойства материалов. Однако все они имеют недостатки и определенные противоречия с фундаментальными правилами построения уравнений состояния. Предыдущие работы авторов представленных исследований устанавливают общие подходы к построению энергетически нелинейных моделей деформирования композиционных материалов с рекомендациями по расчету их констант на основе широкого спектра экспериментов. Оказалось, что набор необходимых экспериментов должен включать эксперименты по сложным напряженным состояниям, большинство из которых технически нереализуемы. В другой работе авторов в 2021 году с использованием тензорного пространства нормированных напряжений потенциал деформации был сформулирован в квазилинейной форме, построенный в главных осях ортотропии материалов и установлено, что для определения констант достаточно данных простейших экспериментов. Наряду с очевидными преимуществами введенного потенциала, у него есть один недостаток, который заключается в замене реальных нелинейных диаграмм прямыми лучами с минимальной погрешностью. Несмотря на безусловную адекватность квазилинейного потенциала, использование такого уровня приближений приводит к количественным ошибкам. Поэтому здесь предлагаются упрощенные нелинейные уравнения состояния для композиционных материалов при определенияи материальных функций которых достаточно простейших экспериментов. Эти уравнения основаны на общих законах механики, на основе которых рассчитываются константы материальных полиномов для углеграфитового композита с учетом ограничений Друкера.

Ключевые слова: материальные функции, нелинейная деформационная анизотропия, структурная ортотропия, определяющие уравнения, тензоры деформаций и напряжений, метод наименьших квадратов, главные оси ортотропии

1. INTRODUCTION

The designs of unique structures, especially critical parts of apparatuses and machines are continuously being improved, which has caused the appearance of special materials with increased deformation and strength characteristics with a minimum mass of the objects being examined. Along with this, similar materials have certain properties that contradict classical theories [1 – 7]. Mainly, these materials include chaotically filled with nano-modifiers and fibers, fibrous composites, fiberglass, graphitoplastics and boroplastics.

The discrepancy between the mechanical properties of these new, as well as many materials traditionally used in engineering, such as concrete and reinforced concrete [8, 9], cast iron [10], fluoroplast [11], carbon-graphite [12, 13], is the sensitivity of their physical and mechanical properties to the type of stress state. Some of these compositions are isotropic [8 – 12], and most are anisotropy of the type of orthotropy and transversal isotropy [1 – 8, 13]. At the same time, over the past 50 years, equations of state have been proposed for isotropic materials in many studies based on various hypotheses, which are largely contradictory, and as demonstrated in [8], all these equations have serious drawbacks and are contradictory. In contrast to these theories, in the works [8, 14, 15], sufficiently universal and free from such shortcomings defining relations were formulated and investigated for applicability to the calculation of a wide class of materials. These relations have energy consistency and are formulated in vector and tensor normalized stress spaces. At the same time, classes of structurally anisotropic materials have been covered by theoretical studies only in individual publications, often under-researched to the level of applicability to design calculations and are not fully systematized [1 – 7, 13, 16, 17].

In the light of the above, the purpose of the presented publication is to demonstrate the application of the normalized tensor space of normalized stresses for postulating nonlinear equations of state in relation to orthotropic materials with deformation anisotropy.

2. FORMULATION OF THE PROBLEM: METHODS AND RESULTS OF CONSTRUCTING NONLINEAR STATE EQUATIONS FOR COMPOSITE MATERIALS. DEFINITION OF MATERIAL FUNCTIONS AND THEIR LIMITATIONS

Research [18] was devoted to an attempt to apply the technique of normalized stress tensor spaces to the formulation of a nonlinear version of the theory of deformation of orthotropic materials with deformation anisotropy acquired during loading in compliance with all the rules for postulating the form of specific additional stress work for continuous deformable media [19]. It has been demonstrated [8, 18] that in equations with full consideration of physical nonlinearity, even with quasi-linear approximations of experimental deformation diagrams, it is necessary to involve a wide range of experiments, including complex stress-strain states, in calculating the constants of the equations of state. Often, for this purpose, it requires the use of wide sets of tests in a plane stress state, spatial (triaxial) experiments in the main planes of orthotropy, including both stretching and compression. However, this is not the most difficult. It is much more difficult to perform tests for joint shifts in two or three main material planes of orthotropy. Conducting such tests at the current level of development of the experimental base is practically impossible for technical reasons and therefore there is not enough information in the scientific literature about the results of such experiments. In the work of the authors published in 2021 [20], using the tensor space of normalized stresses, a quasi-linear form of the deformation potential for orthotropic materials is formulated, taking into account the manifestation of deformation anisotropy. In addition to the potential itself and the equations of state arising from it, a method for calculating the constants of these equations using experimentally determined technical characteristics is also developed there, and the limitations arising from the complete proof of the uniqueness theorem are evaluated. This potential and the equations of state resulting from it have a sufficiently high accuracy, do not contradict the laws of classical mechanics and are free from obvious drawbacks characteristic of well-known theories proposed by other authors. However, it is impossible to achieve further improvement and increase the accuracy of computational models of structures made of composite materials without replacing quasi-linear equations of state with nonlinear ones, which, undoubtedly, should have the smallest error of theoretical predictions relative to experimental data. At the same time, a simple statement of the problem will not be enough, since the difficulties that arise in obtaining experimental data in full do not allow us to establish a set of necessary technical constants. Therefore, it is proposed here to formulate direct nonlinear equations of the relationship between strain and stress tensors for composite orthotropic materials sensitive to the type of stress state in a form close to the generalized Hooke's law with modification by the type of the theory of small elastic-plastic deformations, but using normalized stress spaces.

The proposed version of the equations of state should be universal for any type of stress state and allows to establish one-to-one relationships between deformations and stresses with the involvement of a system of simple experiments, technically feasible and sufficient to fully determine the nonlinear material functions introduced into these equations and taking into account the complex of complicated mechanical properties.

The proposed nonlinear coupling equations of strain and stress tensors for an orthotropic material with deformation anisotropy are recommended to be formulated as:

$$e_{11} = \left[A_{1111}(\sigma_i) + B_{1111}(\sigma_i)\,\alpha_{11}\right]\sigma_{11} + \left[A_{1122}(\sigma_i) + B_{1122}(\sigma_i)(\alpha_{11} + \alpha_{22})\right]\sigma_{22} + \\ + \left[A_{1133}(\sigma_i) + B_{1133}(\sigma_i)(\alpha_{11} + \alpha_{33})\right]\sigma_{33};$$

$$e_{22} = \left[A_{1122}(\sigma_i) + B_{1122}(\sigma_i)(\alpha_{11} + \alpha_{22})\right]\sigma_{11} +$$

$$
\begin{aligned}
&+\left[A_{2222}\left(\sigma_i\right)+B_{2222}\left(\sigma_i\right)\alpha_{22}\right]\sigma_{22}+\\
&+\left[A_{2233}\left(\sigma_i\right)+B_{2233}\left(\sigma_i\right)\left(\alpha_{22}+\alpha_{33}\right)\right]\sigma_{33};\\
e_{33} &= \left[A_{1133}\left(\sigma_i\right)+B_{1133}\left(\sigma_i\right)\left(\alpha_{11}+\alpha_{33}\right)\right]\sigma_{11}+\\
&+\left[A_{2233}\left(\sigma_i\right)+B_{2233}\left(\sigma_i\right)\left(\alpha_{22}+\alpha_{33}\right)\right]\sigma_{22}+\\
&+\left[A_{3333}\left(\sigma_i\right)+B_{3333}\left(\sigma_i\right)\alpha_{33}\right]\sigma_{33};\\
\gamma_{12} &= C_{1212}\left(\sigma_i\right)\tau_{12}; \quad \gamma_{23} = C_{2323}\left(\sigma_i\right)\tau_{23}; \gamma_{13} = C_{1313}\left(\sigma_i\right)\tau_{13},
\end{aligned}
\tag{1}
$$

where $A_{ijkm}\left(\sigma_i\right)$, $B_{ijkm}\left(\sigma_i\right)$ and $C_{ijkm}\left(\sigma_i\right)$ – material nonlinear functions of stress intensity determined by the deformation characteristics of an orthotropic material; $\alpha_{ij} = \sigma_{ij} / S$ – components of normalized stresses; $\sigma_i = \sqrt{3S_{ij}S_{ij}/2}$ – intensity of stresses; $S_{ij} = \sigma_{ij} - \delta_{ij}\sigma$ – stress deviator; $S = \sqrt{\sigma_{ij}\sigma_{ij}}$ – the modulus of the total stress vector (the norm of the tensor stress space); (*i, j, k, m*=1,2,3).

According to the nature of the experimental data changes, it is found that it is advisable to represent the nonlinear material functions of the equations of state (1) as power polynomials, whose coefficients depend on the experimentally established deformed characteristics of the material under study obtained from experiments on uniaxial stretching and compression along the main axes of orthotropy and on shifts in the three main material planes. Mathematical processing of empirical results was carried out using the least squares method implemented in the Microcal Origin Pro 8.0 software package (Microcal Software Inc.). The method of calculating the constants of the equations of state considered in [18], in the case of physical nonlinearity of orthotropic materials in the presence of deformation anisotropy, material functions can be determined in the form of dependencies associated with the experiments carried out:

$$
\begin{aligned}
A_{kkkk}\left(\sigma_i\right) &= 0,5\left[1/E_k^{+}\left(\sigma_i\right)+1/E_k^{-}\left(\sigma_i\right)\right];\\
B_{kkkk}\left(\sigma_i\right) &= 0,5\left[1/E_k^{+}\left(\sigma_i\right)-1/E_k^{-}\left(\sigma_i\right)\right];\\
A_{kkmm}\left(\sigma_i\right) &= -0,5\left[\nu_{km}^{+}\left(\sigma_i\right)/E_m^{+}\left(\sigma_i\right)+\nu_{km}^{-}\left(\sigma_i\right)/E_m^{-}\left(\sigma_i\right)\right];\\
B_{kkmm}\left(\sigma_i\right) &= -0,5\left[\nu_{km}^{+}\left(\sigma_i\right)/E_m^{+}\left(\sigma_i\right)-\nu_{km}^{-}\left(\sigma_i\right)/E_m^{-}\left(\sigma_i\right)\right];\\
C_{kmkm}\left(\sigma_i\right) &= 1/G_{km}\left(\sigma_i\right);\ k,m=1,2,3,
\end{aligned}
\tag{2}
$$

where $E_k^{\pm}\left(\sigma_i\right) = a_k^{\pm} + m_k^{\pm}\sigma_i + n_k^{\pm}\sigma_i^2$;

$\nu_{km}^{\pm}\left(\sigma_i\right) = \lambda_{km}^{\pm} + \beta_{km}^{\pm}\sigma_i + \mu_{km}^{\pm}\sigma_i^2$;

$G_{km}\left(\sigma_i\right) = g_{km} + p_{km}\sigma_i + q_{km}\sigma_i^2$; $E_k^{\pm}\left(\sigma_i\right)$, $\nu_{km}^{\pm}\left(\sigma_i\right)$, $G_{km}\left(\sigma_i\right)$ – functions that depend on the intensity of stresses and represent nonlinear interpretations of deformation modules, transverse deformation coefficients and shear modules of orthotropic material in the corresponding directions of the main material axes and planes (the «+» sign corresponds to the characteristics obtained from experiments on axial tension, and the «–» sign corresponds to axial compression); $a_k^{\pm}$, $m_k^{\pm}$, $n_k^{\pm}$, $\lambda_{km}^{\pm}$, $\beta_{km}^{\pm}$, $\mu_{km}^{\pm}$, g_{km}, p_{km}, q_{km} – coefficients of approximation polynomials obtained as a result of processing experimental data on the deformation of materials by the least squares method.

It is advisable to carry out the determination of material functions, taking into account approximate limitations traditional for the mechanics of orthotropic materials [19]:

$$
\begin{aligned}
\nu_{km}^{+}(\sigma_i)/E_m^{+}(\sigma_i) &= \nu_{mk}^{+}(\sigma_i)/E_k^{+}(\sigma_i);\\
\nu_{km}^{-}(\sigma_i)/E_m^{-}(\sigma_i) &= \nu_{mk}^{-}(\sigma_i)/E_k^{-}(\sigma_i).
\end{aligned}
\tag{3}
$$

The deformation of the composite «carbon fiber-carbon AVCOMod 3a» was considered as a reference material with a twofold anisotropy,

experimental data for which were borrowed from works [6, 13], which presented the results of tests for uniaxial tension and compression in the directions along the main axes of orthotropy and for a net shift in three mutually orthogonal main material planes. Mathematical processing of experimental data on the deformation of the AVCOMod 3 composite allowed us to present the coefficients of the polynomials in Table. 1. Deformation diagrams of the composite under consideration, constructed according to experimental data and their theoretical representations according to model (1) are shown in Fig. 1 – 4.

In the previous work [20], the uniqueness theorem of solutions for the quasilinear deformation potential, which determines approximate relationships of strain and stress tensors for composite materials with complicated properties of the type under consideration, was substantiated and proved. In this [20] and other works [8, 18, 21] it is established that the proof of the uniqueness theorem when postulating any equations of state is finally brought to the verification of Drucker's postulate

$$\delta e_{ij}\delta\sigma_{ij} \geq 0, \qquad (4)$$

within the framework of which restrictions are defined, imposing on material functions. For the accepted nonlinear equations of state (1), the components of the complete Sylvester matrix take the form:

$$D_{11} = \frac{\partial e_{11}}{\partial \sigma_{11}};\ D_{12} = \frac{\partial e_{11}}{\partial \sigma_{22}};\ D_{13} = \frac{\partial e_{11}}{\partial \sigma_{33}};$$
$$D_{14} = \frac{\partial e_{11}}{\partial \tau_{13}};\ D_{15} = \frac{\partial e_{11}}{\partial \tau_{23}};\ D_{16} = \frac{\partial e_{11}}{\partial \tau_{12}};$$
$$D_{22} = \frac{\partial e_{22}}{\partial \sigma_{22}};\ D_{23} = \frac{\partial e_{22}}{\partial \sigma_{33}};\ D_{24} = \frac{\partial e_{22}}{\partial \tau_{13}};$$
$$D_{25} = \frac{\partial e_{22}}{\partial \tau_{23}};\ D_{26} = \frac{\partial e_{22}}{\partial \tau_{12}};\ D_{33} = \frac{\partial e_{33}}{\partial \sigma_{33}};$$
$$D_{34} = \frac{\partial e_{33}}{\partial \tau_{13}};\ D_{35} = \frac{\partial e_{33}}{\partial \tau_{23}};\ D_{36} = \frac{\partial e_{33}}{\partial \tau_{12}};$$
$$D_{44} = \frac{\partial \gamma_{13}}{\partial \tau_{13}};\ D_{45} = \frac{\partial \gamma_{13}}{\partial \tau_{23}};\ D_{46} = \frac{\partial \gamma_{13}}{\partial \tau_{12}};$$
$$D_{55} = \frac{\partial \gamma_{23}}{\partial \tau_{23}};\ D_{56} = \frac{\partial \gamma_{23}}{\partial \tau_{12}};\ D_{66} = \frac{\partial \gamma_{12}}{\partial \tau_{12}};$$
$$D_{ij} = D_{ji}. \qquad (5)$$

It is established that the polynomial constants representing the material functions of the AVCOMod 3a composite [6, 13] given in Table 1, taking into account the quadratic forms (5), satisfy the Sylvester criterion arising from the requirements of the Drucker postulate [8, 18, 20, 21].

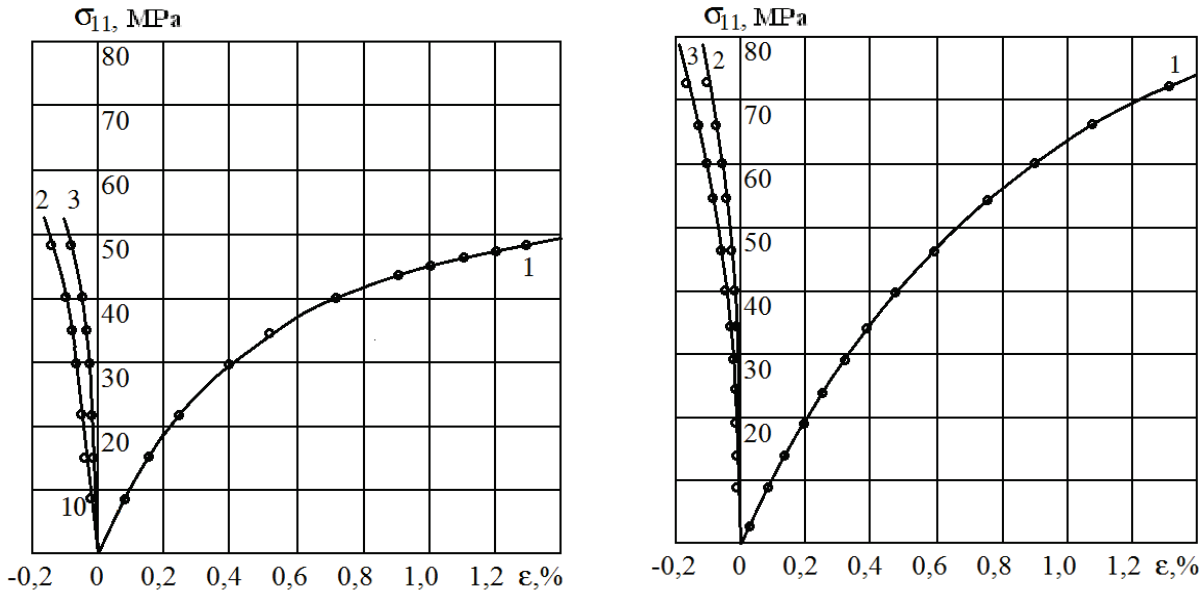
3. DISCUSSION OF THE ADEQUACY OF THE INTRODUCED EQUATIONS OF STATE TO THE EXPERIMENTAL DATA

Figures 1-4 confirm the adequacy of the postulated equations of state (1) to experimentally established diagrams for stretches, compressions in the main axes of orthotropy and shifts in the corresponding planes for reference samples of the AVCOMod 3a composite [6, 13]. It should be noted that the nonlinear model (1) has a number of advantages over the known equations formulated by other authors, such as S.A.Ambartsumyan [16], C.W.Bert–L.N.Reddy [2, 13], R.M.Jones–D.A.R.Nelson [4, 6] and A.A.Zolochevsky [7] in relation to calculations, especially of spatial structures made of orthotropic composite AVCOMod 3a [6, 13]. In particular, the model (1) is free from physically unjustified restrictions imposed on the coefficients of material functions, the absence of piecewise equations of state and the presence of a mechanism for the influence of changes in the type of stress state on the dependence of deformations on stresses. In addition, the error of theoretical approximations (1) of reference experimental

diagrams compared with other theories [2, 3, 6, 7, 13], judging by Fig. 1 – 4, it is minimal, and when the coordinate system rotates, it has a higher accuracy.

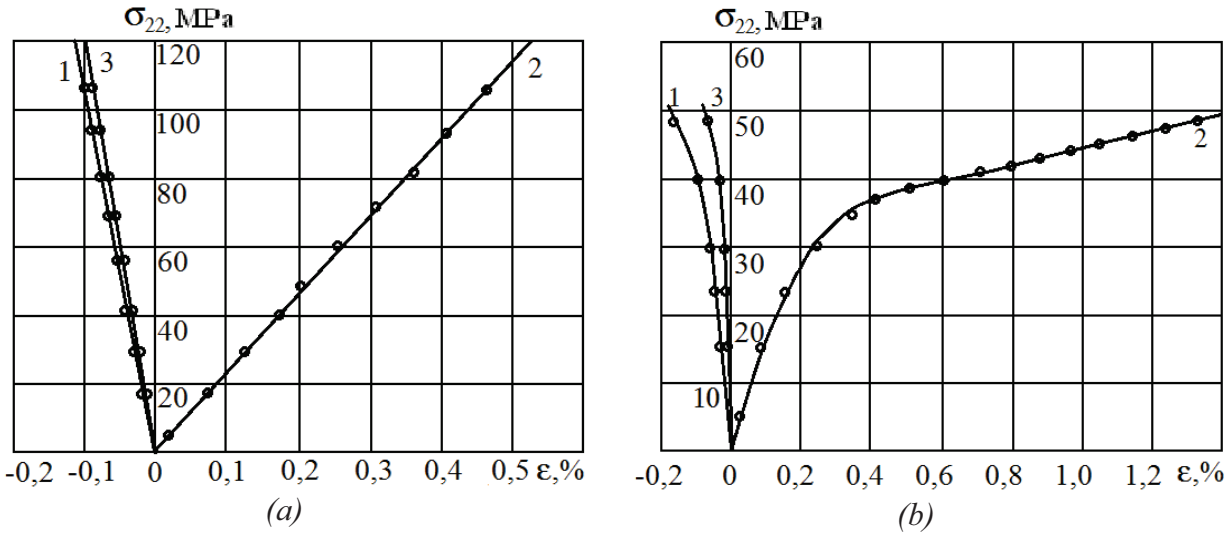
Table 1. Constants of composite material AVCOMod 3a [6, 13]

Type of sample test	Technical parameter	Constants of polynomials of material functions		
Uniaxial stretching along the main axes of orthotropy	$E_k^+(\sigma_i)$	$a_1^+=1{,}058\cdot10^{10}$, Pa	$m_1^+=62{,}829$	$n_1^+=1{,}535\cdot10^{-6}$, Pa^{-1}
		$a_2^+=2{,}864\cdot10^{10}$, Pa	$m_2^+=-105{,}476$	$n_2^+=5{,}893\cdot10^{-7}$, Pa^{-1}
		$a_3^+=2{,}301\cdot10^{10}$, Pa	$m_3^+=88{,}349$	$n_3^+=3{,}711\cdot10^{-6}$, Pa^{-1}
	$\nu_{km}^+(\sigma_i)$	$\lambda_{12}^+=0{,}158$	$\beta_{12}^+=-3{,}1\cdot10^{-9}$, Pa^{-1}	$\mu_{12}^+=2{,}19\cdot10^{-17}$, Pa^{-2}
		$\lambda_{21}^+=0{,}103$	$\beta_{21}^+=-1{,}8\cdot10^{-9}$, Pa^{-1}	$\mu_{21}^+=9{,}1\cdot10^{-18}$, Pa^{-2}
		$\lambda_{13}^+=0{,}203$	$\beta_{13}^+=2{,}15\cdot10^{-9}$, Pa^{-1}	$\mu_{13}^+=6{,}15\cdot10^{-17}$, Pa^{-2}
		$\lambda_{23}^+=0{,}104$	$\beta_{23}^+=0{,}87\cdot10^{-10}$, Pa^{-1}	$\mu_{23}^+=6{,}74\cdot10^{-17}$, Pa^{-2}
		$\lambda_{31}^+=0{,}146$	$\beta_{31}^+=-0{,}15\cdot10^{-10}$, Pa^{-1}	$\mu_{31}^+=6{,}97\cdot10^{-17}$, Pa^{-2}
		$\lambda_{32}^+=0{,}1884$	$\beta_{32}^+=-1{,}15\cdot10^{-2}$, Pa^{-1}	$\mu_{32}^+=1{,}914\cdot10^{-4}$, Pa^{-2}
Uniaxial compression along the main axes of orthotropy	$E_k^-(\sigma_i)$	$a_1^-=9{,}988\cdot10^{9}$, Pa	$m_1^-=-12{,}943$	$n_1^-=6{,}71\cdot10^{-7}$, Pa^{-1}
		$a_2^-=2{,}326\cdot10^{10}$, Pa	$m_2^-=-436{,}81$	$n_2^-=-6{,}08\cdot10^{-7}$, Pa^{-1}
		$a_3^-=5{,}14\cdot10^{9}$, Pa	$m_3^-=-129{,}15$	$n_3^-=-78{,}3\cdot10^{-6}$, Pa^{-1}
	$\nu_{km}^-(\sigma_i)$	$\lambda_{12}^-=0{,}118$	$\beta_{12}^-=-1{,}46\cdot10^{-9}$, Pa^{-1}	$\mu_{12}^-=2{,}14\cdot10^{-17}$, Pa^{-2}
		$\lambda_{21}^-=0{,}06$	$\beta_{21}^-=1{,}77\cdot10^{-9}$, Pa^{-1}	$\mu_{21}^-=2{,}95\cdot10^{-17}$, Pa^{-2}
		$\lambda_{13}^-=0{,}264$	$\beta_{13}^-=-1{,}12\cdot10^{-9}$, Pa^{-1}	$\mu_{13}^-=3{,}01\cdot10^{-17}$, Pa^{-2}
		$\lambda_{23}^-=0{,}189$	$\beta_{23}^-=2{,}16\cdot10^{-9}$, Pa^{-1}	$\mu_{23}^-=2{,}1\cdot10^{-17}$, Pa^{-2}
		$\lambda_{31}^-=0{,}134$	$\beta_{31}^-=-0{,}46\cdot10^{-10}$, Pa^{-1}	$\mu_{31}^-=5{,}82\cdot10^{-17}$, Pa^{-2}
		$\lambda_{32}^-=0{,}07793$	$\beta_{32}^-=-0{,}465\cdot10^{-2}$, Pa^{-1}	$\mu_{32}^-=9{,}0167\cdot10^{-5}$, Pa^{-2}
Shift in the main planes of orthotropy	$G_{km}(\sigma_i)$	$g_{12}=4{,}07\cdot10^{9}$, Pa	$p_{12}=-1{,}6$	$q_{12}=-8{,}38\cdot10^{-6}$, Pa^{-1}
		$g_{23}=1{,}723\cdot10^{9}$, Pa	$p_{23}=16{,}899$	$q_{23}=-1{,}1\cdot10^{-5}$, Pa^{-1}
		$g_{31}=2{,}43\cdot10^{9}$, Pa	$p_{31}=-54{,}455$	$q_{31}=-1{,}97\cdot10^{-5}$, Pa^{-1}



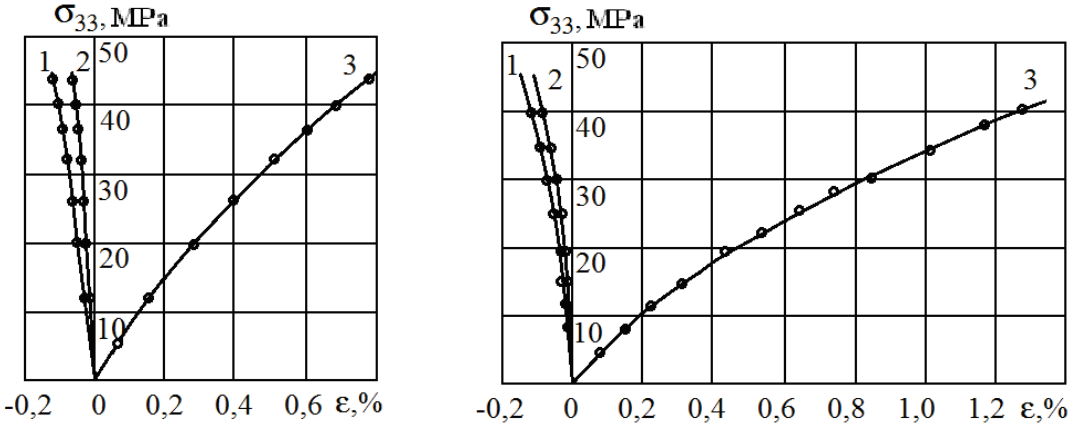
(a) *(b)*

Figure 1. Deformation diagrams along the x_1 axis: (a) stretching; (b) compression; 1 – longitudinal deformation ε_{11}; 2, 3 – transverse deformations ε_{22} and ε_{33}; ⭘ – experimental data; —— – nonlinear approximations



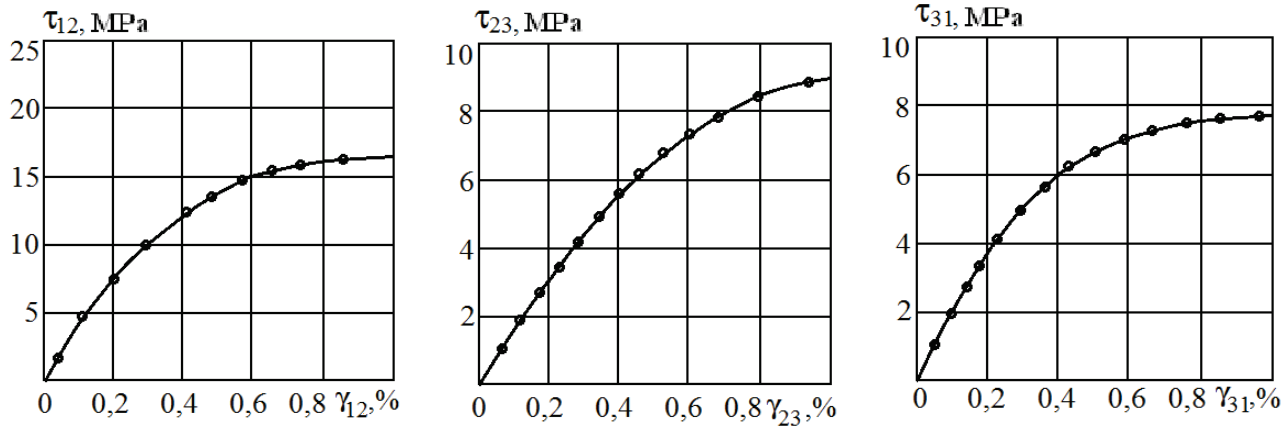
(a) *(b)*

Figure 2. Deformation diagrams along the x_2 axis: (a) stretching; (b) compression; 1, 3 – transverse deformations ε_{11} and ε_{33}; 2 – longitudinal deformation ε_{22}; ⭘ – experimental data;—— – nonlinear approximation



(a) *(b)*

Figure 3. Deformation diagrams along the x_3 axis: (a) stretching; (b) compression; 1, 2 – transverse deformations ε_{11} and ε_{22}; 3 – ongitudinal deformation ε_{33}; ○ – experimental data; —— – nonlinear approximation



(a) *(b)* *(c)*

Figure 4. Deformation diagrams on a net shift in the main planes of orthotropy: (a) in the plane x_1x_2; (b) n the plane x_2x_3; (c) n the plane x_1x_3; ○ – experimental data; —— – nonlinear approximation

REFERENCES

1. **Schmueser D.W.** Nonlinear Stress-Strain and Strength Response of Axisymmetric Bimodulus Composite Material Shells / D.W. Schmueser // AIAA Journal. – 1983. – Vol. 21. – No. 12. – pp. 1742 – 1747.
2. **Reddy L.N.** On the Behavior of Plates Laminated of Bimodulus Composite Materials / L.N.Reddy, C.W.Bert // ZAMM. – 1982. – Vol. 62. – No. 6. – pp. 213 – 219.
3. **Jones R.M.** Modeling Nonlinear Deformation of Carbon-Carbon Composite Material / R.M.Jones // AIAA Journal. – 1980. – Vol. 18. – No. 8. – pp. 995 – 1001.
4. **Kayumov R.A.** Identification of mechanical characteristics of fiber-reinforced composites / R.A.Kayumov, S.A.Lukankin, V.N.Paimushin, S.A.Kholmogorov // Scientific Notes of the Kazan University. Physical and mathematical sciences. – 2015. – Vol. 157. – Book 4. – pp. 112 – 132.

5. **Shafigullin L.N.** Development of the recommendations on selection of glass-fiber reiforced polyurethanes for vehicle parts / L.N.Shafigullin, A.A.Bobrishev, V.T.Erofeev, A.A. Treshchev, A.N.Shafigullina // International Journal of Applied Engineering Research. – 2015. – Vol. 10. – No. 23, – pp. 43758–43762.
6. **Jones R.M.** Modeling Nonlinear Deformation of Carbon-Carbon Composite Material / R.M.Jones // AIAA Journal. – 1980. – Vol. 18. – № 8. – pp. 995 – 1001.
7. **Zolochevsky A.A.** Calculation of anisotropic shells made of different-modulus materials under non-axisymmetric loading / A.A.Zolochevsky, V.N.Kuznetsov // Dynamics and strength of heavy machines. – Dnepropetrovsk: Publisher Name DSU. – 1989. – pp. 84 – 92.
8. **Treschev** A.A. Theory of deformation and strength of different resistant materials / A.A.Treschev. – Tula: Publisher Name TulSU. – 2020. – 359 p.
9. **Tasuji M.E**. Stress-Strain Response and Fracture of Concrete in Biaxial Loading / M.E.Tasuji, F.O.Slate, A.H.Nilson // ACI Journa. – 1979. – No. 7. – pp. 806–812.
10. **Pisarenko G.S.** Deformation and strength of materials under complex stress state / G.S.Pisarenko, A.A.Lebedev. – Kiev: Publisher Name Naukovadumka. – 1976. – 416 p.
11. **Elsufyev S.A.** The study of the deformation of fluoroplast under conditions of plane stress state / S.A.Elsufyev, V.M.Chebanov // Studies in elasticity and plasticity. – Leningrad: Publisher Name, Publishing house of Leningrad state University. – 1971. – Vol. 8. – pp. 209–213.
12. **Bozhanov P.V.** Determination of strength criteria in the occurrence of plastic deformations in polycarbonate / P.V.Bozhanov, A.A.Treshchev // Innovations and investments. – 2018. – No. 12. – pp. 323–326.
13. **Bert C.W.** Models for Fibrous Composite with Different Properties in Tension and Compression / C.W.Bert // Transaction of the ASME 1977. – Vol. 99 H. – Ser. D. – No. 4. – pp. 344–349.
14. **Matchenko N.M.** Determining ratios of isotropic multi-resistive media, Part 2. Nonlinear ratios. / N.M.Matchenko, L.A.Tolokonnikov, A.A.Treshchev // News of the Academy of Sciences. Solid State Mechanics. – 1999. – No. 4. – pp. 87–95.
15. **Treschev A.A.** Constitutive relations for isotropic materials allowing quasilinear approximation of the deformation law / A.A.Treschev, A.A.Bobrishev, L.N.Shafigullin // IOP Conference Series: Materials Science and Engineering. Vol. 481 (2019) UNSP012014. Doi: 10.1088/1757-899X/481/1/ 012014, pp. 1 – 7.
16. **Ambartsumian S.A.** Basic equations and of the ratio of the heterogeneous theory of elasticity of an anisotropic body / S.A.Ambartsumian // News USSR Academy of Sciences. Solid State Mechanics. – 1969. – No. 3. – pp. 51–61.
17. **Lomakin E.V.** Relations of the theory of elasticity for an anisotropic body, the deformation characteristics of which depend on the type of stress state / E.V.Lomakin // News USSR Academy of Sciences. Solid State Mechanics. – 1983. – No. 3. – pp. 63–69.
18. **Treshchev A.A.** Potential dependence between deformations and stresses for orthotropic physically nonlinear materials / A.A.Treshchev // Fundamental and applied problems of engineering and technology. – 2017. – No. 4-1 (324). – pp. 71–74.
19. **Green A.** Large elastic deformations and nonlinear mechanics of a continuous medium / A.Green, J.Adkins. – Moskow: Publisher Name Mir. – 1976. – 416 p.
20. **Treshchev A.A.** Mathematical defining equations of deformation of materials with double anisotropy / A.A.Treshchev, Yu.A.Zavyalova, M.A.Lapshina, A.E.Gvozdev, O.V.Kuzovleva,

E.S.Krupitsyn // Chebyshevskii Sbornik. – 2021. – Vol. 22. – No. 4(80). – pp. 369 – 383.
21. **Tursunov B.S.** On the properties of the stress potential of elastic bodies / B.S.Tursunov // AMM. – 1970. – Vol. 34. – Issue 1. – pp. 15 – 22.

СПИСОК ЛИТЕРАТУРЫ

1. **Schmueser D.W.** Nonlinear Stress-Strain and Strength Response of Axisymmetric Bimodulus Composite Material Shells / D.W. Schmueser // AIAA Journal. – 1983. – Vol. 21. – No. 12. – pp. 1742 – 1747.
2. **Reddy L.N.** On the Behavior of Plates Laminated of Bimodulus Composite Materials / L.N.Reddy, C.W.Bert // ZAMM. – 1982. – Vol. 62. – No. 6. – pp. 213 – 219.
3. **Jones R.M.** Modeling Nonlinear Deformation of Carbon-Carbon Composite Material / R.M.Jones // AIAA Journal. – 1980. – Vol. 18. – No. 8. – pp. 995 – 1001.
4. **Каюмов Р.А.** Идентификация механических характеристик армированных волокнами композитов / Р.А.Каюмов, С.А.Луканкин, В.Н.Паймушин, С.А.Холмогоров // Ученые записки Казанского университета. Физико-математические науки. – 2015. – Т. 157. – Кн. 4. – С. 112–132.
5. **Shafigullin L.N.** Development of the recommendations on selection of glass-fiber reiforced polyurethanes for vehicle parts / L.N.Shafigullin, A.A.Bobrishev, V.T.Erofeev, A.A. Treshchev, A.N.Shafigullina // International Journal of Applied Engineering Research. – 2015. – Vol. 10. – No. 23, – pp. 43758–43762.
6. **Jones R.M.** Modeling Nonlinear Deformation of Carbon-Carbon Composite Material / R.M.Jones // AIAA Journal. – 1980. – Vol. 18. – № 8. – pp. 995 – 1001.
7. **Золочевский А.А.** Расчет анизотропных оболочек из разномодульных материалов при неосесимметричном нагружении / А.А.Золочевский, В.Н.Кузнецов // Динамика и прочность тяжелых машин. – Днепропетровск: ДГУ, 1989. – С. 84–92.
8. **Трещев А.А.** Теория деформирования и прочности разносопротивляющихся материалов / А.А. Трещев // Тула: ТулГУ, 2020. – 359 с.
9. **Tasuji M.E**. Stress-Strain Response and Fracture of Concrete in Biaxial Loading / M.E.Tasuji, F.O.Slate, A.H.Nilson // ACI Journa. – 1979. – No. 7. – pp. 806–812.
10. **Писаренко Г.С.** Деформирование и прочность материалов при сложном напряженном состоянии / Г.С.Писаренко, А.А.Лебедев. – Киев: Наукова думка, 1976. – 416 с.
11. **Елсуфьев С.А.** Исследование деформирования фторопласта-4 при линейном и плоском напряженном состояниях / С.А.Елсуфьев // Механика полимеров. – 1968. – №4. – С. 742–746.
12. **Божанов П.В.** Определение прочностных критериев при возникновении пластических деформаций в поликарбонате / П.В.Божанов, А.АТрещев // Инновации и инвестиции. – 2018. – №12. – С. 323–326.
13. **Bert C.W.** Models for Fibrous Composite with Different Properties in Tension and Compression / C.W.Bert // Transaction of the ASME 1977. – Vol. 99 H. – Ser. D. – No. 4. – pp. 344–349.
14. **Матченко Н.М.** Определяющие соотношения изотропных разносопротивля-ющихся сред. Ч. 2. Нелинейные соотноше-ния / Н.М.Матченко, Л.А.Толоконников, А.А.Трещев // Изв. РАН. МТТ. – 1999. – №4. – С. 87–95.
15. **Treschev A.A.** Constitutive relations for isotropic materials allowing quasilinear approximation of the deformation law /

A.A.Treschev, A.A.Bobrishev, L.N.Shafigullin // IOP Conference Series: Materials Science and Engineering. Vol. 481 (2019) UNSP012014. Doi: 10.1088/ 1757-899X/481/1/ 012014, pp. 1 – 7.
16. **Амбарцумян С.А.** Основные уравнения и соотношения разномодульной теории упругости анизотропного тела / С.А.Амбарцумян // Изв. АН СССР. МТТ. – 1969. – №3. – С. 51–61.
17. **Ломакин Е.В.** Соотношения теории упругости для анизотропного тела, деформационные характеристики которых зависят от вида напряженного состояния / Е.В.Ломакин // Изв. АН СССР. МТТ. – 1983. – №3. – С. 63–69.
18. **Трещев А.А.** Потенциальная зависимость между деформациями и напряжениями для ортотропных физически нелинейных материалов / А.А.Трещев // Фундаментальные и прикладные проблемы техники и технологии. – 2017. – № 4-1 (324). – С. 71 – 74.
19. **Грин А.** Большие упругие деформации и нелинейная механика сплошной среды / А.Грин, Дж.Адкинс. – М.: Мир, 1965. – 456 с.
20. **Treshchev A.A.** Mathematical defining equations of deformation of materials with double anisotropy / A.A.Treshchev, Yu.A.Zavyalova, M.A.Lapshina, A.E.Gvozdev, O.V.Kuzovleva, E.S.Krupitsyn // Chebyshevskii Sbornik. – 2021. – Vol. 22. – No. 4(80). – pp. 369 – 383.
21. **Турсунов Б.С.** О свойствах потенциала напряжений упругих тел / Б.С.Турсунов // ПММ. – 1970. – Т. 34. – Вып. 1. – С. 15–22.

Aleksander Anatolyevich Treshchev, Doctor of Technical Sciences, Professor, Head of the Department of Construction, Building Materials and Structures, Tula State University, Corresponding Member of RAACS; 300012, Russia, Tula, Lenin Ave. 92. Phone: +7 (905) 622-90-58. E-mail: taa58@yandex.ru.

Александр Анатольевич Трещев, доктор технический наук, профессор, заведующий кафедрой «Строительство, строительные материалы и конструкции» Тульского государственного университета, член-корреспондент РААСН; 300012, г. Тула, Проспект Ленина, 92, Тел.: +7 (905) 622-90-58. E-mail: taa58@yandex.ru.

*Nikita Sergeevch Yushchen*co, graduate student of the department "Construction, building materials and structures" of Tula State University; 300012, Russia, Tula, Lenin Ave. 92. Phone: +7 (953) 190-11-06. E-mail: yushenko_1972@bk.ru

Никита Сергеевич Ющенко, аспирант кафедры «Строительство, строительные материалы и конструкции» Тульского государственного университета, член-корреспондент РААСН; 300012, г. Тула, Проспект Ленина, 92, Тел.: +7 (953) 190-11-06. E-mail: yushenko_1972@bk.ru

Alexander Anatolyevich Bobryshev, Kazan Federal University, 423812, Russia, Naberezhnye Chelny, Süümbike Avenue. Phone: +7 (927) 671-50-46. E-mail: taa58@yandex.ru

Александр Анатольевич Бобрышев, кандидат технический наук, доцент Казанского федерального университета; 423812, Набережные Челны, Проспект Сююмбеке. Тел.: +7 (927) 671-50-46. E-mail: borisov800@mail.ru.

DOI:10.22337/2587-9618-2023-19-2-120-135

STRENGTH AND DURABILITY OF CONCRETES WITH A SUPER ABSORBENT POLYMER ADDITIVE

Kamil B. Sharafutdinov [1], Ksenia A. Saraykina [1], Galina G. Kashevarova [1,2], Yana A. Sanyagina [3], Vladimir T. Erofeev [2,3], Nikolai I. Vatin [2,4]

[1] Perm National Research Polytechnic University, Perm, RUSSIA
[2] NIISF RAASN, Moscow, RUSSIA
[3] National Research Mordovian State University name N.P. Ogaryov, Saransk, RUSSIA
[4] Saint-Petersburg Polytechnic University name Peter the Great-Petersburg, Sankt-Peterburg, RUSSIA

Abstract. The article presents an analysis of the results of experimental studies of the effect of different types of a super absorbent polymer additive on the strength of different types of concrete. The study is aimed at the effectiveness of a new type of super absorbent additive in concrete structures. In the course of full-scale experiments, it was possible to identify the optimum dosage of SAP for fine-grained and heavy concretes. In addition, the results showed that the strength of concrete remains unchanged if the dosage of super absorbent polymer additive (SAP) is 0.5% of the weight of cement or less. The possibility of modern intelligent technologies (artificial neural networks) to predict the properties of concrete mixture and hardened concrete at given values of input parameters (SAP dosage and W/C), influence on concrete characteristics (slump of the cone, bending strength, compressive strength) has also been shown.

Keywords: new generation concretes, intelligent concretes, super absorbent additives, properties of concretes and concrete mixes, slump of the cone, strength, property prediction, neural systems

ПРОЧНОСТЬ И ДОЛГОВЕЧНОСТЬ БЕТОНОВ С СУПЕРВПИТЫВАЮЩЕЙ ПОЛИМЕРНОЙ ДОБАВКОЙ

К.Б. Шарафутдинов [1], К.А. Сарайкина [1], Г.Г. Кашеварова [1,2], Я.А. Санягина [3], В.Т. Ерофеев [2,3], Н.И. Ватин [2,4]

[1] Пермский Национальный исследовательский политехнический Университет, г. Пермь, РОССИЯ
[2] Научно-исследовательский институт строительной физики Российской академии архитектуры и строительных наук, г. Москва, РОССИЯ
[3] Национальный исследовательский Мордовского государственный университет имени Н.П. Огарева, г. Саранск, РОССИЯ
[4] Санкт-Петербургский политехнический университет им. Петра Великого, г. Санкт-Петербург, РОССИЯ

Аннотация. В работе представлен анализ результатов экспериментальных исследований влияния супервпитывающей полимерной добавки разных типов на прочность различных видов бетона, проведенных разными авторами. Изучение эффективности применения нового вида суперабсорбирующей добавки в бетонных конструкциях – такова цель данного исследования. В ходе проведения натурных экспериментов удалось выявить оптимальную дозировку САП для мелкозернистых и тяжелых бетонов. Кроме того, результаты исследований показали, что прочность бетона остается неизменной, если дозировка добавки суперабсорбирующего полимера (САП)составляет 0,5% от массы цемента или менее. Также показана возможность использования современных интеллектуальных технологий (искусственных нейронных сетей) для прогнозирования свойств бетонной смеси и затвердевшего бетона при заданных значениях входных параметров (дозировки САП и В/Ц), влияния на характеристики бетона (расплыв конуса, прочность на изгиб, прочность на сжатие).

Ключевые слова: бетоны нового поколения, интеллектуальные бетоны, супервпитывающие добавки, свойства бетонов и бетонных смесей, расплыв конуса, прочность, прогнозирование свойств, нейронные системы

INTRODUCTION

As it is known, the quality of concrete structures mainly depends on the following three parameters: compressive strength, permeability and resistance to aggressive media. The effective solution of the problem to obtain high-quality concretes is possible due to optimization of their composition, activation of components of concrete mixtures, as well as modification of materials structure by complex additives, which have different functional purpose and contribute to regulation of properties of both concrete mixtures and hardened concretes [1]. However, it should be noted that in the course of concrete products and reinforced concrete structures are often subjected to cracking. This reduces their quality and reduces the expected service life. And the cracks can be caused by both force loads and unfavorable environmental factors. Another reason for cracks in concrete is autogenous shrinkage.

To extend the service life of structures, minimizing the propagation of cracks in concrete is extremely important. Thus, there is an urgent economic incentive to develop concrete which is capable of self-repairing.

Animal and plant organisms are known to have a natural ability to cure small injuries in a relatively short period of time without any external influence. Back in 1712, the French scientist R. Rehomur suggested the term "regeneration", which means the process of restoration by the organism of the damaged structures. The papers [2, 3] described processes of regeneration of animal and plant organisms, from which it follows that regeneration can occur by tissue growth on the injured surface, restructuring of the remaining part of the organ into a new one or by growth of the organ remnant without changing its shape.

Numerous works by foreign and Russian researchers such as V. Achal [4], Chun Xiang Qian [5], W. De Muynck [6], V. Ramarkrichnan [7], J. Y. Wang [8], V. T. Erofeev, V. F. Smirnov, M. G. Brujako [9, 10, 11] have been devoted to creation of technology of concrete modified by various additives and the problem of restoration of strength and durability of self-repairing reinforced concrete structures during crack repair.

A number of authors were engaged in the development of various chemical methods for creating self-repairing concrete [12, 13]. According to one of the modern methods the restorative agent is placed inside microcapsules collapsing with cracking of concrete. Cracks are filled with the released restorative agent which can be epoxy resins [14], silicon dioxide solutions in alkali [15] etc. After the microcapsule is used up a permanent cavity is formed in its location in concrete [16]. Encapsulating tubes can be one of the tools for "treatment" of concrete [17]. Continuous glass tubes can be used to seal large cracks, allowing the replacement of the reducing agent [18]. Their use also gives the possibility of supplying an additional agent [19]. However, it should be considered that the use of some chemicals originally designed to seal cracks increases the fragility of the concrete. Thus, there is a risk of reducing the service life of concrete when implementing the above approaches.

Economic feasibility and expediency of using additives remain the key factors that affect the effectiveness of an additive [20, 21]. With a rather large nomenclature of domestic and imported chemical additives, the task to apply new types of concrete chemical modifiers remains relevant. It follows that these directions of research of SAP in concrete are the most promising.

The strength of hardened concrete is influenced by both the type of SAP additive and the characteristics of the components of the concrete mixture. In addition, the characteristics of the mixture and the hardened concrete depend on the size of SAP particles, the method of production and the dosage of the polymer. A number of experiments were conducted previously [22], which showed the dependence of the strength of hardened concrete on different dosages of SAP, W/C ratio and the curing time of concrete. The results of the experiments led to the conclusion that the strength of hardened concrete decreases with increasing the dosage of SAP. The correct ratio of water to cement in the mixture is a determining factor affecting the strength of

concrete. The rate of concrete strength gain also depends on the addition of super absorbent polymer. The results of experiments [23] investigating the properties of hardening concrete with the addition of SAP, showed that the strength of concrete specimens with SAP on the 7th day of hardening is much lower than the strength of concrete specimens without polymer, if the W/C ratio is constant when kneading the mixture. On the 14th day of hardening, specimens with and without SAP are identical in compressive strength. On the 28th day of hardening the compressive strength of concrete with a dosage of 0.33% of the cement mass increases by 5%. Experiments conducted in [22] also showed that the addition of SAP in a dosage equal to 0.3% does not cause a noticeable decrease in the strength on the 28th day of concrete curing. According to studies by other authors [25], the compressive strength of concrete increases up to 7% at a dosage of SAP at 3% of the weight of cement. Comparable results were obtained in [26], and [27] reported a slight increase in compressive strength only after adding 0.3% SAP combined with anti-shrinkage additive. Meanwhile, other studies have reported that dosages of 0.3% SAP do not increase the compressive strength. For example, an experiment with three types of SAP was conducted in [28], and all of them led to a decrease in the compressive strength of concrete by 5-15%. Comparable results were obtained in [29]: the compressive strength of concrete at a dosage of 0.3% of the weight of cement decreased by 10-12% after 7 and 28 days of hardening.

Analysis of studies conducted by the various authors allows us to conclude that there is an optimal dosage for each type of SAP. And the experimental results are often not comparable due to differences in the type of SAP, the composition of the concrete mixture and its W/C ratio. Despite this problem, the use of SAP can be an important tool to improve the quality of construction materials. Experimental studies will allow to investigate the effectiveness of the use of the tested types of SAP.

The present study focuses on the investigation of concrete with the addition of super absorbent polymers that can absorb a large amount of liquid, hold it for a long time and gradually release it back. This property of SAP allows to solve the problem of increasing the strength of concrete due to the effect of internal curing. The SAP particles will gradually release the absorbed water, which ensures a more complete hydration of cement during the hardening of concrete. Internal curing can reduce the risk of cracking in the early stages of hardening and thus increase the strength of the concrete. The described effect can be useful in modern construction, where high-strength concretes with low W/C ratios are applied.

The purpose of the study is to investigate concrete mixtures and hardened concretes modified with a super absorbent additive for further development of effective concrete compositions.

Research Objectives:

1. To evaluate the super absorbent additive as a potential modifier for the development of effective concrete compositions.
2. To define the regularities of changes in the rheological and structural-mechanical characteristics of concrete depending on the dosage of the additive.
3. To consider prospects of using neural network technologies in order to establish the possibility of crack curing and determine the autogenous shrinkage of concrete with SAP additive.
4. The obtained results will help to identify further prospects for the use of the studied types of SAP in concrete structures.

MATERIALS AND METHODS

Portland cement CEM I 42.5 N produced by Gornozavodskcement LLC, Perm region, Russia, was used as a binder.

As an additive was selected super absorbent polymer (SAP) manufactured by the Korean company "GV Holdings Co". Its absorption capacity is 400 g of water per 1 g of SAP, the average particle size is 300 microns. Since the

chosen additive had not been investigated before, the first stage of the research was to conduct experiments with different dosages of SAP and W/C ratios of concrete mortar. The purpose of this study was to determine the effectiveness of this type of SAP as an additive in concrete. The super absorbent polymer was added to the dry mixture of aggregate and cement. Then it was stirred manually before adding water.

A series of concrete specimens on fine aggregate as well as on a mixture of fine and coarse aggregate were investigated. In the first, fine river sand fraction of 0-2,5 mm was applied. In the second case, the same sand and dolomite crushed stone fraction of 5-10 mm were used.

Two series of specimens were molded for the experiment. The first series was performed in the form of 4×4×16 cm beams, the second one contained specimens-cubes with a rib size of 10 cm.

Two series of specimens were made of fine-grained concrete, each with four different compositions. The first four mixtures were prepared according to the normal consistency of the concrete mortar (cone slump of each was 106-115 mm). For the remaining four mortar mixes, a W/C ratio of 0.5 was adopted as constant. This value was chosen in order to obtain the cone slump of 106-115 mm at a SAP dosage equal to 1%. Cone slump of the mortar was determined after each mixture was stirred. Table 1 shows the compositions of the experimental mortars and concretes. The latter ones were formed with a constant ratio W/C = 0.55, the slump of the cone was determined after mixing each composition.

Table 1. Experimental compositions for the specimens

Composition No	SAP, % of the cement mass	W/C ratio	The quantity of materials for 1m^3 of mortar and concrete, kg				
			Cement	Sand	Crushed stone	Water	SAP
1-1	0	0.42	650	1950	–	273	0
1-2	0.25	0.44	650	1950	–	286	1.625
1-3	0.5	0.46	650	1950	–	299	3.25
1-4	1	0.5	650	1950	–	325	6.5
2-1	0	0.5	650	1950	–	273	0
2-2	0.25	0.5	650	1950	–	286	1.625
2-3	0,5	0.5	650	1950	–	299	3.25
2-4	1	0.5	650	1950	–	325	6.5
3-1	0	0.55	365	850	1200	200	0
3-2	0.5	0.55	365	850	1200	200	1.825

Concrete specimens were cured under normal temperature and humidity conditions for 28 days before compression testing. Each of the series of specimens was tested on the 28th day of hardening in accordance with modern regulatory documents.

RESULTS AND DISCUSSION

Among chemical additives in the construction practice the preference is given to additives of poly-functional action providing maximum use of positive and minimization of negative properties of individual additives. At the first stage of research the rheological properties were considered, namely, the influence of additive SAP on the water-cement ratio and slumping was determined. At the same time, it is important to identify how much it is feasible to reduce or increase water consumption on gravitational slumping of cement compositions.

When forming test specimens No. 1-4 of fine-grained concrete, the dependence of W/C on SAP dosage for the normal consistency of the mortar was determined. Increasing the dosage of SAP led to an increase in the water consumption of the mixture. With the use of SAP from 0 to 1%, the dependence of W/C on its dosage turned out to be linear (Fig. 1). This dependence is applicable only to the raw materials used in this experiment and only if the dosage of SAP is from 0 to 1% of the cement mass.

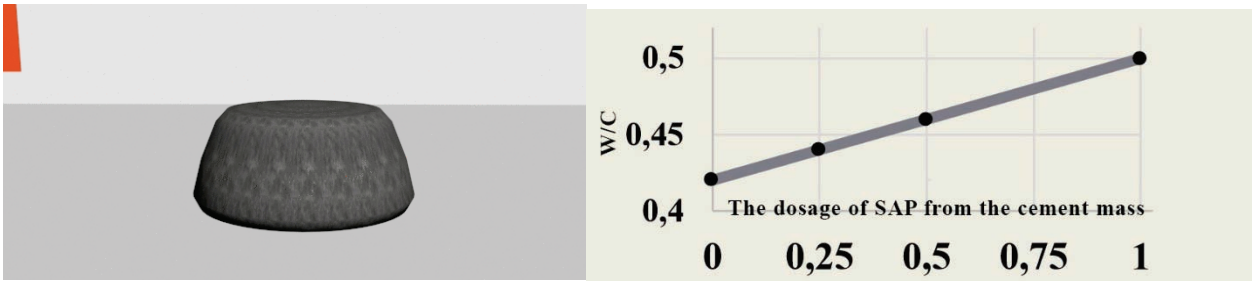


Figure 1. W/C ratio for cone slump of 106-115 mm depending on the dosage of SAP

At the same stage, the dependence of the influence of the quantity of additive on cone slump at a constant water-cement ratio was revealed. Increasing the dosage of SAP led to a decrease in cone slump at a constant W/C equal to 0.5 (Fig. 2).

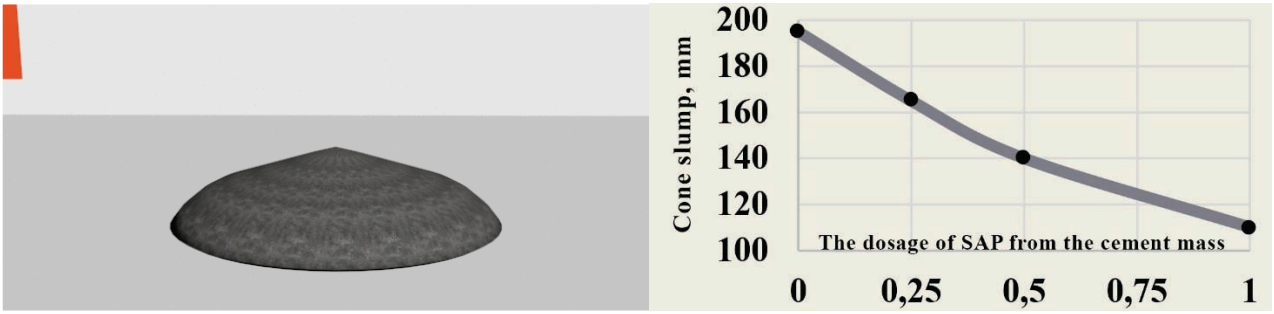


Figure 2. Cone slump depending on the dosage of SAP at a constant W/C ratio equal to 0.5

The detected dependence is not linear, it is limited by the permissible values of cone slump and is also applicable only for raw materials used in this experiment, and only if the dosage of SAP is from 0 to 1% of the weight of cement. The performance of the additive is very often evaluated by the physical and mechanical properties of the resulting concrete. Among the physico-mechanical properties of structural materials are the strength indicators.

A comparative assessment of the effect of SAP additive on the strength of cement composite was performed. The strength values determined in accordance with the standards and its average values have been determined. The dependences of bending and compressive strength of concrete specimens on the dosage of the studied type of SAP were obtained (Fig. 3, 4).

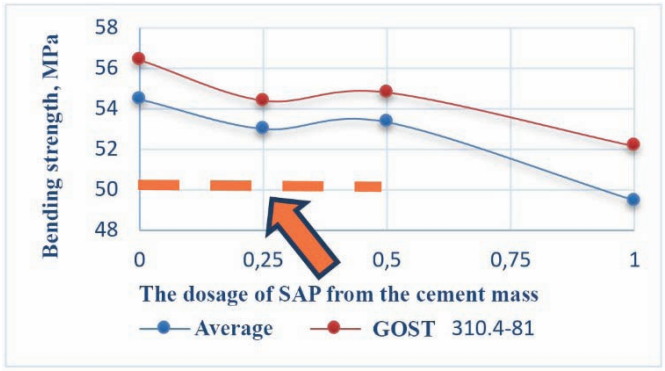
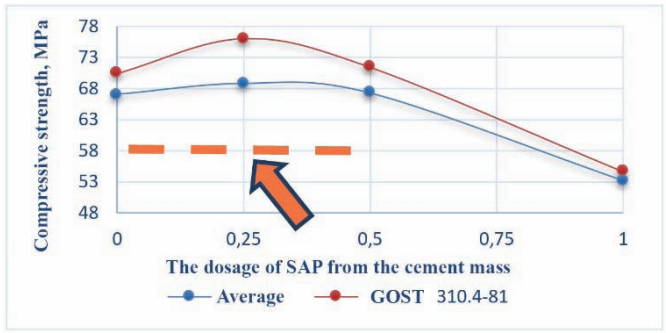
cone slump = const	
cone slump = const	

Figure 3. Dependence of the bending strength and compressive strength on the SAP dosage at a constant cone flowequal to 106-115 mm

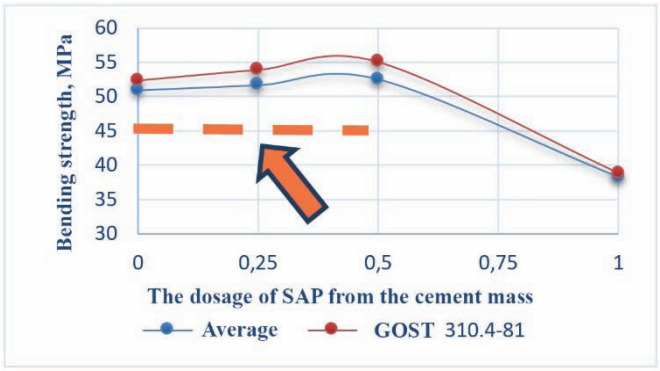
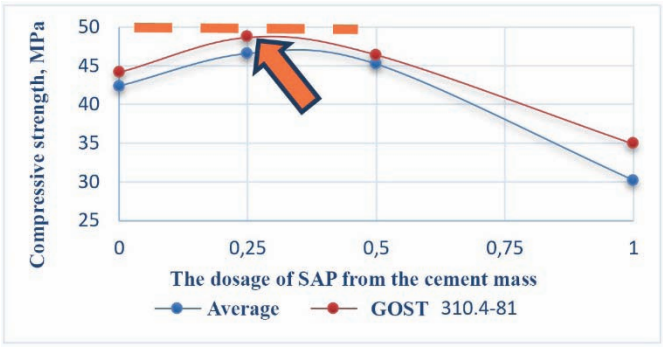
W/C = const	
W/C = const	

Figure 4. Dependence of the bending strength and compressive strength of concrete depending on the SAP dosage at a constant W/C ratio equal to 0.5

Fig. 3 shows the dependence at a constant cone slump equal to 106-115 mm. Fig. 4 provides the relationship for a constant W/C ratio of 0.5. The above curves can be represented in the form of the surface shown in Fig. 5, which is formed by three quantities: W/C, the percentage of SAP additive and the strength of the concrete. This allows the results of the study to be seen in a more comprehensible way.

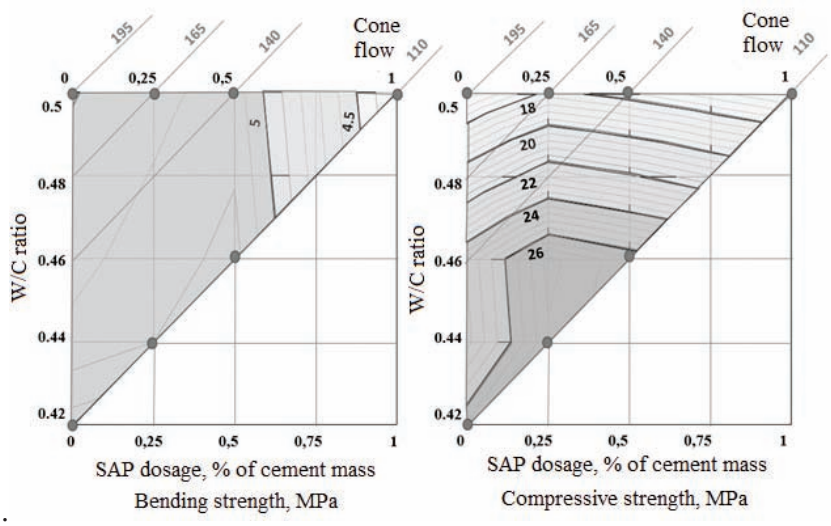
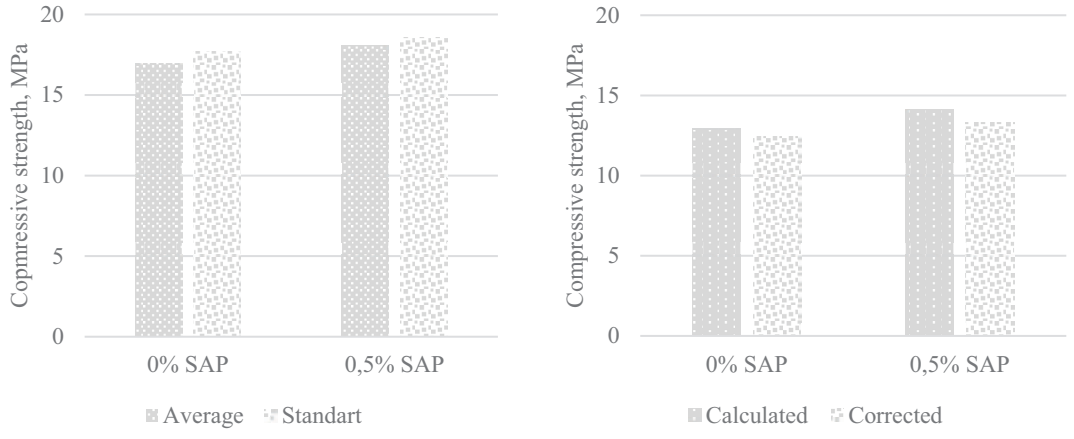


Figure 5. Dependence of the bending strength and compressive strength depending on the SAP dosageand concreteW/C ratio

Analysis of the results shows that the bending and compressive strength of fine-grained concrete does not change at dosages up to 0.5%. However, it decreases by 20-25% when the dosage is increased to 1%. It can be concluded that for further studies of this type of SAP should be selected its dosage not more than 0.5% of the weight of cement. The compressive strength of concrete increases insignificantly with the dosage of the additive, equal to 0.25% of the weight of cement.

It is interesting to compare the test results of mortar mixes with the results obtained by testing specimens of heavy concrete (Fig. 6). Only the additive dosage equal to 0.5% of the weight of cement was investigated in this study, and the compressive strength of concrete was taken as a parameter of properties.



A *B*

Figure 6. Compressive strength of heavy (A) concrete and fine-grained (B) concrete

The results show that the inclusion of SAP in an amount of 0.5% of the weight of cement increases the compressive strength of heavy concrete by 9% at a constant W/C equal to 0.55. The strength of fine-grained concrete under the same conditions increased by 7%.

As the experimental data accumulate, their generalization and statistical processing become relevant. The solution of this problem allows to pass to the creation of prediction methods for the set of concrete properties.

In 2000-2020s there is a growing interest in theory and practice of artificial neural networks for research of structure-property relations of different materials. Depending on a type of a property they can solve the problems of classification (at a discrete set of values of properties), and also the problems of regression (at continuous values of modelled property).

Neural networks, in a certain sense, represent an alternative to the traditional regression analysis and open up the possibility of creating materials with predetermined properties.

A neural network trained on the information gathered as a result of the study can predict the properties of the obtained material. This allows to optimally plan further studies and reduce the number of necessary experiments.

Due to the ability to approximate nonlinear dependences of arbitrary form, neural networks are best suited for modeling and predicting the physical and mechanical properties of concretes, depending on such parameters as the composition of mortar and mixtures, temperature, pressure, etc. [30, 31, 32].

This study was conducted on the eight types of concrete compositions in which only the dosage of SAP and W/C varied. All other parameters were the same, so the named variables can be taken as input values. As a result of the study, data such as mortar slump, flexural strength, and compressive strength were obtained for each concrete mixture (see Table 2). These values are the output data.

To create a primitive version of the neural network, the Python programming language was applied. As a training sample, the results of the experiments on the compositions No. 1-8 shown in Table 2 were used. The values of the table were normalized in the range from 0 to 1 with respect to the maximum values of the output data and are presented in Table 3.

Table 2. Neural network base

Mixture №	Input parameters		Output parameters – Results		
	SAP, % of cement mass	W/C ratio	Slump flow, mm	Bending strength, MPa	Compressive Strength, MPa
1	0	0.42	120	5.44	26.84
2	0.25	0.44	120	5.3	27.54
3	0.5	0.46	120	5.33	26.92
4	1	0.5	120	4.96	21.29
5	0	0.5	195	5.09	16.96
6	0.25	0.5	165	5.17	18.64
7	0.5	0.5	140	5.25	18.57
8	1	0.5	120	3.83	12.07

Table 3. Training matrix for neural network

Mixture№	Inputparameters		Outputparameters–Results		
	X1	X2	Y1	Y2	Y3
1	0	0.84	0.615	1	0.974
2	0.25	0.88	0.615	0.974	1
3	0.5	0.92	0.615	0.979	0.977
4	1	1	0.615	0.911	0.773
5	0	1	1	0.935	0.616
6	0.25	1	0.846	0.95	0.676
7	0.5	1	0.718	0.965	0.674
8	1	1	0.615	0.704	0.438

To determine the prospects of applying the neural network, new compositions were selected for which the input values were known: the dosage of SAP and W/C, while the output values of cone slump, bending and compressive strength were unknown. New normalized input values were fed into the trained neural network (Table 4). Here is also the result of the neural network.

Table 4. Input and output parameters of neural network

Mixture №	Input parameters		Output parameters - Results		
	X1	X2	Y1	Y2	Y3
Neiro-1	0.75	1	0.656	0.917	0.713
Neiro-2	0.3	1	0.751	0.983	0.823
Neiro-3	1	1.2	0.662	0.924	0.722

After converting the obtained values from normalized to calculated values, the results of the neural network presented in Table 5 were obtained.

Table 5. Results of neural network

Mixture№	Inputparameters		Outputparameters–Results		
	SAP, % ofcementmass	W/C ratio	Slump flow, mm	Bending strength, MPa	Compressive strength, MPa
Neiro-1	0.75	0.5	128	4.988	19.636
Neiro-2	0.3	0.5	146	5.347	22.665
Neiro-3	1	0.6	129	5.026	19.884

The obtained values allow predicting the properties of the concrete mixture and hardened concrete at given values. It can be assumed that the investigated type of SAP does not reduce the strength of concrete at dosages up to 0.5% of the weight of cement, therefore it can be used to improve other characteristics of concrete. Inclusion of SAP into the concrete mixture causes the increase of W/C, therefore the effect of its application in combination with plasticizers and anti-shrinkage additives should be accounted for more effective use of the additive.

The interest in the theory and practice of artificial neural networks lies in their ability to approximate non-linear dependences of arbitrary

type by means of algorithms, which the neural networks themselves find.
The disadvantage of the presented system is the absence of a large training sample, so the neural network may have errors.

CONCLUSIONS

1. The possibility of obtaining effective concretes with improved physical-mechanical and operational characteristics by their modification with a super absorbent additive has been theoretically substantiated and confirmed experimentally.
2. The dependence of changes in the characteristics of the quality of concrete mixture depending on the presence of the introduced additive has been established. Increasing the dosage of SAP increases water consumption of concrete mixture, cone slump decreases at a constant W/C ratio. The dependence of the ratio W/C on the dosage of SAP to achieve the slump of the cone 106-115 mm proved to be linear
3. The most effective impact of the additive on the compressive strength can be recognized as follows: the dosage of super absorbent additive in an amount of 0.5% of the weight of cement increases the compressive strength of fine-grained concrete to 7% at a constant ratio W / C = 0.5 and increases the compressive strength of heavy concrete to 9% at a constant ratio W / C = 0.55. The increase in the dosage of SAP to 1% of the weight of cement decreases the strength of hardened concrete to 20-25% and significantly reduces the slumping of heavy concrete.
4. The obtained results allow further comparative experiments to determine autogenous shrinkage and the possibility of crack curing. The results of the research will also help to substantiate the effectiveness of the presented type of SAP in concrete structures. It can be effective in reducing autogenous shrinkage of concrete without reducing its strength, and may also find application in the creation of self-curing concrete.

ACKNOWLEDGMENTS

Funding: The research was funded by the Ministry of Science and Higher Education of the Russian Federation as the grant Self-Healing Construction Materials (contract No. 075-15-2021-590 dated 04.06.2021).

REFERENCES

1. **Kalashnikov V.I., Erofeev V.T., Moroz M.N.** [et al.] Nanogidrosilikatnyye tekhnologii v proizvodstve betonov [Nanohydrosilicate technologies in the production of concrete] // Stroitelnye materialy. 2014. No. 5.P. 88–91 (In Russian). https://cyberleninka.ru/article/n/nanogidrosilikatnye-tehnologii-v-proizvodstve-betonov
2. **Ghosh S.K.** (ed.) Self-healing materials: fundamentals, design strategies, and applications, Wiley WCH, Weinheim. – 2009. – P. 183–218.
3. **Hua Xia.** Self-healing of Engineered Cementitious Composites (ECC) in Concrete Repair System / Hua Xia // MASc thesis, Delft University of Technology, Netherlands. – 2010. –P. 1–56.
4. **Achal V**. Microbial remediation of defects in building materials and structures: PhD thesis. – India: Thapar University, Patiala, 2010. – P. 1–263.
5. **Chun Xiang Qian**. Cementation of sand grains based on carbonate precipitation induced by microorganism / Chun Xiang Qian, Qingfeng Pan, Ruixing Wang. – 2010. – Vol. 53(8) – P. 2198–2206. https://doi.org/10.1007/s11431-009-3189-z
6. **De Muynck W.** Bacterial carbonate precipitation as an alternative surface treatment for concrete / W. De Muynck, C. Kathelijn, N. De Belie. // Construction and Building Materials. – 2008. – Vol. 22(5). – P. 875–885. https://doi.org/10.1016/j.conbuildmat.2006.12.011

7. **Ramakrishan V**. A novel technique for repairing cracks in high performance concrete using bacteria / V. Ramakrishan, S.S. Bang, K.S. Deo // Proc. international conference on high performance high strength concrete, Perth, Australia. – 1998. – P. 597–618. https://www.researchgate.net/publication/284463206_A_novel_technique_for_repairing_cracks_in_high_performance_concrete_using_bacteria
8. **Wang J.Y., Snoeck D., Vlierberghe S.V., Verstraete W., De Belie N.** Application of hydrogelencapsulated carbonate precipitating bacteria for approaching a realistic self-healing in concrete / J.Y. Wang, D. Snoeck,S.V. Vlierberghe, W. Verstraete, N. De Belie // Construction and Building Materials. – 2014. – Vol. 68. – P. 110–119. https://doi.org/10.1016/j.conbuildmat.2014.06.018
9. Khimicheskiye aspekty protsessa ustraneniya treshchin betona s pomoshchyu bakteriy / V. T. Erofeyev. V. T. Fomichev // Internet-zhurnal «Transportnyye sooruzheniya». – 2018. – № 3. – T. 5. S.12. – Rezhim dostupa: https://t-s.today/PDF/13SATS318.pdf.
10. Bakterii dlya polucheniya samovosstanavlivayushchikhsya betonov / V. T. Erofeyev. V. F. Smirnov // Internet-zhurnal «Transportnyyesooruzheniya. – 2018. – № 4. T. 5.– S.6 – Rezhimdostupa: https://t-s.today/PDF/07SATS418.pdf.
11. Biomodifitsirovaniye stroitelnykh materialov bakteriyami s ureaznoy aktivnostyu / M.G. Bruyako, A.I. Grigoryeva, D.S. Golotenko, A.A. Podsevalova / Stroitelstvo i rekonstruktsiya – zhurnal FGBOU VO «OGU im. I. S. Turgeneva». – № 2 (88). – 2020. – S. 5–15. https://doi.org/10.33979/2073-7416-2020-88-2-5-15
12. Bobrishev A. A., Shafigullin L. N., Erofeev V. T., Treshchev A. A., Sotnikov M. I., Vyacheslav A. Study of effects of redispersable latex powders on hardening kinetics of cement-sand composites.https://www.scopus.com/record/display.uri?eid=2-s2.0-84991711531&origin=resultslist&sort=cp-f&src=s&st1=Study+of+effects+of+redispersable+latex+powders+on+hardening+kinetics+of+cement-sand+composites&sid=b71ac3837a9795fac76fa3cdb136ea56&sot=b&sdt=b&sl=110&s=TITLE-ABS-KEY%28Study+of+effects+of+redispersable+latex+powders+on+hardening+kinetics+of+cement-sand+composites%29&relpos=0&citeCnt=3&searchTerm=
13. Arabi N. Formation of C-S-H in calcium hydroxide-blast furnace slag-Quartz-water system In autoclaving conditions / N. Arabi, R. Jauberthie, N. Chelghoum, L. Molez // Advances in Cement Research. – 2015. – 27(3). – P. 153–162.https://doi.org/10.1680/adcr.13.00069
14. **Kamada T**. The effects of surface preparation on the fracture behavior of ECC / T. Kamada, V.C. Li // concrete repair system, Cementand Concrete Composites. – 2000. – Vol.22, № 6. – P. 422–431. https://doi.org/10.1016/S0958-9465(00)00042-1
15. **Bang S.S**. Calcite precipitation in duced by polyurethane immobilized Sporos arc in a pasteurii / S.S. Bang, J.K. Galinat, V. Ramakrishnan // Enzyme and Microbial Technology. – 2001. – Vol. 28, № 4 – P. 404–409. https://doi.org/10.1016/S0141-0229(00)00348-3
16. **Sahmaran M.** Durability properties of micro-cracked ECC containing high volumes flyash / M. Sahmaran, V. C. Li // Cement and Concrete Research. – 2009. – Vol. 39. – № 11. – P. 1033–1043.https://doi.org/10.1016/j.cemconres.2009.07.009
17. **Mookhoek S.D**. Self-healing behaviour in man-made engineering materials: bioinspired but taking into account their intrinsic character /S.D. Mookhoek, S.

Vander Zwaag, N.H. van Dijk, H.M. Jonkers, W.G. Sloof // Philosophical Transactions A: Mathematical, Physical and Engineering Science. – 2009. – Vol. 367, № 3. – P. 1689–1704. https://doi.org/10.1098/rsta.2009.0020

18. **Lyu K., She W., Miao C., Chang H., Gu Y.** Quantitative characterization of pore morphology in hardened cement paste via SEM-BSE image analysis. Constr. Build. Mater. 2019; 202: 589–602. https://doi.org/10.1016/j.conbuildmat.2019.01.055
19. **Song Y, Zhou J, Bian Z, Dai G.** Pore structure characterization of hardened cement paste by multiple methods. Adv Mater Sci Eng2019; 2019: 1–18. https://doi.org/10.1155/2019/3726953
20. **Wang J, Dong S, Zhou C, Ashour A, Han B.** Investigating pore structure of nano-engineered concrete with low-field nuclear magnetic resonance. J Mater Sci 2021; 56(1): 243–59. https://doi.org/10.1007/s10853-020-05268-0
21. **Wang J.Y.** Diatomaceous earth as a protective vehicle for bacteria applied for self-healing concrete / J. Y. Wang, N. De Belie, W. Verstraete // Journal of Industrial Microbiology and Biotechnology. – 2012. – Vol. 39, № 4. – P. 567–577. https://doi.org/10.1007/s10295-011-1037-1
22. **Olawuyi B.J., Babafemi A.J. and Boshoff W.P.** 2021 Early-age and long-term strength development of high-performance concrete with SAP Construction and Building Materials 267121798. https://doi.org/10.1016/j.conbuildmat.2020.121798
23. **Li L., Dabarera A.G.P. and Dao V.** 2020 Time-zero and deformational characteristics of high performance concrete with and without superabsorbent polymers at early ages Construction and Building Materials 264120262.https://doi.org/10.1016/j.conbuildmat.2020.120262
24. **Tan Y., Lu X., He R., Chen Hand Wang Z.** 2020 Influence of superabsorbent polymers (SAPs) type and particle size on the performance of surrounding cement-based materials Construction and Building Materials270 121442.https://doi.org/10.1016/j.conbuildmat.2020.121442
25. **Popov D.Yu., Lesovik V.S., Mechtcherine V.S.** The Influence of Superabsorbent Polymer on the Performance of Concrete // Bulletin of BSTU named after V. G. Shukhov, 2016. – № 11. – P. 1–7. DOI: 10.12737/22455
26. **Sensale G.R., Goncalves A.F.** Effects of Fine LWA and SAP as Internal Water Curing Agents // International Journal of Concrete Structures and Materials. – 2014. – V/ 8. – P. 229–238. https://doi.org/10.1007/s40069-014-0076-1
27. **Liu J., Farzadnia N., Shi C. and Ma X.** 2019 Shrinkage and strength development of UHSC incorporating a hybrid system of SAP and SRA Cement and Concrete Composites 97 175-189. https://doi.org/10.1016/j.cemconcomp.2018.12.029
28. **Silva E., Alejandro M.R.M, Lopes A.N. M., Dias R.T.F.** Effect of sap on the autogenous shrinkage and compressive strength of high-strength fine-grained concrete // Springer Nature. – 2020. – P. 2211–0852. https://www.researchgate.net/publication/341600761_EFFECT_OF_SAP_ON_THE_AUTOGENOUS_SHRINKAGE_AND_COMPRESSIVE_STRENGTH_OF_HIGH-STRENGTH_FINE-GRAINED_CONCRETE
29. **Meyst L., Kheir J., Roberto J.T.F., Tittelboom K.V.** The Use of Superabsorbent Polymers in High Performance Concrete to Mitigate Autogenous Shrinkage in a Large-Scale Demonstrator Sustainability 12. – 2020. – 2(11), 4741; https://doi.org/10.3390/su12114741.
30. **A.N. Gorban**. Obobshchennaya approksimatsionnaya teorema I vychislitelnyye vozmozhnosti neyronnykh

setey. Sib. zhurn. vychisl. matem.. 1998. tom 1. nomer 1. 11–24.
31. **N.M. Galbershtam, I.I. Baskin, V.A. Palyulin, N.S. Zefirov**. “Neyronnyye seti kak metod poiska zavisimostey struktura – svoystvo organicheskikh soyedineniy”. Usp. khim.. 72:7 (2003). 706–727; Russian Chem. Reviews. 72:7 (2003). 629–649.https://doi.org/10.1070/RC2003v072n07ABEH000754
32. **Jiang, G., Keller, J., Bond, P.L**. and 1 more Predicting concrete corrosion of sewers using artificial neural network // Water Research, 2016.https://doi.org/10.1016/j.watres.2016.01.029

СПИСОК ЛИТЕРАТУРЫ

1. **Калашников В.И.** Суспензионно-наполненные бетонные смеси для порошково-активированных бетонов нового поколения / В. И. Калашников, В.Т. Ерофеев, О.В. Тараканов // Изв. вузов. Стр-во. – 2016. – № 4. – С. 38–37. https://www.elibrary.ru/item.asp?id=28153441
2. **Ghosh S.K.** (ed.) Self-healing materials: fundamentals, design strategies, and applications, Wiley WCH, Weinheim. – 2009. – P. 183–218.
3. **Hua Xia.** Self-healing of Engineered Cementitious Composites (ECC) in Concrete Repair System / Hua Xia //MASc thesis, Delft University of Technology, Netherlands. – 2010. –P. 1–56.
4. **Achal V**. Microbial remediation of defects in building materials and structures: PhD thesis. – India: Thapar University, Patiala, 2010. – P. 1–263.
5. **Chun Xiang Qian.** Cementation of sand grains based on carbonate precipitation induced by microorganism / Chun Xiang Qian, Qingfeng Pan, Ruixing Wang. – 2010. – Vol. 53(8) – P. 2198–2206. https://doi.org/10.1007/s11431-009-3189-z
6. **De Muynck W.** Bacterial carbonate precipitation as an alternative surface treatment for concrete / W. De Muynck, C. Kathelijn, N. De Belie. // Construction and Building Materials. – 2008. – Vol. 22(5). – P. 875–885. https://doi.org/10.1016/j.conbuildmat.2006.12.011
7. **Ramakrishan V.** A novel technique for repairing cracks in high performance concrete using bacteria / V. Ramakrishan, S.S. Bang, K.S. Deo // Proc. international conference on high performance high strength concrete, Perth, Australia. – 1998. – P. 597–618. https://www.researchgate.net/publication/284463206_A_novel_technique_for_repairing_cracks_in_high_performance_concrete_using_bacteria
8. **WangJ. Y., Snoeck D., Vlierberghe S.V., Verstraete W., De Belie N.** Application of hydrogelencapsulated carbonate precipitating bacteria for approaching a realistic self-healing in concrete / J. Y. Wang, D. Snoeck, S. V. Vlierberghe, W. Verstraete, N. De Belie // Construction and Building Materials. – 2014. – Vol. 68. – P. 110–119. https://doi.org/10.1016/j.conbuildmat.2014.06.018
9. Химические аспекты процесса устранения трещин бетона с помощью бактерий / В. Т.Ерофеев, В. Т.Фомичев // Интернет-журнал «Транспортные сооружения». –2018. –№3. – Т. 5. С.12. – Режим доступа: https://t-s.today/PDF/13SATS318.pdf.
10. Бактерии для получения самовосстанавливающихся бетонов / В. Т.Ерофеев, В. Ф. Смирнов // Интернет-журнал «Транспортные сооружения.– 2018.–№4. Т.5.– С.6 – Режим доступа: https://t-s.today/PDF/07SATS418.pdf.
11. Биомодифицирование строительных материалов бактериями с уреазной активностью / М.Г. Бруяко, А.И. Григорьева, Д.С. Голотенко, А.А. Подсевалова / Строительство и

реконструкция – журнал ФГБОУ ВО «ОГУ им. И. С. Тургенева».– № 2 (88). – 2020. – С. 5–15. https://doi.org/10.33979/2073-7416-2020-88-2-5-15

12. **Bobrishev A.A., Shafigullin L.N., Erofeev V.T., Treshchev A.A., Sotnikov M.I., Vyacheslav A.** Study of effects of redispersable latex powders on hardening kinetics of cement-sand composites. https://www.scopus.com/record/display.uri?eid=2-s2.0-84991711531&origin=resultslist&sort=cp-f&src=s&st1=Study+of+effects+of+redispersable+latex+powders+on+hardening+kinetics+of+cement-sand+composites&sid=b71ac3837a9795fac76fa3cdb136ea56&sot=b&sdt=b&sl=110&s=TITLE-ABS-KEY%28Study+of+effects+of+redispersable+latex+powders+on+hardening+kinetics+of+cement-sand+composites%29&relpos=0&citeCnt=3&searchTerm=
13. **Arabi N.** Formation of C-S-H in calcium hydroxide-blast furnace slag-Quartz-water system Inautoclavingconditions / N. Arabi, R. Jauberthie,N. Chelghoum, L. Molez // Advances in Cement Research. – 2015. – 27(3). – P. 153–162. https://doi.org/10.1680/adcr.13.00069
14. **Kamada T.** The effects of surface preparation on the fracture behavior ofECC / T. Kamada, V. C. Li // concrete repair system,Cementand Concrete Composites. – 2000. – Vol.22, № 6. – P. 422–431.https://doi.org/10.1016/S0958-9465(00)00042-1
15. **Bang S.S**. Calcite precipitation in duced by polyurethane im mobilized Sporosarcinapasteurii / S.S. Bang, J. K. Galinat, V. Ramakrishnan // Enzyme and Microbial Technology. – 2001. – Vol. 28, № 4 – P. 404–409. https://doi.org/10.1016/S0141-0229(00)00348-3
16. **Sahmaran M.** Durability properties of micro-cracked ECC containing high volumes flyash / M. Sahmaran, V.C. Li // Cement and Concrete Research. – 2009. – Vol. 39. – № 11. – P. 1033–1043.https://doi.org/10.1016/j.cemconres.2009.07.009
17. **Mookhoek S.D**. Self-healing behaviour in man-made engineering materials: bioinspired but taking into account their intrinsic character / S.D. Mookhoek, S. Vander Zwaag, N.H. van Dijk, H.M. Jonkers, W.G. Sloof // Philosophical Transactions A: Mathematical, Physical and Engineering Science. – 2009. – Vol. 367, № 3. – P. 1689–1704. https://doi.org/10.1098/rsta.2009.0020
18. **Lyu K, She W, Miao C, Chang H, Gu Y**. Quantitative characterization of pore morphology in hardened cement paste via SEM-BSE image analysis. Constr. Build. Mater. 2019; 202: 589–602. https://doi.org/10.1016/j.conbuildmat.2019.01.055
19. **Song Y, Zhou J, Bian Z, Dai G.** Pore structure characterization of hardened cement paste by multiple methods. Adv Mater Sci Eng. 2019; 2019:1–18. https://doi.org/10.1155/2019/3726953
20. Wang J, Dong S, Zhou C, Ashour A, Han B. Investigating pore structure of nano-engineered concrete with low-field nuclear magnetic resonance. J Mater Sci 2021; 56(1):243–59.https://doi.org/10.1007/s10853-020-05268-0
21. **Wang J.Y.** Diatomaceous earth as a protectivevehicle for bacteria applied for self-healing concrete / J.Y. Wang, N. De Belie, W. Verstraete // Journal of Industrial Microbiology and Biotechnology. – 2012. – Vol. 39, № 4. – P. 567–577. https://doi.org/10.1007/s10295-011-1037-1
22. **Olawuyi B.J., Babafemi A.J. and Boshoff W.P.** 2021 Early-age and long-term strength development of high-performance concrete with SAP Construction and

Building Materials 267121798. https://doi.org/10.1016/j.conbuildmat.2020.121798

23. **Li L., Dabarera A.G.P. and Dao V.** 2020 Time-zero and deformational characteristics of high performance concrete with and without superabsorbent polymers at early ages Construction and Building Materials 264120262.https://doi.org/10.1016/j.conbuildmat.2020.120262
24. **Tan Y., Lu X., He R., Chen Hand Wang Z**. 2020 Influence of superabsorbent polymers (SAPs) type and particle size on the performance of surrounding cement-based materials Construction and Building Materials270 121442. https://doi.org/10.1016/j.conbuildmat.2020.121442
25. **Popov D.Yu., Lesovik V.S., Mechtcherine V.S.** The Influence of Superabsorbent Polymer on the Performance of Concrete // Bulletin of BSTU named after V.G. Shukhov, 2016. – № 11. – P. 1–7.DOI: 10.12737/22455
26. **Sensale G.R., Goncalves A.F.** Effects of Fine LWA and SAP as Internal Water Curing Agents // International Journal of Concrete Structures and Materials. – 2014. – V/ 8. – P. 229–238. https://doi.org/10.1007/s40069-014-0076-1
27. **Liu J., Farzadnia N., Shi C. and Ma X.** 2019 Shrinkage and strength development of UHSC incorporating a hybrid system of SAP and SRA Cement and Concrete Composites97 175-189. https://doi.org/10.1016/j.cemconcomp.2018.12.029
28. **Silva E., Alejandro M.R.M, Lopes A.N.M., Dias R.T.F**. Effect of sap on the autogenous shrinkage and compressive strength of high-strength fine-grained concrete // Springer Nature. – 2020. – P. 2211–0852. https://www.researchgate.net/publication/341600761_EFFECT_OF_SAP_ON_THE_AUTOGENOUS_SHRINKAGE_AND_COMPRESSIVE_STRENGTH_OF_HIGH-STRENGTH_FINE-GRAINED_CONCRETE
29. **Meyst L., Kheir J., Roberto J.T.F., Tittelboom K.V.** The Use of Superabsorbent Polymers in High Performance Concrete to Mitigate Autogenous Shrinkage in a Large-Scale Demonstrator Sustainability12. – 2020. – 2(11), 4741; https://doi.org/10.3390/su12114741.
30. **А.Н. Горбань,** Обобщенная аппроксимационная теорема и вычислительные возможности нейронных сетей, Сиб. журн. вычисл. матем., 1998, том 1, номер 1, 11–24.
31. **Н.М. Гальберштам, И.И. Баскин, В.А. Палюлин, Н.С. Зефиров,** “Нейронные сети как метод поиска зависимостей структура - свойство органических соединений”, Усп. хим., 72:7 (2003), 706–727; RussianChem. Reviews, 72:7 (2003), 629–649. https://doi.org/10.1070/RC2003v072n07ABEH000754
32. **Jiang, G., Keller, J., Bond, P.L.** and 1 more Predicting concrete corrosion of sewers using artificial neural network // Water Research, 2016. https://doi.org/10.1016/j.watres.2016.01.029

Sharafutdinov Kamil Bulatovich, postgraduate student of the Department of "Building Structures and Computational Mechanics" Perm National Research Polytechnic University; 109 Kuibyshev str., Perm, 614010, Russia; tel. +7(342) 219-83-61, e-mail: kamil_sh@bk.ru

Saraikina Ksenia Aleksandrovna, Candidate of Technical Sciences, Associate Professor of the Department of "Construction Engineering and Materials Science" Dean of the Faculty of Construction Perm National Research Polytechnic University; 109 Kuibyshev str., Perm, 614010, Russia; tel. +7(342) 219-81-72, e-mail: k.a.saraykina@pstu.ru

Galina G. Kashevarova, Corresponding Member of Russian Academy of Architecture and Construction Sciences, Professor, Dr.Sc., Head of department “Building constructions and computational mechanics”, Perm National Research Polytechnic University; Russia,

614010, Perm, ul. Kuibyshev, 109; phone +7 (342) 219-83-61, e-mail: ggkash@mail.ru.

Yana A. Sanyagina, Competitor of the Department of Building Materials and Technologies, National Research Mordovian State University name N.P. Ogaryov; 430005, Republic of Mordovia, Saransk, st. Bolshevik, d. 68; E-mail: sanyagina@mail.ru.

Vladimir T. Erofeev, Academician of the RAACS, Professor, Doctor of Technical Sciences, Director of the Institute of Architecture and Construction, National Research Mordovian State University name N.P. Ogaryov; 430005, Republic of Mordovia, Saransk, st. Bolshevik, d. 68; tel. +7(8342) 48-25-64; E-mail: erofeevvt@bk.ru.

Nikolai I. Vatin, Professor, Doctor of Technical Sciences, Chief Researcher, St. Petersburg Polytechnic University name Peter the Great; 109992, Moscow, st. Solyanka, 14; E-mail: vatin_ni@spbstu.ru

Шарафутдинов Камил Булатович, аспирант кафедры ««Строительные конструкции и вычислительная механика» Пермского национального исследовательского политехнического университета; 614010, Россия, г. Пермь, ул. Куйбышева, 109;тел. +7(342) 219-83-61, e-mail:kamil_sh@bk.ru

Сарайкина Ксения Александровна, к.т.н., доцент кафедры "Строительный инжиниринг и материаловедение" декан строительного факультета Пермского национального исследовательского политехнического университета; 614010, Россия, г. Пермь, ул. Куйбышева, 109;тел. +7(342) 219-81-72, e-mail: k.a.saraykina@pstu.ru

Кашеварова Галина Геннадьевна, член-корреспондент РААСН, доктор технических наук, профессор, заведующая кафедрой «Строительные конструкции и вычислительная механика» Пермского национального исследовательского политехнического университета; 614010, Россия, г. Пермь, ул. Куйбышева, 109;тел. +7(342) 219-83-61, e-mail: ggkash@mail.ru

Санягина Яна Александровна, соискатель кафедры строительных материалов и технологий Национального исследовательского Мордовского государственного университета имени Н.П. Огарева; 430005, Республика Мордовия, г.Саранск, ул. Большевистская, д. 68; E-mail: sanyagina@mail.ru

Ерофеев Владимир Трофимович, академик РААСН, профессор, доктор технических наук, директор института архитектуры и строительства Национального исследовательского Мордовского государственного университета имени Н.П. Огарева; 430005, Республика Мордовия, г. Саранск, ул. Большевистская, д. 68; тел. +7(8342) 48-25-64; E-mail: <url> erofeevvt@bk.ru

Ватин Николай Иванович, профессор, доктор технических наук, главный научный сотрудник, Санкт-Петербургский политехнический университет имени Петра Великого; 109992, Москва, ул. Солянка, 14; E-mail: vatin_ni@spbstu.ru

International Journal for Computational Civil and Structural Engineering, 19(2) 136–149 (2023)

DOI:10.22337/2587-9618-2023-19-2-136-149

EXPERIMENTAL AND THEORETICAL STUDIES OF DYNAMIC CHARACTERISTICS OF WOODEN FRAME BUILDINGS

Tatiana L. Dmitrieva, Kristina A. Podshivalova

Federal State Budget Educational Institution of Higher Education «Irkutsk National Research Technical University», Irkutsk, RUSSIA

Abstract: The research carried out in this paper is reduced to studying the design features of wooden frame structures and analyzing the nature and degree of influence of individual structural elements on the work of the frame as a whole based on a comparison of experimental and theoretical data. The results of the studies with the evaluation of natural oscillations are the basis for the correct modeling of structural systems when performing static and dynamic calculations.

Keywords: wooden frame buildings, dynamic characteristics, natural oscillation frequencies

ЭКСПЕРИМЕНТАЛЬНО-ТЕОРЕТИЧЕСКИЕ ИССЛЕДОВАНИЯ ДИНАМИЧЕСКИХ ХАРАКТЕРИСТИК ДЕРЕВЯННЫХ КАРКАСНЫХ ЗДАНИЙ

Дмитриева Т.Л., Подшивалова К.А.

Федеральное государственное бюджетное образовательное учреждение высшего образования «Иркутский национальный исследовательский технический университет», г. Иркутск, РОССИЯ

Аннотация: Проводимые в данной работе исследования сводятся к изучению особенностей конструирования деревянных каркасных сооружений и анализу характера и степени влияния отдельных конструктивных элементов на работу каркаса в целом на основе сопоставления экспериментальных и теоретических данных. Результаты исследований с оценкой показателей собственных колебаний лежат в основе корректного моделирования конструктивных систем при выполнении статических и динамических расчетов.

Ключевые слова: деревянные каркасные здания, динамические характеристики, частоты собственных колебаний

INTRODUCTION

The construction of buildings and structures with a wooden load-bearing frame is currently being increasingly used, both in the world and in domestic practice. There is a tendency to increase the number of floors of wooden frame housing construction. A serious advantage of frame structures is the fact that, having a low weight, high spatial strength and stability, they allow you to build buildings on lightweight foundations.

The article is devoted to the study of the dynamic characteristics of wooden frame buildings. The relevance of the presented topic is due to the need to further reduce the cost of frame construction in compliance with the standards of structural reliability, safety and energy efficiency by improving the design schemes performed on the basis of an in-depth study of the nature and degree of influence of the elements of the frame and cladding on the spatial strength and rigidity of the structure. Such studies are of absolute practical importance for objects being built in seismically active zones.

The basis of the load-bearing skeleton of the buildings in question is a wooden frame formed

by racks, bindings and floor beams, which are combined into a single spatial scheme using various rigidity elements in the form of struts, sheathing, diaphragms, etc. The spatial strength and immutability of the system can be realized in different design variants: due to the joint work of the main elements of the frame with diagonal bracing elements in the plane of walls and ceilings, or due to the joint work of the frame and sheathing, in the absence of bracing connections. Combined variants are also possible, combining the joint work of all elements – braces, paneling in the form of plates or composite boards made of boards, profiled sheet, etc.

The calculation of wooden frame structures is a complex task that requires taking into account many factors. It should be noted that one of the main problems in the design of such structures is associated with their modeling in computational complexes, namely, the difficulty of analyzing and taking into account factors affecting their stress-strain state, since wood as a structural material, due to natural anisotropy, has a significantly greater spread of mechanical characteristics compared to such materials, like steel and concrete. Additional and very important parameters for modeling and calculation in software and computing complexes are the deformation characteristics of joints. Most often, nodal joints are assembled on nagel-type joints that have a certain malleability.

These problems contributed to the development of new methods and approaches to the calculation of wooden frame structures [1-17]. So, Saule Tulebekova and co-authors in their work investigated the effect of operational load on the rigidity of frame high-rise buildings made of glued beams [18]. P.V. Maksimov, A.I. Volkov in their work consider the features of numerical calculation of VAT of frame wooden structures using the finite element method and give recommendations for taking into account the complex physical and mechanical properties of wood, implementation of numerical counting in the ANSYS package [19].

In this article, the analysis of the influence of individual structural elements on the work of the frame as a whole is carried out by comparing experimental and theoretical data. For this purpose, the following tasks were set:

1. Production of an experimental fragment of a frame structure in different structural variants – a frame, a frame with plywood sheathing, a frame with diagonal braces, a frame with diagonal braces and an outer plywood sheathing.
2. Conducting experimental studies of the dynamic characteristics of fragments using the RSV-150 vibration measuring system.
3. Modeling of the computational schemes of the test fragments in the SCAD Office and Lira soft package.
4. Analysis of experimental and theoretical data to assess the comparability of the results of experimental and theoretical studies.
5. Drawing up recommendations based on the data obtained on improving the calculation methods of wooden frame structures in software and computing complexes.
6. Preparation of recommendations for the program of further studies of the dynamic characteristics of wooden frame systems, assemblies and parts.

1. EXPERIMENTAL STUDY OF NATURAL VIBRATIONS OF STRUCTURES OF WOODEN FRAME BUILDINGS

To identify the dynamic characteristics of natural vibrations of structures, the RSV-150 Polytec vibration meter was used, which is a universal device used to measure vibrations of structures located at short and long distances (from 5 to 300 m).

The sensor head contains an optical detector module with an infrared laser beam. It also contains a green “binding” laser and a video camera used to indicate the object of study. The controller includes a decoder of the speed of the measured signal, as well as electronic control

modules for the sensor head and its power supply. To perform vibration measurement, a beam of a helium-neon laser is directed at an oscillating object and reflected from it. Due to the occurrence of the Doppler effect, the speed and movement of the oscillating object form a frequency or phase modulation, which is restored in the signal processing module using appropriate demodulators (or decoders). The speed information is recovered from the frequency modulation of the Doppler signal, the displacement signal is recovered from the simultaneously available phase modulation. The values of the velocities or movements of an object are recorded at equal very small intervals (from thousandths to millionths of a second), forming discretized functions of time, and digitized on electronic media, stored in the PC memory.

Polytec Vibrometer Software (VibSoft) is used to display and analyze measurement results using a PC. Next, a high-precision spectral display of measurement results is carried out using Fourier transforms. Spectral functions are also stored in the PC memory in separate files. With the help of this device, the frequency of natural vibrations of the object in the longitudinal and transverse directions was determined.

The object under study is a fragment of a frame structure. The fragment is a rectangular structure with dimensions of 2.08x1.56 m. The height of the walls is 2.08 m. The frame is made of a grade 1 board with a cross section of 120x40mm. The cladding on the outside is made of plywood with a thickness of 9 mm.

Dynamic characteristics were tested for four different combinations of the frame in order to study the effect of each element on the spatial rigidity of the structure as a whole:

Frame 1 – Frame without braces. The frame consists of vertical racks, upper and lower strapping, horizontal jumpers.

Frame 2 is a frame with inclined braces.

Frame 3 is a frame with plywood covering on the outside of the fragment.

Frame 4 – Frame with braces and plywood sheathing (so-called full frame).



Figure 1. Frame 1



Figure 2. Frame 2



Figure 3. Frame 3



Figure 4. Frame 4

To exclude noise processes, noise vibrations were measured, followed by spectral mapping of frequency peaks characteristic of noise processes (Fig. 5).

The displacement values were measured horizontally along the transverse and longitudinal axes of the structure.

The fixation of oscillatory processes was loaded in digitized form into the memory of the PC hard disk. Further, the oscillations were subjected to spectral mapping to detect the frequency peak characteristic of the impact.

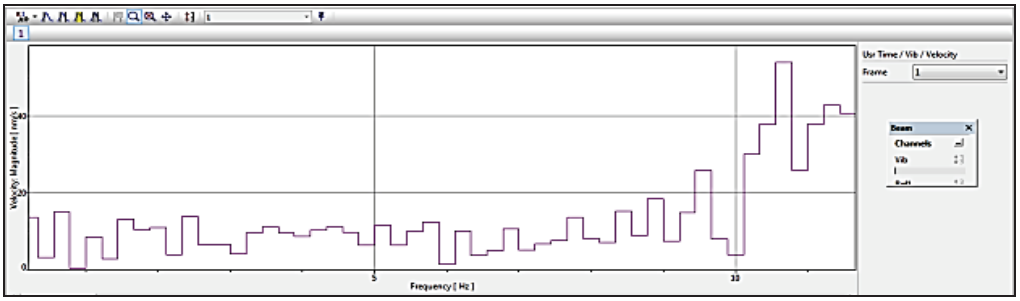


Figure 5. Spectral display of noise vibrations

The distances from the measuring equipment to the building had values from 7 to 10 m, which satisfies the conditions of effective measurements of the RSV-150 device.

The results of spectral mapping are presented in Figures 6-13.

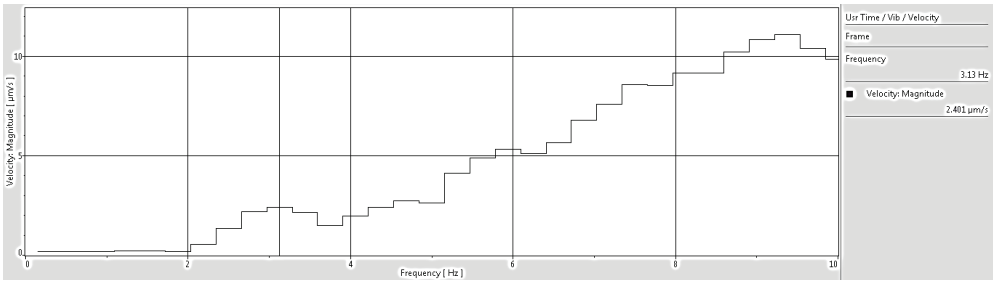


Figure 6. Frame 1. Time interval and spectral mapping of oscillatory processes in the longitudinal direction

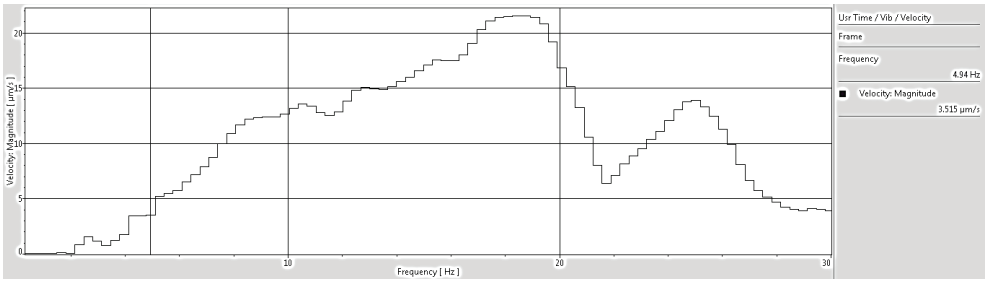


Figure 7. Frame 1. Spectral mapping of oscillatory processes in the transverse direction

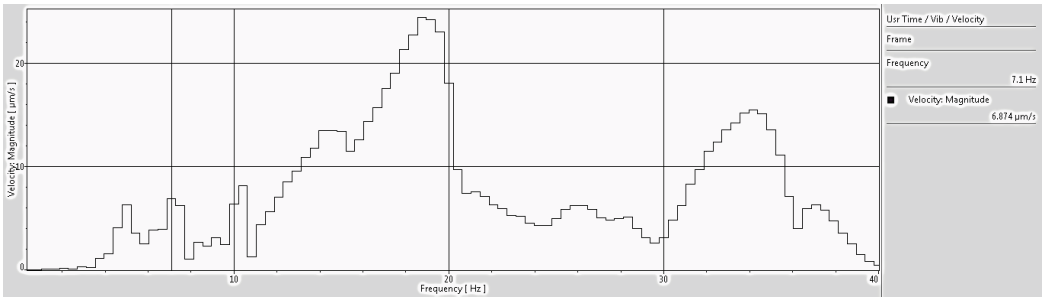


Figure 8. Frame 2. Spectral mapping of oscillatory processes in the longitudinal direction

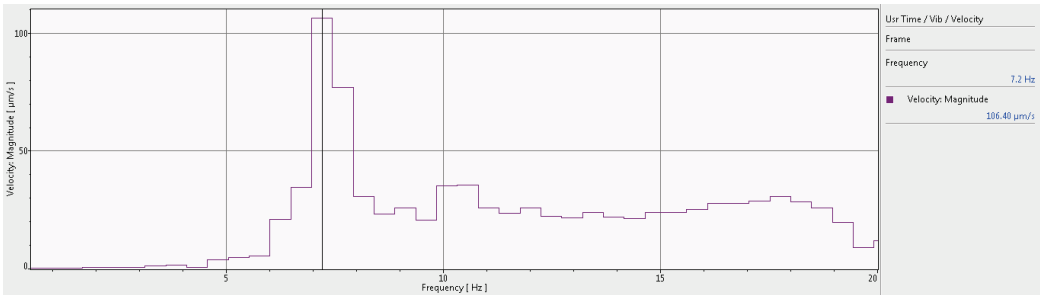


Figure 9. Frame 2. Spectral mapping of oscillatory processes in the transverse direction

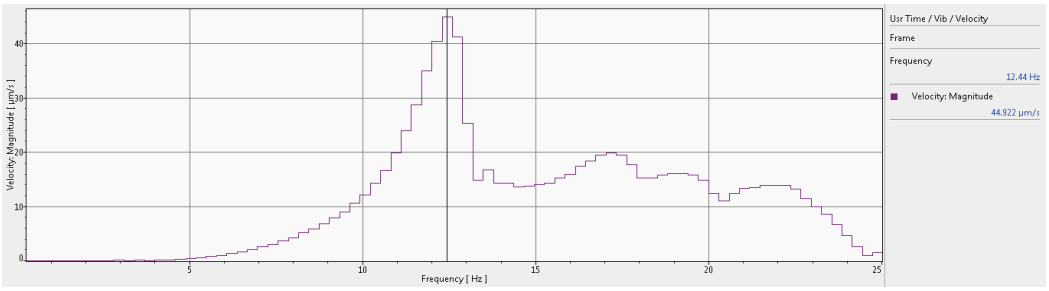


Figure 10. Frame 3. Spectral mapping of oscillatory processes in the longitudinal direction

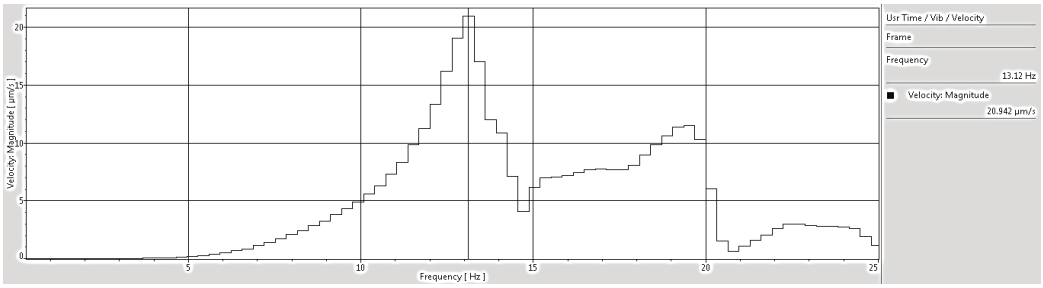


Figure 11. Frame 3. Spectral mapping of oscillatory processes in the transverse direction

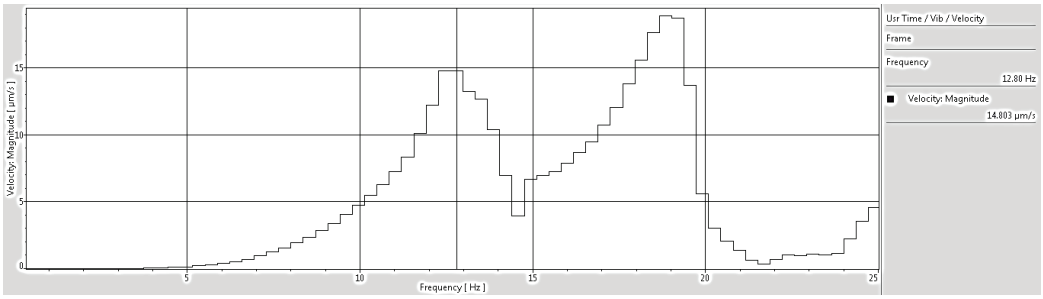


Figure 12. Frame 4. Spectral mapping of oscillatory processes in the longitudinal direction

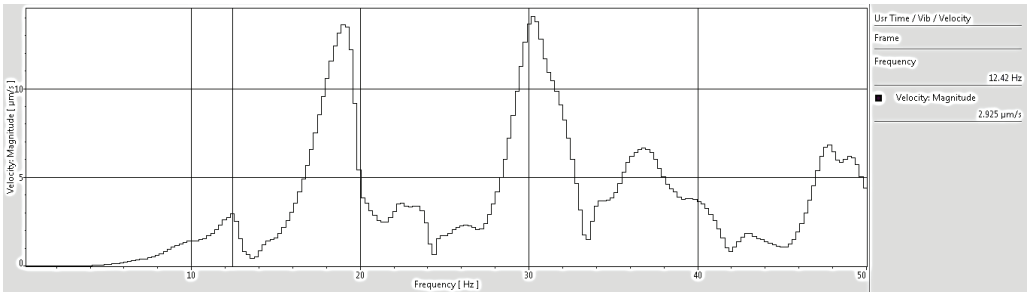


Figure 13. Frame 4. Spectral mapping of oscillatory processes in the transverse direction

2. MODELING AND CALCULATION OF THE STUDIED OBJECTS IN SCAD OFFICE AND LIRA SOFT PCS

The frame struts, lintels and lower strapping were modeled in the form of core elements. The connections of the racks with the horizontal surface of the concrete floor of the laboratory are set in the form of a hinge-fixed support, limiting movement along the X, Y, Z axes and the average Z racks for some variants of the design schemes. To obtain the dynamic characteristics of natural oscillations, a modal analysis was carried out based on the transformation of the static load of its own weight from the considered variant of the structural scheme of the fragment into masses.

To model wooden frame structures, it is necessary to take into account the nodal connections of elements: racks with strapping, braces and horizontal spacers with a frame, a frame with a skin, which in this case are attached to screws. These compounds are malleable, which causes difficulty in modeling in computational complexes.

In the SCAD Office PC, when modeling rod elements, there is no possibility of taking into account the orthotropic properties of wood and the elements are set to be isotropic. The lamellar elements of plywood sheaths are set to be otrotropic.

In the Lira Soft PC, on the contrary, when modeling rod elements, it is possible to take into account the orthotropic properties of wood, but at the same time the plate elements of plywood sheaths are set to be isotropic.

In the study of dynamic characteristics in computational complexes, many variants of computational schemes were created, and this paper presents the most successful of all with a description of the modeling tools used.

2.1 Frame 1

The frame has a hinged coupling of racks with strapping and jumpers. The corner and paired pillars of the frame fragment are connected by combining displacements, thereby modeling a malleable (conditionally hinged) joint.

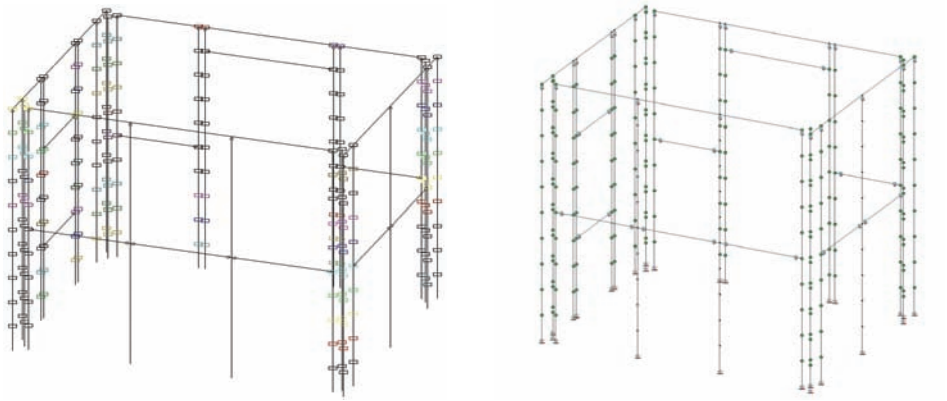


Figure 14. Frame 1. Model in PVC SCAD Office and Lira Soft

Table 1. The results of natural oscillations of the fragment of the frame 1 in SCAD Office and Lira Soft

SCAD Office	Lira Soft
X - 2,92 Гц	X - 2,7 Гц
Y - 6,03 Гц	Y - 5,54 Гц

2.2 Frame 2

Additionally, we model diagonal braces in the form of rod elements in the frame. The connection of the braces with the pillars of the main frame is made pivotally.

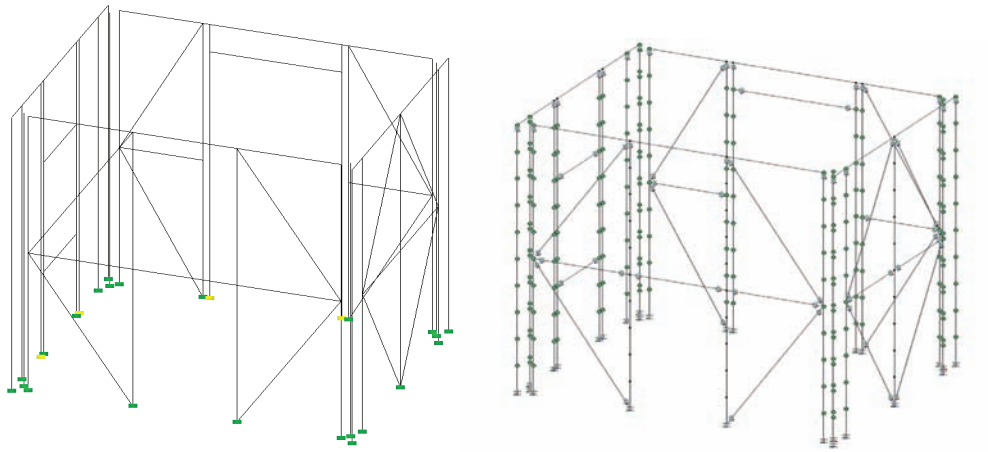


Figure 15. Frame 2. Model in PVC SCAD Office and Lira Soft

Table 2. The results of the natural oscillations of the fragment of the frame 2 in SCAD Office and Lira Soft

SCAD Office	Lira Soft
X - 6,49 Гц	X – 6,64 Гц
Y - 7,17 Гц	Y – 8,52 Гц

2.3 Frame 3

Plywood panels in the form of plate elements with a thickness of 9 mm were added to the design scheme and diagonal braces were removed. Characteristics of the cladding material: elastic modulus X = 400000 kN/m2, elastic modulus Y = 10000000 kN/m2. Poisson's ratio V_{XY} = 0.45, V_{YX}=0.02. The shear modulus G_{XY}=500000 kN/m2.

The frame with the skin is connected pivotally by introducing a connection in the form of a combination of movements.

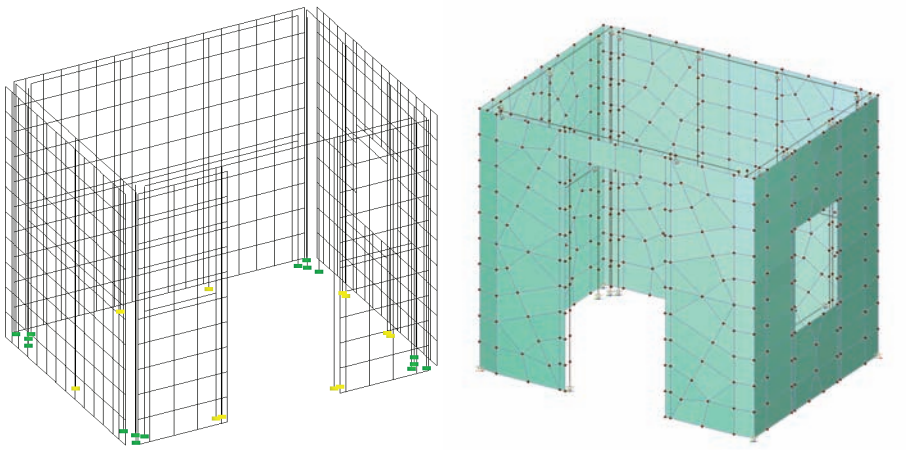


Figure 16. Frame 3. Model in PVC SCAD Office and Lira Soft

Table 3. Results of natural oscillations of a fragment of the frame 3 in SCAD Office and Lira Soft

SCAD Office	Lira Soft
X - 15,74 Гц	X - 15,88 Гц
Y - 8,80 Гц	Y - 10,20 Гц

2.4 Frame 4

Diagonal braces are reintroduced into the design scheme of the frame with plywood sheathing. The core elements are connected to each other pivotally. The plywood skin is attached with the help of the "movement unification" tool.

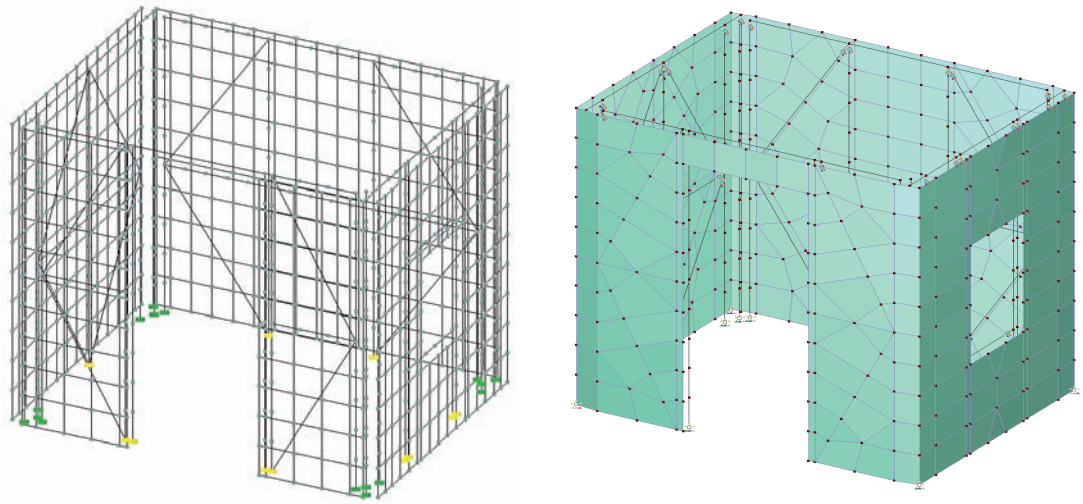


Figure 17. Frame 4. Model in PVC SCAD Office and Lira Soft

Table 4. Results of natural oscillations of a fragment of the frame 4 in SCAD Office and Lira Soft

SCAD Office	Лира Софт
X - 16,82 Гц	X - 16,26 Гц
Y - 13,43 Гц	Y - 10,87 Гц

3. COMPARATIVE ANALYSIS OF THE VALUES OF DYNAMIC CHARACTERISTICS OBTAINED BY THEORETICAL NUMERICAL CALCULATION AND EXPERIMENTAL METHODS

A comparative analysis of the values obtained by measuring the dynamic characteristics of a fragment of a wooden frame with the values obtained as a result of modeling the frame in the computing complexes SCAD Office and Lira Soft.

The purpose of the analysis was to identify errors in experimental data and theoretical numerical calculations, which are manifested due to incomplete consideration of the natural origin of wood and inaccuracy of modeling nodal joints of structural elements in calculation complexes.

Another, no less important, task is a comparative analysis of the dynamic characteristics of 4 combinations of a fragment of a wooden frame and a conclusion about the need to install diagonal braces to increase the strength of the building.

Based on the results obtained, we will form a general summary table 5.

Table 5. Summary table of natural oscillation frequency

№	Name of the measurement	Direction of measurement	Values from SCAD Office, Hz	Value from Lira Soft, Hz	Values from the VibSoft, Hz	The coefficient of reduction to the indicators of the VibSoft	
						SCAD Office	Lira Soft
1	2	3	4	5	6	7	8
1	Frame 1	Longitudinal direction	2,92	2,7	3,13	1,07	1,16
		Transverse direction	6,03	5,54	4,94	0,82	0,89
2	Frame 2	Longitudinal direction	6,49	6,64	7,1	1,09	1,07
		Transverse direction	7,17	8,52	7,2	1,00	0,85
3	Frame 3	Longitudinal direction	15,74	15,88	12,44	0,79	0,78
		Transverse direction	8,8	10,2	13,12	1,49	1,29
4	Frame 4	Longitudinal direction	16,82	16,26	12,8	0,76	0,79
		Transverse direction	13,43	10,87	12,42	0,92	1,14

The natural oscillation frequencies of the system are determined by the formula:

$$w_0 = \sqrt{\frac{EJ}{m}} \quad (1)$$

where EJ is the rigidity of the system; m is the mass of the system.

Then the rigidity of the system is determined by the formula:

$$EJ = w_0^2 m \quad (2)$$

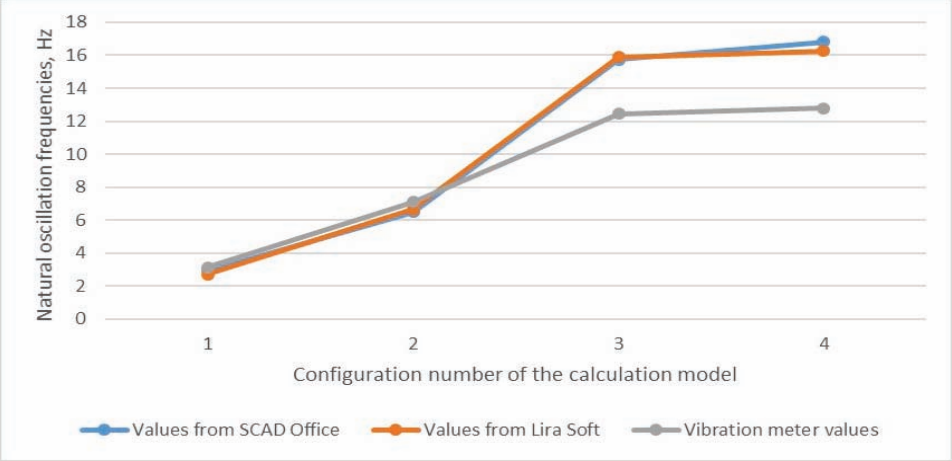


Figure 18. Indicators of natural oscillation frequencies in the longitudinal direction of the frame fragment

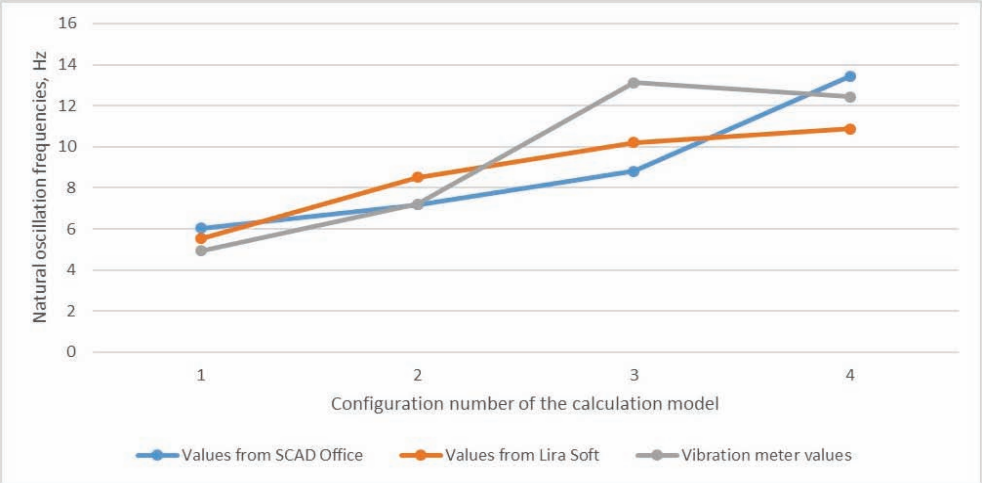


Figure 19. Indicators of natural oscillation frequencies in the transverse direction of the frame fragment

Table 6. Summary table of the rigidity of the frame system

№	Name of the measurement	Direction of measurement	System weight, kN	Rigidity of the SCAD Office system (EJ), kN m^2	Rigidity of the system (EJ) Lira Soft, kN m^2	Stiffness (EJ) of the experimental fragment, kN m^2	The coefficient of reduction to the indicators of the VibSoft	
							SCAD Office	Lira Soft
1	2	3	4	5	6	7	8	9
1	Frame 1	Longitudinal direction	2,18	18,55	15,86	21,31	1,15	1,34
		Transverse direction	2,18	79,11	66,77	53,09	0,67	0,80
2	Frame 2	Longitudinal direction	2,55	107,43	112,45	128,58	1,20	1,14
		Transverse direction	2,55	131,12	185,15	132,22	1,01	0,71
3	Frame 3	Longitudinal direction	2,83	701,67	714,21	438,29	0,62	0,61
		Transverse direction	2,83	219,33	294,66	487,52	2,22	1,65
4	Frame 4	Longitudinal direction	3,20	906,62	847,26	525,04	0,58	0,62
		Transverse direction	3,20	578,00	378,65	494,33	0,86	1,31

Comparing the data obtained as a result of theoretical numerical calculations and experimental studies given in Tables 5 and 6, it can be concluded that the greatest increase in the rigidity of the frame is achieved when using a structural variant with plywood cladding. In addition, correction coefficients were calculated that allow us to bring the characteristics of the natural oscillation frequencies (Table 5, columns 7, 8) and the rigidity of structures (Table 6, columns 8, 9) obtained in the SCAD

Office and Lira Soft software complexes to the indicators of the VibSoft.

It should also be noted that the nodes connecting the elements to each other are elastic, since they are made using nagel-type connections. Modeling of such nodes with the help of hinges or rigid fastening does not correspond to their actual work in the structure. To account for and evaluate these features, several different types of calculation schemes with different combinations of frame elements were considered and analyzed. The obvious disadvantage of the calculation systems used is the lack of the possibility of taking into account the orthotropic properties of wood when modeling elements using rod and plate elements. The results of the simulation indicate the absolute need for further improvement of the SCAD Office and Lira Soft software complexes in terms of taking into account the features of the anisotropic structure of wood and the nonlinear operation of nodes and parts in wooden frame systems.

CONCLUSION

Based on a comparative analysis of numerical calculations and experimental dynamic characteristics of fragments of wooden frame structures, the following conclusions are made:

1. It is proved that there is no need to use braces in the frames of buildings with sheathing at the standard step of the racks. The use of braces in combination with the skin does not significantly increase the performance compared to the option without braces: in the longitudinal direction by about 20% and 1.4% in the transverse direction.

2. Comparison of the results of numerical calculations and experimental data of natural vibration frequencies of wooden frame buildings revealed the need to introduce correction coefficients to the stiffness indicators or natural vibration frequencies obtained in the calculation complexes.

3. The numerical calculation revealed significant difficulties in modeling wooden frame structures. The SCAD Office and Lira Soft software systems used do not allow modeling a design scheme that would reflect the actual operation of nodes, such as the coupling of racks with cladding, diagonal braces with racks, horizontal jumpers with racks.

Further studies to assess the dynamic characteristics of wooden frame buildings should include static and dynamic tests of individual components and parts with an in-depth study of their strength and deformability indicators. Of course, it is necessary to increase the number of studied objects, which will reduce the error of the data obtained.

REFERENCES

1. **Biswajit Chand, Hemant B. Kaushik, Sandip Das,** Lateral load behavior of connections in Assam-type wooden houses in the Himalayan region of India, Construction and Building Materials, Volume 261, 2020, 119904, ISSN 0950-0618, https://doi.org/10.1016/j.conbuildmat.2020.119904.
2. **Kehinde J. Alawode, Krishna Sai Vutukuru, Amal Elawady, Arindam Gan Chowdhury,** Review of wind loading on roof to wall connections in low-rise light wood-frame residential buildings, Journal of Wind Engineering and Industrial Aerodynamics, Volume 236, 2023, 105360, ISSN 0167-6105, https://doi.org/10.1016/j.jweia.2023.105360.
3. **Pan Yu, Qingshan Yang, Siu-seong Law**, Lateral performances of traditional wooden frame with loose penetrated mortise-tenon connection and column foot models, Journal of Building Engineering, Volume 47, 2022, 103793, ISSN 2352-7102, https://doi.org/10.1016/j.jobe.2021.103793.
4. **F. Asdrubali, B. Ferracuti, L. Lombardi, C. Guattari, L. Evangelisti, G. Grazieschi**, A review of structural, thermo-physical,

acoustical, and environmental properties of wooden materials for building applications, Building and Environment, Volume 114, 2017, Pages 307-332, ISSN 0360-1323, https://doi.org/10.1016/j.buildenv.2016.12.033.

5. **Si-Qi Li, Analysis** of an empirical seismic fragility prediction model of wooden roof truss buildings, Case Studies in Construction Materials, Volume 17, 2022, e01420, ISSN 2214-5095, https://doi.org/10.1016/j.cscm.2022.e01420.
6. **Jianyang Xue, Guoqi Ren, Liangjie Qi, Xin Zhang,** Lateral behavior of glued-laminated timber frame infilled with light-wooden-frame wall hybrid system: Experimental and numerical analysis, Structures, Volume 30, 2021, Pages 352-367, ISSN 2352-0124, https://doi.org/10.1016/j.istruc.2021.01.022.
7. **Burova O.A., Labudin B.V., Melekhov V.I., Tsarev E.G.** Low-rise wooden housing construction on the way out of the crisis // Actual problems of the forest complex. 2009. №24.
8. **Smirnova N.V.** Development of construction of frame houses and recommendations for their construction // Science, technology and education. 2016. №8 (26).
9. **Alendorf E.V**. About the state of frame wooden housing construction in Russia // Actual problems of the forest complex. 2008. No.2.
10. **Shakirzyanov R.A., Shakirzyanov F.R.** Dynamics and stability of structures: A textbook. − 2nd reprint ed. − Kazan: Publishing house of Kazan State Architect.-builds. un-ta, 2015. − 120 p.
11. **T.L. Dmitrieva, K.A. Podshivalova, D.O. Molchanov, K.M. Beloborodov** – Current approaches to the modeling and calculation wood frame building, taking into account the joint work of the load-bearing elements of the frame and cladding. Baikal Forum 2020.IOP Conf. Series: Earth and Environmental.
12. **Di Wu, Yoshihiro Yamazaki, Sayoko Sawada, Hiroyasu Sakata**, Experiment-based numerical simulation of hybrid structure consisting of wooden frame and rigid core, Engineering Structures, Volume 182, 2019, Pages 473-486, ISSN 0141-0296, https://doi.org/10.1016/j.engstruct.2018.12.085.
13. **Christian Mergel, Klaus Menrad**, Thomas Decker, Wood or not? An analysis of regional differences in wooden residential building permits in Germany, Journal of Cleaner Production, Volume 376, 2022, 134328, ISSN 0959-6526, https://doi.org/10.1016/j.jclepro.2022.134328.
14. **Ting Guo, Na Yang, Haibin Zhou, Shuangyong Wang,** In-plane behavior of Chuan-Dou style wooden frames with infill under cyclic loading, Structures, Volume 41, 2022, Pages 1311-1328, ISSN 2352-0124, https://doi.org/10.1016/j.istruc.2022.05.058.
15. **Jochen Köhler, John Dalsgaard Sørensen, Michael Havbro Faber,** Probabilistic modeling of timber structures, Structural Safety, Volume 29, Issue 4, 2007, Pages 255-267, ISSN 0167-4730, https://doi.org/10.1016/j.strusafe.2006.07.007.
16. **Philipp Dietsch, Stefan Winter**, Structural failure in large-span timber structures: A comprehensive analysis of 230 cases, Structural Safety, Volume 71, 2018, Pages 41-46, ISSN 0167-4730, https://doi.org/10.1016/j.strusafe.2017.11.004.
17. **Zhan Shu, Zheng Li, Minjuan He, Xiuzhi Zheng, Tingting Wu**, Seismic design and performance evaluation of self-centering timber moment resisting frames, Soil Dynamics and Earthquake Engineering, Volume 119, 2019, Pages 346-357, ISSN 0267-7261, https://doi.org/10.1016/j.soildyn.2018.08.038.
18. **Saule Tulebekova, Kjell Arne Malo, Anders Rønnquist, Petter Nåvik** Modeling stiffness of connections and non-structural elements for dynamic response of taller glulam timber frame buildings, Engineering Structures, Volume

261,2022,114209, ISSN 0141-0296, https://doi.org/10.1016/j.engstruct.2022.114209/
19. **Maksimov P.V., Volkov A.I.** – Calculation of frame wooden structures with the use of FEM // Bulletin of PNRPU. 2012. №1.

СПИСОК ЛИТЕРАТУРЫ

1. **Biswajit Chand, Hemant B. Kaushik, Sandip Das**, Lateral load behavior of connections in Assam-type wooden houses in the Himalayan region of India, Construction and Building Materials, Volume 261, 2020, 119904, ISSN 0950-0618, https://doi.org/10.1016/j.conbuildmat.2020.119904.
2. **Kehinde J. Alawode, Krishna Sai Vutukuru, Amal Elawady, Arindam Gan Chowdhury**, Review of wind loading on roof to wall connections in low-rise light wood-frame residential buildings, Journal of Wind Engineering and Industrial Aerodynamics, Volume 236, 2023, 105360, ISSN 0167-6105, https://doi.org/10.1016/j.jweia.2023.105360
3. **Pan Yu, Qingshan Yang, Siu-seong Law**, Lateral performances of traditional wooden frame with loose penetrated mortise-tenon connection and column foot models, Journal of Building Engineering, Volume 47, 2022, 103793, ISSN 2352-7102, https://doi.org/10.1016/j.jobe.2021.103793.
4. **F. Asdrubali, B. Ferracuti, L. Lombardi, C. Guattari, L. Evangelisti, G. Grazieschi,** A review of structural, thermo-physical, acoustical, and environmental properties of wooden materials for building applications, Building and Environment, Volume 114, 2017, Pages 307-332, ISSN 0360-1323, https://doi.org/10.1016/j.buildenv.2016.12.033.
5. **Si-Qi Li,** Analysis of an empirical seismic fragility prediction model of wooden roof truss buildings, Case Studies in Construction Materials, Volume 17, 2022, e01420, ISSN 2214-5095, https://doi.org/10.1016/j.cscm.2022.e01420
6. **Jianyang Xue, Guoqi Ren, Liangjie Qi, Xin Zhang**, Lateral behavior of glued-laminated timber frame infilled with light-wooden-frame wall hybrid system: Experimental and numerical analysis, Structures, Volume 30, 2021, Pages 352-367, ISSN 2352-0124, https://doi.org/10.1016/j.istruc.2021.01.022.
7. **Бурова О.А., Лабудин Б.В., Мелехов В.И., Царев Е.Г.** Малоэтажное деревянное домостроение на пути выхода из кризиса // Актуальные проблемы лесного комплекса. 2009. №24.
8. **Смирнова Н. В.** Развитие строительства каркасных домов и рекомендации по их возведению // Наука, техника и образование. 2016. №8 (26).
9. **Алендорф Э.В.** О состоянии каркасного деревянного домостроения в России // Актуальные проблемы лесного комплекса. 2008. №2.
10. **Шакирзянов Р.А., Шакирзянов Ф.Р.** Динамика и устойчивость сооружений: Учебное пособие. − 2-е перераб. изд. − Казань: Изд-во Казанск. гос. архитект.-строит. ун-та, 2015. − 120 с.
11. **T.L. Dmitrieva, K.A. Podshivalova, D.O. Molchanov, K.M. Beloborodov** – Current approaches to the modeling and calculation wood frame building, taking into account the joint work of the load-bearing elements of the frame and cladding. Baikal Forum 2020.IOP Conf. Series: Earth and Environmental.
12. **Di Wu, Yoshihiro Yamazaki, Sayoko Sawada, Hiroyasu Sakata**, Experiment-based numerical simulation of hybrid structure consisting of wooden frame and rigid core, Engineering Structures, Volume 182, 2019, Pages 473-486, ISSN 0141-0296, https://doi.org/10.1016/j.engstruct.2018.12.085.
13. **Christian Mergel, Klaus Menrad**, Thomas Decker, Wood or not? An analysis of regional differences in wooden

residential building permits in Germany, Journal of Cleaner Production, Volume 376, 2022, 134328, ISSN 0959-6526, https://doi.org/10.1016/j.jclepro.2022.134328.
14. **Ting Guo, Na Yang, Haibin Zhou, Shuangyong Wang**, In-plane behavior of Chuan-Dou style wooden frames with infill under cyclic loading, Structures, Volume 41, 2022, Pages 1311-1328, ISSN 2352-0124, https://doi.org/10.1016/j.istruc.2022.05.058.
15. **Jochen Köhler, John Dalsgaard Sørensen, Michael Havbro Faber**, Probabilistic modeling of timber structures, Structural Safety, Volume 29, Issue 4, 2007, Pages 255-267, ISSN 0167-4730, https://doi.org/10.1016/j.strusafe.2006.07.007.
16. **Philipp Dietsch, Stefan Winter,** Structural failure in large-span timber structures: A comprehensive analysis of 230 cases, Structural Safety, Volume 71, 2018, Pages 41-46, ISSN 0167-4730, https://doi.org/10.1016/j.strusafe.2017.11.004.
17. **Zhan Shu, Zheng Li, Minjuan He, Xiuzhi Zheng, Tingting Wu,** Seismic design and performance evaluation of self-centering timber moment resisting frames, Soil Dynamics and Earthquake Engineering, Volume 119, 2019, Pages 346-357, ISSN 0267-7261, https://doi.org/10.1016/j.soildyn.2018.08.038.
18. **Saule Tulebekova, Kjell Arne Malo, Anders Rønnquist, Petter Nåvik** Modeling stiffness of connections and non-structural elements for dynamic response of taller glulam timber frame buildings, Engineering Structures, Volume 261,2022,114209, ISSN 0141-0296, https://doi.org/10.1016/j.engstruct.2022.114209
19. **Максимов П.В., Волков А.И.** – Расчет каркасных деревянных конструкций с применением МКЭ // Вестник ПНИПУ. 2012. №1.

Tatiana Lvovna Dmitrieva - Doctor of Technical Sciences, Professor of the Department of Mechanics and Resistance of Materials, Federal State Budget Educational Institution of Higher Education «Irkutsk National Research Technical University» (INRTU), 83, Lermontov str., Irkutsk, 664074, Russia, dmitrievat@list.ru , +7 (3952) 40-54-25

Podshivalova Kristina Aleksandrovna - Postgraduate student of the Center for Software Engineering, Senior Lecturer of the Department "Construction Production", Federal State Budget Educational Institution of Higher Education «Irkutsk National Research Technical University» (INRTU), 83, Lermontov str., Irkutsk, 664074, Russia, 1295536@mail.ru , +7 (3952) 40-54-25

Татьяна Львовна Дмитриева - д.т.н., профессор кафедры «Механика и сопротивление материалов», Федеральное государственное бюджетное образовательное учреждение высшего образования «Иркутский национальный исследовательский технический университет» (ФГБОУ ВО «ИРНИТУ»), 83, ул. Лермонтова, г. Иркутск, 664074, Россия, dmitrievat@list.ru , +7 (3952) 40-54-25

Подшивалова Кристина Александровна - аспирант центра программной инженерии, старший преподаватель кафедры «Строительное производство», Федеральное государственное бюджетное образовательное учреждение высшего образования «Иркутский национальный исследовательский технический университет» (ФГБОУ ВО «ИРНИТУ»), 83, ул. Лермонтова, г. Иркутск, 664074, Россия, 1295536@mail.ru , +7 (3952) 40-54-25)

DOI:10.22337/2587-9618-2023-19-2-150-160

CALCULATION MODEL OF A MULTI-STOREY REINFORCED CONCRETE FRAME WITH COMPLEXLY STRESSED BEAMS UNDER ACCIDENTAL IMPACT

Violetta S. Moskovtseva [1,2], Sergey S. Fedorov [3], Margarita A. Amelina [1]

[1] Federal State Budgetary Educational Institution of Higher Education "South-West State University", Kursk, RUSSIA
[2] Scientific Research Institute of Construction Physics of the Russian Academy of Architecture and Construction Sciences, Moscow, RUSSIA
[3] National Research Moscow State University of Civil Engineering, Moscow, RUSSIA

Annotation. A computational model is presented for determining deformations in complexly stressed beams of a structurally non-linear reinforced concrete frame in a transcendental state caused by a special emergency action in the form of a sudden removal of one of the structural elements. The determination of the stress-strain state after the formation of spatial cracks in the reinforced concrete elements of the frame was carried out using the calculated spatial section. At the same time, dynamic additional loads in the design section of the reinforced concrete frame element from a special impact are determined on an energy basis using the "bending moment-curvature" and "torque-angle of rotation" diagrams. The considered calculation algorithm includes the determination of forces in compressed concrete, longitudinal and transverse reinforcement for primary and secondary design schemes and verification of special limit state criteria. The results of a numerical analysis of the effect of cracking, the ratio of torque and bending moment on the stress state in transverse and longitudinal reinforcement and on the dissipative properties of a frame structural system are presented.

Keywords: reinforced concrete frame, cracks, dynamic additional loads, complex resistance, spatial section

РАСЧЕТНАЯ МОДЕЛЬ МНОГОЭТАЖНОЙ ЖЕЛЕЗОБЕТОННОЙ РАМЫ СО СЛОЖНОНАПРЯЖЕННЫМИ РИГЕЛЯМИ В ЗАПРЕДЕЛЬНОМ СОСТОЯНИИ

В.С. Московцева [1,2], С.С. Федоров [3], М.А. Амелина [1]

[1] Федеральное государственное бюджетное образовательное учреждение высшего образования «Юго-Западный государственный университет», г. Курск, РОССИЯ
[2] Научно-исследовательский институт строительной физики Российской академии архитектуры и строительных наук, г. Москва, РОССИЯ
[3] Национальный исследовательский Московский государственный строительный университет, г. Москва, РОССИЯ

Аннотация. Приведена расчетная модель для определения деформаций в сложнонапряженных ригелях железобетонной конструктивно нелинейной рамы в запредельном состоянии, вызванном особым аварийным воздействием в виде внезапного удаления одного из конструктивных элементов. Определение напряженно деформированного состояния после образования пространственных трещин в железобетонных элементах рамы выполнено с использованием расчетного пространственного сечения. При этом динамические догружения в расчетном сечении железобетонного элемента рамы от особого воздействия определены на энергетической основе с использованием диаграмм «изгибающий момент-кривизна» и «крутящий момент -угол поворота». Рассмотренный алгоритм расчета включает определение усилий в сжатом бетоне, продольной и поперечной арматуре для первичной и вторичной расчетных схем и проверку критериев особого предельного состояния. Приведены результаты численного анализа влияния трещинообразования, соотношения крутящего и изгибающего момента на напряженное состояние в поперечной и продольной арматуре и на диссипативные свойства рамной конструктивной системы.

Ключевые слова: железобетонная рама, трещины, динамические догружения, сложное сопротивление, пространственное сечение

INTRODUCTION

The problem of ensuring the safety of structural systems always remains the main priority of scientific, design and construction activities. In recent decades, due to the constant growth in the types and intensity of various impacts on buildings and structures, there is a constant need to improve ways to protect structural systems from such impacts, including the so-called special and emergency ones. This caused the appearance in Russia and some other countries of new regulations aimed at providing such protection, in particular, Russian State Standard GOST 27751-2014 with Amendment No. 1, SP 385.1325800.2018 with Amendments No. 1, 2, 3, SP 296.1325800.2017. These documents contain general provisions regarding the consideration of special effects, the scope of the provisions given in these standards, ways to protect different types of structural systems during their design. However, many of the provisions presented here look like criteria requirements without detailing how to ensure these requirements in the design. At the same time, as shown in [1-3], these criterion requirements remain within the framework of the traditional approach of the limit states method. At the same time, the concepts of "special impact", "special limit state" and "criteria for a special limit state" introduced in these documents for the calculated parameters do not adequately reflect the physical essence of the deformation of structural systems made of various materials under various stress states at the stages of deformation that go beyond limits of criteria for limit states established experimentally [4-14]. For example, in [1, 15] it is shown that the coefficient of dynamic additional loads and the parameter of survivability of a structural system depend on the material, the topology of the structure, the stage of deformation, and other factors. But this is not taken into account in the requirements of the norms and most studies and publications in the field under consideration. The change in the dissipative properties of the material depending on the load level at which the system is dynamically additionally loaded by a special emergency effect is also not taken into account. The article under consideration presents a computational model, algorithm and results of numerical studies of static-dynamic deformation of reinforced concrete elements of a multi-storey reinforced concrete frame with complexly stressed crossbars in a transcendental state with an analysis of its dissipative properties depending on the type and level of stress state.

METHODS

The solution of the considered problem of computational analysis of the parameters of deformation of a reinforced concrete frame in the limiting and translimiting states is carried out in relation to a fragment of a reinforced concrete frame-rod structural system of the frame of a multi-storey building with a complex stress state in the crossbars under the combined action of torsional and bending moments from the forces Pi applied to the crossbars of the first floor with eccentricity e (Fig. 1 a, b). The calculation scheme of the frame is adopted in two versions: primary - at given loads before the application of a special impact and secondary - under the action of the same loads on the frame, but with the application of a special impact in the form of a sudden removal of one of the columns of the first floor of the frame.

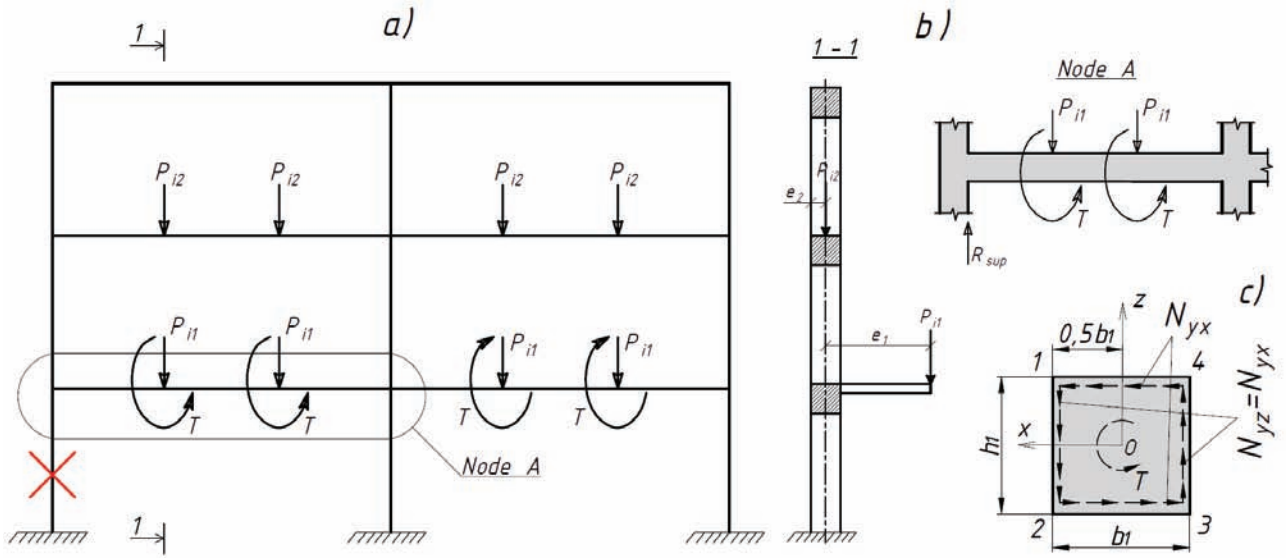


Figure 1. Scheme of application of loads (a, b) and scheme of flows of tangential forces from the action of torque along the design contour of a box section 1-2-3-4 (c)

Reinforcement of the frame structure is made as follows (Fig. 2). The crossbar is reinforced in the upper and lower zones with symmetrical longitudinal reinforcement from reinforcing bars, determined by the calculation for a given load and a special effect. The transverse reinforcement of the crossbar is adopted in the form of closed clamps designed for the combined action of the transverse force, torsional and bending moments. The step of the clamps is different in the support zone in the areas of the joint action of the torques of the bending moments and in the middle part of the span of the crossbars.

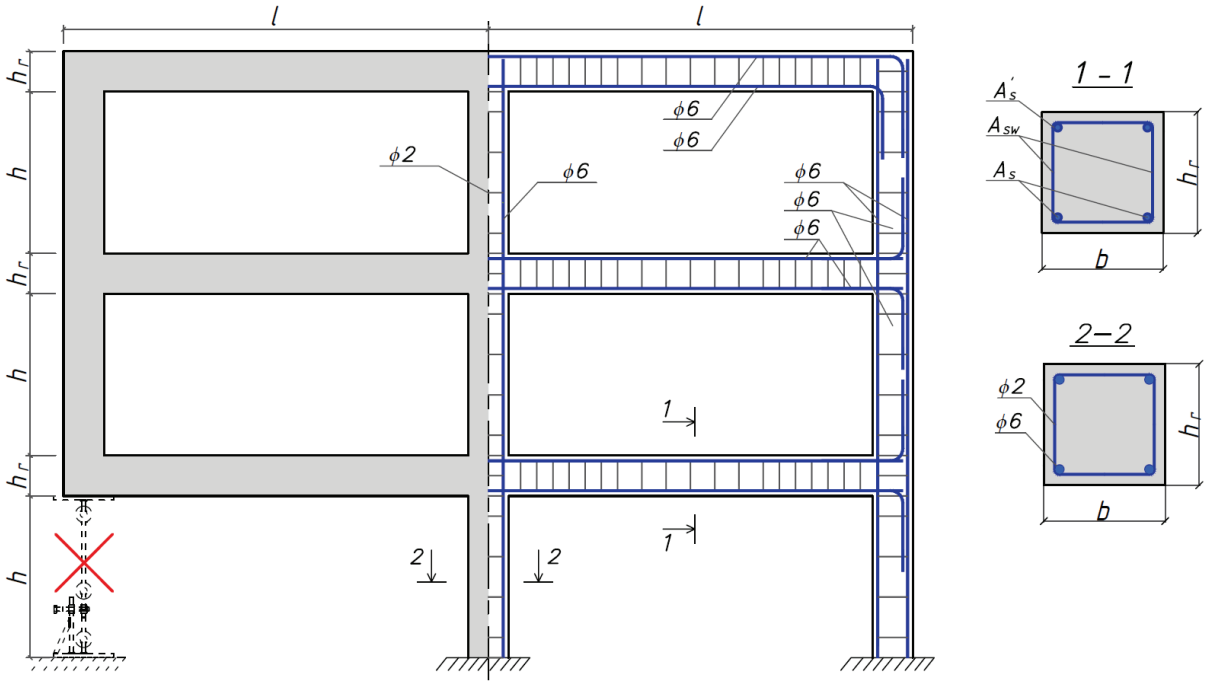


Figure 2. Scheme of formwork and reinforcement of a reinforced concrete frame

The calculation scheme for determining the stress-strain state in the section after the formation of spatial cracks in the crossbars of the frame was adopted on the basis of the hypotheses and main provisions of the deformation model proposed in [16, 17]. In the calculation, the given rectangular section of the crossbar is modeled by a box-shaped section. At the same time, an additional hypothesis is introduced that the scheme of the calculated spatial section in the limiting and transcendental states (Fig. 3) does not change after the application of a special impact. Depending on the ratio of torque and bending moment T/M and, accordingly, the nature of the stress state of the element, the angles of inclination of the spatial crack can change α.

The algorithm for calculating the frame according to the primary and secondary design schemes includes the following steps.

1. In the primary design scheme for given design loads P_i applied to the frame with eccentricity e and the initial stiffness of the sections of the frame elements B_0, the forces in the crossbars are determined and the condition for the formation of a spatial crack from these forces is checked.
2. If a spatial crack formed in the most stressed section of the crossbar, the stiffness of the crossbar section is calculated taking into account cracks B_1 [18] and the frame is recalculated under the same load.
3. One of the structural elements is removed from the primary design scheme of the frame, for example, the rack of the first floor of the frame, and the reaction in this rack, determined from the calculation according to the primary design scheme, is applied to the secondary design scheme thus obtained in the direction of the axis of the remote rack with the opposite sign.

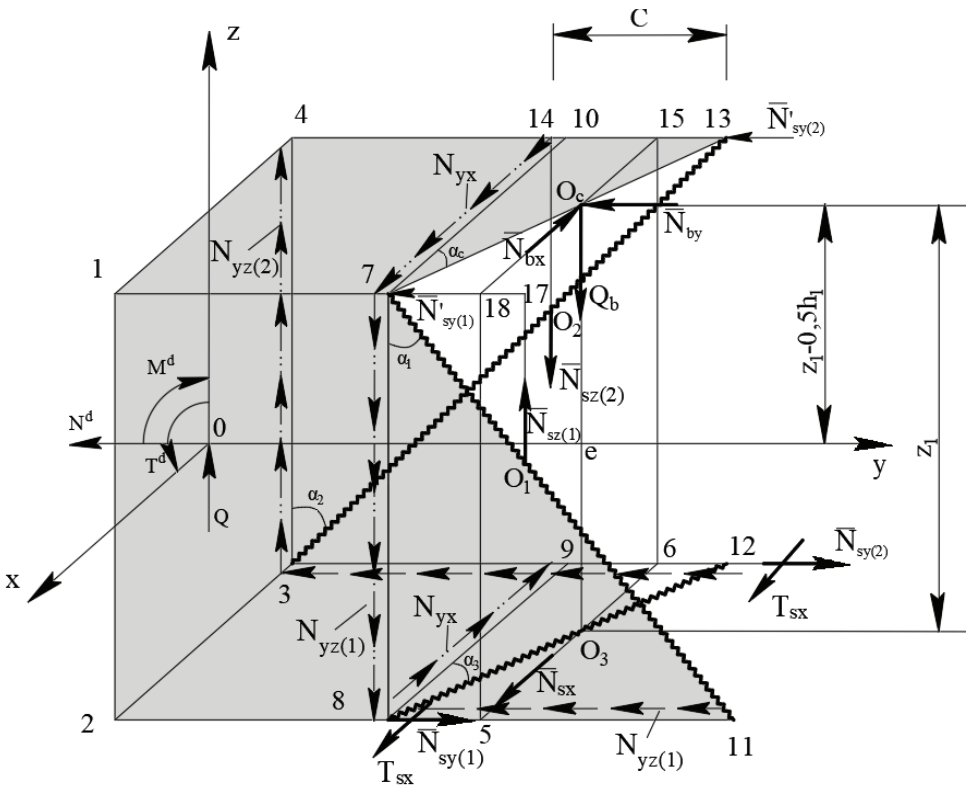


Figure 3. Calculation scheme of the crossbar section after the formation of a spatial crack with the joint application of torsional and bending moments in the limiting and transcendental states

4. Using the analytical dependence to determine the increment of dynamic forces and dynamic deformations obtained in the frame system under the considered influences [19], dynamic forces, dynamic curvatures and dynamic angles of rotation in the considered spatial section of the crossbar with a crack are calculated.
5. A diagram of the calculated spatial section is built (see Fig. 3) and for this section, the shear longitudinal $\bar{N}_{by}$ and transverse $\bar{N}_{by}$ forces in compressed concrete, the forces in the transverse reinforcement located on the left $\bar{N}_{sz(1)}$ and right $\bar{N}_{sz(2)}$ sides of the element section, the forces in the longitudinal tensile reinforcement located on the left $\bar{N}_{sx(1)}$ are calculated and on the right $\bar{N}_{sz(2)}$ at the lower edge of the crossbar section according to the formulas obtained from the conditions of statics, physical and deformation relations for the considered design section.
The value of the transverse force perceived by the concrete of the compressed zone, with some approximation, can be determined by the formula (1):

$$Q_b \approx \frac{\phi_{b2} R_{bt} b h_0^2}{C} \cdot \beta_Q \qquad (1)$$

where, φ_{b2}–is a coefficient taken equal to 1.5; R_{bt} - design resistance of concrete to axial tension; b - crossbar width; h_0 - working height of the crossbar; C - the length of the horizontal projection of the most dangerous inclined section (cut span).
The value of the longitudinal shear force in compressed concrete:

$$\bar{N}_{bx} = N_{yx} b_1 = \frac{Tb_1}{2(b_1+Z_1)}, \qquad (2)$$

where, $\bar{N}_{bx}$ - tangential force from torque T; b_1 – is the horizontal distance between the rods; Z_1 - the distance from the tensile reinforcement $2F_s$ to the center of gravity of the concrete of the compressed zone.
The value of the longitudinal force in compressed concrete:

$$\bar{N}_{by} = \frac{M}{Z_1} - \left(\frac{T}{4(b_1+Z_1)} - \frac{(Q-Q_b)}{4Z_1}\right)(Z_1 tg\alpha_1 - b_1 tg\alpha_c) - \left(\frac{T}{4(b_1+Z_1)} + \frac{(Q-Q_b)}{4Z_1}\right) * * (Z_1 tg\alpha_2 - b_1 tg\alpha_c) - \frac{Tb_1(tg\alpha_3 - tg\alpha_c)}{4(b_1+Z_1)} \qquad (3)$$

where, M – is the bending moment in the crossbar; α_c – is the slope angle of the compressed zone line; Q_b – transverse force perceived by the concrete of the compressed zone.
The total forces in the clamps are equal to:

$$\left.\begin{aligned} \bar{N}_{sz(1)} &= N_{yz(1)} Z_1 = \frac{TZ_1}{2(b_1+Z_1)} - \frac{(Q-Q_b)}{2}, \\ \bar{N}_{sz(2)} &= N_{yz(2)} Z_1 = \frac{TZ_1}{2(b_1+Z_1)} + \frac{(Q-Q_b)}{2} \end{aligned}\right\}, \qquad (4)$$

where, $N_{yz(1)}, N_{yz(2)}$ – shear forces in clamps located on the left and right sides of the cross section; Z_1 – the distance from the tension reinforcement $2F_s$ to the center of gravity of the concrete of the compressed zone of the concrete; T – torque; Q_b – transverse force perceived by the concrete of the compressed zone.

$$\begin{cases} N_{sy(1)} = 0.5N_{by} + t_{yz(1)} d_1 \cdot tg\alpha_1 + 0.5N \\ N_{sy(2)} = 0.5N_{by} + t_{yz(1)} d_1 \cdot tg\alpha_2 + 0.5N \end{cases}. \qquad (5)$$

When calculating forces in longitudinal and transverse reinforcement and compressed concrete of a three-dimensional section, the values of torque T_{n-1}^d and bending moment M_{n-1}^d obtained from the calculation according to the secondary design scheme are used, taking into account dynamic additional loads from special effects.
6. The criteria for a special limit state established by the requirements are checked (SP 385.1325800.2018 "Protection of buildings and structures against progressive collapse" with Amendments No. 1, 2, 3) for the values of curvatures and angles of rotation and limiting longitudinal and transverse deformations for compressed concrete of the section and

stretched longitudinal and transverse reinforcement.

Numerical studies and analysis of results

To evaluate the effectiveness of the proposed calculation model, a calculation of a reinforced concrete frame was carried out, the test results of which are given in publications [20, 21]. In accordance with the above algorithm, the static calculation of the frame according to the primary and secondary design schemes was performed with the following initial data: frame span l = 1050 mm, storey height h = 450 mm, crossbar section height hr =100 mm, crossbar section width b = 100 mm. Reinforcement of the crossbar and above the first floor A_s and A'_s is taken from rods with a diameter of 6 mm. The transverse reinforcement is adopted in the form of closed clamps made of wire with a strength equivalent to A240 with a diameter of 2 mm. The pitch of the transverse reinforcement on the supporting sections is 40 mm in a span of 60 mm. Frame construction concrete adopted B15.

In accordance with the algorithm, dynamic curvatures and dynamic angles of rotation were calculated using the formulas given in [19] for two variants of the stress state: option 1 - under the load Pi when there are no cracks in the frame crossbars and option 2 - under the load Pi at which inclined spatial cracks. As a result of the calculation for these options, the values of bending and torque moments were calculated in the original n-fold statically indeterminate frame, in the frame with the left post removed according to the secondary design scheme and the moments calculated according to the secondary design scheme, but taking into account the dynamic additional loading from the considered special impact (Fig. 4). The values of the coefficient of dynamic additional loading were determined as the ratio of the dynamic moment in the n-1 system to the static moments in the same system according to the formula:

$$\theta = \frac{M^d_{n-1}}{M^{st}_{n-1}}. \qquad (6)$$

According to formulas (4)-(5), the stress values in the longitudinal and transverse working reinforcement located on the left and right in the design section were calculated (see Fig. 3).

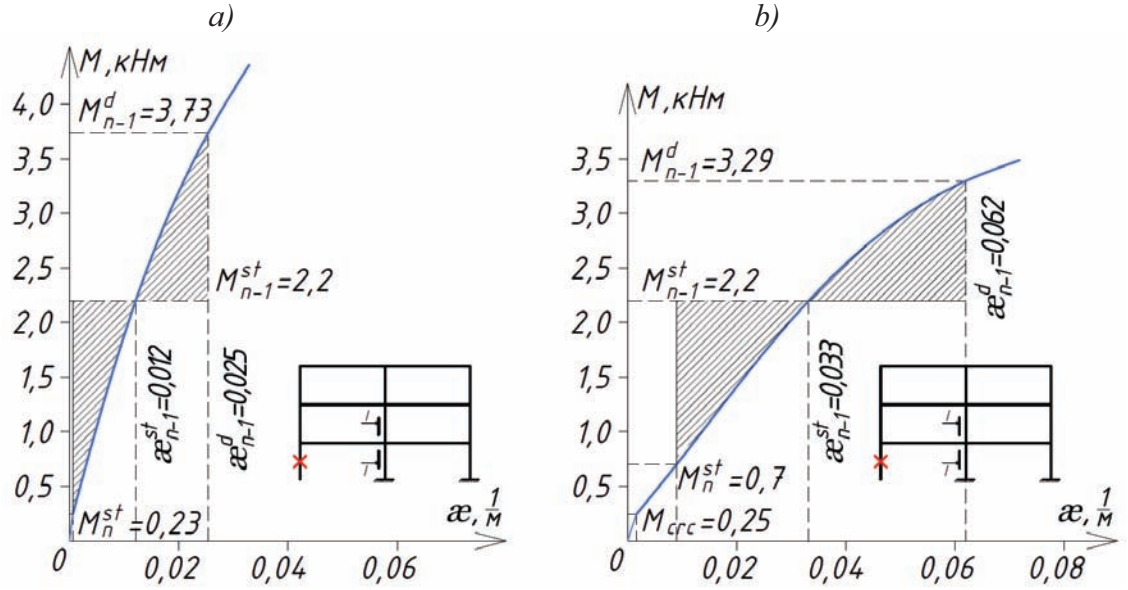


Figure 4. Diagrams of static-dynamic deformation of section 1-1 after an emergency impact when it is applied to a frame without cracks from the action of loads Pi (a) and in a frame with cracks (b)

Analyzing the results obtained (Fig. 5 a), it can be seen that with an increase in the ratio of torque to bending moment (ξ), the stress state in the clamps of the crossbar located to the left and right of the calculated section increases. The stresses in the longitudinal reinforcement located on the left and right at the lower edge of the section, on the contrary, decrease.

From a comparison of the obtained dependences for stresses in longitudinal and transverse reinforcement according to the results of calculation for the first and second options (without cracks - dependence 1 and with cracks - dependence 2 in Figure 5b in crossbars when design loads Pi are applied at the first stage of loading), it can be seen that the stress state in the transverse and longitudinal reinforcement under loading of a frame with cracks is significantly greater by a special effect than when the frame is loaded when there are no cracks in it under the design load. It follows from this that the dissipative properties of reinforced concrete frames with cracks under operational load are higher than in structures without cracks. The same applies to the stressed state: the dissipative properties of the crossbar loaded with torque and bending moment increase with increasing ratio ξ (Fig. 5b).

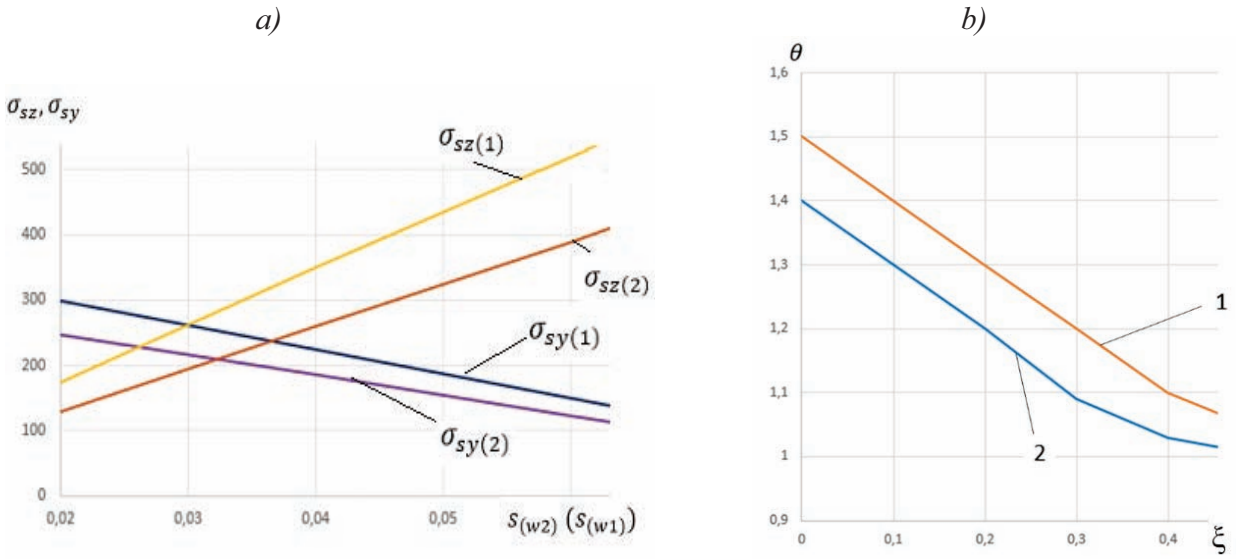


Figure 5. Dependences for stresses in the clamps «$\sigma_{sz}-s_{w2}$» and stresses in the longitudinal working reinforcement «$\sigma_{sy}-s_{w1}$» (a) and the dependence of the coefficient of dynamic additional loads θ on the ratio of torque to bending moment ξ in the design cross section of the crossbar (b): 1- when applying a special effect to the frame without cracks; 2- the same, to the frame with cracks

CONCLUSIONS

The parameters of the stress-strain state in the complexly stressed design section of the crossbar under the considered loading mode are determined based on the model of the spatial section passing through the spatial crack. The limiting state of the calculated section is determined by the deformation criteria for concrete and reinforcement.

1. A deformation model and an algorithm for calculating a multi-storey reinforced concrete frame with complexly stressed crossbars, in a transcendental state caused by a special emergency impact, are built.
2. The determination of dynamic forces in complexly stressed crossbars under the combined action of bending and torsional moments, loaded with an operational static load and dynamic additional loading in the form of a

sudden removal of one of the structures from the frame structural system, was performed on an energy basis using deformation diagrams of the design section "bending moment - curvature" and "torque - angle of rotation".

3. The parameters of the stress-strain state in the complexly stressed design section of the crossbar under the considered loading mode are determined based on the model of the spatial section passing through the spatial crack. The limiting state of the calculated section is determined by the deformation criteria for concrete and reinforcement.

4. The proposed model of static-dynamic deformation of complexly stressed reinforced concrete elements can be used in the design of protection of reinforced concrete frames of multi-storey buildings from progressive collapse.

REFERENCES

1. **Kolchunov V.I., Fedorova N.V., Savin S.Yu**. (2022) Dinamicheskie effekty v staticheski neopredelimyh fizicheski i konstruktivno nelinejnyh sistemah [Dynamic effects in statically indeterminate physically and structurally nonlinear systems]. *Industrial and civil engineering.* No. 9. pp.42-51. (in Russian)
2. **Kodysh E.N.** (2018) Proektirovanie zashchity zdanij i sooruzhenij ot progressiruyushchego obrusheniya s uchetom vozniknoveniya osobogo predel'nogo sostoyaniya [Designing the protection of buildings and structures from progressive collapse, taking into account the occurrence of a special limiting state]. *Industrial and civil engineering.* No. 10. pp. 95-101. (in Russian)
3. **Eremeev P.G.** (2022) Metody proektirovaniya na progressiruyushchee obrushenie: garmonizaciya rossijskih i mezhdunarodnyh normativnyh dokumentov [Design methods for progressive collapse: harmonization of Russian and international regulatory documents]. *Industrial and civil engineering.* No 4. pp. 23-28. (in Russian)
4. **Fedorova N.V., Ngoc V.T.** (2019) Deformation and failure of monolithic reinforced concrete frames under special actions. *Journal of Physics: Conference Series,* Vol.1425, pp.012033.
5. **Lin K., Lu X., Li Y., Guan H.** (2019) Experimental study of a novel multi-hazard resistant prefabricated concrete frame structure. *Soil Dynamics and Earthquake Engineering.* Vol.119. pp.390–407.
6. **Fedorova N.V., Kolchunov V.I., Vu N. T., Iliushchenko T.A.** (2021) Determination of stiffness parameters of reinforced concrete structures using the decomposition method for calculating their survivability. *IOP Conference Series: Materials Science and Engineering.* Vol. 1030. No. 1. pp. 012078.
7. **Geniev G.A., Kolchunov V.I., Klyueva N.V.** (2004) Prochnost' i deformativnost' zhelezobetonnyh konstrukcij pri zaproektnyh vozdejstviyah [Strength and deformability of reinforced concrete structures under design impacts]: monograph. Moscow: ASV. (in Russian)
8. **Kolchunov Vl.I., Demyanov A.I., Matveev M.I.** (2020) Osnovnye rezul'taty eksperimental'nyh issledovanij zhelezobetonnyh konstrukcij kruglogo secheniya pri kruchenii s izgibom [The main results of experimental studies of reinforced concrete structures of circular cross section in torsion with bending]. *Buildings and Reconstruction*, No. 3 (89). pp. 3-13. (in Russian)
9. **Li S., Shan S., Zhai C., Xie L**. (2016) Experimental and numerical study on progressive collapse process of RC frames with full-height infill walls. *Engineering Failure Analysis*. Vol. 59. pp. 57-68.
10. **Sheffield C., Kersul A., Hoon V., Amini A.** An instrumented full-scale building progressive collapse test. *Proc., 14th Int. Symp. on* Interaction of the Effects of Munitions with Structures, Seattle. 2011

11. **Yi W.J., He Q.F., Xiao Y., Kunnath S.K.** (2008) Experimental study on progressive collapse-resistant behavior of reinforced concrete frame structures. *ACI Structural Journal.* Vol. 105. No. 4. pp.433.
12. **Yu J., Tan K.H.** (2013) Experimental and numerical investigation on progressive collapse resistance of reinforced concrete beam column sub-assemblages. *Engineering Structures.* Vol. 55. pp. 90-106.
13. **Yu J., Tan K.H.** (2014) Special detailing techniques to improve structural resistance against progressive collapse. *Journal of Structural Engineering*. Vol. 140. No 3. pp.04013077.
14. **Fedorova N. V., Vu N. T., Iliushchenko T.A.** (2020). The effect of energy dissipation on the dynamic response of reinforced concrete structure. *IOP Conference Series: Materials Science and Engineering*. Vol. 962. No 2. pp.022063.
15. **Fedorova N.V., Khalina T.A.** (2017) Issledovanie dinamicheskih dogruzhenij v zhelezobetonnyh konstruktivnyh sistemah pri vnezapnyh strukturnyh perestrojkah [Investigation of dynamic loading in reinforced concrete structural systems during sudden structural changes]. *Industrial and civil engineering.* No. 5, pp. 32-36 (in Russian)
16. **Karpenko N.I., Kolchunov Vl.I., Kolchunov V.I., Travush V.I., Demyanov A.I**. (2021) Deformirovanie zhelezobetonnyh konstrukcij pri izgibe s krucheniem [Deformation of reinforced concrete structures during bending with torsion]. *Stroitelnye materialy*. No. 6. pp. 47-56. (in Russian)
17. **Karpenko N.I., Kolchunov Vl.I., Travush V.I.** (2021) Calculation model of a complex stress reinforced concrete element of a boxed section during torsion with bending. *Russian Journal of Building Construction and Architecture*. No. 3 (51). pp. 7-26.
18. **Golyshev A.B., Kolchunov Vl.I.** (2009) Soprotivlenie zhelezobetona [Reinforced concrete resistance]. Kyiv: Osnova (in Russian)
19. **Fedorova N.V., Moskovtseva V.S., Amelina M.A., Demyanov A.I.** (2023) Opredelenie dinamicheskih usilij v slozhnonapryazhennyh elementah zhelezobetonnyh ram pri osobom vozdejstvii [Determination of dynamic forces in complexly stressed elements of reinforced concrete frames under special impact]. *News of higher educational institutions. Construction.* No 2. (in Russian)
20. **Kolchunov V.I., Moskovtseva V.S.** (2022) ZHivuchest' zhelezobetonnyh karkasov mnogoetazhnyh zdanij so slozhnonapryazhennymi elementami [Survivability of reinforced concrete frames of multi-storey buildings with complex stress elements]. *Structural mechanics of engineering constructions and buildings.* No. 18(3). pp.195-203. (in Russian)
21. **Fedorova N.V., Moskovtseva V.S., Savin S.Yu.** (2022) Deformirovanie i razrushenie zhelezobetonnyh ram so slozhnonapryazhennymi elementami v zapredel'nyh sostoyaniyah [Deformation and destruction of reinforced concrete frames with complexly stressed elements in transcendent states]. *Collection of scientific papers of the RAASN. Russian Academy of Architecture and Building Sciences*, Vol. 2. pp. 458-468. (in Russian)

СПИСОК ЛИТЕРАТУРЫ

1. **Колчунов В.И., Федорова Н.В., Савин С.Ю.** Динамические эффекты в статически неопределимых физически и конструктивно нелинейных системах // Промышленное и гражданское строительство, 2022, № 9. С.42-51.
2. **Кодыш Э.Н.** Проектирование защиты зданий и сооружений от прогрессирующего обрушения с учетом возникновения особого предельного состояния // Промышленное и

гражданское строительство, 2018, № 10. С. 95-101.
3. **Еремеев П.Г.** Методы проектирования на прогрессирующее обрушение: гармонизация российских и международных нормативных документов // Промышленное и гражданское строительство, 2022, №4. С.23-28.
4. **Fedorova N.V., Ngoc V.T.** Deformation and failure of monolithic reinforced concrete frames under special actions // Journal of Physics: Conference Series – 2019. – Т. 1425 – С.012033.
5. **Lin K., Lu X., Li Y., Guan H.** Experimental study of a novel multi-hazard resistant prefabricated concrete frame structure // Soil Dynamics and Earthquake Engineering. 2019. Vol.119. Pp.390–407.
6. **Fedorova N.V., Kolchunov V.I., Vu N. T., Iliushchenko T.A.** Determination of stiffness parameters of reinforced concrete structures using the decomposition method for calculating their survivability // IOP Conference Series: Materials Science and Engineering. 2021 Т.1030. №.1. С.012078.
7. **Гениев Г.А., Колчунов В.И., Клюева Н.В. и др.** Прочность и деформативность железобетонных конструкций при запроектных воздействиях: монография. М.: АСВ, 2004. – 216 с.
8. **Колчунов Вл.И., Демьянов А.И., Матвеев М.И.** Основные результаты экспериментальных исследований железобетонных конструкций круглого сечения при кручении с изгибом // Строительство и реконструкция, 2020. № 3 (89). С. 3-13.
9. **Li S., Shan S., Zhai C., Xie L.** Experimental and numerical study on progressive collapse process of RC frames with full-height infill walls // Engineering Failure Analysis. 2016. Т. 59. С.57-68.
10. **Sheffield C., Kersul A., Hoon V., Amini A.** An instrumented full-scale building progressive collapse test // Proc., 14th Int. Symp. on Interaction of the Effects of Munitions with Structures, Seattle. – 2011.
11. **Yi W.J., He Q.F., Xiao Y., Kunnath S.K.** Experimental study on progressive collapse-resistant behavior of reinforced concrete frame structures // ACI Structural Journal. – 2008. Т. 105. № 4. С.433.
12. **Yu J., Tan K.H.** Experimental and numerical investigation on progressive collapse resistance of reinforced concrete beam column sub-assemblages // Engineering Structures. 2013. Т. 55. С.90-106.
13. **Yu J., Tan K.H.** Special detailing techniques to improve structural resistance against progressive collapse // Journal of Structural Engineering. – 2014. – Т. 140. – № 3. – С.04013077.
14. **Fedorova N. V., Vu N. T., Iliushchenko T.A.** The effect of energy dissipation on the dynamic response of reinforced concrete structure // IOP Conference Series: Materials Science and Engineering. 2020. Т. 962. №2. С.022063.
15. **Федорова Н.В., Халина Т.А.** Исследование динамических догружений в железобетонных конструктивных системах при внезапных структурных перестройках // Промышленное и гражданское строительство. 2017, №5, С. 32-36.
16. **Карпенко Н.И., Колчунов Вл.И., Колчунов В.И., Травуш В.И., Демьянов А.И.** Деформирование железобетонных конструкций при изгибе с кручением // Строительные материалы. 2021. № 6. С. 47-56.
17. **Karpenko N.I., Kolchunov Vl.I., Travush V.I.** Calculation model of a complex stress reinforced concrete element of a boxed section during torsion with bending // Russian Journal of Building Construction and Architecture. 2021. № 3 (51). С. 7-26.
18. **Голышев А.Б., Колчунов Вл.И.** Сопротивление железобетона. – К.: Основа, 2009. – 432 с.

19. **Федорова Н.В., Московцева В.С., Амелина М.А., Демьянов А.И.** Определение динамических усилий в сложнонапряженных элементах железобетонных рам при особом воздействии // Известия вузов. Строительство. 2023. №2.
20. **Колчунов В.И., Московцева В.С.** Живучесть железобетонных каркасов многоэтажных зданий со сложнонапряженными элементами // Строительная механика инженерных конструкций и сооружений, 2022. №18(3). С.195-203.
21. **Федорова Н.В., Московцева В.С., Савин С.Ю.** Деформирование и разрушение железобетонных рам со сложнонапряженными элементами в запредельных состояниях // Сборник научных трудов РААСН. Российская академия архитектуры и строительных наук, 2022. Том 2. С. 458-468

Moskovtseva Violetta Sergeevna, Graduate Student, Engineer of the Department of Unique Buildings and Structures, Southwest State University (SWSU), 94, 50 let Oktyabrya st, Kursk, 305040, Russia, e-mail: lyavetka1@mail.ru тел. (4712) 22-24-61

Fedorov Sergey Sergeevich, Candidate of Technical Sciences, Associate Professor, Head of the Department of Engineering Graphics and Computer Modeling, National Research Moscow State University of Civil Engineering, 26 Yaroslavskoye Shosse, Moscow, 129337, Russian Federation; fedorovss@mgsu.ru

Amelina Margarita Andreevna, Student of the Department of Unique Buildings and Structures, Southwest State University (SWSU), 94, 50 let Oktyabrya st, Kursk, 305040, Russia, e-mail: margo.dremova@mail.ru тел. (4712) 22-24-61

Московцева Виолетта Сергеевна, аспирант, инженер кафедры Уникальных зданий и сооружений, Федеральное государственное бюджетное образовательное учреждение высшего образования «Юго-Западный государственный университет» (ФГБОУ ВО «ЮЗГУ») д. 94, ул. 50 лет Октября, г. Курск, 305040, Россия, e-mail: lyavetka1@mail.ru тел. (4712) 22-24-61

Федоров Сергей Сергеевич, кандидат технических наук, доцент, заведующий кафедрой инженерной графики и компьютерного моделирования, Федеральное государственное бюджетное образовательное учреждение высшего образования «Национальный исследовательский Московский государственный строительный университет» (НИУ МГСУ), д. 26, Ярославское шоссе, г. Москва, 129337, Россия, fedorovss@mgsu.ru

Амелина Маргарита Андреевна, студент кафедры Уникальных зданий и сооружений, Федеральное государственное бюджетное образовательное учреждение высшего образования «Юго-Западный государственный университет» (ФГБОУ ВО «ЮЗГУ») д. 94, ул. 50 лет Октября, г. Курск, 305040, Россия, e-mail: margo.dremova@mail.ru тел. (4712) 22-24-61

International Journal for Computational Civil and Structural Engineering, 19(2) 161–171(2023)

DOI:10.22337/2587-9618-2023-19-2-161-171

NUMERICAL ANALYSIS OF ANTISEISMIC SLIDING BELT PERFORMANCE

Oleg V. Mkrtychev, Salima R. Mingazova

National Research Moscow State University of Civil Engineering, Moscow, RUSSIA

Abstract: One of the effective methods for ensuring seismic resistance of buildings and structures located in seismic-prone areas is the use of an active seismic protection system. The most common at present is an active seismic protection system based on seismic isolation. Seismic isolations in the form of rubber-metal (RMB) and pendulum sliding bearings (PSB) have gained great popularity in our country and abroad. Also known seismic isolation in the form of a sliding belt at the foundation level. Unlike RMB and PSB, the sliding belt is easier to manufacture, install, maintain, however, it is less studied and there are still a lack of sufficient design justifications. In this study, the effectiveness of a seismic isolating sliding belt at the foundation level with PTFE plates was investigated: a methodology for calculating a building with seismic isolating sliding belt at the foundation level using the direct dynamic method was developed; studies were conducted on the influence of the friction coefficient of the friction minimization component on the effectiveness of the anti-seismic sliding belt using the example of a 9-story monolithic reinforced concrete building under one-component seismic excitation. As a result of the calculations, graphs of relative displacements and accelerations, stress intensity, also pictures with displacement isofields, stress intensity and deformations were obtained. The analysis of the obtained results shows that the most effective component for friction minimization is the use of PTFE plates.

Keywords: active seismic protection, seismic isolation, sliding belt, PTFE, direct dynamic method

ЧИСЛЕННЫЙ АНАЛИЗ ЭФФЕКТИВНОСТИ РАБОТЫ АНТИСЕЙСМИЧЕСКОГО СКОЛЬЗЯЩЕГО ПОЯСА

О.В. Мкртычев, С.Р. Мингазова

Национальный исследовательский Московский государственный строительный университет, г. Москва, РОССИЯ

Аннотация: Одним из эффективных методов обеспечения сейсмостойкости зданий и сооружений, расположенных в сейсмоопасных районах, является использование системы активной сейсмозащиты. Наиболее распространенным в настоящее время является система активной сейсмозашиты, основанная на сейсмоизоляции. Большую популярность в нашей стране и за рубежом получили сейсмоизоляции в виде резинометаллических (РМО) и маятниковых скользящих опор (МСО). Также известна сейсмоизоляция в виде скользящего пояса в уровне фундамента. В отличие от РМО и МСО, скользящий пояс является более простым в изготовлении, в установке, в обслуживании, однако она мало изучена и для данной системы сейсмозащиты до сих пор отсутствуют в необходимом объеме расчетные обоснования. В данной работе проводилось исследование эффективности работы сейсмоизолирующего скользящего пояса в уровне фундамента с фторопластовыми пластинами: разработана методика расчета здания с сейсмоизолирующим скользящим поясом в уровне фундамента прямым динамическим методом; проведены исследования влияния коэффициента трения компонента минимизации трения на эффективность антисейсмического скользящего пояса на примере 9-тиэтажного монолитного железобетонного здания при однокомпонентном сейсмическом воздействии. В результате проведенных расчетов были получены графики относительных перемещений и ускорений, интенсивности напряжений, а также картины с изополями перемещений, интенсивности напряжений и деформаций. Анализ полученных результатов показывает, что наиболее эффективным в качестве компонента минимизации трения является применение фторопластовых пластин.

Ключевые слова: активная сейсмозащита, сейсмоизоляция, скользящий пояс, фторопласт, прямой динамический метод

INTRODUCTION

The catastrophic consequences of earthquakes are well known. Approximately 25% of the territory of the Russian Federation is located in earthquake-prone areas, where there is a probability of earthquakes with intensity up to 9 points on the MSK-64 scale. In this regard, ensuring the seismic resistance of buildings and structures erected in earthquake-prone areas is one of the urgent and practically important problems in construction.

At present, to ensure seismic resistance of buildings and structures, various systems of active seismic protection are used (with switch-off ties [1], systems of gravity type, systems with dynamic vibration dampers, with suspended supports, pendular sliding supports (PSS), rubber-metal supports (RMS) [2, 3, 4], with a sliding belt device in the foundation level). In our country and abroad, seismic protection in the form of RMS is most widely used. However, this type of active seismic protection has a number of disadvantages: high cost, complexity of installation and maintenance.

Seismic protection in the form of a seismic-isolating sliding belt at the foundation level is also known. However, this type of seismic protection is less popular, compared to RMS, since it is poorly investigated and currently it lacks the necessary calculation justifications in its entirety.

Development and research of active seismic protection were engaged by many domestic and foreign scientists. The problem of seismic resistance of buildings and constructions was addressed in the studies of Eisenberg [1, 5], Plevkov and Malganov [6], Djinchvelashvili and Mkrtichev [7], Uzdin [8], Kelly [9], Kani [10] and other researchers. The studies of Chudnetzov and Soldatov [11], Kuznetsov and Chen Xiatin [12] are dedicated to seismic protection through a seismic-isolating sliding belt. The effectiveness of this type of seismic protection has been demonstrated.

Despite the fact that seismic isolation as a sliding belt at the foundation level is quite well known and has practical applications, the issues regarding the development of adequate mathematical models and corresponding calculation methods remain unstudied so far.

The objective of the study is to assess the efficiency of application of the seismic isolating sliding belt at the foundation level with fluoroplastic plates to increase the seismic resistance of the building under the action of heavy earthquakes using the time-history dynamic method.

In order to achieve the preset objective, the following tasks were accomplished:

1. The existing mathematical models describing the actual performance of the seismic isolating sliding belt at the foundation level were analyzed;
2. The existing methods of calculation of building structures for the action of seismic loads have been analyzed;
3. The method of calculation of simple and complex systems with seismic-isolating sliding belt using time-history dynamical method has been developed;
4. Calculation scheme of the system "building-seismic isolation-foundation" describing its actual operation under seismic load is simulated;
5. The analysis of the obtained results is performed.

METHODS

To ensure the seismic resistance of buildings and structures erected in earthquake-prone areas, various methods of seismic protection are used: passive (traditional) and active. Currently, passive methods of seismic protection are the main in the construction practice. The use of the traditional approach to ensuring seismic resistance implies an increase in sections and an increase in the load-bearing elements. This leads to an increase in the mass of the structure and, as a consequence, an increase in inertial seismic forces. It is advisable in many cases to use active methods of seismic protection, e.g. seismic isolation and seismic shaking. Let's consider in more detail the principle of seismic isolation.

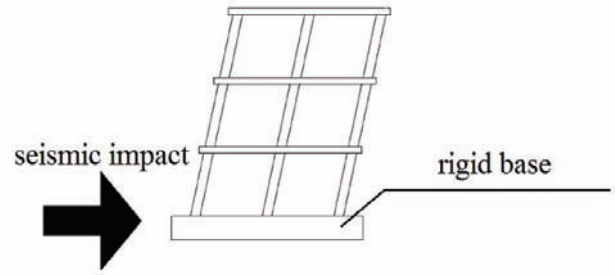


Figure 1. Deformed scheme of an uninsulated building under seismic action

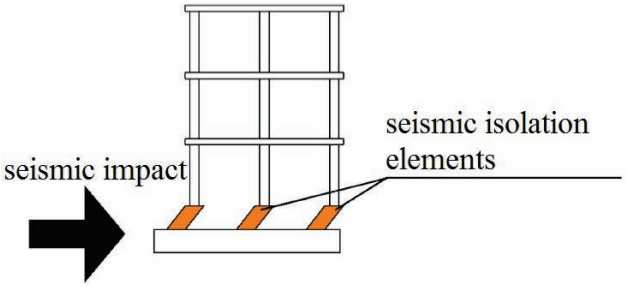


Figure 2. Deformed scheme of an isolated building under seismic action

The reduction of seismic impacts on buildings and structures is achieved through the introduction of special structural elements - seismic isolators (Fig. 1, 2), because of which the structure becomes more pliable. And this leads to increase of displacements in the upper part of the structure. Consequently, acceleration of concentrated masses, as well as seismic inertial forces are decreased [13].

Let's consider an example of seismic protection system with a sliding belt device (Fig.3).

The basis for the operation of seismic isolation in the form of a sliding belt at the foundation level is the sliding device, which includes friction minimization components and components for limiting large horizontal displacements.

There are various materials used as a friction minimization component: elastic coating graphite, stainless steel, fluoroplastic plates (PTFE), etc. When the total inertial force exceeds a certain value in the support elements of the seismic isolation device, slippage occurs. This leads to a decrease in the acceleration peaks in the system.

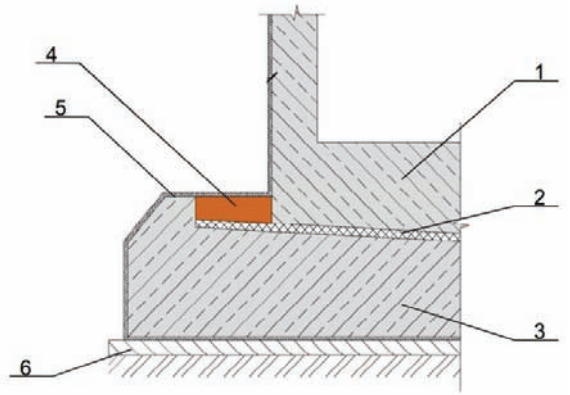


Figure 3. Scheme of seismic isolating sliding belt: 1) lower part of the building at foundation level 2) fluoroplastic plates 3) foundation 4) damper (coarse sand) 5) waterproofing 6) concrete layer

In this study, the effect of the friction coefficient on the efficiency of the antiseismic sliding belt was investigated. The following materials were considered as friction minimization component: PTFE over PTFE (PTFE+PTFE) with friction coefficient 0.052; PTFE over steel (PTFE+Steel) with friction coefficient 0.07; steel over steel (Steel+Steel) with friction coefficient 0.15.

Differential equations of motion of the system with a finite number of degrees of freedom in matrix form [14]:

$$M\ddot{u} + C\dot{u} + Ku = f^a \qquad (1)$$

where $\mathbf{u}$ is the unknown vector of nodal displacements;

$\dot{\mathbf{u}} = \mathbf{v}$ is the nodal velocity vector;

$\ddot{\mathbf{u}} = \mathbf{a}$ is the nodal acceleration vector;

$\mathbf{M}$ is the mass matrix;

$\mathbf{C}$ is the damping matrix;

$\mathbf{K}$ is the stiffness matrix;

$\mathbf{f}^a$ is the vector of applied loads.

Solution of system (1) can be obtained by using explicit and implicit schemes of direct integration of motion equations. If methods implementing implicit scheme of integration are used, expression (1) at a moment of time t_{n+1} can be represented in the form:

$$\mathbf{M}\ddot{\mathbf{u}}_{t+\Delta t} + \mathbf{C}\dot{\mathbf{u}}_{t+\Delta t} + \mathbf{K}\mathbf{u}_{t+\Delta t} = \mathbf{f}^a_{t+\Delta t} \qquad (2)$$

The difference approximation of the nodal accelerations $\ddot{\mathbf{u}}$, velocities $\dot{\mathbf{u}}$ and displacements $\mathbf{u}$ has the form:

$$\ddot{\mathbf{u}}_{t+\Delta t} = \frac{1}{\alpha \Delta t^2}\left(\mathbf{u}_{t+\Delta t} - \mathbf{u}_t\right) - \frac{1}{\alpha \Delta t}\dot{\mathbf{u}}_t - \left(\frac{1}{2\alpha} - 1\right)\ddot{\mathbf{u}}_t \quad (3)$$

$$\dot{\mathbf{u}}_{t+\Delta t} = \mathbf{u}_t - \Delta t\left(1-\delta\right)\ddot{\mathbf{u}}_t + \delta \Delta t \ddot{\mathbf{u}}_{t+\Delta t} \quad (4)$$

$$\mathbf{u}_{t+\Delta t} = \mathbf{u}_t + \mathbf{u}_t \Delta t + \left[\left(\frac{1}{2} - \alpha\right)\ddot{\mathbf{u}}_t + \alpha \ddot{\mathbf{u}}_{t+\Delta t}\right]\Delta t^2 \quad (5)$$

where α and δ are the integration parameters.

Using the explicit scheme of integration of the equation of motion of the system, obtain:

$$\mathbf{M}\ddot{\mathbf{u}}_t + \mathbf{C}\dot{\mathbf{u}}_t + \mathbf{K}\mathbf{u}_t = \mathbf{f}_t^{\,a} \quad (6)$$

Acceleration vector:

$$\mathbf{a}_t = \mathbf{M}^{-1}\left(\mathbf{f}_t^{ext} - \mathbf{f}_t^{\text{int}}\right) \quad (7)$$

where $\mathbf{f}_t^{ext}$ is the external force vector; $\mathbf{f}_t^{\text{int}}$ is the internal force vector.

Velocity and displacement vectors at the corresponding step:

$$\mathbf{v}_{t+\Delta t/2} = \mathbf{v}_{t-\Delta t/2} + \mathbf{a}_t \Delta t \quad (8)$$

$$\mathbf{u}_{t+\Delta t} = \mathbf{u}_t + \mathbf{v}_{t+\Delta t/2}\frac{\Delta t_t + \Delta t_{t+\Delta t}}{2} \quad (9)$$

The calculation was performed using an explicit integration scheme.

The calculation model of a 9-story monolithic reinforced concrete building (Figures 4, 5) with seismic insulation on a rigid soil base was adopted as the object of study.

The structural scheme of the building is cross-wall. The spatial stiffness of the structure is ensured due to the combined work of the walls and stiffening cores with the discs of the monolithic slabs. Bearing elements of the structure are made of concrete of B25 class, and steel reinforcement of A500 class. The height of the typical floor of 3.0 m. The length of the building - 24.7 m, width - 19.8 m, height - 30.9 m. The thickness of the walls and cores is 0.2m and 0.25m; floor slabs is 0.22m. Beams of rectangular cross-section are 0.4x0.56m.

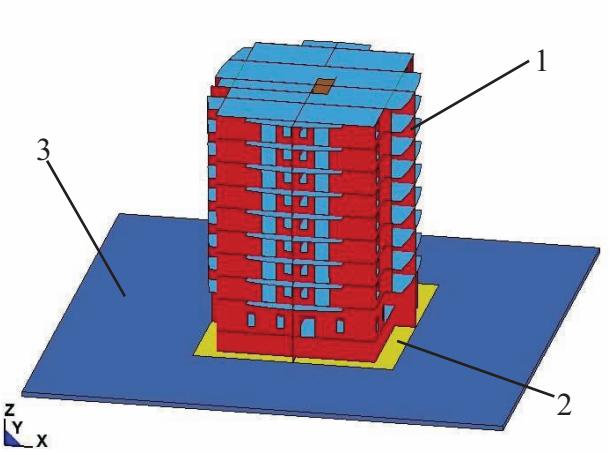


Figure 4. Finite-element model of a building with seismic isolation: 1-Building; 2 -contact surface (PTFE+PTFE/ PTFE+Steel/ Steel+Steel); 3- rigid soil base

The calculation was performed using time-history nonlinear dynamic method in a multi-purpose finite-element software package LS-DYNA. In the computational scheme, bar and spatial finite-element shells were used.

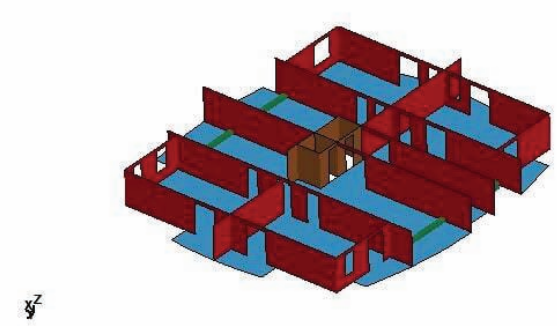


Figure 5. Finite element model of the typical floor of the building

The intensity of the earthquake is 9 on the MSK-34 scale. Figure 6 shows a one-component accelerogram of the external seismic effect.

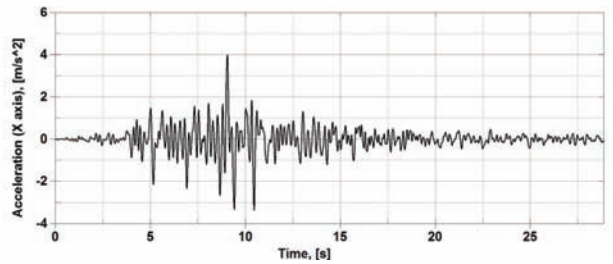


Figure 6. Accelerogram (component X)

The main results of the study are presented below (Fig.7-13, Table 1). Based on the calculation results obtained, the analysis of building operation under seismic impact with seismic-isolating sliding belt was performed using different types of friction minimization components (fluoroplastic on fluoroplastic; fluoroplastic on steel; steel on steel).

RESULTS

The graphs of relative displacements (Fig.7, 9), stress intensity (Fig.8), as well as pictures with displacement iso-fields (Fig.10), stress intensity (Fig.11, 13) and strain intensity (Fig.12) are presented below.

The main results of the study are given in Table 1. Analysis of the results shows that using PTFE+PTFE as a friction minimization component leads to 2 times lower relative movements of the whole building and 1.6 times lower relative accelerations, and to a considerable stress reduction in a certain wall element of the most loaded layer of the building.

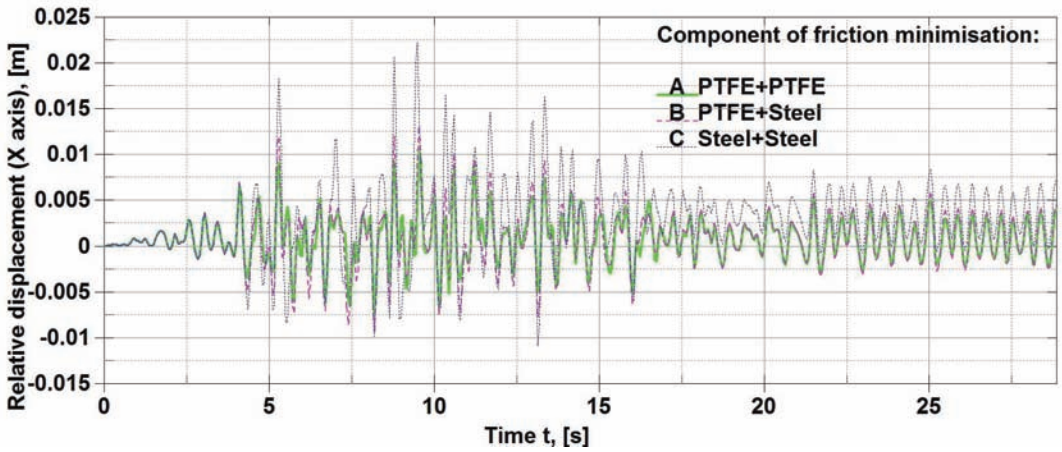


Figure 7. Displacement of the upper point of the building with respect to the soil base along the X-axis, [m]

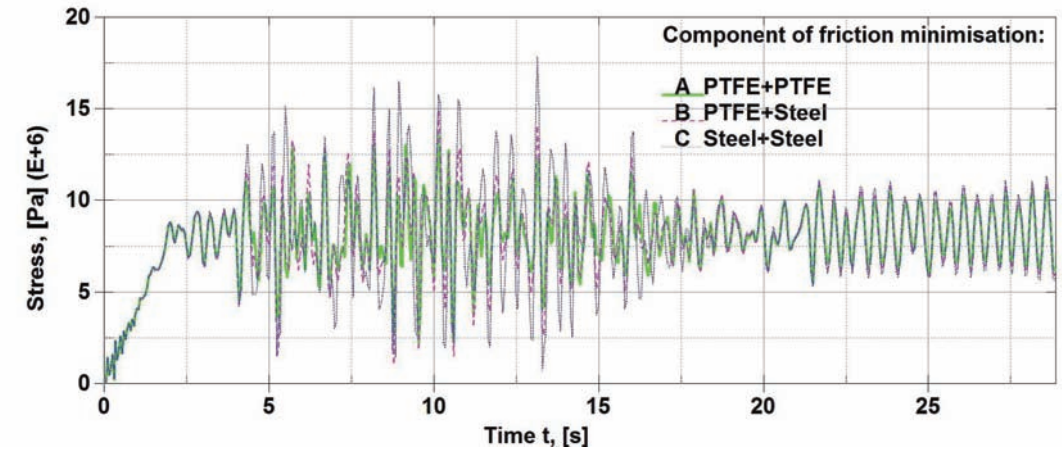


Figure 8. Stress intensity in the wall element (#160) of the 1st tier of the building, [Pa]

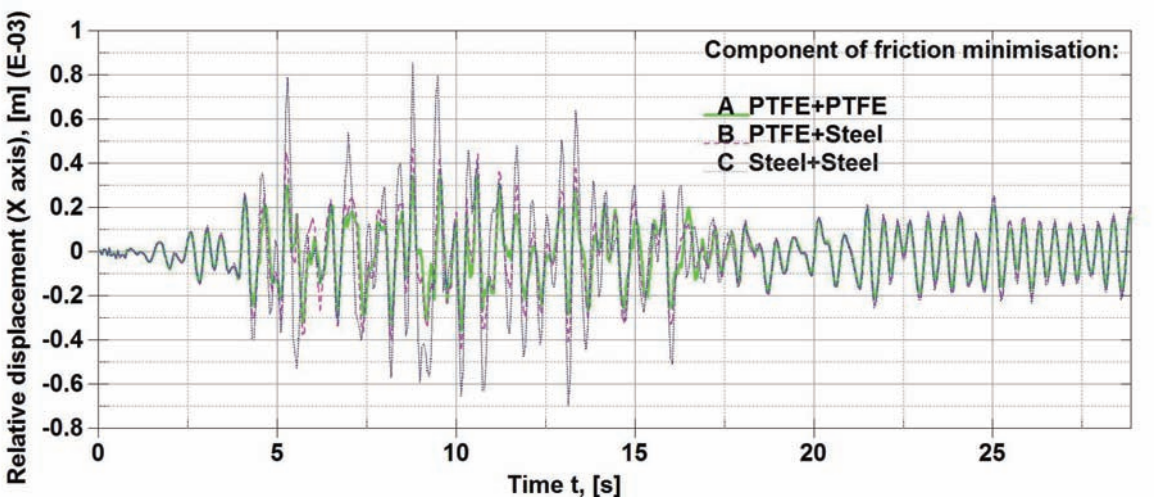
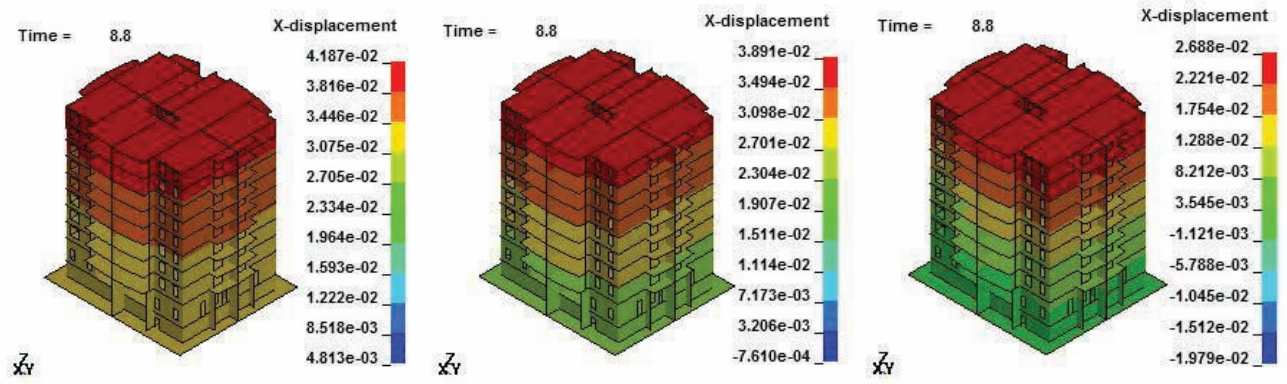
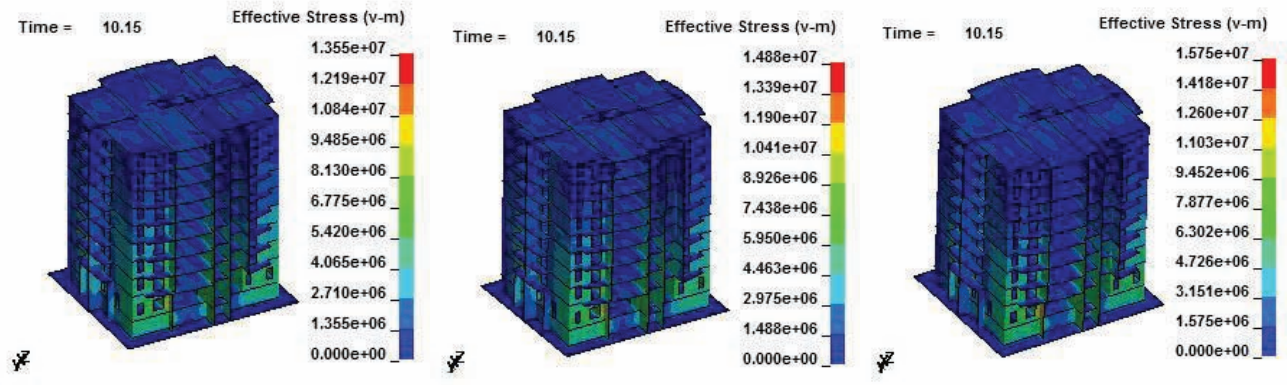


Figure 9. Displacement of the upper point of the 1st floor of the building with respect to the bottom of the building along the X axis, [m]



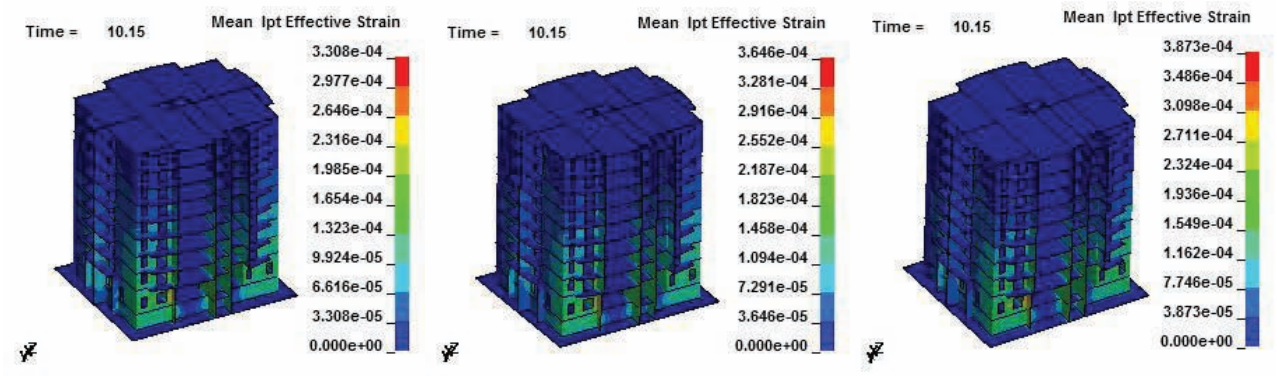
a) *b)* *c)*

Figure 10. Isopoles of displacements along the X-axis at the time t =8.8s: a) PTFE+PTFE; b) PTFE+Steel; c) Steel+Steel, [m]



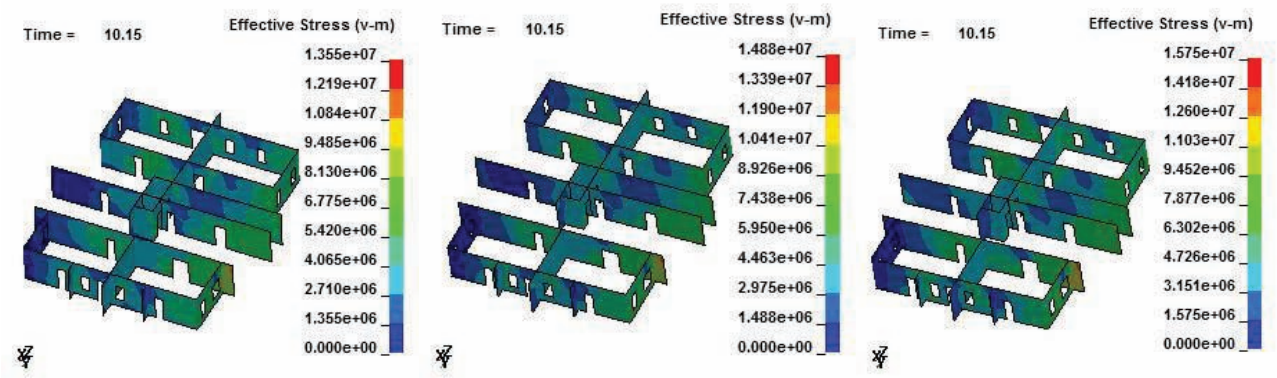
a) *b)* *c)*

Figure 11. Isopoles of stress intensity at time t =10.15s: a) PTFE+PTFE; b) PTFE+Steel; c) Steel+Steel, [Pa]



а) *б)* *в)*

Figure 12. Isopoles of strain intensity at time t =10.15s:
a) PTFE+PTFE; b) PTFE+Steel; c) Steel+Steel



а) *б)* *в)*

Figure 13. Isopoles of the stress intensity at time t = 10.15s
1st tier of the building: a) PTFE+PTFE; b) PTFE+Steel; c) Steel+Steel, [Pa]

Table 1. Main results of the study

	PTFE+PTFE	PTFE+Steel	Steel+ Steel
Relative displacement of the top of the building $\Delta u_{x.max}$, mm	10.30	13.00	22.20
Relative acceleration of the top of the building $a_{x.max}$, m/s^2	1.99	2.36	3.20
Stress in the wall element of the 1st floor of the building σ_{max}, (N/m^2)·10^7	1.35	1.49	1.78

CONCLUSIONS

The study provides evidence that the most effective component of friction minimization in a 9-story reinforced concrete monolithic building with seismic-insulating sliding belt at foundation level under earthquake conditions is PTFE+PTFE. Using PTFE+PTFE as the friction minimization component leads to the highest displacement (sliding) of the building (Fig.10), which in turn is accompanied by the lowest relative displacements. According to relative displacements diagram for the whole building (Fig.7) and the most loaded floor of the building

(Fig.9) it is evident that relative displacements under using PTFE+PTFE as friction minimization component are twice less than displacements under using Steel+Steel friction minimization component. The stress intensity diagram for the most loaded floor (Fig.8) and the isopoles of stress and strain intensity for the whole building and the most loaded floor (Figs.11-13) show that the least stresses and strains appear when sliding belt with PTFE plates is applied.

Fluoroplastic has a number of advantages. Its performance can withstand temperatures from -269 to +260°C. It does not absorb water, is chemically resistant to acids, alkalis and organic solvents, does not combust, is resistant to fungi and bacteria, does not age. The service life of the material exceeds 20 years, and is listed in the Guinness Book of Records as the most slippery material.

Research results show high efficiency of seismic protection in the form of a sliding belt at the foundation level with fluoroplastic plates when providing seismic resistance of buildings and structures. This type of seismic isolation allows to reduce considerably seismic loads on the above-ground part of the building structures, to increase the reliability of their operation during earthquakes and to reduce the material capacity and construction cost estimates. Unlike the popular RMS, seismic protection in the form of a sliding belt at the foundation level does not require factory production and can be made directly at the construction site. The simplicity of installation and maintenance of this seismic protection system also belongs to the number of advantages. The proposed approach of ensuring the seismic resistance of buildings and structures is practically acceptable and does not require substantial expenditures for anti-seismic measures.

REFERENCE

1. **Eisenberg J.M.** Sooruzheniya s vyklyuchayushchimisya svyazyami dlya sejsmicheskih rajonov [Structures with switchable joints for seismic areas]. Moscow. Stroizdat, 1976, 232 c.
2. **Mkrtychev O.V., Dzhinchvelashvili G.A, Bunov A.A.** Study of lead rubber bearings operation with varying height buildings at earthquake. Procedia Engineering, 2014, Vol.91, pp. 48-53.
3. **Mkrtychev O.V., Bunov A.A.** Nadezhnost' zhelezobetonnyh zdanij s sistemoj sejsmoizolyacii v vide rezinometallicheskih opor pri zemletryasenii [Reliability of reinforced concrete buildings with seismic isolation system in the form of rubber-metal supports during earthquake]. AKB Publishing House, Moscow, 2016, 121 c.
4. **Mkrtychev O.V., Bunov A.A.** A research on performance efficiency of rubber metal support structures // IOP Conf. Series: Materials Science and Engineering 269, 2017, 012067, doi:10.1088/1757-899X/269/1/012067.
5. **Eisenberg Y.M., Akbiev R.T, Granovsky A.V., Smirnov V.I, Chigrin S.I.** Sejsmicheskaya bezopasnost': issledovaniya, normy, proektirovanie [Seismic safety: research, standards, design] // Industrial and Civil Engineering, 2007, №3, P. 22-25.
6. **Plevkov V.S., Malganov A.I.** Zhelezobetonnye i kamennye konstrukcii sejsmostojkih zdanij i sooruzhenij [Reinforced concrete and stone structures of sarthquake-resistant buildings and structures] // Association of Construction Universities Publishing House, 2010, 290 p.
7. **Mkrtichev O.V.** Bezopasnost' zdanij i sooruzhenij pri sejsmicheskih i avarijnyh vozdejstviyah [Safety of buildings and structures under seismic and emergency impacts] // Monograph. Moscow, 2010, 152c.
8. **Uzdin A.M., Sandovich T.A., Samih Amin Al-Nasser-Mohomad**. Osnovy teorii sejsmostojkogo stroitel'stva zdanij i sooruzhenij [Fundamentals of theory of earthquake engineering of buildings and struc-

tures]. St. Petersburg: VNIIH Publishing House. B.E. Vedenev, 1993, 176 c.
9. **Kelly J.M.** Base isolation in Japan, 1988 // Report to the National Science Foundation. Report No. UCB/EERC-88/20. University of California, Berkeley, 1991, 90 p.
10. **Kani N.** Current state of seismicisolation design // The 14th World Conference on Earthquake Engineering. Beijing, 2008, pp.110-120.
11. **Chudnetsov V.P., Soldatova L.L.** Zdaniya s sejsmoizolyacionnym skol'zyashchim poyasom i uprugimi ogranichitelyami peremeshchenij [Buildings with seismic insulating sliding belt and elastic limiters of displacement] // Earthquake Engineering: Ref. 14, 1979, No.5, pp. 1-3.
12. **Kuznetsova V.D., Chen Xiatin.** Skol'zyashchij poyas s ftoroplastom sejsmostojkogo zdaniya [Sliding belt with fluoroplastic seismic-resistant building] // Engineering and Construction Journal, No.3, 2011.
13. **Polyakov V.S., Kilimnik L.Sh, Cherkashin A.V.** Sovremennye metody sejsmozashchity zdanij [Modern methods of seismic protection of buildings] // Moscow: Stroyizdat, 1989, 320 p.
14. **Clough R., Penzien J.** Dinamika sooruzhenij [Dynamics of structures]. Moscow. Stroyizdat, 1979, 316 c.
15. **Kuznetsov V.D., Lyadsky V.A.** Sejsmoizolyaciya obshchestvennyh zdanij na osnove ftoroplasta [Seismic insulation of public buildings based on fluoroplastic]. Engineering and Construction Journal, №3, 2010, Saint-Petersburg, c. 61-64.
16. **Abakarova A.D., Zainulabidova H.R**. Ocenka oblastej racional'nogo primeneniya sistemy sejsmoizolyacii zdanij so skol'zyashchim fundamentnym poyasom [Assessment of areas of rational application of seismic isolation system of buildings with a sliding foundation belt] // Bulletin of Daghestan State Technical University. Technical Sciences, №1(40), 2016, p.77-85.
17. **Zainulabidova H.R.** Ocenka vliyaniya etazhnosti zdanij na effektivnost' ispol'zovaniya sistem sejsmoizolyacii so skol'zyashchim poyasom [Assessing the impact of building storeys on the efficiency of seismic isolation systems with a sliding belt]. Science Week 2015. Collection of theses of reports XXXVI final scientific and technical conference of teachers, employees, postgraduates and students of Federal State Budgetary Educational Institution of Higher Professional Education Dagestan State Technical University. 2015. C.138-140.
18. **Davydova G.V., Ermoshin A.A., Uzdin A.M., Rumyantsev A.Y.** Ocenka peremeshcheniya zdanij s sejsmoizolirovannym skol'zyashchim poyasom [Assessment of building displacement with seismic insulated sliding belt]. Earthquake Resistant Construction. Safety of Structures, No.3, 2007, c. 34-37.
19. **Apsemetov M.C., Andashev A.J., Shamshiev N.U., Apsemetov A.M.** Kolebaniya modeli maloetazhnyh zdanij s sejsmoizoliruyushchim poyasom pri sejsmicheskih vozdejstviyah [Vibrations of model of low-rise buildings with seismic insulating belt under seismic impacts]. Vestnik of International Institute of Management. Arkhangelsk, №1, 2018, c.68-73.
20. **Gian Michele Calvi, Paolo M. Calvi, Matteo Moratti.** Seismic isolation of buildings using devices based on sliding between surfaces with variable friction coefficient // DOI 10.1007/s41062-017-0081-8. Innov. Infrastruct. Solut, 2017.

СПИСОК ЛИТЕРАТУРЫ

1. **Айзенберг Я.М.** Сооружения с выключающимися связями для сейсмических районов. Москва. Строиздат, 1976, 232 с.
2. **Mkrtychev O.V., Dzhinchvelashvili G.A, Bunov A.A.** Study of lead rubber bearings operation with varying height buildings at

earthquake. Procedia Engineering, 2014, Vol.91, pp. 48-53.
3. **Мкртычев О.В., Бунов А.А.** Надежность железобетонных зданий с системой сейсмоизоляции в виде резинометаллических опор при землетрясении. Издательство АСВ. Москва, 2016, 121 с.
4. **Mkrtychev O.V., Bunov A.A.** A research on performance efficiency of rubber metal support structures // IOP Conf. Series: Materials Science and Engineering 269, 2017, 012067, doi:10.1088/1757-899X/269/1/012067.
5. **Айзенберг Я.М., Акбиев Р.Т., Грановский А.В., Смирнов В.И., Чигрин С.И.** Сейсмическая безопасность: исследования, нормы, проектирование // Промышленное и гражданское строительство, 2007, №3, с. 22-25.
6. **Плевков В.С., Мальганов А.И.** Железобетонные и каменные конструкции сейсмостойких зданий и сооружений // Издательство Ассоциации строительных вузов, 2010, 290 с.
7. **Мкртычев О.В.** Безопасность зданий и сооружений при сейсмических и аварийных воздействиях // монография. Москва, 2010, 152с.
8. **Уздин А.М., Сандович Т.А., Самих Амин Аль-Насер-Мохомад.** Основы теории сейсмостойкого строительства зданий и сооружений. Санкт-Петербург: Издательство ВНИИГ им. Б.Е. Веденеева, 1993, 176 с.
9. **Kelly J.M.** Base isolation in Japan, 1988 // Report to the National Science Foundation. Report No. UCB/EERC-88/20. University of California, Berkeley, 1991, 90 p.
10. **Kani N.** Current state of seismicisolation design // The 14th World Conference on Earthquake Engineering. Beijing, 2008, pp.110-120.
11. **Чуднецов В.П., Солдатова Л.Л.** Здания с сейсмоизоляционным скользящим поясом и упругими ограничителями перемещений // Сейсмостойкое строительство: Реф. сб./ЦИНИС, Сер. 14, 1979, Вып.5, с.1-3.
12. **Кузнецова В.Д., Чэнь Сятин.** Скользящий пояс с фторопластом сейсмостойкого здания // Инженерно-строительный журнал, №3, 2011.
13. **Поляков В.С., Килимник Л.Ш., Черкашин А.В.** Современные методы сейсмозащиты зданий // Москва: Стройиздат, 1989, 320 с.
14. **Р.Клаф, Дж.Пензиен.** Динамика сооружений. Москва. Стройиздат, 1979, 316 с.
15. **Кузнецов В.Д., Лядский В.А.** Сейсмоизоляция общественных зданий на основе фторопласта. Инженерно-строительный журнал, №3, 2010, Санкт-Петербург, с. 61-64.
16. .**Абакарова А.Д., Зайнулабидова Х.Р.** Оценка областей рационального применения системы сейсмоизоляции зданий со скользящим фундаментным поясом // Вестник Дагестанского государственного технического университета. Технические науки, №1(40), 2016, с.77-85.
17. **Зайнулабидова Х.Р.** Оценка влияния этажности зданий на эффективность использования систем сейсмоизоляции со скользящим поясом. Неделя науки – 2015. Сборник тезисов докладов XXXVI итоговой научно-технической конференции преподавателей, сотрудников, аспирантов и студентов ФГБОУ ВО Дагестанский государственный технический университет, 2015, с.138-140.
18. **Давыдова Г.В., Ермошин А.А., Уздин А.М., Румянцев А.Ю.** Оценка перемещения зданий с сейсмоизолированным скользящим поясом. Сейсмостойкое строительство. Безопасность сооружений, №3, 2007, с. 34-37.
19. **Апсеметов М.Ч., Андашев А.Ж., Шамшиев Н.У., Апсеметов А.М.** Колебания модели малоэтажных зданий с сейсмоизолирующим поясом при сейсмических воздействиях. Вестник Международного Института Управления. Архангельск, №1, 2018, с.68-73.

20. **Gian Michele Calvi, Paolo M. Calvi, Matteo Moratti.** Seismic isolation of buildings using devices based on sliding between surfaces with variable friction coefficient // DOI 10.1007/s41062-017-0081-8. Innov. Infrastruct. Solut, 2017.

Mkrtichev Oleg Vartanovich — PhD (technical sciences), professor, head of department "Resistance of materials", Federal state budget educational institution of higher education "NATIONAL RESEARCH MOSCOW STATE UNIVERSITY OF CIVIL ENGINEERING" (MGSU), 129337, Moscow, Yaroslavskoe shosse, 26, +7 (499) 183-34-83, mkrtychev@yandex.ru

Mingazova Salima Rafilovna — Postgraduate student of the department " Resistance of materials Federal state budget educational institution of higher education "NATIONAL RESEARCH MOSCOW STATE UNIVERSITY OF CIVIL ENGINEERING" (MGSU), 129337, Moscow, Yaroslavskoe shosse, 26, +7 (910) 013-31-50, salima.mingazova@yandex.ru

Мкртычев Олег Вартанович — доктор технических наук, профессор, заведующий кафедрой «Сопротивление материалов», Федеральное государственное бюджетное образовательное учреждение высшего образования «Национальный исследовательский Московский государственный строительный университет» (НИУ МГСУ), 129337, г. Москва, Ярославское шоссе, д. 26, +7 (499) 183-34-83, mkrtychev@yandex.ru

Мингазова Салима Рафиловна — аспирант кафедры «Сопротивление материалов», Федеральное государственное бюджетное образовательное учреждение высшего образования «Национальный исследовательский Московский государственный строительный университет» (НИУ МГСУ), 129337, г. Москва, Ярославское шоссе, д. 26, +7 (910) 013-31-50, salima.mingazova@yandex.ru

International Journal for Computational Civil and Structural Engineering, 19(2) 172–187(2023)

DOI:10.22337/2587-9618-2023-19-2-172-187

RESUDIAL STRESSES IN I-BEAMS AND ITS EFFECT ON RODS BUCKLING

Denis V. Konin [1], Alexander I. Fimkin [2], Alexander R. Olurombi [1]

[1] TSNIISK named after V. A. Koucherenko JSC Research Center of Construction, Moscow, RUSSIA
[2] Russian University of Transport, Moscow, RUSSIA

Abstract: Stability calculation of steel rods should consider residual stresses, as well as local imperfections (bends, buckling). Codes of EU, USA, PCR considering difference between welded and rolled I-beams on compression and compression with bending. Coefficient of longitudinal bending has values that consider the presence of different values of residual stresses for welded and rolled I-beams. Russian code for the design of steel structures (SP 16.13330) for conditionally centrally compressed rods does not distinguish between methods of I-beams production.

To determine residual stresses, a wide range of Russian profiles with different thin-walled was studied. Residual stresses for small-sized profiles were carried out by partitioning, for large I-beams - by drilling blind holes. The actual values of residual stresses in flanges and walls are established; most suitable curves for their approximation are selected. The actual shape of I-beams was also measured with a laser scanner. According to the results of curvature measuring, the limit and average values of local flanges deflection are established.

Considering experimental studies, FE-modeling of rods with residual stresses was performed for both rolled and welded I-beams. In addition to code eccentricities, local shape imperfections were modeled. It is established that rolled I-beams show higher values of critical forces than welded ones by 8-16%. This is true for steels C355 and C390 with a lambda-factor of more than 4, and for C255 with lambda-factor more than 3. According to the study, a coefficient is proposed that increases the bearing capacity of rolled I-beams for medium and large flexibilities.

Keywords: steel, stability, residual stress, section method, hole-drilling method, local buckling, rolled I-beam, welded I-beam, FE-modelling

ОСТАТОЧНЫЕ НАПРЯЖЕНИЯ В ДВУТАВРАХ И ИХ ВЛИЯНИЕ НА УСТОЙЧИВОСТЬ СТЕРЖНЕЙ

Д.В. Конин [1], А.И. Фимкин [2], А.Р. Олуромби [1]

[1] ЦНИИСК им. В.А. Кучеренко АО «НИЦ «Строительство», г. Москва, РОССИЯ
[2] Российский университет транспорта, г. Москва, РОССИЯ

Аннотация: Расчет стальных стержней на устойчивость должен учитывать наличие остаточных напряжений, а также наличие местных несовершенств формы (погибы, выпучивания). В нормах Евросоюза, США, КНР учтено отличие сварных и прокатных двутавров при работе на сжатие и сжатие с изгибом. Коэффициент продольного изгиба имеет значения, учитывающие наличие разных величин остаточных напряжений для сварного и прокатного двутавра. В отличие от указанных норм, российский свод правил по проектированию стальных конструкций (СП 16.13330) для центрально сжатых стержней не делает различия между способом производства двутавров.

Для определения величин остаточных напряжений был изучен широкий диапазон профилей российского производства с различной тонкостенностью. Остаточные напряжения для профилей небольших размеров проведены методом секционирования, для крупных двутавров – методом сверления глухих отверстий. Установлены фактические значения остаточных напряжений по полкам и стенкам, подобраны наиболее подходящие кривые для их аппроксимации. Также проведено измерение действительной формы двутавров лазерным сканером. По результатам анализа кривизны поверхности установлены предельные и средние значения местных погибей полок.

С учетом экспериментальных исследований выполнено КЭ-моделирование стержней с остаточными напряжениями как для прокатных и сварных двутавров из различных сталей. Кроме нормативных эксцентриситетов моделировались локальные несовершенства формы. Установлено, что прокатные

двутавры показывают большие значения критических сил, чем сварные на 8-16%. Это справедливо для сталей с С355 и С390 при условной гибкости более 4, а для С255 условной гибкости более 3. По результатам исследования предложен коэффициент, увеличивающий несущую способность прокатных двутавров для средних и больших гибкостей.

Ключевые слова: сталь, устойчивость, остаточные напряжения, секционирование, сверление отверстий, местная потеря устойчивости, прокатной двутавр, сварной двутавр, КЭ-моделирование

INTRODUCTION

In the studies of domestic [1, 2] and foreign authors [3, 4, 5] in the mid-20th century, it was established that residual stresses affect the performance of compressed steel bars. The following significant studies [6, 7, 8, 9] established the laws of development of residual stresses in I-beams, pipes, as well as other construction profiles. Based on the generalization of studies on the influence of residual stresses on rolled and welded sections, a document [10] was compiled. This document formed the basis for the creation of relevant provisions of Eurocode 3: Design of steel structures. Residual stresses along with other imperfections are considered in the standards for the calculation of structures by reduction factor φ for relevant buckling mode.

Let us compare the buckling curves for steel compressed rods according to the current standards. Figures 1, 2 show a comparison of the curves of the reduction factor φ from the current SP 16.13330.2016 "Steel Structures" (solid lines), from Eurocode 3 (European Union), from GB50017-2003 (PRC), from Steel Construction Manual 13th Edition (ASTM, USA). A comparison shows the following. Curves *a* and *b* follow practically the same trajectory and the deviation within the range of conditional flexibility from 0.4 to 4 is not more than 3% (0.8% on average), the curve c of SP 16.13330.2016 has a difference of up to 4.5% from the corresponding curve of Eurocode 3. The most advantageous in terms of material consumption are curves *a* and a_0. The sections of *a* type in SP 16.13330.2016 include closed pipes regardless of the method of production, and in Eurocode 3 are hot-rolled pipes, rolled I-beams in calculations in the plane of greater stiffness, as well as any I-beams in calculations in any direction from steel S460 (a_0). The curve a_0 gives φ values 6-7% higher than a from Eurocode 3 or from SP 16.13330.2016. This curve was introduced in Eurocode 3 based on several studies by European researchers in recent years [11, 12, 13, 14]. The Eurocode 3 accepts the most inefficient curve for column-type I-beams (height and width are the same). The difference in the performance of welded and rolled I-beams was identified and investigated abroad quite a long time ago [4, 8] and accounted for in the norms. SP 16.13330.2016 does not take into account the type of I-beam (column, beam, wide flange), the type of steel, the method of manufacture when evaluating the bearing capacity of centrally compressed elements. It also does not consider the direction of the design axes. I-beam in the plane of the flanges and in the plane of the wall is calculated using a single curve *b*. Eurocode 3 also has a curve *d*, which accounts for the negative effects of residual stresses in welded I-beams when calculating in the plane of the flanges, which are composed of two or more sheets.

In the range λ from 0.4 to 6 the value of the reduction factor φ according to ASTM is higher by 6.1% in comparison with curve b of Eurocode 3 and by 6.9% in comparison with curve b of SP 16.13330. The factor φ from GB50017-2003 (PRC) generally repeats the values of one from SP 16.13330. However, there is a separate curve for welded jambo-profiles, which considers the negative influence of welding stresses. These conclusions were drawn on the basis of several studies, including the investigation of I-beams made of high-strength steels [15, 16, 17].

It should be noted that modern RF standards have not been corrected in terms of specification of reduction factors φ for quite a long time. At

the same time, the values of factors in the 1980s were derived with regard to foreign experimental data on the values of residual stresses [1, 2]. The values of residual stresses were studied by some researchers in the 1980s after the beginning of the rolling mill for the production of wide-shelved I-beams in Nizhny Tagil [18]. Modern studies of residual stresses in rolled and welded sections were not aimed at updating the regulatory documents, but are devoted to important particular issues of the influence of residual stresses on the stress-strain state of certain structures. In particular, papers [19, 20] provide an investigation of stresses in tubular sections. In papers [21, 22] small I-beams and C-profiles are considered. Papers [23, 24] and etc. consider residual stresses from the standpoint of technological peculiarities of manufacturing.

Since there is no systematic research of residual stresses of I-beams in the part of their influence on stability of compressed beams, objectives and tasks of the current study are formulated. The objective of the study is to determine residual stresses in I-beams made of different steels produced in the Russian Federation, and to estimate the influence of residual stresses on the performance of compressed struts. One of the tasks is to estimate the difference between residual stresses in rolled and welded I-beams.

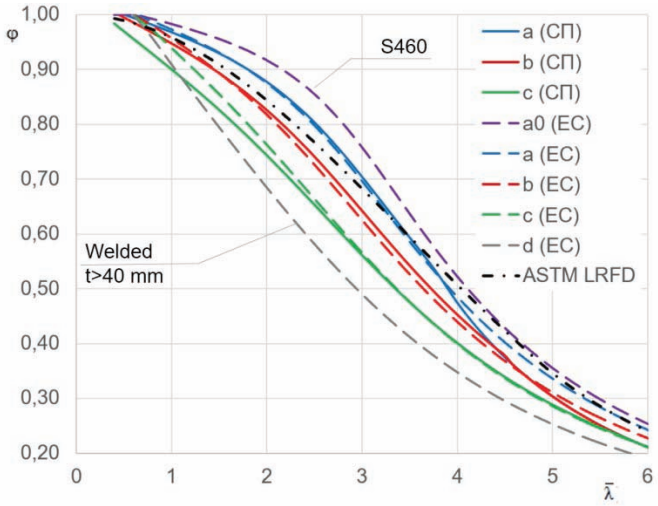


Figure 1. Graph $\varphi - \bar{\lambda}$ for SP 16.13330, Eurocode 3, ASTM

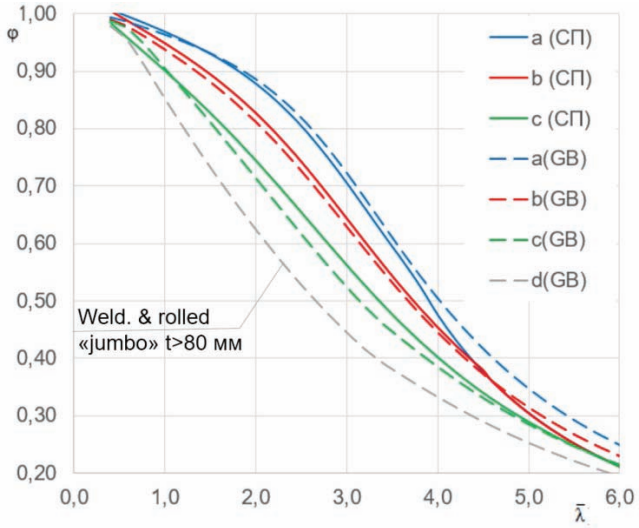


Figure 2. Graph $\varphi - \bar{\lambda}$ for SP 16.13330, GB50017-2003)

METHODS

A. Determination of residual stresses and real shape

To construct the residual stress diagrams, 10 samples selected from rolled I-beams produced in Russia according to GOST R 57837-2017 were investigated. Actual dimensions of the investigated sections and their mechanical characteristics are given in Table 1. In the table and further in the text the following designations are adopted: *L* is the length of the sample, *h* is the height of the I-beam, *b* is the shelf width, s is the wall thickness, *t* is the shelf thickness, h_w is the distance in light between the flanges, σ_y, σ_u are the yield strength and ultimate strength of steel according to test results. Relative lengths *L/h* of the studied samples are from 4.1 to 4.8. This means that the length of the samples did not affect the distribution of residual stresses. So, the determined residual stresses can be extended to all rod lengths (except for "short" ones, in which the *L/h* ratio is less than 3). As was shown in [3], the specimen length *L/h*>4 ensures that the residual stresses are unchanged when the specimen is cut out of the whole rod. Table 1 also shows that a wide range of profiles with different thinness *n=h/s* has been studied. The most "thin-walled" profiles are 15DK1 (A1) and 20Sh2 (A9), which have a parameter n of about 26. The least "thin-walled" profile is 20K8 (A6), which has parameter n about 13. The range of the studied profiles by parameter n covers almost all I-beams according to GOST R 57837-2017, which are used in structures as compressed rods. Such profiles belong to the K (column) type. The *h/b* ratio for them is approximately equal to 1 and ranges from 0.97 (20K1 A3) to 1.16 (20K8 A6). Also, for comparison were studied I-beam's type SH (wide-strip), for which *h/b* is approximately equal to 1.3 (20Sh2 (A9), 20Sh3 (A10). The specimens were made of C255 and C390 steels. The ratio σ_y/σ_u shows high plastic properties of steels and is from 0.63 (20Sh3 (A10) to 0.79 (15DK1 A1). The high plastic properties of the steels are also confirmed by the value of relative elongation from 30 to 39%, as well as the values of impact toughness values above 150 J/cm2.

Table 1. Studied profiles

Profile and steel	Dimensions based on measurement results (average values), mm						Profile's parameters				Steel characterisitics, MPa		
	L	*h*	*b*	*s*	*t*	h_w	*L/h*	*n = h/s*	*s/h*	*h/b*	σ_y	σ_u	σ_y/σ_u
1	2	3	4	5	6	7	8	9	10	11	12	13	14
A1 C255 15DK1	749	157	158	6.7	7.1	142.8	4.8	26.2	0.04	0.99	337	429	0.79
A2 C255 15DK3	689	161	153.9	9.2	11.3	138.4	4.3	20.0	0.06	1.05	301	443	0.68
A3 C255 20K1	832	192	198	7.2	9.9	172.2	4.3	30.2	0.04	0.97	280	423	0.66
A4 C255 20K3	822	201	200	11.1	13.6	173.8	4.1	22.7	0.06	1.01	273	422	0.65
A5 C390 20K3	816	200	199	10.3	13.6	172.8	4.1	22.7	0.05	1.01	403	539	0.75
A6 C390 20K8	971	231	200	19.8	28.9	173.2	4.2	13.0	0.09	1.16	383	531	0.72
A7 C390 30K7	1340	316	301	14.7	22.9	270.2	4.2	21.8	0.05	1.05	399	538	0.74
A8 C390 40K3	1659	409	401	16.5	23.6	361.8	4.1	25.4	0.04	1.02	403	563	0.72
A9 C255 20SH2	870	197	150	8.2	10.8	175.4	4.4	26.5	0.04	1.31	286	434	0.66
A10 C255 20SH3	845	202	150.5	9.8	12.7	177.3	4.2	22.7	0.05	1.35	266	422	0.63

Measurements of residual stresses in I-beams A3, A4, A5, A7, A8, A9 were performed by hole drilling method, in I-beams A1, A2, A10 - by sectioning method. I-beam A6 was tested by two methods to verify both methods and to control measurements.

The method of sectioning is based on cutting out of the specimen by two cross-section cuts a narrow fragment (temple), on the surface of which on the contour are previously glued strain gauges FLA-3-11 (24 to 36 pieces depending on the size of the I-beam). Strain gauge readings are measured throughout the cutting process. Fig. 3 shows a schematic diagram of the method. When the temple is cut, residual stresses are released in it. This causes changes in the readings of strain gauges. Based on these changes, the relative deformations ε in the measuring points and then the residual stresses are calculated assuming a linear stress state on the surface of the I-beam [25, 26].

The hole-drilling method is based on ASTM: E837 "Standard Test Method for Determining Residual Stresses by the Hole-Drilling Strain-Gauge Method". A strain-gauge socket (figure 4) is glued to the surface of the object under study and a hole is drilled in the center of the socket. Depending on the size of the I-beam, from 13 to 19 FRS-3-11 sockets were glued. The hole-drilling method does not release the strains from their own residual stresses completely. Therefore, the stresses cannot be calculated directly from the measured strains. It is necessary to have correction factors obtained computationally or experimentally. The computational method is based on the well-known solution of the problem of elasticity theory on the tension of a strip with a hole. The development of this solution using FEM is applied in the above-mentioned standard.

To identify the actual shape and dimensions of I-beams, surface scanning of specimens up to 5 m long was performed by HandyScan laser scanner. According to the results of scanning the surface maps of I-beams were constructed and analyzed. It was established that the curvature of the flange overhang is 1/100 0.5b in average and never exceeds 1/50 0.5b. For example, for the largest I-beam 40K3 the average value of the overhang curvature will be 2.01 mm, which was adopted in the further FE analysis).

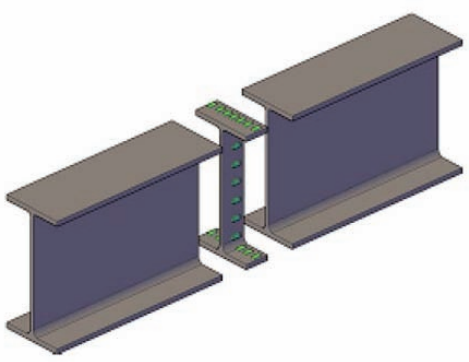


Figure 3. Sectioning method

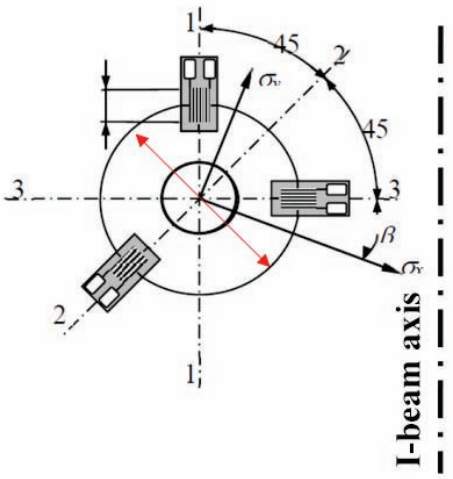


Figure 4. Socket of three strain gauges for the drilling method

B. Finite element modeling

A parametric finite-element model in Ansys Workbench was applied to solve the buckling problem of a centrally compressed I-beam profile. Solid finite elements in the form of hexahedrons ("Structural 3D Solid45") were used for modeling. Element size and mesh density were selected through successive iterative analyses. The first trial calculation was performed with a rough mesh, then a finer mesh was partitioned, the step was decreased by 20-30%. The results of the calculations were used to evaluate the change of critical load, if the difference of calculations with

different meshes in neighboring iterations was more than 0.5%, the mesh was reduced further and a new calculation was performed. The mesh densification was continued until the difference of critical loads in neighboring iterations was less than 0.5%. To specify the boundary conditions, the end nodes of the FE model of an I-beam were joined by an absolutely rigid finite element (one at each end), which had a hinged attachment at an eccentricity distance from the central axis of the profile. The eccentricity was set in the plane of least stiffness of an I-beam (a plane parallel to the flanges and passing through the center of gravity of the section). The compressive load was modeled by the movement of one hinged support along the initial axis of the rod. The modeling considered the elastoplastic properties of the steel. The σ-ε diagrams of the steels were assumed in accordance with SP 16.13330.2016 "Steel structures" in the form of piecewise linear functions. The plasticity criterion was taken as the von Mises criterion. Temperature fields were applied to the finite-element models of I-beams to set residual stresses. The temperature on the elements was set so that the final stresses in the I-beam corresponded to the test results for rolled I-beams and to the results of theoretical calculations for welded sections. An iterative type of solving a numerical problem by the Newton-Raphson method was used. This type of calculation is performed step by step according to the deformed scheme. The number of iterations for the considered models was from 30 to 80. The models were loaded until the appearance of necking in the diagram "longitudinal reaction of the support vs. displacement of the support". The maximum on this diagram was assumed to be the critical load of the model. Totally 324 models were created and calculated: 9 I-beam sections, given in table 1; for each section models with six slenderness ratios (λ =1; 2; 3,14; 4; 5; 6) were created; for each section and flexibility 3 kinds of steel were given for C255, C355 and C390; for each model residual stresses corresponding to rolled or welded version were specified. The general view of one of the models is shown in Figure 5.

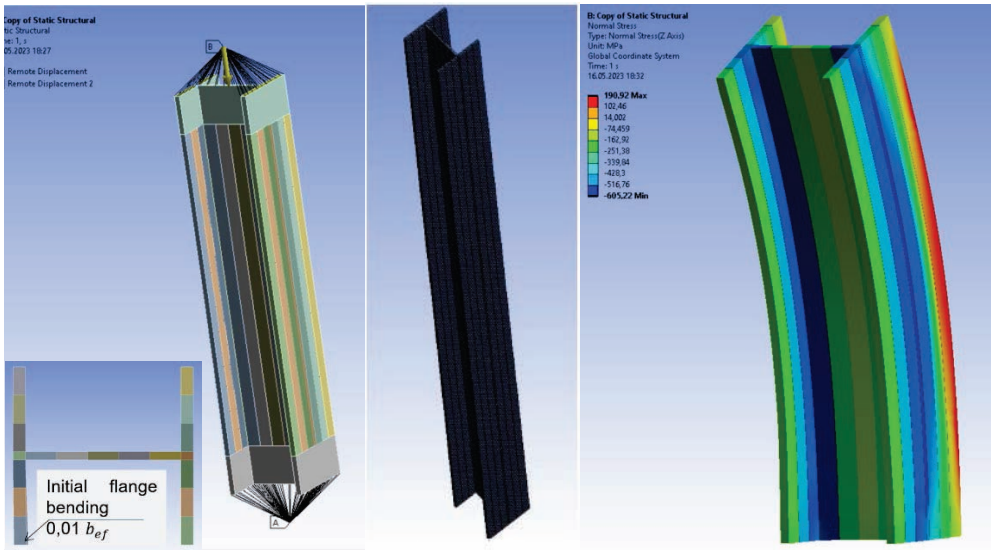


Figure 5. FE model of the rod

RESULTS AND DISCUSSION

A. Residual stresses

The measurement results of residual stresses are highly variable and should be analyzed by averaging and identifying general patterns. Averaging is performed by calculating average values from measurements of residual stresses in the similar elements at the same distance from the edges (for the flanges) or from the middle of the wall on the left and right surfaces. Figures 6 and 7 show the relative values of

residual stresses $\bar{\sigma}_{res}$ calculated with respect to the actual yield strength σ_y of a particular specimen $\bar{\sigma}_{res} = \sigma_{res}/\sigma_y$ in the relative coordinates $\bar{x}$ and $\bar{y}$. The coordinates are counted from the center of gravity of the section and calculated using the formulas формулам $\bar{x} = x_i/0{,}5b$ and $\bar{y} = y_i/0{,}5h_w$.. Fig. 6 and Figure 7 also show dashed lines for comparison the theoretical values of residual stresses for rolled I-beams taken from the authors Alpstein, Tebedge, Spoorenberg [8, 4, 12] and for welded I-beams according to [10, 13] (calculated for the weld with full penetration by automatic welding for profile-analogues).

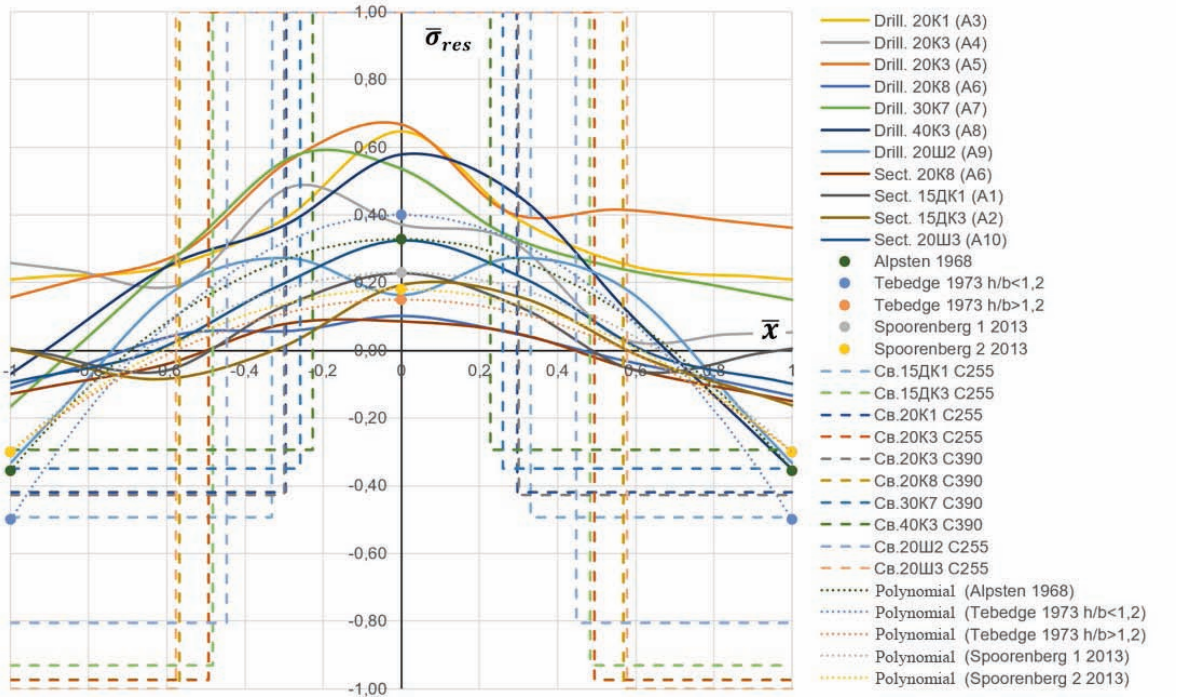


Figure 6. Measured residual stresses in I-beam flanges (solid lines)

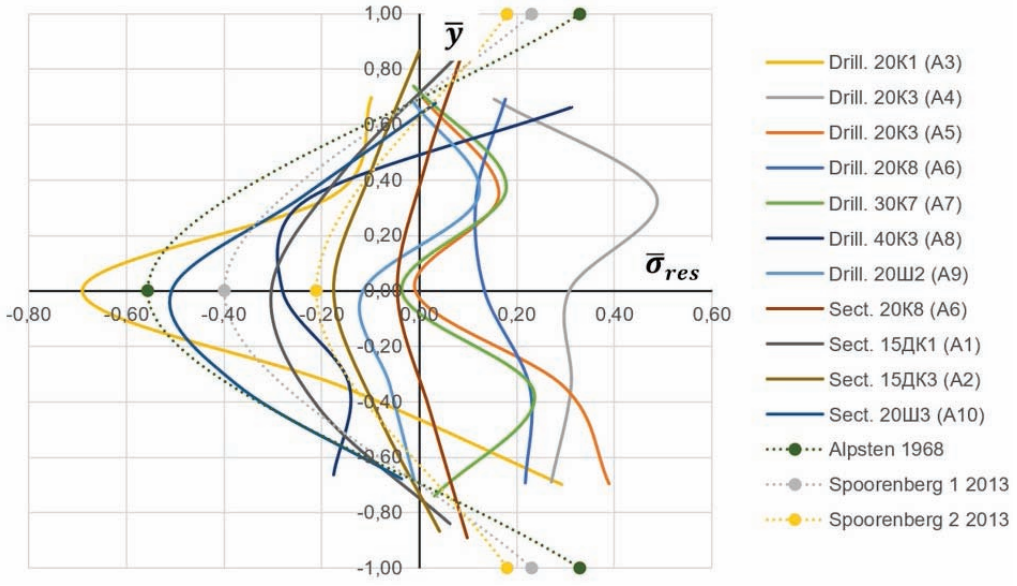


Figure 7. Measured residual stresses in I-beam walls (solid lines)

The best match with the actually measured stresses was demonstrated by the Spoorenberg dependences [12]. The closest to the theoretical value of residual stresses is the profile A9 20Sh2 (the difference in tensile and compressive stresses is 16 and 10%, respectively). The most far from the theoretical values is the most "thick-walled" profile A6 20K8 (the difference in tensile and compressive stresses is minus 171% and minus 125%, respectively). This means that the actual stresses are much lower than those predicted by theoretical studies. These differences are confirmed by two independent measurements of residual stresses in the I-beam. According to all considered theoretical dependences I-beams of Sh type (A9 and A10) most accurately describe the distribution of actual residual stresses. This is probably due to the fact that most of the profiles studied abroad refer to beams or wide-shelves. Correlation of the magnitude of deviations with the yield strength or thin-walled profiles is not revealed. The residual stresses in the wall have less correlation with the theoretical results (see Figure 7). For example, for some I-beams (A4 20K3, A7 30K7, A6 20K8 and others) the values of residual stresses which do not change sign and do not have parabolic form were recorded. This circumstance requires additional investigation and accumulation of statistical data for different I-beam producers. It should be noted that the distribution of residual stresses along the wall significantly depends on the production method as well as the position of the I-beam during cooling [4, 18]. Residual stresses in the wall practically do not affect the operation of the rod in eccentric compression [13, 14].

B. Performance of compressed rods

According to the results of the finite element analysis for buckling under central compression, the critical loads were calculated. On the basis of these loads the reduction factors were obtained by the formula 1, which is a modified formula 7 of SP 16.13330.2016 under the action on the rod of the critical force.

$$\varphi = \frac{N_{cr}}{\gamma_c A R_y} \quad (1)$$

where N_{cr} is the critical load based on the results of finite element modeling; A is the cross-sectional area by assortment; R_y is the design value of the yield strength of steel, $\gamma_c = 1$. According to the results of the analyses (Fig. 9), six dependences φ-λ were obtained for each type of section for three variants of steels and two versions of design (rolled, welded). Analyzing the obtained results, certain regularities can be noted. It is observed in all cases that I-beam section in welded version has lower factor φ than in rolled version. This can be noted on all the considered slenderness ratios and steel variants. The decrease in the load capacity is caused precisely by residual stresses, since the calculated models had the same geometric and mechanical characteristics and differed only in the initial internal stresses. During the detailed consideration of the stress-strain state of models and the estimation of influence of residual stresses a considerable influence of initial form imperfections on the character of stability loss and total bearing capacity has been noted. For welded I-beams, where residual stresses reach yield strength, distribution of stresses and strains over the section has an irregular character. That is, plastic deformations have a local character at the initial stages of loading. The maximum stresses are displaced from the outermost fibers inside the section. There are local stress concentrators which do not have significant influence for ideal shape of I-beam which is straight prism, but play significant role in the presence of local form imperfections. Figure 10 shows the graphs of φ-λ for an I-beam 30K7 as an example. The solid lines show the dependences for the rolled sections and the dashed lines for the welded ones. The red solid line is the curve for section type b in accordance with Table D.1 of SP 16.13330.2016. The detected deviations based on the results of detailed 3D scanning of the shape and dimensions of I-beam sections do not exceed the

limits set by the I-beam standards. Nevertheless, these deviations, taken into account in the FE modeling, had a significant impact on the nature of the buckling of the models. Local eccentricities in the flanges reached 2-3 mm, which caused additional bending moments and deformations of the section. In combination with local stress concentrators resulting from residual stresses, the eccentricities in the flanges led to local deformations having an avalanche-like character (Fig. 9). There was a local buckling, which immediately led to the loss of overall stability. This type of exhaustion of bearing capacity was most clearly observed in welded I-beams with relatively flexible flanges, for example, 20K1 and 15DK1. In rolled I-beams the loss buckling was also observed, but its effect on the final bearing capacity was less.

In the area of small slenderness ratios ($\bar{\lambda}$ ≈1÷3) the reduction factors obtained by numerical calculations are lower than the normative ones. This is characteristic of all welded and rolled profiles made of steel C355 and higher. In the area of medium slenderness ratios ($\bar{\lambda}$ ≈3÷6) the calculated reduction factors approximately coincide with the normative ones, and at large slenderness ratios ($\bar{\lambda}$ ≈6÷8) the bearing capacity according to the finite-element analysis is higher than that according to the normative calculation. The discrepancy between the results obtained and the method [12] is due to the fact that the numerical simulation takes into account not only the initial imperfections of the bars, but also local form imperfections and residual stresses. Residual stresses in combination with local form imperfections increase their influence with decreasing slenderness ratios. At large slenderness ratios, random eccentricities have a significant effect on bearing capacity, with profiles losing their overall stability earlier than local stability. The most unfavorable variations of residual stresses which can arise in the I-beam are taken into account in the FE modeling. The residual stresses obtained from the test results have been extended to the whole body of the profile, although in the real I-beam the residual stresses may be variable along the length and have less influence on the bearing capacity, being smaller in magnitude.

The analysis of the obtained $\varphi - \bar{\lambda}$ dependences shows that the factor φ decreases as the steel strength increases. This is observed in all the profiles considered both in the group of rolled I-beams and in the group of welded I-beams. Comparing the ratio of factors φ for different steels, a ratio $\frac{\varphi_{C390}}{\varphi_{C255}} = 0.975 \ldots 0.985$ is obtained at $\bar{\lambda}$=1. That is, the values of the coefficients are close enough. When $\bar{\lambda}$=6 the ratio $\frac{\varphi_{C390}}{\varphi_{C255}} = 0.715 \ldots 0.743$.. The decrease in the ratio $\frac{\varphi_{C390}}{\varphi_{C255}}$ with increasing slenderness ratio is explained by the fact that the conditional slenderness takes into account the strength characteristics of the material in a simplified form, and the given diagram of steel behavior according to SP 16.13330 is piecewise linear, but not curvilinear. A statistically reliable model of elastoplastic deformation for different steels in the section of transition from linear performance to yield point is required for more accurate modeling of I-beam operation depending on residual stresses, form imperfections and steel type. This issue is still open and requires further investigations.

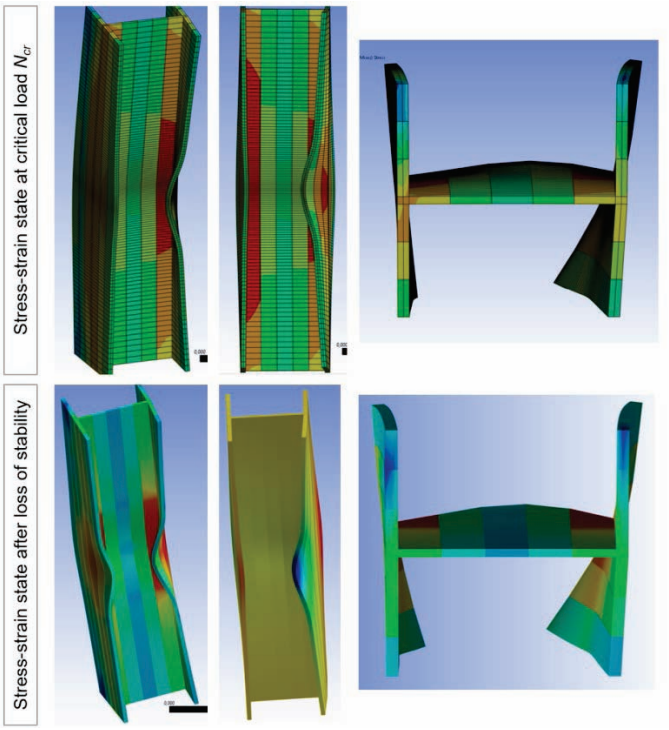


Figure 9. Stress-strain state for 30K7 profile at critical load (up) and after loss of stability (down)

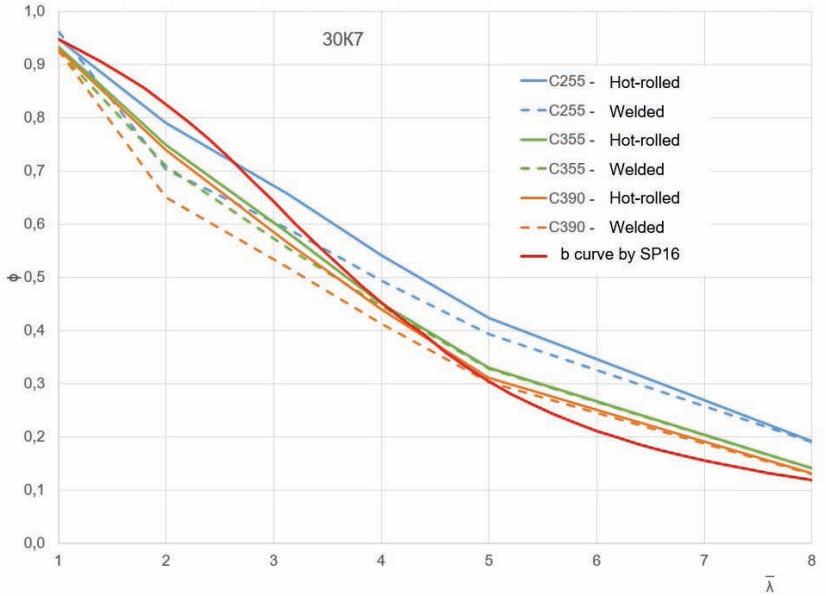


Figure10. Graph $\varphi - \bar{\lambda}$ for 30K7 profile

To evaluate the influence of I-beam section manufacturing method on its bearing capacity under central compression, it is necessary to consider the change in bearing capacity of sections of the same geometry and steel, but with different design - welded and rolled. For this purpose, let us analyze the ratio of the corresponding critical forces $N_{cr.Roll}/N_{cr.Weld}$ on the range of considered slenderness ratios $\bar{\lambda}$ (figure 11 - example for I-beam 30K7). The graph $\frac{N_{cr.Roll}}{N_{cr.Weld}} - \bar{\lambda}$ has a noticeable maximum in the range $\bar{\lambda} = 2 \div 4$, and this is typical for all the considered profiles and steel types. When

$\bar{\lambda} = 1$ the difference between the rolled version and the welded version is small. At high slenderness ratio $(\bar{\lambda} = 6 \div 8)$ the difference in bearing capacity of two versions is also not very large, the ratio $\frac{N_{cr.Roll}}{N_{cr.Weld}} - \bar{\lambda}$ does not exceed the value 1.03. The greatest difference of reduction factors is observed in the range of slenderness ratios $\bar{\lambda} = 2 \div 4$, at that for different profiles $\frac{N_{cr.Roll}}{N_{cr.Weld}} = 1{,}08 \div 1{,}16$. The highest values of $\frac{N_{cr.Roll}}{N_{cr.Weld}}$ are observed for profiles 40K3, 15DK3, 20Sh3.

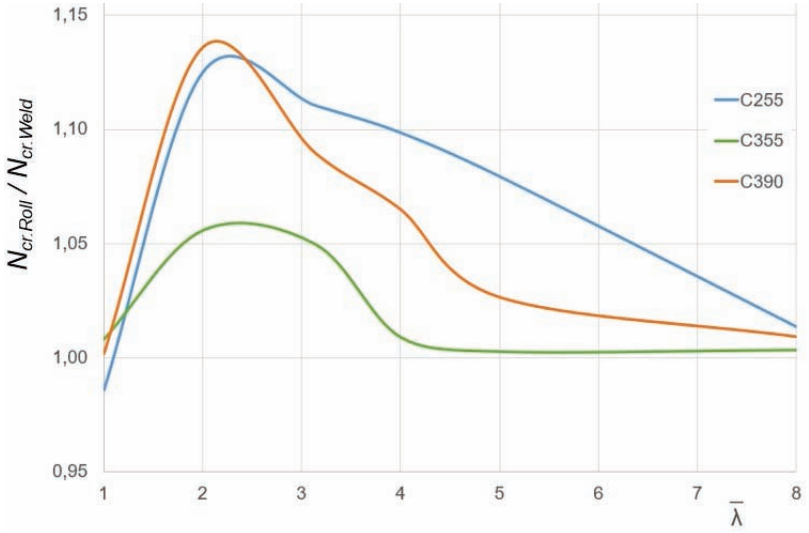


Figure 11. Graph $N_{cr.Roll}/N_{cr.Weld}$ for 30K7 profile

Let's compare the bearing capacity of the rolled I-beam, obtained from the results of numerical calculation, with the normative calculation according to SP 16.13330.2016. For this purpose let's consider the graph of the ratio $N_{cr.Roll}/N_{cr.Weld}$ as a function of $\bar{\lambda}$ (Figure 12 - example for 30K7). At small slenderness ratio $\bar{\lambda}$ = 1 the calculated values practically coincide with the normative estimate, the values $N_{cr.Roll}/N_{cr.Weld}$ are about unity. At slenderness ratio ratio $\bar{\lambda}$ = 2 the ratio $N_{cr.Roll}/N_{cr.Weld}$ is in many cases below unity, that is the numerical calculation of the rolled I-beam shows a lower carrying capacity than required by standards. The exception is the 20K type I-beams of C255 steel, for these cases $N_{cr.Roll}/N_{cr.Weld}$ is always greater than unity and constantly increases with increasing slenderness. For other profiles the growth of $N_{cr.Roll}/N_{cr.Weld}$ with increasing slenderness becomes true only when $\bar{\lambda} \geq 3$. In general, it can be said that the bearing capacity at numerical calculation is greater than the normative one for steels with strength characteristics C355 and higher at $\bar{\lambda}$ >4, and for C255 at $\bar{\lambda}$ >3.

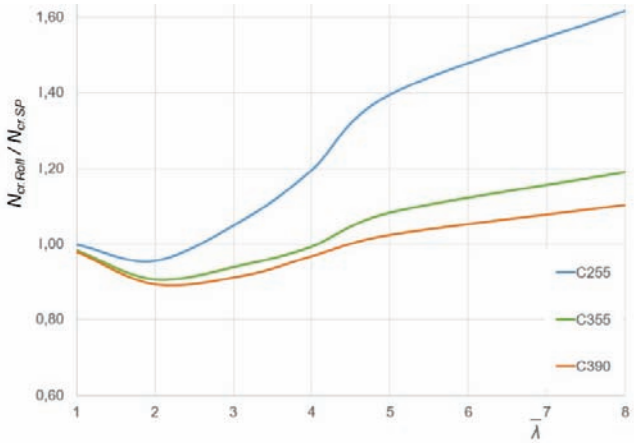


Figure 12. Graph $N_{cr.Roll}/N_{cr.SP}$ for 30K7 profile

C. Proposals for considering the effect of residual stresses in codes

The dependences "φ-λ " obtained by the results of the FE-analysis represent one of the worst-case scenarios of I-beams operation under

central compression when local form imperfections, the highest residual stresses and random eccentricities are acting in combination. For the calculation of standard structures, the normative checking according to SP 16.13330.2016 is sufficient. Reliability coefficients and behavior conditions laid down in the norms sufficiently prevent the influence of initial imperfections. Nevertheless, the results of the study showed that the rolled profiles behave more effectively in central compression than the welded ones. Based on the data obtained, in order to improve the normative methodology for calculation of I-beams in central compression, we can propose the coefficient k_{res}, increasing the bearing capacity of rolled I-beams for medium and large slenderness, in the following form:

$$k_{res(255)} = \begin{cases} 1; for\ \bar{\lambda} \leq 3 \\ 0{,}1\bar{\lambda} + 0{,}7; for\ \bar{\lambda} > 3 \end{cases} \quad (2)$$

$$k_{res(390)} = \begin{cases} 1; for\ \bar{\lambda} \leq 5 \\ 0{,}2\bar{\lambda} + 0{,}9; for\ \bar{\lambda} > 5 \end{cases} \quad (3)$$

The normative checking of the welded I-beam stability in central compression is recommended, as before, in accordance with paragraph 7.1.3 of SP 16.13330.2016. In turn, the test of buckling under the central compression of a rolled I-beam should be performed according to the formula (4), which accounts for a coefficient ofk_{res}:

$$\frac{N}{k_{res}\varphi R_y \gamma_c} \leq 1 \quad (4)$$

CONCLUSION

1. A study provides the results of investigation of actual residual stresses in rolled I-beams. Measurements of residual stresses were carried out on the entire range of rolled sections of the Russian Federation (GOST R 57837-2017) by proven methods: sectioning and drilling holes. The patterns of residual stresses distribution in flanges and walls of rolled I-beams have been revealed.
2. The shape of rolled I-beams has been measured. It was found that the bending of I-beam flange after rolling averages 0.01 b_{ef}.
3. By the whole range of cross-sections of the Russian product range (GOST R 57837), as well as by the most widespread range λ (from 1 to 6) the FE-models taking into account imperfections of two-beam shape and distribution of residual stresses were created.
4. The difference between the performance of welded and rolled sections, caused by different distribution of residual stresses, is covered by the existing reliability coefficients laid down in the normative documents.
5. According to the results of investigations, it was established that the rolled sections of domestic production behave in compression more effectively than the welded ones.
6. The calculation of critical structures in order to increase the efficiency of steel consumption for small eccentricities, it can be proposed to use the coefficient k_{res}, which increases the bearing capacity of rolled I-beams according to equations (2) and (3).

REFERENCES

1. **Belskij G.E.** O predel'nyh sostoyaniyah elementov metallicheskih konstrukcij pri szhatii (rastyazhenii) s izgibom [On the limiting states of elements of metal structures under compression (tension) with bending] Bel'skij, G.E. *Stroitel'naya mekhanika i raschet sooruzhenij*. 1973. No 2. Pp. 51-57. (In Russian)
2. **Belskij G.E.** K raschetu stal'nyh kolonn so slozhnym poperechnym secheniem [To the calculation of steel columns with a complex cross-section] Bel'skij, G.E., Gil'dengorn, L.A. *Stroitel'naya mekhanika i raschet sooruzhenij.* 1981. No 6. Pp. 68-73. (In Russian)
3. **Huber A. W., Beedle, L. S.** Residual stress and the compressive strength of steel.

Welding Journal, 33 (12), P. 589, (December 1954), Reprint No. 96 (54-3)
4. **Alpsten G.A.** Thermal residual stresses in hot-rolled steel members. Alpsten, G.A. Fritz Laboratory Reports. P. 329, Lehigh University. Lehigh, 1968. 118 p.
5. **Yang C.H.** Residual stress and the yield strength of steel beams. Yang, C.H., Beedle, L.S., Johnston, B.G. Welding Journal. 1952. Vol. 131. Pp. 205-316.
6. **Odar E.** Residual stresses in welded built-up T-1 shapes / Odar, E., Nishino F. // Fritz Laboratory Reports. Paper 177, Lehigh University. Lehigh, 1965. 41 p.
7. **NagarajaRao N.** Residual stresses in welded shapes / NagarajaRao, N., Estuar, F., Tall, L. // The Welding Journal. – 1964. – Vo. 43 (July). – pp. 295-349.
8. **Tebedge Negussie,** "Residual stresses in structural steel shapes--a summary of measured values, February 1973 (74-12)" (1973) Fritz Laboratory Reports. 337.34.
9. **Young B.W.** Residual stresses in hot-rolled members, IABSE reports of the working commissions, No 23, 1972
10. Manual on Stability of Steel Structures (Second Edition) / ECCS, 1976, p. 321.
11. **K.J.R. Rasmussen, G.J. Hancock**, Tests of high strength steel columns, J. Constr. Steel Res. 34 (1) (1995) 27–52.
12. **Spoorenberg R.C.** Experimental investigation on residual stresses in heavy wide flange QST steel sections. Spoorenberg, R.C., Snijder, H.H., L.-G. Cajot, May, M.S. Journal of Constructional Steel Research. 2013. No 89. Pp. 63-74.
13. **M. Abambres Wai-Meng Quach**. Residual stresses in steel members: a review of available analytical expressions. International Journal of Structural Integrity, Vol. 7 Iss 1 (2016) Pp. 70 – 94.
14. **H. Pasternak B. Launert, T. Kannengießer, M. Rhode.** Residual stresses and imperfections in welded high-strength I-shape sections. Insights and Innovations in Structural Engineering, Mechanics and Computation. Zingoni (Ed.) 2016 Taylor & Francis Group, London. Pp. 1139-1146.
15. **Y.B. Wang G.Q. Li, S.W. Chen, F.F. Sun,** Experimental and numerical study on the behavior of axially compressed high strength steel columns with H-section, Eng. Struct. 43 (2012) 149–159.
16. **G. Shi H.Y. Ban, F.S.K. Bijlaard**, Tests and numerical study of ultra-high strength steel columns with end restraints, J. Constr. Steel Res. 70 (2012) Pp. 236–247.
17. **H.Y Ban, G. Shi, Y.J. Shi, Y.Q. Wang**, Overall buckling behavior of 460 MPa high strength steel columns: experimental investigation and design method, J. Constr. Steel Res. 74 (2012) Pp. 140–150.
18. **Pozdeev A.A., Nyashin U.I., Trusov P.V.** Ostatochnye napryazheniya. Teoriya i prilozheniya [Residual stresses. Theory and applications] «Nauka». Moscow, 1982, 111 p. (In Russian)
19. **Golodnov A.I., Balashova O.S.** K opredeleniyu ostatochnogo napryazhennogo sostoyaniya v svarnyh elementah korobchatogo profilya [To determine the residual stress state in the welded elements of the box profile] Sovremennoe promyshlennoe i grazhdanskoe stroitel'stvo, No 3 Tom 6 (2010), Donbasskaya nac. akademiya stroitel'stva i arhitektury. Pp. 153-158. (In Russian)
20. **Golodnov A.I., Kozlova O.N.** Vliyanie ostatochnogo napryazhennogo sostoyaniya na ustojchivost' szhatyh elementov iz trub [The effect of the residual stress state on the stability of compressed elements from pipes] Metallicheskie konstrukcii, No 4. Tom 13 (2007), Donbasskaya nac. akademiya stroitel'stva i arhitektury. Pp. 181-186. (In Russian)
21. **Ivanov A.P., Ivanova I.A.** Raspredelenie ostatochnyh napryazhenij v goryachekatanyh prokatnyh profilyah [Distribution of residual stresses in hot-rolled rolling profiles] Sbornik nauchnyh trudov UkrNIPSK im. V.M.

Shimanovskogo. No. 2, 2008. Pp. 5-12. (In Russian)
22. **Psyuk V.V.** Issledovanie ostatochnogo napryazhyonnogo costoyaniya v prokatnyh dvutavrah [Investigation of the residual stress state in rolling I-beams] Psyuk, V.V., Golodnov A.I., Karapetyan, S.H. Sbornik nauchnyh trudov Donbasskogo gosudarstvennogo tekhnicheskogo universiteta. 2012. No 37. Pp. 50-58. (In Russian)
23. **Kolmogorov G.L., Kuznecova E.V., Tiunov V.V.** Tekhnologicheskie ostatochnye napryazheniya i ih vliyanie na dolgovechnosti i nadezhnost' metalloizdelij [Technological residual stresses and their impact on the durability and reliability of metal products] Perm, PNIPU. 2012. 226 p. (In Russian)
24. **Kartaushin S.I.** Modelirovanie i raschet ostatochnyh napryazhenij v prokatnyh profilyah [Modeling and calculation of residual stresses in rolling profiles] Kartaushin, S.I., Hramova, D.A., Bil'dyuk, N.A. Izvestiya vysshih uchebnyh zavedenij. Mashinostroenie. 2017. No 6 (687). Pp. 28-34. (In Russian)
25. **Fimkin A.I.** Ocenka dostovernosti raschetno-eksperimental'noj interpolyacionnoj metodiki opredeleniya ostatochnyh napryazhenij s pomoshch'yu chislennogo eksperimenta [Evaluation of the reliability of the computational and experimental interpolation technique for determining residual stresses using a numerical experiment] Stroitel'naya mekhanika i raschet sooruzhenij, No 5 (250). 2013. Pp. 29-35. (In Russian)
26. **Fimkin A.I.** Primenenie metoda regulyarizacii Tihonova dlya opredeleniya ostatochnyh napryazhenij [Application of Tikhonov regularization method for determination of residual stresses] Stroitel'naya mekhanika inzhenernyh konstrukcij i sooruzhenij, No 4. 2009. Pp. 48-55. (In Russian)

СПИСОК ЛИТЕРАТУРЫ

1. **Бельский Г.Е.** О предельных состояниях элементов металлических конструкций при сжатии (растяжении) с изгибом / Бельский, Г.Е. // Строительная механика и расчет сооружений. – 1973. - №2. – с. 51-57.
2. **Бельский Г.Е.** К расчету стальных колонн со сложным поперечным сечением / Бельский, Г.Е., Гильденгорн, Л.А. // Строительная механика и расчет сооружений. – 1981. - №6. – с. 68-73.
3. **Huber A. W., Beedle, L. S.** Residual stress and the compressive strength of steel. Welding Journal, 33 (12), p. 589, (December 1954), Reprint No. 96 (54-3)
4. **Alpsten G.A.** Thermal residual stresses in hot-rolled steel members. Alpsten, G.A. Fritz Laboratory Reports. P. 329, Lehigh University. Lehigh, 1968. 118 p.
5. **Yang C.H.** Residual stress and the yield strength of steel beams. Yang, C.H., Beedle, L.S., Johnston, B.G. Welding Journal. 1952. Vol. 131. Pp. 205-316.
6. **Odar E.** Residual stresses in welded built-up T-1 shapes. Odar, E., Nishino F. Fritz Laboratory Reports. Paper 177, Lehigh University. Lehigh, 1965. 41 p.
7. **NagarajaRao N.** Residual stresses in welded shapes / NagarajaRao, N., Estuar, F., Tall, L. The Welding Journal. 1964. Vol. 43 (July). Pp. 295-349.
8. **Tebedge, Negussie,** "Residual stresses in structural steel shapes--a summary of measured values, February 1973 (74-12)" (1973) Fritz Laboratory Reports. 337.34.
9. **Young B.W.** Residual stresses in hot-rolled members, IABSE reports of the working commissions, No 23, 1972
10. Manual on Stability of Steel Structures (Second Edition). ECCS, 1976, p. 321.
11. **K.J.R. Rasmussen, G.J. Hancock,** Tests of high strength steel columns, J. Constr. Steel Res. 34 (1) (1995) 27–52.
12. **Spoorenberg R.C.** Experimental investigation on residual stresses in heavy

wide flange QST steel sections. Spoorenberg, R.C., Snijder, H.H., L.-G. Cajot, May, M.S. Journal of Constructional Steel Research. 2013. No 89. Pp. 63-74.
13. **M. Abambres Wai-Meng Quach**. Residual stresses in steel members: a review of available analytical expressions. International Journal of Structural Integrity, Vol. 7 Iss 1 (2016) Pp. 70 – 94.
14. **H. Pasternak B. Launert, T. Kannengießer, M. Rhode.** Residual stresses and imperfections in welded high-strength I-shape sections. Insights and Innovations in Structural Engineering, Mechanics and Computation – Zingoni (Ed.) 2016 Taylor & Francis Group, London. Pp. 1139-1146.
15. **Y.B. Wang G.Q. Li, S.W. Chen, F.F. Sun**, Experimental and numerical study on the behavior of axially compressed high strength steel columns with H-section, Eng. Struct. 43 (2012) 149–159.
16. **G. Shi H.Y. Ban, F.S.K. Bijlaard**, Tests and numerical study of ultra-high strength steel columns with end restraints, J. Constr. Steel Res. 70 (2012) Pp. 236–247.
17. **H.Y. Ban, G. Shi, Y.J. Shi, Y.Q. Wang**, Overall buckling behavior of 460 MPa high strength steel columns: experimental investigation and design method, J. Constr. Steel Res. 74 (2012) Pp. 140–150.
18. **Поздеев А.А., Няшин Ю.И., Трусов П.В.** Остаточные напряжения. Теория и приложения. – Изд. «Наука». – М., 1982., 111 с.
19. **Голоднов А.И., Балашова О.С.** К определению остаточного напряженного состояния в сварных элементах коробчатого профиля / Современное промышленное и гражданское строительство, №3. Том 6 (2010), Донбасская нац. академия строительства и архитектуры. – с. 153-158.
20. **Голоднов А.И., Козлова О.Н.** Влияние остаточного напряженного состояния на устойчивость сжатых элементов из труб / Металлические конструкции, №4. Том 13 (2007), Донбасская нац. академия строительства и архитектуры. – с. 181-186.
21. **Иванов А.П., Иванова И.А**. Распределение остаточных напряжений в горячекатаных прокатных профилях / Сборник научных трудов УкрНИПСК им. В.М. Шимановского. Вып. 2, 2008. С. 5-12.
22. **Псюк В.В.** Исследование остаточного напряжённого состояния в прокатных двутаврах / Псюк, В.В., Голоднов А.И., Карапетян, С.Х. // Сборник научных трудов Донбасского государственного технического университета. – 2012. – Выпуск 37. – с. 50-58.
23. **Колмогоров Г.Л.** Кузнецова Е.В., Тиунов В.В. Технологические остаточные напряжения и их влияние на долговечности и надежность металлоизделий. – Пермь: Изд-во ПНИПУ. – 2012. – 226 с.
24. **Картаушин С.И.** Моделирование и расчет остаточных напряжений в прокатных профилях / Картаушин, С.И., Храмова, Д.А., Бильдюк, Н.А. // Известия высших учебных заведений. Машиностроение. – 2017. - №6 (687). – с. 28-34.
25. **Фимкин А.И.** Оценка достоверности расчетно-экспериментальной интерполяционной методики определения остаточных напряжений с помощью численного эксперимента / Строительная механика и расчет сооружений, №5 (250). – 2013. – с. 29-35.
26. **Фимкин А.И.** Применение метода регуляризации Тихонова для определения остаточных напряжений / Строительная механика инженерных конструкций и сооружений, №4. – 2009. – с. 48-55.

Denis V. Konin - PhD, deputy director for scientific work Research Institute of Building Constructions (TSNIISK) named after V. A. Koucherenko JSC Research Center of Construction: 6, 2nd Institutskaya street, 109428, Moscow, Russia; +7-926-853-99-73. E-mail: konden@inbox.ru

Alexander I. Fimkin - PhD, head of the laboratory of the Department of "Construction Mechanics" Russian university of transport: 9-9, Obraztsova street, 127994, Moscow, Russia; +7-919-779-83-19. E-mail:smlab@yandex.ru

Alexander R. Olurombi - PhD, leading researcher of the Laboratory of high-rise buildings and structures of the department of metal structures Research Institute of Building Constructions (TSNIISK) named after V. A. Koucherenko JSC Research Center of Construction, 6, 2nd Institutskaya street, 109428, Moscow, Russia; +7-925-855-53-57. E-mail: alexolrich@gmail.com

Конин Денис Владимирович - кандидат технических наук, заместитель директора по научной работе Центрального научно-исследовательского института строительных конструкций (ЦНИИСК) им. В.А. Кучеренко АО «Научно-исследовательский центр (НИЦ) «Строительство»): 109428, Россия, г. Москва, 2-я Институтская ул., д. 6; +7-926-853-99-73. E-mail: konden@inbox.ru

Александр Иванович Фимкин - кандидат технических наук, заведующий лабораторией кафедры «Строительная механика» Российского университета транспорта: 127994, Россия, г. Москва, ул. Образцова, д. 9, стр. 9; +7-919-779-83-19.E-mail:smlab@yandex.ru

Александр Ричардович Олуромби - кандидат технических наук, ведущий научный сотрудник лаборатории высотных зданий и сооружений отдела металлических конструкций Центрального научно-исследовательского института строительных конструкций (ЦНИИСК) им. В.А. Кучеренко АО «Научно-исследовательский центр (НИЦ) «Строительство»: 109428, Россия, г. Москва, 2-я Институтская ул., д. 6; +7-925-855-53-57. E-mail: alexolrich@gmail.com

DOI:10.22337/2587-9618-2023-19-2-188-204

ACOUSTIC EMISSION-BASED DAMAGE DETECTION IN STEEL FRAMED STRUCTURE- A REVIEW

Mr. Anupam Kumar Biswas [1,2], Dr. Aloke Kumar Datta [1], Dr. Pijush Topdar [1], Dr. Sanjay Sengupta [2]

[1] NIT Durgapur, Durgapur, INDIA

[2] Dr. B.C. Roy Engineering College, Durgapur, INDIA

Abstract: Steel structures are commonly utilized in vast areas in industries, and also now a days they are used in residential settings as well. Structures made of steel is a better alternative as their constructions have high strength, light weight and quick compared to other construction materials. Steel structure degradation is frequently related to an engineering system's underperformance and leads to collapse. Therefore, it is essential to identify the problem and take remedial steps to make sure that structures function as intended throughout their design lives. Among the best non-destructive assessment methods for finding problems is acoustic emission (AE). The current study evaluates the available literature on this method in a few major areas and discusses historical advances in each category. The pros and cons of each approach are discussed, and future study directions are suggested. This review examines the fundamental Acoustic Emission techniques and contemporary research to identify damage in different types of steel structures using various localization approaches. This research aims to find the ideal placement for a real-time sensor to detect deterioration in a steel-framed construction. Finally, the artificial intelligence techniques used to identify deterioration in the steel frame construction are discussed.

Keywords: Acoustic Emission; AE Technique; Structural Damage detection; Steel Frame Structure

ОБНАРУЖЕНИЕ ПОВРЕЖДЕНИЙ В СТАЛЬНЫХ РАМНЫХ КОНСТРУКЦИЯХ АКУСТИЧЕСКИМ МЕИОДОМ: АНАЛИТИЧЕСКИЙ ОБЗОР

Г-н Анупам Кумар Бисвас [1,2], д-р Алоке Кумар Датта [1], д-р Пиюш Топдар [1], д-р Санджай Сенгупта [2]

[1] Национальный институт технологий Дургапура, г. Дургапур, ИНДИЯ

[2] Инженерный колледж им. д-ра Б. К. Роя, г. Дургапур, ИНДИЯ

Аннотация: Стальные конструкции широко используются в промышленности, а в настоящее время они применяются и в жилых зданиях. Конструкции из стали являются лучшей из альтернатив, так как их конструкции обладают высокой прочностью, малым весом и быстровозводимостью по сравнению с другими строительными материалами. Деградация стальных конструкций часто связана с недостаточной эффективностью инженерных систем и приводит к их разрушению. Поэтому очень важно выявить проблему и принять меры по ее устранению, чтобы убедиться, что конструкции функционируют так, как предполагалось, в течение всего проектного срока службы. Одним из лучших неразрушающих методов оценки для поиска повреждений является акустическая эмиссия (АЭ). В данном исследовании оценивается доступная литература по этому методу в нескольких основных областях и обсуждаются исторические достижения в каждой из категорий. Обсуждаются плюсы и минусы каждого подхода, а также предлагаются направления будущих исследований. В данном обзоре рассматриваются фундаментальные методы акустической эмиссии и современные исследования по выявлению повреждений в различных типах стальных конструкций с использованием различных подходов к обнаружению повреждений. Цель данного исследования - найти оптимальное расположение датчика для обнаружения повреждений в стальных конструкциях в режиме реального времени. В заключение обсуждаются методы искусственного интеллекта, используемые для выявления повреждений в стальных конструкциях.

Ключевые слова: акустическая эмиссия; метод акустической эмиссии; обнаружение структурных повреждений; стальная рама

1. INTRODUCTION

Steel, a blend of carbon and iron alloy, is one of the most often used materials in the industry due to its wear- and heat-resistant properties, strength, and fatigue resistance. Among all structural building materials, it is the most widely applicable and adaptable, enabling it to flex without splitting and making it particularly effective at absorbing and dispersing energy. Steel is renowned for providing a framework in architecture that is unmatched by any other substance. Because steel has such high tension and compression strengths, flexibility, and malleability, its components are designed to withstand the elements. Structural steel can take many different forms, including I-beams, Z-beams, HSS-beams, L-beams (angle), structural channels (C-beams with cross sections), T-beams, Rail profiles, bars, rods, plates, open joists made of web steel, and so on. Modern research is becoming increasingly interested in managing any expensive infrastructure. From a techno-economic standpoint, preserving these infrastructural facilities in overall and physical infrastructures in specific is essential. The technical and scientific communities are concerned about departing from their usual functioning. Such deviations or malfunctions are sometimes brought on by structural damage resulting from poor design or construction, an excessive load, ageing, or a natural disaster. Such structural damages call for appropriate corrective action if a structure is to last the whole of its design life. However, the location of the harm and the evaluation of its scope are necessary for such treatments.

An abrupt reorganisation of stresses in a substance results in the formation of an elastic wave known as acoustic emissions. In instance, for damage identification & structure health management, it is often used in non-destructive testing (NDT) of substances including constructions. The fracture activity is quite sensitive to by the AE technique. The benefit of the acoustic emission (AE) approach is that it allows actual structure surveillance by quickly identifying injury which works as an emission source. In other words, the building can be watched in actual. The structure is equipped with AE sensors that detect damage in real-time. Installing detectors inside a building to identify damages in actual time is expensive. As a consequence, in order to conserve money, the quantity of sensors used for structural health surveillance must be reduced to a minimum. The motion of certain fault, including a fracture that might begin but then propagate, which is the reason of acoustic emission waves, results in the redistribution of a stress field within the sample & produces the subsequent AE waves. Rapid energy transfer from a material's interior, which may be caused by factors including crack nucleation or expansion, material dislocations, or yielding, causes high-frequency stress waves [1]. A sensor can capture AE waves, which may be analyzed to learn more about the emission source [2]. The results of the literature review show that analytical studies make up the majority of research on the placement of AE sensors for real-time monitoring in steel-framed buildings, but no such real-world trials where been performed [3-6]. Various structural damage localization strategies are documented in the literature for this situation; among them, the acoustic AE methodology is significant and shows promise for usage in steel structural health monitoring applications. As a result, this article examines steel frame structure damage and categorization based on acoustic emission.

2. IMPORTANT AE PARAMETRIC FEATURES

The parametric features are commonly utilized in AE NDT to study and analyze damage in an object.

AE Event: The parameterization properties of the elasticity waves are created within the substrate are shown by the time domain or frequency domain of the acoustic wave signal. During AE testing, it is the whole AE wave representation.

AE Hit: An AE hit occurs when the AE signals from one channel surpasses the consumer threshold. A test of numerous platforms or an AE event may have multiple hits.

Maximum Amplitude (Amplitude): Greatest amplitude is the maximum amplitude of an AE hit as expressed in voltage or decibels (dB). AE waves that are not captured as AE signals have a peak amplitude lower than the threshold line specified by the user.

Count: The number of pulses in an AE hit that are more than a consumer threshold value is known as a count.

Rise Time: Rise time is the time required for an AE to increase from its initial threshold crossing amplitude to its peak amplitude.

Duration: An AE impact's duration is measured from its initial threshold crossing amplitude to its final threshold crossing amplitude.

Energy: Energy is the collective term for the region beneath the detecting envelope during an AE hit.

Peak Frequency: The frequency component (kHz) in an AE wave spectrum corresponding to the highest amplitude is called the peak frequency.

Frequency on Average: It is the typical frequency of an AE impact. It may be planned by dividing "count" by "duration" and is related to both count and period. It can unevenly predict the signal frequency (once the AE waveform is impossible to store). The entire signal is an acoustic emission effect signal.

Center Frequency: The frequency component (kHz) related to the centre of gravity is what is referred to as the centre frequency in an AE wave spectrum.

Initial Frequency: The beginning frequency of an AE spectrum is indicated by this value. It's calculated by dividing the quantity of "counts" till the peak by the "rise time."

Reverberation Frequency: The connection among total count with beginning count is divided by the connection among period as well as rising time to obtain the reverberation frequency.

RA Score: To determine it, divide the lengthened duration by the highest amplitude (amplitude). It is the inverse of the gradient in the AE signal waveform which indicates the kind of fractures in the unit of ms/V.

b-value; Ib-value: These characteristics constitute a novel technique based on the cumulative event frequency–magnitude distribution, specifically designed for seismic applications. The b-Value approach was originally designed to analyze seismic data populations, but it has since been effectively used on the subject of corrosion [8].
The b-value is defined as:

$$-\mathrm{mathbflogmathit}N = \mathrm{mathit}a - \mathrm{mathit}b\left(\frac{\mathrm{mathit}A_{\mathrm{mathit}d\mathrm{mathit}B}}{20}\right)$$

N refers to the sum of events with an amplitude greater than $\mathrm{mathit}A_{\mathrm{mathit}d\mathrm{mathit}B}$ where $\mathrm{mathit}A_{\mathrm{mathit}d\mathrm{mathit}B}$.b is the event magnitude. B is referred to as the b-value. The enhanced b-value (Ib-value) was presented in [7] as a means of resolving the problems with defining amplitude range and N.

$$\mathrm{mathit}I\mathrm{mathit}b = \frac{\left(\mathrm{mathbflog}_{10}\mathrm{mathit}N(\mathrm{mathit}\omega_1) - \mathrm{mathbflog}_{10}\mathrm{mathit}N(\mathrm{mathit}\omega_2)\right)}{\left(\mathrm{mathit}\sigma(\mathrm{mathit}\alpha_1 + \mathrm{mathit}\alpha_2)\right)}$$

where N(ω1) and N(ω2) are the overall amount of AE events with amplitudes greater than μ – $\mathrm{mathit}\alpha_1\sigma$, and μ + $\mathrm{mathit}\alpha_2\sigma$ accordingly. μ is the mean value of the magnitude distributions

for a certain collection of events, mathitα_1 and mathitα_2 are empiric constants, but also σ is the standard deviation of the magnitude distribution for every set of occurrences [9].

3. AE SENSORS AND DATA ACQUISITION

In actual AE experiments, the piezoelectric sensor is frequently utilized as an AE sensor. Typically, the sensor is of the contact type but has a piezoelectric element protected by a tough metal shell as well as an electric connector for conducting the produced electrical impacts. The sensor structure is powered by the lead zirconate titanate piezoelectric effect (PZT). This kind of sensor is reasonably priced, sensitive, as well as works well in AE investigations to convert mechanical device to electric signal.

The frequency requested in the experiment influences the choice of an appropriate AE sensor. Choosing the appropriate AE sensor for AE testing depends on the frequency response of the propagating elastic wave because the propagation path as well as process to the AE sensor both seriously affect this frequency response.

The proper sensor for AE tests to pressure vessels, storage vessels, heat transfer, pipes, reactor, aerial lift gadgets, nuclear power plants, including biomedical regions are suitably formulated depends on their essential frequency band. According to the frequency band for AE evaluations used by various businesses, sensors are divided into three categories: low-frequency range sensors (20-100 kHz), middle or standard range sensors (100-400 kHz), but also high-frequency range sensors (400 kHz). Companies like Physical Acoustic Corporation (PAC), Vallen System Company, as well as others [10–13] create sensors for the type of commercial AE sensor with high sensitivity.

3.1 AE Wave Propagation and Source Location

The transmission of high-frequency acoustic emission waves may be strongly affected by signal attenuation but also distortion depending on the material, including steel, concrete, or brick/mortar. In Table 1, the highest source sensor distances & typical AE wave velocities for steel are contrasted with those for other building materials. Variation in wave velocity can found with different materials like lesser velocity in brick masonry whereas increasing trend can be seen concrete and steel respectively.

Table 1. Typical AE wave velocities and maximum source-sensor distances for various construction materials.

Materials	The velocity of waves used [m/s]	References
Clay brick masonry	500-2000	[27]
Concrete	2500-4000	[27]
Steel	4000-5500	[27]

The AE approach can be used to locate faults before assessing the damage progression including fracture type by utilising a number of sensors or source location approaches including triangulation [14–17]. Acoustic emission sources in masonry are hard to locate due to the orthotropic structure of the brick and mortar levels, which results in the elastic wave propagating at varied speeds and directions. Second, the porous material's high wave attenuation limits the maximum source sensor distance. Bricks and blocks have higher AE wave velocities than mortar joints. Brick and concrete contacts so serve as reflecting surfaces. As a result, it is advised that every sensor undergo a recognition limit study during site surveillance.

3.2 Source Localization Methods

In this literature, we are using AE technique where several approaches are there for locating sources. Few of them are classified are Wavelet Transform Analysis, Wavelet Transform Analysis and Modal Location (WTML) method, Finite Element Analysis and Geometric Method.

3.2.1 Source Localization by Wavelet Transform Analysis

Wavelet Transform (WT) is a time-frequency analysis-based mathematical process for analyzing

non-stationary signals such as transient AE waves. The wavelet is a time-based signal that is an oscillating signal with one or more cycles. Based on location and scale, this wavelet is utilized to decompose the waveform into several component portions called coefficients. WT gives high frequency and temporal coefficients in two dimensions. The wavelet coefficient represents the wavelet's proportion of correlation with the waveform, and its value indicates the data's third dimension, the amplitude or intensity associated with it. The wavelet technique can view the waveform signal's frequency and time (position). WT fair value indicates that a wave is localized in time and has finite energy. Because of this localized quality, time-domain analysis of given signals can be performed without loss of information.

Rao et al. [18] introduced proof pressure testing of pressure vessels, and acoustic emission (AE) monitoring is used to detect any crack growth-related phenomena. When performing AE monitoring, it is common to discover that the background noise is extremely high. Along with the noise, the signal contains different phenomena such as crack propagation, fastener rubbing, leaks, and so on. Due to noise, identifying the signature of the original signals associated with the above phenomena becomes challenging. In such cases, the wavelet processing technique is more appropriate for analyzing AE signals. The AE data is de-noised using the wavelet processing technique. The de-noised signal is categorized to determine a signature corresponding to the type of phenomenon. In such cases, the wavelet processing technique is more appropriate for analyzing AE signals. The AE data is de-noised using the wavelet processing technique.

3.2.2 Source Localization by Finite Element Analysis

Researchers have recently attempted using the AE approach to use Finite Element Analysis (FEA) for damage localization. However, source severity evaluation requires additional information that can be provided by FE analysis with laboratory fatigue tests. Future years will see an increase in fatigue. Finding damage areas in steel bridges is best accomplished with the AE method. To discover harm from fatigue cracks at welds with shear stud movement at the steel-concrete interface, worldwide and local arrays of the time of arrival source location approaches might be consumed. FE analysis is also useful for detecting regions that are likely to be problematic.

Ai, Li, et al [19] proposed a Finite Element (FE) assessment of a bridge particle is associated to field research location results, confirming regions of likely crack location. The flexural as well as extensional Lamb modes' appearance but also dispersive activity in digitised AE signals were identified. Bandpass frequency filtering is used to demonstrate modal isolation by comparing the frequency properties of the two states. This space is utilized to compute the source-to-sensor distance. AE bridge surveillance might be consumed to position both anticipated but also unforeseen sources, giving precise information on a problem area.

3.2.3 Source Localization by Geometric Method

The triangulation method is used to map the locations of acoustic generators throughout the past three decades. To locate the audio origin in a two-dimensional workstation, three randomly arranged AE sensors are used for sound waves arrival time analysis (i.e. plane surface). On the basis of the path variances among the first, second, as well as third sensors, that have calculated by multiplying the variations in arrival times to the sensors as well as the wave velocity, the position of the acoustic signal was determined analytically utilising polar coordinates in relation to a reference sensor.

Kosnik et al. [20] proposed Two substantial steel Interstate Highway arches, one with a cantilever through truss another with a trapezoidal box girder, were subjected to acoustic emission (AE) analysis on specifics. Quantification activity levels in areas where cracks are confirmed or assumed to exist by observing AE under typical service loads (e.g., live traffic and wind). Cluster analysis offered valuable insight into the horizontal web's acoustic emission characteristics. The clustering approach was first created to monitor the welding

process. As a result, many AE events are identified in a highly confined cluster. While other techniques, such as ultrasonic testing, need up-close access to the crack, AE testing may find and describe a crack within a larger area, making it a more forgiving method in terms of access and precision. A steel bridge detail's stress field is frequently complex, with highly localized stress concentrations. AE is most suited to monitoring small areas of a few tens of square feet in high-stress places like connections.

3.3 Damage Diagnostics in Steel Structure with AE

Damage placement, damage recognition, then damage accumulation recognition are the three stages of damage detection with AE. The initial layer is concerned with determining the damage beginning criteria, regardless of the injury. The impact is then localised using a network of AE sensors but several localization techniques in the second level. In the end, signal processing, supervised classification, then unsupervised clustering methods are used to extract the damage from the AE dataset.

The acoustic emission signals were investigated by Amer, A. Ould, et al. [21] to identify the acoustic fingerprints connected to a certain damage mechanism. Signals from plastic deformation or the spread of fatigue fractures can be differentiated using an unsupervised classification method. Both these processes seem to be the main causes of acoustic emissions in isotropic materials. The key findings are classifying auditory signals into different classifications using multivariate statistical approaches. In austenitic stainless-steel alloys, a number of phenomena, including plastic deformation, martensitic transition, including fatigue fracture propagation, serve as AE sources. At varied total strain amplitudes, AE examined the low cycle fatigue of 304L stainless steel. An association among auditory signals with injury development is revealed by the increase in the EA's activation during fatigue tests. However, when the AE variables are in an area repair mode, even though the aspects mentioned regarding the damage correlating are unsure but also make allocating a signal to damage which happened challenging, the areas identified regarding the harm correlating are uncertain but also present in the area recovery mode for the fatigue tests. Different AE sources are categorized using the k-means cluster technique.

Arvindan, Sivasuriyan, and colleagues [22] looked on structural health monitoring (SHM) together with damage assessments for constructing buildings. The FEM was used to evaluate injury in steel bracing utilising weighted least squares and Bayesian estimation techniques in the first phases of the Eigen-sensitivity-based FE design. The research evaluated scenarios for evaluation including self-monitoring, as well as fault detection but also building evaluation by adding sensors while assuming weaknesses. Modern methods for collecting information & sensor technology enable routine real-time building surveillance. When analysing real-time experiments using analysis methods with sophisticated software, numerical modelling approaches known as the finite element method (FEM) and finite element analysis (FEA) are said. As a result, complicated analyses, such as stiffness and damping, can be carried out very easily and reliably using the FEM technique, even for multi-story buildings.

3.4 Literature Survey on Structural Health Monitoring by Acoustic Emission Technique

In the realm of structural health monitoring (SHM), acoustic emission can be employed for fault recoginition or condition monitoring. It is frequently used in the disciplines of non-destructive testing (NDT), non-destructive evaluation (NDE), with non-destructive monitoring (NDM) for various engineering applications because it is a non-invasive approach. Since its inception, similar applications of AE in seismology have been well documented.

The AE design to material testing is also frequently employed. The splitting, breakage, & unfavourable characteristics of structural parts, flexible components, brittle materials, as well as other components, along with composite materials, are

assessed for a range of manufacturing but also biomedical uses. Furthermore, several smart AE tests are used to examine micro-structural studies as well as metallurgical characteristics of many materials. The AE method is also used to monitor various aeronautical structures. Because many sensors may be conveniently attached to various areas of aerospace structures, the AE approach can perform damage monitoring at a microscopic level as well as damage location in multidimensional characteristics. Wireless AE sensing devices are used in various smart AE techniques to provide real-time wireless monitoring [23]. The next section describes the approaches to Acoustic Emission Techniques, which detect the damages in different structures.

3.4.1 Damage Detection based on Acoustic Emission Techniques

The acoustic emission (AE) approach was proposed by Di et al. [24] which involved 36 direct pull-out experiments to observe the bonding behaviour of steel bars and fiber-reinforced polymer (FRP) in self-compacting concrete (SCC). The FRP reinforced samples get a lower bond strength with a greater corresponding slip value than the steel-reinforced samples because of their low elastic modulus with varying surface treatment. However, acoustic emissions systems can only predict how much damage is there in the material and how long the components will survive on a qualitative basis.

Adamczak-Bugno et al. [25] proposed the acoustic emission signal (AE) in the diagnostics of procedural services is discussed in this article. One area of technology where the AE technique can be applied is in the monitoring of steel structure's technical condition. The ability to record and analyze the AE signal proved useful in diagnosing this structure. Moreover, metal deformation causes a weak AE, and the creation and growth of fractures are frequently accompanied by a significant AE, particularly in additional hard materials, i.e. those with less deformability with advanced strength. The link between AE signals and destructive processes paves the way for more research into statistical, probabilistic models that describe structural durability variations while considering actual working conditions and the severity of damage development assessed "in-situ."

Khan et al. [26] presented an external force (such as altering pressure, load, or temperature), a microfracture within the body to release energy in the form of an AE wave, which is detected by a sensor and turned into an electrical signal for inspection. Many studies are currently being conducted on the theories underlying AE production, transmission, and inspection in numerous domains as a vital health monitoring tool for NDT. a "feature view of AE" depends on historical, current, with future perspectives; Smarter structural health monitoring techniques with industrial as well as structural approaches, as well as an "AE monitoring" methodology utilizing theoretical & experimental perspectives. Parametric analysis but also AE source location are two main features of the AE approach in structural health monitoring.

Verstrynge et al. [27] proposed the literature on applying acoustic emission techniques to masonry structures, focusing on unique issues and current findings. In light of monitoring approaches, wave propagation, source localization, with the crack formation under static, fatigue, as well as creep loads, AE-based methods for damage assessment in masonry are explored. However, the technique's non-invasive nature and great sensitivity offer intriguing possibilities for locating damage, determining the severity of the damage, and determining the degradation rate, particularly for historic masonry structures. Acoustic emission information from periodic measurements were analysed to determine whether the technology might be used for on-site monitoring.

Debonding testing during the acoustic emission (AE) approach was developed by Ghiassiet al. [28] to examine interfacial fracture but also damage propagation in bricks reinforced with GFRP and SRG. Single-lap shear bond tests assess the activity of the bond while AE sensors monitor the development of the fracture. The fracture progress but also active debonding

processes are described utilizing the AE procedure's findings. employing AE techniques to check the health of reinforced masonry constructions on the spot. The findings revealed that AE output could be effectively employed for investigating and interpreting the debonding fracture process.

Świt et al. [29] investigated the method of acoustic emission (AE), which is founded on destructive processes. The outcomes of using the AE approach to find potential candidates have been presented in this article as active damaging processes and monitoring their progression during the normal functioning of diverse machine structures of various kinds. A suitable technique must be designed to identify the beginning of the process of degradation as well as enable monitoring of its progress all across the entire chapter of the formation, not just in subjectively chosen areas. This is because locating as well as monitoring potential damage as well as assessing its effect on the structure of the system are both components of the service life assessment process.

The overall review of the Acoustic Emission Techniques is described in table 2, which is given below.

Table 2. Review of Damage Detection Techniques based on Acoustic Emission Techniques.

Ref. No	**Advantages**	**Limitations**	**Performance Measures**	**Structures/ Technique**
[24]	High strength, lightweight, long-term durability, and low maintenance costs	Damages in materials	more sensitive, larger measuring ranges	FRP and SCC/ AE
[25]	load-bearing capacity and serviceability	Very weak signals	Durability	Steel Structure/AE
[26]	characterizing damage propagation behaviour, overall damage monitoring system	smart applications in structural health monitoring	The event, Hit, Amplitude, Count, Rise Time, Duration, Frequency	General/.Parametric analysis with AE
[27]	Signal attenuation places restrictions on the placement and density of AE sensors.	Algorithms for locating sources and correcting waveforms in various brickwork types	Amplitude And Energy	Masonry structures
[28]	Due to its low weight-to-strength proportion & adaptability in regards to application, FRPs are a strong option.	due to the AE wave's considerable attenuation and disruption	arrival time, amplitude, count, period and energy, threshold, but also sampling frequency	Bricks
[29]	Assessments are designed to encompass the entire material being evaluated but can be carried out under real operational loads.	how long the components will last	Durability, safety, and usability	Machine structures/ Destructive processes

Based on the current works, we can infer that numerous works have been done for Acoustic Emission based on various constraints such as sensors, wave and propagation, source localization, and signal approaches outperforming other constraints.

3.4.2 Review of damage detection in steel frame structure

Black, C. J et al. [30] introduced the information offered to possible participants in the blind test on damage detection for a steel frame and the answer. The data for this test came from a one-third-scale steel frame structure finite element model. Damage was mimicked by removing members or modifying member attributes in a small area. The cost and time necessary to restore a structure could be greatly reduced if the degree and location of damage could be estimated using modal analysis techniques.

Modal flexibility (MF)-based methodologies in vibration-based damage detection (VBDD) were used by Bernagozzi, G. et al. [31] to establish an experimental flexibility matrix of materials that may be produced from recognized natural frequencies with the mode shapes. Using operational mode analytic methods, these properties can be obtained from ambient vibration (AV) information. Modal flexibility (MF)-based procedures in vibration-based damage detection (VBDD) are able to generate empirical versatility matrices of structures from known natural frequencies and mode shapes. Using functional mode analytic methods, these qualities can be extrapolated from ambient vibration signals.

Modal parameter changes were introduced by Dohler M. et al. [32]. However, in a recommended and successfully utilized subspace-based damage identification test, estimation of the modal properties is omitted. The new test, designed to resist shifting excitation qualities, performed substantially better in this environment, detecting damage far earlier than a preceding traditional test for damage identification. The applications in which the stimulation is ambient & uncontrolled should benefit from the supplied test resistive to excitation changes. The new procedure is anticipated to further accurately as well as earlier identify defects.

A wavelet-based structural damage identification method was proposed by Hou Z et al. [33]. It is regarded as a typical Fourier transform with a flexible window size and location. Its ability to analyse local information with a "zoom lens with changing focus" to generate a variety of levels of analysis including estimates of the original signal is one of wavelet analysis' strongest points. A detectability map explores the effects of noise level and damage severity.

The overall review of the steel frame structure is described in table 3, which is given below.

Table 3. Review of damage detection in the steel frame structure

Citation	**Technique Used**	**Advantages**	**Limitations**	**Performance Measures**	**Structures**
[30]	Modal Analysis Techniques/finite element model	The Cost And Time Required To Repair A Structure Could Be Significantly Reduced	Invisible to determine damage	White noise, Maximum Amplitude	Steel frame

[31]	Modal Flexibility/ambient vibration	By recognising the stories with routes, harm locations can be determined.	Modal Truncation Errors	Ambient Vibration	Plane shear-type
[32]	Subspace	Early but More Reliable Damage Detection	The Reversibility Of Generated Damages ensures Fatigue Crack, The Reproducibility Of Test Series.	Ambient Vibration, Threshold	Steel frame
[33]	Wavelet	Excessive Response, Crack Growth	Effects Of Noise Intensity And Damage Severity	Reliable, Efficient, And Low Cost	Steel frame

Based on those mentioned above, we may conclude that the steel frame structure has been utilized for various purposes such as noise level, amplitude, ambient vibration, threshold, piezoelectric sensor, Plane shear-type, and Finite Element Model.

3.4.3 Acoustic Emission in Steel Frame with Machine Learning Technique

To find steel fractures, the digital data was analysed then categorised using a deep learning algorithm after being normalised to reduce background noise. The deep learning-based AE method was applied locally to identify steel faults. The distinctive aspect of the research is the effective detection but also localization of steel cracks utilising a single AE sensor and an AE signal-based deep learning system.

Since the cracking method (strength properties or shearing) is connected to the underlying physical principles, Das et al. [34] established the Crack mode classification as a massively important technique to determine the harm status of a structural for good preservation to promote structural security with reliability. In this study, a framework was developed. The automatic probabilistic classification of cracks in cementitious components uses AE signals. The framework was utilised to analyse AE data from samples of direct stress Strain Hardening Cementitious Composite (SHCC) and bending Steel Fiber Reinforced Concrete (SFRC) beams. It is demonstrated that the cracking modes of the proposed ML method accord with composite theory expectations.

Azimi, M. et al. [35] developed various SHM applications by reviewing recent publications in SHM that use developing DL-based approaches. A better understanding is presented in form of many DL techniques, including deep neural networks, transfer learning, and others. Along with some of the latest innovations consumed for SHM, such as sensors including unmanned aerial vehicles, the method as well as application of vibration-based but also vision-based monitoring are explained (UAVs). The study is concluded with a discussion of the advantages and disadvantages of DL-based methods in SHM arrangements.

A straightforward experimental method was created by Paulraj, Murugesa Pandiyan, and colleagues to keep the steel plate in compliance with the supported boundary condition [36]. The steel structure's vibration patterns are collected using a simple methodology based on impact testing. Under typical circumstances, the steel plate's vibration signals are recorded. The Fishman criterion is used to determine the network's performance. SHM aims to assure

high reliability and low maintenance costs over the structure's lifetime. The vibrating signal that travels through a steel plate when an impulse force is applied can detect damage. To recover the characteristics from the vibration analysis, feature extraction methods based on frame energy-based statistical time-domain signal processing techniques are created.

Structural damage detection, a hybrid method based on ANNs but also genetic algorithms, was proposed by Betti et al. [37]. Accelerations caused by ambient vibrations were observed as the frame's damage grew worse, as well as the damaged entity was determined by the depth of the cut. At every stage of damage, the fundamental characteristics of the steel frame (natural frequencies & modal geometries) were examined. The fact that the training could be performed on any structure due to the indexes' extensive range of attributes is one of the main benefits of feeding the system with the four indices stated above.

Table 4. Review of Acoustic Emission with Machine Learning

Citation	Technique Used	Advantages	Limitations	Performance Measures	Structures
[34]	Machine learning	Structural Safety, Durability	limitation, need for huge training set, plus loss of physical interpretations	RA values and Average frequency	Tensile or Shear
[35]	Deep Learning; Machine Learning	Performance By Cross-Validation, Accuracy.	Image-Processing For Crack Detection.	Feature Extraction, Pattern Classification, And Regression	Steel frame
[36]	Artificial Neural Network	high reliability, less maintenance	Energy that manifests as vibration is impacted	Activation Function, Learning Rate, And Momentum	steel structure
[37]	Artificial neural networks	Training is performed with different structures	Identifying A Proper Fitness Function; Non-Optimal Solution	Size, The Mutation and The Crossover Rate, The Elitism Rate, The Selection Methods	Three-Storey Steel Structure

Based on those mentioned earlier, we may conclude that acoustic emission with machine learning has been utilized for various purposes, such as Artificial neural networks, Deep Learning, and Machine Learning.

4. DISCUSSION

Various strategies for improving the accuracy of the AE parameters source locations and mechanisms have been devised, with some employed and others requiring more

investigation. With recently improved sensor techniques and signal processing techniques, there is a lot of potential for frequency-domain investigations of AE; however, recent research has only extracted a small amount of data from the frequency-domain of AE. Because of the differentiation between high- and low-frequency ranges, AE can be examined in specific frequency bands. Moreover, Acoustic Emission with Machine Learning for detecting damages in steel. By using mean amplitude and standard deviation of the amplitude distributions, another important parameter, the b-value, is improved. However, the attenuation effect on the amplitude distribution is often overlooked, leading in a decrease in the b-value. The AE approach appears useful in structural health monitoring of industrial buildings with steel making up the majority of the structural elements, which is the most significant finding. According, to the findings, all the problems evaluated could be recognized using acoustic emissions. Therefore, real-time damage identification in a steel-framed structure is accomplished using our Acoustic emission approach.

5. CHALLENGES AND FUTURE DIRECTIONS

It is possible to do research to modify normal AE practises for concrete to be used in masonry. It would be a huge advancement to develop high-sensitivity, reliable, as well as integrated AE sensors for site surveillance.

1. In order to advance in this field, fibre optics with multi-frequency spectrum sensors are now being utilised. To provide a strong connection among AE data as well as the damage mechanism, the majority of sites surveillance concentrates on a single degrading event or places sensors close to active fracture areas. Devoted filtration methods with multi-sensor systems might be advantageous for applications in noisy environments (such as crossings) but several damage mechanisms (such as creep and salt efflorescence). Our understanding of AE signal propagation has recently increased with to advancements in instrumentation, sensors, signal processing, & data fusion techniques.
2. Considering current developments in high-speed digital waveform-based AE devices, large quantities of AE waveforms signals are now digitised then saved for evaluation. These developments have led to a greater comprehension of AE signal transmission in relation of directed acoustic patterns, especially when coupled with innovations in high fidelity, highly sensitive wideband detectors as well as the creation of contemporary PC-based signal processing techniques. The approach, later named "Modal AE," can shift away from the conventional focus on data analysis thus significantly improve AE's structural health monitoring capabilities.
3. Future SHM is anticipated to be enhanced by modern AE programs that make use of different modelling software & artificial intelligence technology. Future discussions are likely to focus on topics like newer, smaller sensors, monitoring systems, features but also grouping analytics, even AE monitoring in harsh environments, to name just a few. For sustainable communities, more effective AE procedures are needed now more than ever.

6. CONCLUSION

AE is a significant application method for monitoring structures because of its non-invasive nature and great sensitivity. The steel framework may be simply changed and expanded if necessary. Steel is a dimensionally accurate material produced using modern computer technology. Steel buildings allow for long spans. In order to lay a solid foundation for future developments as well as improve the use of AE sensing in steel, this review study offered a thorough literature review on damage identification in steel frame structures utilising the acoustic emission technique. In this review,

we examined the application of acoustic emission to detect but also categorise harm to steel frames.

REFERENCES

1. **Emission, Mark, F.** Carlos-Acoustic. Heeding the Warning Sounds from Materials. *ASTM Standardisation News.* 2003.
2. **Holford, K.M. and Lark, R.J.** Acoustic emission testing of bridges, in Inspection and monitoring techniques for bridges and civil structures. *G. Fu, Editor. 2005, Wood head Publishing Limited and CRC*. P.183-215.
3. **Udwadia, Firdaus, E.** Methodology for optimum sensor locations for parameter identification in dynamic systems. *Journal of Engineering Mechanics.* 1994, 120(2), p. 368-390.
4. **Shah, P.C., and Udwadia, F.E.** A methodology for optimal sensor locations for identification of dynamic systems. 1978, p.188-196.
5. **Datta, A.K., Shrikhande, M., and Paul, D.K.** On the optimal location of sensors in multi-storeyed buildings. *Journal of earthquake engineering.* 2002, 6(1), p. 17-30.
6. **Li, Z.N., Tang, J., and Li, Q.S.** Optimal sensor locations for structural vibration measurements. *Applied Acoustics.* 2004, 65(8), p.807-818
7. **Calabrese, L., Galeano, M., Proverbio, E**. The use of b-value and Ib-value of acoustic emission in monitoring hydrogen-assisted cracking of martensitic stainless steel. *Int. J. Micro struct. Mater. Prop.* 2017, 12, p.165–182.
8. **Behnia, A., Chai, H.K., Shiotani, T.** Advanced structural health monitoring of concrete structures with the aid of acoustic emission. Constr. *Build. Mater.* 2014, 65, p.282–302.
9. **Shiotani, T., Yuyama, S., Li, ZW., Ohtsu, M.** Application of AE improved b-value to quantitative evaluation of fracture process in concrete materials. *J. Acoust. Emiss.* 2001, 19, p.118–133.
10. MISTRAS Group Inc. Express-8 AE System user's Manual, Rev 0, Part#: 7050-1000. *Physical Acoustic Corporation,* 2014
11. **Hatano, H., Watanabe, T.** Reciprocity calibration of acoustic emission transducers in Rayleigh wave and longitudinal wave sound field. *The Journal of the Acoustical Society of America.* 1997, 101, p.1450-1455
12. **Hsu, N.N., Breckenridge, F.R.** Characterization and calibration of acoustic emission sensors. *Materials Evaluation.* 1981, 39, p.60-68
13. Vallen Systeme GmbH. Acoustic Emission Sensors Specification; 2015. *Available from: http://www.vallen.de/zdownload/pdf/sov1507.pdf [Accessed 2018-07-03]*
14. **Shehadeh M., Steel J.A., Reuben R.L.** Acoustic emission source location for steel pipe and pipeline applications: the role of arrival time estimation. *Proceedings of the Institution of Mechanical Engineers Part E-Journal of Process Mechanical Engineering.* 2006, 220(E2), p.121-133.
15. **Shetty N., Livitsanos G., Van Hemelrijck D., Aggelis D.G., Wevers M., Verstrynge E.** Characterization of mechanical behaviour of masonry under compression using acoustic emission. *in 8th International Conference on Acoustic Emission Kyoto, Japan.* 2016, p.365-370
16. **Shah S.P., Li Z.** Localization of micro cracking in concrete under uniaxial tension. *ACI Materials Journal.* 1994, 91(4), p.372–381.
17. **Grosse C.U., Reinhardt H.W., Dahm T.** Localization and classification of fracture types in concrete with quantitative acoustic emission measurement techniques. *NDT & E International.* 1997, 30(4), p.223-230
18. **Rao, S.S., & Subramanian, B.** Analysis of Acoustic Emission Signals using Wavelet

Transformation Technique. *Defense Science Journal*. 2008, 58(4), p.559.

19. **Ai, L., Greer, B., Hill, J., Soltangharaei, V., & Ziehl, R.A.P.** Finite element modelling of acoustic emission in dry cask storage systems generated by cosine bell sources. *In AIP Conference Proceedings.* 2019, 2102(1), 130001.
20. **Kosnik, D.E., Hopwood, T., & Corr, D.J**. Acoustic emission monitoring for assessment of steel bridge details. *In AIP Conference Proceedings,* 2011, 1335(1), 1410-1417.
21. **Amer, A.O., Gloanec, A.L., Courtin, S., & Touze, C.** Characterization of fatigue damage in 304L steel by an acoustic emission method. *Procedia Engineering.* 2013, 66, p. 651-660.
22. **Sivasuriyan, A., Vijayan, D.S., Górski, W., Wodzyński, Ł., Vaverková, M.D., & Koda, E.** Practical implementation of structural health monitoring in multi-story buildings. *Buildings*. 2021, 11(6), p. 263
23. **Colada, M., Prevorovsky, Z.** Remote AE monitoring of fatigue crack growth in complex aircraft structures. *In: Proceedings, 30th European Conference on Acoustic Emission Testing & 7th International Conference on Acoustic Emission,* 2012, p. 12-15.
24. **Di, Bo, Jingkai Wang, Haotian Li, Jinhang Zheng, Yu Zheng, and Gangbing Song.** Investigation of bonding behaviour of FRP and steel bars in self-compacting concrete structures using acoustic emission method. *Sensors.* 2019, 19(1), 159.
25. **Adamczak-Bugno, A., Swit, G., & Krampikowska, A.** Application of the Acoustic Emission Method in the Assessment of the Technical Condition of Steel Structures. *In IOP Conference Series: Materials Science and Engineering.* 2019, 471(3), p. 032041.
26. **Khan, M.T.I.** Structural Health Monitoring by Acoustic Emission. Structural Health Monitoring from Sensing to Processing. 2018, 23.
27. **Verstrynge, E., Lacidogna, G., Accornero, F., & Tomor, A.** A review on acoustic emission monitoring for damage detection in masonry structures. *Construction and Building Materials.* 2021, 268, 121089.
28. **Ghiassi, B., Verstrynge, E., Lourenço, P.B., & Oliveira, D.V.** Characterization of debonding in FRP-strengthened masonry using the acoustic emission technique. *Engineering Structures*. 2014, 66, p.24-34.
29. **Świt, G.** Acoustic emission method for locating and identifying active, destructive processes in operating facilities. *Applied Sciences.* 2018, 8(8), p.1295.
30. **Black, C.J., & Ventura, C.E.** Blind test on damage detection of a steel frame structure. In Society for Experimental Mechanics. *Inc, 16 the International Modal Analysis Conference.* 1998, 1, p. 623-629.
31. **Bernagozzi, G., Ventura, C.E., Allahdadian, S., Kaya, Y., Landi, L., & Diotallevi, P.P.** Application of modal flexibility-based deflections for damage diagnosis of a steel frame structure. *Procedia Engineering*. 2017, 199, p.2026-2033.
32. **Döhler, M., & Hille, F.** Subspace-based damage detection on steel frame structure under changing excitation. In *Structural Health Monitoring.* 2014, 5, p. 167-174.
33. **Hou, Z., Noori, M.N., & St Amand, R.** Wavelet-based approach for structural damage detection. *Journal of Engineering Mechanics.* 2000, 126(7), p.677.
34. **Das, A.K., Suthar, D., & Leung, C.K.** Machine learning-based crack mode classification from unlabeled acoustic emission waveform features. *Cement and Concrete Research*. 2019, 121, p.42-57.
35. **Azimi, M., Eslamlou, A.D., Pekcan, G.** Data-Driven Structural Health Monitoring, and Damage Detection through Deep Learning: State-of-the-Art Review.

Sensors. 2020, 20, p.2778. https://doi.org/10.3390/s20102778

36. **Paulraj, M.P., Yaacob, S., Majid, M.A., Kazim, M.N.F.M., & Krishnan, P.** Structural steel plate damage detection using non-destructive testing, frame energy-based statistical features, and artificial neural networks. *Procedia Engineering.* 2013, 53, p.376-386.
37. **Betti, M., Facchini, L., & Biagini, P.** Damage detection on a three-story steel frame using artificial neural networks and genetic algorithms. *Meccanica*, 2015, 50(3), p.875-886.

СПИСОК ЛИТЕРАТУРЫ

38. **Emission, Mark, F.** Carlos-Acoustic. Heeding the Warning Sounds from Materials. *ASTM Standardisation News.* 2003.
39. **Holford, K.M. and Lark, R.J.** Acoustic emission testing of bridges, in Inspection and monitoring techniques for bridges and civil structures. *G. Fu, Editor. 2005, Wood head Publishing Limited and CRC*. P.183-215.
40. **Udwadia, Firdaus, E.** Methodology for optimum sensor locations for parameter identification in dynamic systems. *Journal of Engineering Mechanics.* 1994, 120(2), p. 368-390.
41. **Shah, P.C., and Udwadia, F.E.** A methodology for optimal sensor locations for identification of dynamic systems. 1978, p.188-196.
42. **Datta, A.K., Shrikhande, M., and Paul, D.K.** On the optimal location of sensors in multi-storeyed buildings. *Journal of earthquake engineering.* 2002, 6(1), p. 17-30.
43. **Li, Z.N., Tang, J., and Li, Q.S.** Optimal sensor locations for structural vibration measurements. *Applied Acoustics.* 2004, 65(8), p.807-818
44. **Calabrese, L., Galeano, M., Proverbio, E**. The use of b-value and Ib-value of acoustic emission in monitoring hydrogen-assisted cracking of martensitic stainless steel. *Int. J. Micro struct. Mater. Prop.* 2017, 12, p.165–182.
45. **Behnia, A., Chai, H.K., Shiotani, T.** Advanced structural health monitoring of concrete structures with the aid of acoustic emission. Constr. *Build. Mater.* 2014, 65, p.282–302.
46. **Shiotani, T., Yuyama, S., Li, ZW., Ohtsu, M.** Application of AE improved b-value to quantitative evaluation of fracture process in concrete materials. *J. Acoust. Emiss.* 2001, 19, p.118–133.
47. MISTRAS Group Inc. Express-8 AE System user's Manual, Rev 0, Part#: 7050-1000. *Physical Acoustic Corporation,* 2014
48. **Hatano, H., Watanabe, T.** Reciprocity calibration of acoustic emission transducers in Rayleigh wave and longitudinal wave sound field. *The Journal of the Acoustical Society of America.* 1997, 101, p.1450-1455
49. **Hsu, N.N., Breckenridge, F.R.** Characterization and calibration of acoustic emission sensors. *Materials Evaluation.* 1981, 39, p.60-68
50. Vallen Systeme GmbH. Acoustic Emission Sensors Specification; 2015. *Available from: http://www.vallen.de/zdownload/pdf/sov1507.pdf [Accessed 2018-07-03]*
51. **Shehadeh M., Steel J.A., Reuben R.L.** Acoustic emission source location for steel pipe and pipeline applications: the role of arrival time estimation. *Proceedings of the Institution of Mechanical Engineers Part E-Journal of Process Mechanical Engineering.* 2006, 220(E2), p.121-133.
52. **Shetty N., Livitsanos G., Van Hemelrijck D., Aggelis D.G., Wevers M., Verstrynge E.** Characterization of mechanical behaviour of masonry under compression using acoustic emission. *in 8th International Conference on Acoustic Emission Kyoto, Japan.* 2016, p.365-370

53. **Shah S.P., Li Z.** Localization of micro cracking in concrete under uniaxial tension. *ACI Materials Journal.* 1994, 91(4), p.372–381.
54. **Grosse C.U., Reinhardt H.W., Dahm T.** Localization and classification of fracture types in concrete with quantitative acoustic emission measurement techniques. *NDT & E International.* 1997, 30(4), p.223-230
55. **Rao, S.S., & Subramanian, B.** Analysis of Acoustic Emission Signals using Wavelet Transformation Technique. *Defense Science Journal*. 2008, 58(4), p.559.
56. **Ai, L., Greer, B., Hill, J., Soltangharaei, V., & Ziehl, R.A.P.** Finite element modelling of acoustic emission in dry cask storage systems generated by cosine bell sources. *In AIP Conference Proceedings.* 2019, 2102(1), 130001.
57. **Kosnik, D.E., Hopwood, T., & Corr, D.J**. Acoustic emission monitoring for assessment of steel bridge details. *In AIP Conference Proceedings,* 2011, 1335(1), 1410-1417.
58. **Amer, A.O., Gloanec, A.L., Courtin, S., & Touze, C.** Characterization of fatigue damage in 304L steel by an acoustic emission method. *Procedia Engineering.* 2013, 66, p. 651-660.
59. **Sivasuriyan, A., Vijayan, D.S., Górski, W., Wodzyński, Ł., Vaverková, M.D., & Koda, E.** Practical implementation of structural health monitoring in multi-story buildings. *Buildings*. 2021, 11(6), p. 263
60. **Colada, M., Prevorovsky, Z.** Remote AE monitoring of fatigue crack growth in complex aircraft structures. *In: Proceedings, 30th European Conference on Acoustic Emission Testing & 7th International Conference on Acoustic Emission,* 2012, p. 12-15.
61. **Di, Bo, Jingkai Wang, Haotian Li, Jinhang Zheng, Yu Zheng, and Gangbing Song.** Investigation of bonding behaviour of FRP and steel bars in self-compacting concrete structures using acoustic emission method. *Sensors.* 2019, 19(1), 159.
62. **Adamczak-Bugno, A., Swit, G., & Krampikowska, A.** Application of the Acoustic Emission Method in the Assessment of the Technical Condition of Steel Structures. *In IOP Conference Series: Materials Science and Engineering.* 2019, 471(3), p. 032041.
63. **Khan, M.T.I.** Structural Health Monitoring by Acoustic Emission. Structural Health Monitoring from Sensing to Processing. 2018, 23.
64. **Verstrynge, E., Lacidogna, G., Accornero, F., & Tomor, A.** A review on acoustic emission monitoring for damage detection in masonry structures. *Construction and Building Materials.* 2021, 268, 121089.
65. **Ghiassi, B., Verstrynge, E., Lourenço, P.B., & Oliveira, D.V.** Characterization of debonding in FRP-strengthened masonry using the acoustic emission technique. *Engineering Structures*. 2014, 66, p.24-34.
66. **Świt, G.** Acoustic emission method for locating and identifying active, destructive processes in operating facilities. *Applied Sciences.* 2018, 8(8), p.1295.
67. **Black, C.J., & Ventura, C.E.** Blind test on damage detection of a steel frame structure. In Society for Experimental Mechanics. *Inc, 16 the International Modal Analysis Conference.* 1998, 1, p. 623-629.
68. **Bernagozzi, G., Ventura, C.E., Allahdadian, S., Kaya, Y., Landi, L., & Diotallevi, P.P.** Application of modal flexibility-based deflections for damage diagnosis of a steel frame structure. *Procedia Engineering*. 2017, 199, p.2026-2033.
69. **Döhler, M., & Hille, F.** Subspace-based damage detection on steel frame structure under changing excitation. In *Structural Health Monitoring.* 2014, 5, p. 167-174.
70. **Hou, Z., Noori, M.N., & St Amand, R.** Wavelet-based approach for structural

damage detection. *Journal of Engineering Mechanics.* 2000, 126(7), p.677.

71. **Das, A.K., Suthar, D., & Leung, C.K.** Machine learning-based crack mode classification from unlabeled acoustic emission waveform features. *Cement and Concrete Research*. 2019, 121, p.42-57.
72. **Azimi, M., Eslamlou, A.D., Pekcan, G.** Data-Driven Structural Health Monitoring, and Damage Detection through Deep Learning: State-of-the-Art Review. *Sensors*. 2020, 20, p.2778. https://doi.org/10.3390/s20102778
73. **Paulraj, M.P., Yaacob, S., Majid, M.A., Kazim, M.N.F.M., & Krishnan, P.** Structural steel plate damage detection using non-destructive testing, frame energy-based statistical features, and artificial neural networks. *Procedia Engineering.* 2013, 53, p.376-386.
74. **Betti, M., Facchini, L., & Biagini, P.** Damage detection on a three-story steel frame using artificial neural networks and genetic algorithms. *Meccanica*, 2015, 50(3), p.875-886.

Anupam Kumar Biswas, Research Scholar, Department of Civil Engineering, NIT Durgapur, 713209, W.B India,Assistant Professor, Dr. B.C. Roy Engineering College, Durgapur 713206, W.B India, anupamkumarbiswas123@gmail.com.

Aloke Kumar Datta, Associate Professor, Department of Civil Engineering, NIT Durgapur, Durgapur 713209, W.B India, alokekumardatta1234@gmail.com.

Pijush Topdar, Associate Professor, Department of Civil Engineering, NIT Durgapur, Durgapur 713209, W.B India, pijushtopdar@gmail.com.

Sanjay Sengupta, Associate Professor, Department of Civil Engineering, Dr. B.C. Roy Engineering College, Durgapur, 713206, W.B, India. anjaysengupta321@gmail.com.

Анупам Кумар Бисвас, научный сотрудник, факультет гражданского строительства, НИТ Дургапур, 713209, Западная Индия, доцент, Инженерный колледж им. доктора Б. К. Роя, Дургапур 713206, Индия, anupamkumarbiswas123@gmail.com.

Алок Кумар Дате, доцент кафедры гражданского строительства, NET Durgapur, Дургапур 713209, Западная Индия, alokekumardatta1234@gmail.com.

Пиджуш Топдар, доцент кафедры гражданского строительства, г. Дургапур 713209, Индия, pijushtopdar@gmail.com.

Санджай Сенгупта, доцент кафедры гражданского строительства инженерного колледжа им. доктора Б.К. Роя, Дургапур, 713206, Индия. anjaysengupta321@gmail.com.

О ВОСЬМОМ МЕЖДУНАРОДНОМ СИМПОЗИУМЕ РААСН «АКТУАЛЬНЫЕ ПРОБЛЕМЫ КОМПЬЮТЕРНОГО МОДЕЛИРОВАНИЯ КОНСТРУКЦИЙ И СООРУЖЕНИЙ»

Травуш В.И., Акимов П.А., Белостоцкий А.М., Сидоров В.Н., Монастырев П.В.

Ключевые слова: компьютерное моделирование; конструкции и сооружения; Российская академия архитектуры и строительных наук (РААСН).

1. ОБЩАЯ ИНФОРМАЦИЯ

Восьмой международный симпозиум «Актуальные проблемы компьютерного моделирования конструкций и сооружений» Российской академии архитектуры и строительных наук проходил в период с 17-21 мая 2023 г. в городе Тамбове на базе федерального государственного бюджетного образовательного учреждения высшего образования «Тамбовский государственный технический университет» (далее – ТГТУ), основные организаторы в ТГТУ – член-корреспондент РААСН, проф., д.т.н. П.В. Монастырев, доц., к.т.н. О.В. Евдокимцев. В этом году ТГТУ, одному из ведущих российских вузов, исполнятся 65 лет со дня его образования и 30 лет с момента получения статуса университета в регионе.



Рис. 1. Главный корпус Тамбовского государственного технического университета

Решение о проведении Симпозиума было принято Научным Советом РААСН «Цифровые технологии в строительстве и архитектуре» в июле 2021 года. Первый Симпозиум прошел в 2007 году в Нижнем Новгороде, затем Симпозиумы РААСН проводились в Перми, Новочеркасске, Челябинске, Иркутске, Владивостоке и Новосибирске [1] - [3].

В этом году Симпозиум на площадке ТГТУ собрал более 200 участников из 40 регионов Российской Федерации и зарубежных государств. Было представлено более 190 устных и стендовых докладов, которые опубликованы в сборнике тезисов Симпозиума [1]. В организации и проведении Симпозиума, а также в выступлении с пленарными и секционными докладами приняли участие более 45 членов РААСН. Среди них вице-президент РААСН, академик РААСН, проф., д.т.н. В.И. Травуш; академик-секретарь Отделения строительных наук РААСН, академик РААСН, проф., д.т.н. Н.И. Карпенко; академик РААСН, проф., д.т.н. П.А. Акимов; академик РААСН, проф., д.т.н. А.М. Белостоцкий; академик РААСН, проф., д.т.н. С.С. Каприелов; академик РААСН, проф., д.т.н. В.И. Колчунов; академик РААСН, проф., д.т.н. Л.С. Ляхович; академик РААСН, проф., д.т.н. В.П. Селяев; академик РААСН, проф., д.т.н. В.И. Теличенко; академик РААСН, проф., д.т.н. С.В. Федосов; член-корреспондент РААСН, проф., д.т.н. Г.Г. Кашеварова; член-корреспондент РААСН, проф., д.т.н. Вл.И. Колчунов; член-корреспондент РААСН, проф., д.т.н. С.Б. Крылов; член-корреспондент РААСН, проф., д.т.н. С.А. Кудрявцев; член-корреспондент РААСН, проф., д.т.н. Р.А. Мангушев; член-корреспондент РААСН, проф., д.т.н. И.Т. Мирсаяпов; член-корреспондент РААСН, проф., д.т.н. П.В. Монастырев; член-корреспондент РААСН, проф., д.т.н. В.Л. Мондрус; член-корреспондент РААСН, проф., д.т.н. А.Н. Потапов; член-корреспондент РААСН, д.т.н. В.Е. Румянцева, член-корреспондент РААСН, проф., д.т.н. В.Н. Сидоров; член-корреспондент РААСН, проф., д.т.н. А.А. Трещев и др.

Соорганизаторами 8-го Симпозиума выступили Правительство Тамбовской области, федеральное государственное бюджетное образовательное учреждение высшего образования «Национальный исследовательский Московский государственный строительный университет» (НИУ МГСУ), федеральное государственное бюджетное образовательное учреждение высшего образования «Московский архитектурный институт (государственная академия)» (МАрхИ), федеральное государственное бюджетное образовательное учреждение высшего образования «Новосибирский государственный архитектурно-строительный университет (Сибстрин)» (НГАСУ (Сибстрин)), федеральное государственное бюджетное образовательное учреждение высшего образования «Российский университет транспорта (МИИТ)» (РУТ (МИИТ)), федеральное государственное бюджетное образовательное учреждение высшего образования «Томский государственный архитектурно-строительный университет» (ТГАСУ), акционерное общество «Научно-исследовательский центр СтаДиО» (АО НИЦ СтаДиО).

Спонсорскую поддержку оказали ООО Научно-проектная фирма «СКАД СОФТ», АО «АСКОН», ООО «ЕВРОСОФТ», АО «НИЦ «Строительство», ООО «ТИК-ПРОДЖЕКТ», ООО «Специализированный застройщик «Строительная компания Жупиков», ООО «Бокинский Завод Строительных Конструкций», Ассоциация СРО «Тамбовские строители», Группа компаний «АСБ», Тамбовское отделение 8594 ПАО «Сбербанк России», ООО Проектный институт «Тамбовсельхозтехпроект», ООО «Газстальмонтаж», ООО «Группа компаний «Мегаполис», ООО «МОСТОСТРОЙ», ООО «Тамбовспецстрой».

2. ОСНОВНЫЕ НАУЧНЫЕ НАПРАВЛЕНИЯ, ПРОГРАММА И МЕРОПРИЯТИЯ СИМПОЗИУМА

Работу Симпозиума открыл председатель его Организационного комитета, академик РААСН В.И. Травуш. На торжественном открытии с приветственными обращениями к участникам Симпозиума выступили Министр строительства и жилищно-коммунального хозяйства Российской Федерации И.Э. Файзуллин, Губернатор Тамбовской области М.Б. Егоров, президент РААСН, ректор МАрхИ академик Д.О. Швидковский, ректор ТГТУ М.Н. Краснянский, ректор НИУ МГСУ П.А.Акимов.



Рис. 2. Выступает академик РААСН В.И. Травуш

На пленарных заседаниях Симпозиума были заслушаны доклады: «Компьютерное моделирование уникальных зданий и сооружений на всех этапах жизненного цикла. Опыт 2018-2023 гг., проблемы и решения» (докладчик - академик РААСН А.М. Белостоцкий); «Новые модифицированные бетоны – качество и надежность сооружений в контексте зеленых технологий» (докладчик – академик РААСН С.С. Каприелов); «Живучесть железобетонных рамно-стержневых конструктивных систем при особых воздействиях» (докладчик – академик РААСН В.И. Колчунов); «Инженерные решения задач математической физики в приложении к техническим проблемам строительных наук» (докладчик – академик РААСН С.В. Федосов), «Моделирование шумового режима на объектах с массовым пребыванием людей» (докладчик – А.И. Антонов); «Определение характерных особенностей работы перфорированного резинометаллического виброизолятора с использованием современных программных комплексов, реализующих метод конечного элемента» (докладчик – В.Л. Мондрус); «Численное моделирование колебаний композитных рамных конструкций с учётом демпфирования с памятью» (докладчик – В.Н. Сидоров); «Моделирование многоэтажного железобетонного здания на многослойном деформируемом основании с учетом повреждаемости» (докладчик – А.А. Трещев); «Цифровые и интеллектуальные технологии в диагностике строительных объектов» (докладчик – Г.Г. Кашеварова); «Развитие и совершенствование теории статических расчетов стержневых и пластинчатых систем на произвольном упругом основании» (докладчик – О.В. Козунова); «О развитии и совершенствовании программного комплекса МКЭ для геотехнической практики» (докладчик – Р.А. Мангушев); «Расчетная модель деформирования грунтового основания высотного здания с учетом предыстории загружения» (докладчик – И.Т. Мирсаяпов); «Математическое моделирование механических свойств вязкоупругих материалов с отрицательным коэффициентом Пуассона» (докладчик – М.В. Шитикова).

Доклады Симпозиума были заслушаны и обсуждены по основными научным направлениям:

1. Моделирование нагрузок и воздействий на строительные конструкции, здания, сооружения и комплексы.
2. Технологии информационного моделирования жизненного цикла объекта капитального строительства.
3. Разработка, исследование и развитие численных и численно-аналитических методов расчета конструкций, зданий и сооружений.
4. Нелинейные модели материалов, конструкций зданий и сооружений при расчетном обосновании проектов и оптимальном проектировании.
5. Моделирование конструкций, зданий, сооружений и комплексов на стадиях их возведения, реконструкции, нагружений, сопротивляемости прогрессирующему разрушению.
6. Математическое и компьютерное моделирование в архитектуре, градостроительстве и строительстве.
7. Моделирование материалов и конструкций в нестационарных физико-механических условиях при сложных воздействиях.
8. Моделирование повреждаемости и разрушения конструкций и материалов. Математические модели и методы в системах мониторинга зданий и сооружений.



Рис. 3. Выступает академик РААСН А.М. Белостоцкий



Рис. 4. Участники Симпозиума во время докладов

Научная программа Симпозиума проводилась по восьми секциям: «Моделирование нагрузок и воздействий на строительные конструкции, здания, сооружения и комплексы» (Секция №1. Модераторы - А.М. Белостоцкий и Т.А. Белаш); «Технологии информационного моделирования жизненного цикла объекта капитального строительства» (Секция №2. Модераторы - Н.Г. Келасьев и А.И. Антонов); «Разработка, исследование и развитие численных и численно-

аналитических методов расчета конструкций, зданий и сооружений» (Секция №3. Модераторы - В.К. Ахметов и А.Н. Потапов); «Нелинейные модели материалов, конструкций зданий и сооружений при расчетном обосновании проектов и оптимальном проектировании» (Секция №4. Модераторы - В.В. Лалин и М.В. Шитикова); «Моделирование конструкций, зданий, сооружений и комплексов на стадиях их возведения, реконструкции, нагружений, сопротивляемости прогрессирующему разрушению» (Секция №5. Модератор - Г.Г. Кашеварова); «Математическое и компьютерное моделирование в архитектуре, градостроительстве и строительстве» (Секция №6. Модераторы - В.И. Леденев и Н.Н. Трекин); «Моделирование материалов и конструкций в нестационарных физико-механических условиях при сложных воздействиях» (Секция №7. Модераторы - Т.Л. Дмитриева и А.Н. Мамин); «Моделирование повреждаемости и разрушения конструкций и материалов. Математические модели и методы в системах мониторинга зданий и сооружений» (Секция №8. Модераторы - С.Б. Крылов и Т.А. Низина).



Рис. 5. Н.Н. Баглаев, Г.Г. Кашеварова, А.М. Белостоцкий принимают участие в работе научных секций



Рис. 6. Академик С.С. Каприелов и член-корреспондент В.Е. Румянцева в дискуссии на кофе-брейке

К началу работы Симпозиума его участники получили опубликованный сборник тезисов докладов, проиндексированный в базе данных РИНЦ [4].

В рамках Симпозиума прошло общее собрание членов Центрального территориального отделения РААСН и заседание Отраслевого консорциума «Строительство и архитектура». На заседании были подписаны соглашения о вхождении в Консорциум новых членов.



Рис. 7. Академик РААСН В.И. Травуш, ректор ТГТУ М.Н. Краснянский и советник РААСН В.В. Галишникова на заседании Отраслевого консорциума «Строительство и архитектура»

Состоялись заседания Научных советов Российской академии архитектуры и строительных наук «Цифровые технологии в строительстве и архитектуре» и «Механика разрушения бетона, железобетона и других строительных материалов».

На заседании Научного совета «Цифровые технологии в строительстве и архитектуре» С докладами «О разработке национального программного обеспечения в области архитектуры и строительства" выступили академик А.М. Белостоцкий и советник РААСН, О.В. Кабанцев. С сообщением «О проведении IX Международного симпозиума РААСН «Актуальные проблемы компьютерного моделирования конструкций и сооружений» член-корреспондент В.Н. Сидоров.

На заседании Научного совета «Механика разрушения бетона, железобетона и других строительных материалов» под председательством академика В.П. Селяева обсуждена стратегия работы Научного Совета в ближайшей перспективе, рассмотрен план работы Научного Совета на 2023-2025 гг. Членами Научного совета изложены и обсуждены основные результаты исследований, сформулированы проблемы и задачи в механике разрушения бетона и других строительных композитов.



Рис. 8. Заместители председателя Организационного комитета Симпозиума член-корреспондент РААСН П.В. Монастырев и член-корреспондент РААСН В.Н. Сидоров на заседании Научного совета РААСН «Цифровые технологии в строительстве и архитектуре»

Доклады на круглом столах Симпозиума «Региональные проблемы цифровизации строительной индустрии» под председательством ректора ТГТУ М.Н. Краснянского и «Критерии расчета ответственных зданий и сооружений на особые нагрузки и воздействия» под председательством академика РААСН А.М. Белостоцкого и О.В. Кабанцева сопровождались содержательными выступлениями и полезными дискуссиями.



Рис. 9. Министр градостроительства и архитектуры, главный архитектор Тамбовской области А.А. Филатов принял активное участие в круглом столе Симпозиума «Региональные проблемы цифровизации строительной индустрии»

Ведущими разработчиками программного обеспечения, компаниями АСКОН, СКАД СОФТ, Лира-сервис, Еврософт были проведены мастер-классы.

В рамках культурной программы участники Симпозиума познакомились с достопримечательностями и музеями городов Тамбова и Мичуринска, в год 150-летия со дня рождения великого композитора С.В. Рахманинова приняли участие в масштабном Музыкальном фестивале «Сиреневая ночь» в музее-заповеднике Сергея Рахманинова в с. Ивановка Тамбовской области.



Рис. 10. Музей-заповедник С.В. Рахманинова в с. Ивановка Тамбовской области

ЗАКЛЮЧЕНИЕ

Симпозиум позволил произвести оценку современного состояния российской науки и практики в сфере компьютерного моделирования зданий и сооружений с учётом ретроспективного анализа, осмысления пройденного пути и полученного опыта в период 1990 – 2023 гг., а также прогнозирования и программирования их развития в период до 2035 г.

Организационный и Программный комитеты Симпозиума уверены в несомненной полезности и ценности обмена мнениями представителей науки, бизнеса и власти, которое проходило на разнообразных площадках Симпозиума. Целью этого взаимодействия стала выработка направлений и содержания, механизмов и рычагов эффективного развития, движения к новым успехам и достижениям в области компьютерного моделирования конструкций и сооружений, цифровизации строительной отрасли.

Подробная информация о площадках Симпозиума, фотографии и видеоматериалы приведены на его сайте - http://8apscse.tstu.ru/.

Литература.

1. Травуш В.И. Об истории и основных итогах V международного симпозиума «Актуальные проблемы компьютерного моделирования конструкций и сооружений». // Строительная механика и расчет сооружений, 2014, №5, с. 2-7.

2. Травуш В.И., Акимов П.А., Белостоцкий А.М., Дмитриева Т.Л., Сидоров В.Н. Об истории и основных итогах Пятого международного симпозиума «Актуальные проблемы компьютерного моделирования конструкций и сооружений». // International Journal for Computational Civil and Structural Engineering, Volume 10, Issue 3, 2014, pp. 176-183.

3. В.И. Травуш, П.А. Акимов, А.В. Баенхаев, А.Т. Беккер, А.М. Белостоцкий, Т.Б. Кайтуков, В.Н. Сидоров Об основных итогах шестого международного симпозиума «актуальные проблемы компьютерного моделирования конструкций и сооружений» International Journal for Computational Civil and Structural Engineering, Volume 12, Issue 3, 2016, pp. 125-140.

4. Актуальные проблемы компьютерного моделирования конструкций и сооружений. Тезисы докладов VIII-го международного симпозиума. Под редакцией Сидорова В.Н. и Монастырева П.В. / 2023, 436 стр.
[https://www.elibrary.ru/item.asp?id=52693501&selid=53113693]